ABSTRACT

ELECTRIC FIELD MODEL OF A CYLINDRICAL NEURON AND ITS RESPONSE FOR IMPRESSED STIMULI AND VARIABLE MEMBRANE CONDUCTANCE

By

Thomas Michael Przybylski

The problem studied in this report is the development of a general solution for the electric potentials, fields, and currents in and about a membrane cylinder representing a nerve axon or dendrite. The resulting models are for both the passive response to subthreshold stimulating currents impressed via electrodes, and the active response due to ion-selective changes in the membrane's conductance. Two space variables (radial and axial) plus time are used.

In the development of the appropriate volume-conductor equations, the possibility of an ion-acoustic wave being excited as part of the action potential is considered and rejected. Boundary conditions for both interface and transmembrane boundaries are developed in a general fashion. The Goldman equation for transmembrane potential is shown to hold exactly in cylindrical coordinates.

A model giving the steady-state and transient electrotonic responses to source currents supplied by intracellular or extracellular metallic ring electrodes is developed by use of the Fourier exponential transform on the axial variable and the Laplace transform applied to the time variable. The inverse transforms are found

analytically in the case of the Laplace transform and numerically (with a digital computer) for the Fourier transform. This model involves three volume-conductor regions (intracellular, extracellular, and membrane). Allowing the electrodes to be finite-sized structures eliminates a singularity found in previous solutions. The response of the present model is compared to the response of the core-conductor model, with the result that the responses are virtually the same (except near the electrode) for an intracellular stimulus and totally different for an extracellular stimulus.

Membrane capacitance is calculated directly from surface charge and transmembrane potential and is shown to be a constant. The model also demonstrates that axial currents within the membrane are negligible and can be ignored. Transient responses for step, pulse, and impulse (delta) function stimulus time dependence are presented, with the model's response containing a stimulus artifact. A simulation of a myelinated axon suggests that the action of the myelin sheath is to block action potential generation by preventing the axon membrane from reaching threshold.

A model for two volume-conductor compartments (intracellular and extracellular) is also presented; with its electrotonic response being the same as the three-region model. This reduced model is extended to predict the active response to membrane conductance changes. Responses presented include those due to an ion-selective steady-state high conductance window and simulations of excitatory and inhibitory postysnaptic potentials. The model explicitly contains the individual Nernst potentials in the source terms and has a non-linear response to conductance perturbations.

Appendices include development of error bounds, solution convergence considerations, and details on the computer programming involved.

ELECTRIC FIELD MODEL OF A CYLINDRICAL NEURON AND ITS RESPONSE FOR IMPRESSED STIMULI AND VARIABLE MEMBRANE CONDUCTANCE

By

Thomas Michael Przybylski

A DISSERTATION

Submitted to
Michigan State University
in partial fulfillment of the requirements
for the degree of

DOCTOR OF PHILOSOPHY

Department of Electrical Engineering and Systems Science

1975

ACKNOWLEDGMENTS

The author wishes to express his appreciation to Drs. Kun Mu Chen and Dennis P. Nyquist for their assistance and guidance. A special note of thanks is due Dr. Nyquist for his editorial assistance during the preparation of the manuscript. The bulk of this research was performed while the author was on a National Science Foundation Fellowship.

TABLE OF CONTENTS

LIST OF FIGURES

LIST OF TABLES

CHAPTER 1

INTRODUCTION

The survival of any living organism is dependent upon its ability to interact with its environment. In all but the lowest orders of the animal kingdom, it is the role of the nervous system to provide this necessary integration of the organism with both its internal and external environments. To accomplish this, the nervous system performs a wide variety of functions. These include such things as information input, signal processing, decision making, and output responses in the form of appropriate reactions to environmental demands. In man, this system is composed of billions of highly specialized cells interconnected in an immensely complex network. Even in the simplest of creatures has the understanding of the complete nervous system evaded investigators. However, a great deal of progress has been made towards defining the function and properties of the basic building block of the system: the individual neuron. It is to the problem of formulating a mathematical model for the electrical response of the neuron that this present report addresses itself.

1.1. Description of the System

The primary purpose of this section is to present a very brief description of the system under consideration: the individual

neuron. The reader is referred to the literature for a more complete treatment, with this material intended as an outline of nomenclature for those not familiar with neurophysiology. The present author suggests Katz [40] and Stevens [74] for a basic but thorough treatment; with physiology texts such as Cole [12], Eccles [17] - [19], Ganong [27], Hodgkin [33], Mountcastle [50], Ochs [54], or Ruch and Patton [70] providing more advanced sources.

Functionally, the neuron may be described as a unit that integrates multiple inputs into a single output. This signal processing is essentially an electrical event; with metabolism, cellular structure, and neuronal interconnections all involved in both the generation and processing of the electrical signals. The histology of a typical neuron[1] is illustrated in Figure 1.1. The cell body is referred to as the soma and is identified by the presence of the nucleus (site of genetic code). The dendrites (or dendritic tree) extend from the soma and are specialized for receiving information. The synapses are the junctions at which information passes from one nerve cell to another. Primarily they occur on the dendrites and soma[2]. The structure that carries

---

[1] The phrase "typical neuron" is likely to evoke a smile from any biologist. There is tremendous structural variation between neurons, with the precise role of these variations on neural function poorly understood. The neuron discussed here is perhaps most similar to those of the spinal column or peripheral nerve trunks.

[2] Synapses are also found on axons. These axo-axonal synapses are less frequent than axo-somatic or axo-dendritic synapses and are felt to be the site of presynaptic signal processing. See Stevens [74].

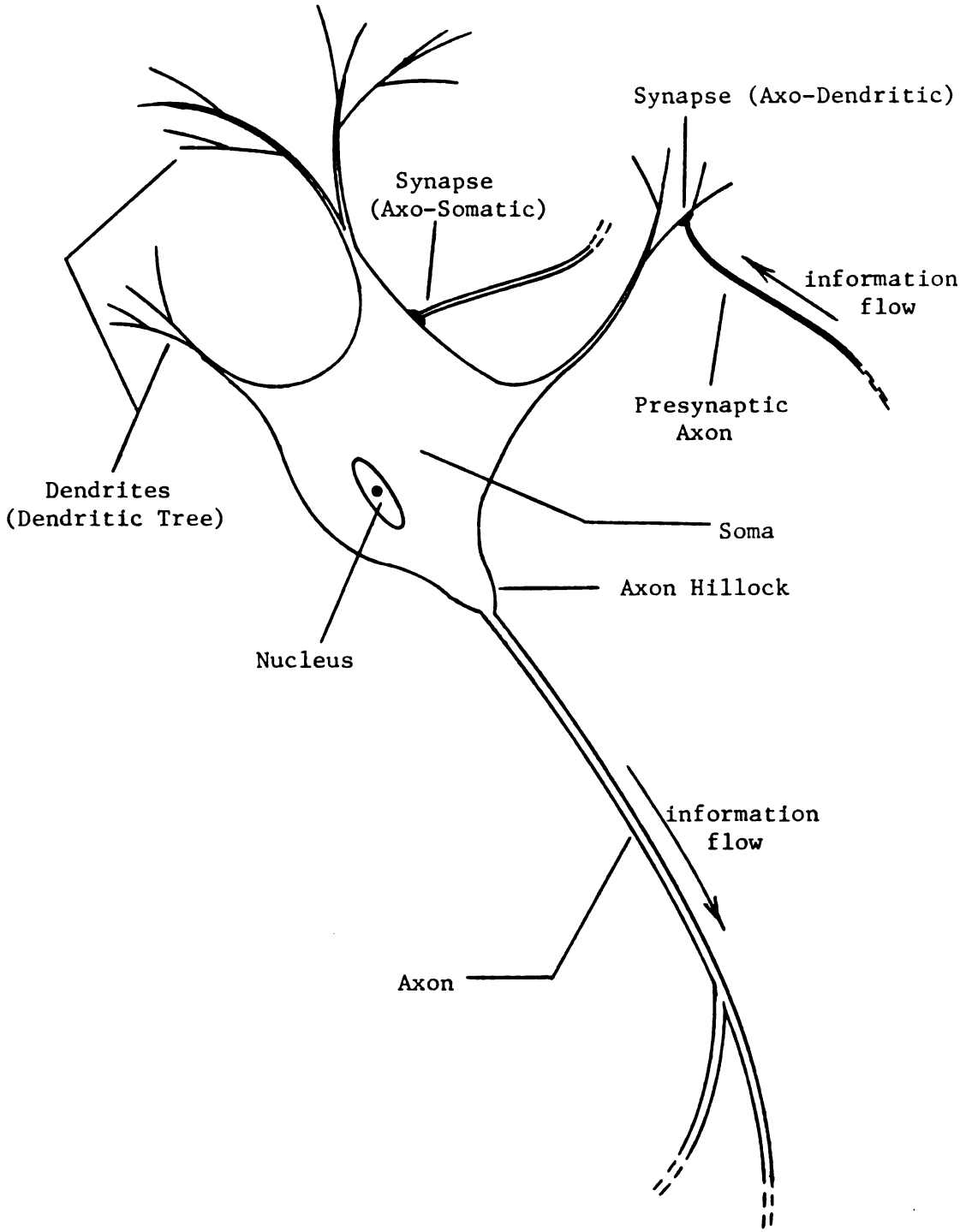

FIGURE 1.1

Schematic Representation of a Typical Neuron

information away from the cell is the axon, a single fiber originating at the axon hillock that may branch to synapse with one or more neurons, muscle cells, or secretory cells. The plasma membrane defines the boundary of the cell and separates the intracellular medium (cytoplasm) from the extracellular (interstitial) fluid.

The physical dimensions of a neuron can vary over a considerable range. The soma normally has a diameter between 2 and 30μ (1μ = 10^{-6} meters). The dendrites can have lengths up to 2 mm. Axons show the largest variation, with lengths ranging from 50μ to 3 meters and diameters from 0.5μ to 1 mm. The membrane thickness lies in the range of 50 to 150 Å (1 Å = 10^{-10} meters).

The cellular fluids contain a variety of inorganic and organic ions. These ions are the charge carriers in the system. An important property of the membrane is its selective permeability to certain ions; thought to be the result of ion-specific channels that sort the ions by their hydrated sizes (see Hille [32]). The ions of primary importance in neural function are sodium (Na^+), potassium (K^+), and chloride (Cl^-). The extracellular fluid has a high concentration of Na^+ and Cl^- ions, and a low concentration of K^+ ions. Conversely, the intracellular medium has K^+ ions in high concentration, with relatively little Na^+ or Cl^- ions present[1]. This distribution of ions causes ionic concentration gradients across the membrane; with the selective permeability of the membrane and a metabolic sodium-potassium pump maintaining the situation.

---

[1] Overall electroneutrality in the cell interior is maintained by the presence of organic anions that cannot pass through the membrane.

The ionic concentration gradients result in a charge separation (or polarization) that maintains a potential difference across (and an electric field within) the cell membrane. In the resting state, this potential difference is about -60 mV, with the sign convention being interior potential with respect to exterior potential[1]. The resting potential is primarily due to a balance between its associated electric field drift fluxes and the diffusion fluxes driven by the concentration gradients of the K^+ and Cl^- ions. This follows from the membrane (in the resting state) being highly permeable to K^+ and Cl^- ions and only slightly permeable to Na^+ ions. The response to reducing the charge separation across the membrane is to reduce the magnitude of the transmembrane potential (V_m); referred to as a depolarization. Increasing the charge separation increases the magnitude of V_m and is called a hyperpolarization.

If the axon's membrane is depolarized past a stability point known as threshold[2], a complicated phenomenon called the nerve impulse is initiated. The nerve impulse is characterized by a very rapid depolarization and reversal of V_m, followed by a slower repolarization to slightly beyond (more negative than)

---

[1] Different authors cite various values for the resting potential. This value is from Katz [40]. Values reported range from -40 to -100 mV, with the differences arising both from the particular cell's ionic profiles and the recording technique used. See Plonsey [60].

[2] Threshold is normally at about V_m = -40 mV. Depolarizations that do not reach threshold fail to excite the nerve impulse and only result in a local spread of potential perturbation.

the resting potential before returning to the resting state. This potential change associated with the nerve impulse is labeled the action potential. The "spike" of the action potential has a duration of about 1 msec and a fixed magnitude[1]. The cause of the action potential is a rapid increase in the membrane's permeability to sodium ions resulting in an influx of positive charge. Repolarization follows from a subsequent increase in the permeability and associated efflux of K^+ ions (see Cole [13] for the classical paper on this subject). Since the ionic motions represent current flows, the permeability of the membrane to an ion species is intimately linked with the electric conductivity of the membrane for that ion species. Alterations in permeability thus represent alterations in conductivity and the two terms are often used interchangeably.

Once the action potential is excited, it propagates along the nerve axon at a velocity between 0.1 and 100 m/sec until it reaches the point where the axon synapses with another cell. The arrival of a nerve impulse at a synapse causes the release of a chemical referred to as the transmitter substance from vesicles in the axon terminals. This transmitter substance forms the information-carrying link between the cells. Its arrival by diffusion at the postsynaptic membrane[2] alters the conductance of that membrane to one or more ion species; resulting in a depolarization

---

[1] The peak of the action potential is a transmembrane potential of about +40 mV so that the magnitude is about 100 mV. The fixed magnitude is a property of the "all or none law", see Stevens [74].

[2] The presynaptic and postsynaptic membranes are separated by a distance of approximately 200 Å known as the synaptic cleft.

or hyperpolarization of the postsynaptic membrane near the synapse. If the postsynaptic cell is a muscle or secretory cell, the result to activity in the presynaptic axon is a muscular contraction or glandular secretion; essentially the output end of the nervous system whereby the organism responds to its environment.

When the postsynaptic cell is another neuron, the depolarization or hyperpolarization passively spreads to the soma where it is spatially and temporally summed with the polarizations due to other synapses. If the result is a supra-threshold depolarization at the axon hillock, an action potential is excited and propagates down the postsynaptic cell's axon to repeat the above-discussed process. This addition of the responses due to many synapses into a single output is the previously mentioned process of neural integration. The signal processing and decision of whether a nerve impulse is excited at the axon hillock are functions of the number, locations, frequency, and time of occurrence of all synapses to the cell's receptor surface. Information is carried in the system either as analog variations in transmembrane potential (as from synapses, referred to as "slow potentials") or in the repetition rate (frequency of occurrence) of action potentials.

From the above brief and sketchy outline of neural function, it is apparent that there are two basic divisions to the electrical response of a neuron. There is the passive response; characterized by hyperpolarizations or subthreshold depolarizations that produce only local effects and do not alter the membrane's conductivity sufficiently to excite an action potential. The second division is the active response due to changes in the conductivity of the membrane to

one or more ion species. These permeability changes can be due to chemical action (synapse) or supra-threshold depolarizations that excite the propagated nerve impulse. This report presents models for both these divisions of bioelectric phenomena. The next section discusses different types of previous models, outlines the specific problem to be attacked, and indicates the relationship of this present effort to previous work.

1.2. Discussion of the Problem and Related Work

Mathematical abstractions or "models" have long been an important tool of the scientist. At their best, they aid in quantifying experimental results, predict new behavior, suggest further experiments, help to discover the underlying mechanisms of phenomena, and assist the investigator in the choice or development of theoretical formulations. As discussed by Cole [11], the development of electrical models for neural function has a history reaching back into the 19th century. However, the real advances in this field have occurred in the last 40 years.

The variety of neural models is nearly as great as the number of investigators. Some models involve phenomena that mimic neural behavior; such as Lille's [47] analogy of nerve impulse transmission that used an iron wire in a bath of strong acid. Other investigators have explored mathematical equations that have stability properties and propagated solutions that in some ways resemble neural phenomena, as seen in the work of Rinzel and Keller [68]. This nearly pure mathematical approach has shown value in developing systems-analysis stability descriptions and state

diagrams (see FitzHugh [24] and [26]), and in exploring the mathematical side of more physical neural models (as in the work of Evans and Shenk [22] on the Hodgkin and Huxley [37] formulation).

The largest class of models can be described as theoretical formulations based upon physical laws and the experimentally observed or implied structure and properties of the system's constituents. To reduce the complexity, the scope of the model is normally only a portion of the neuron or its response. As such, the variety of investigations in this class are nearly unlimited. At one level, investigators seek to explain the properties of the plasma membrane and its active and passive responses. Mullins [51] considers the variable conductivity of the membrane with a model involving ionic channels within the membrane. Offner [55]-[57] uses a more general physiochemical approach; applying kinetics, electrostatics, and diffusion phenomena to arrive at a model for variable conductivity, ionic concentration profiles, and electric fields within the membrane. Cooley and Cohen [14] solved for the response within the membrane to a step in stimulating current. Others (typically Arndt, Bond, and Roper [3], [4]) solve for the fields and concentration profiles of the resting membrane. The common feature of these investigations is that they are confined to the membrane alone and use a planar (cartesian coordinates) description of membrane geometry.

Another group of models based upon neuronal structure are for the electrical behavior of the axon or dendrites; their geometry represented as membrane cylinders. The oldest and most widely used formulation is the core-conductor model. It reduces the

membrane cylinder to a distributed network of resistors, capacitors, and batteries; leading to a one-dimensional cable equation. Its early formulation (see Lorente de No [48]) described passive (subthreshold) events with the membrane modeled as a parallel combination of a fixed conductance and capacitance. The work of Hodgkin and Huxley [34] - [37] extended the cable equation to cover the active response of the action potential. They developed a membrane network based upon the ionic composition of the cellular fluids and the known phenomena of ion-selective membrane conductance alterations during the nerve impulse. From experimental measurements, they found empirical expressions for the membrane conductivities of the individual ion species as functions of transmembrane potential[1]. With their equivalent circuit for the membrane (and different conductance functions) nearly any active neural event can be simulated.

A great number of the investigations since that time have concentrated on verifying and extending the Hodgkin-Huxley model. Finkelstein and Mauro [23] demonstrated the membrane equivalent circuit could be derived from consideration of the system's ionic composition and the bulk parameters of the media. Hoyt [39] explored kinetic factors involved in some of the assumptions inherent in the Hodgkin-Huxley model. FitzHugh [25] and Goldman and Albus [28] alternated the Hodgkin-Huxley membrane with a passive membrane to simulate the conduction of the nerve impulse in a myelinated axon. Others, such as Cooley and Dodge [15] have used

---

[1] Their work was for the membrane of the giant axon of Loligo.

the digital computer to explore the characteristics of the model's response in greater detail. Nagumo, Arimoto, and Yoshizawa [52] developed a simulation in the form of an active pulse transmission line; suggested by cable theory and the Hodgkin-Huxley formulation. Recently, Goldstein and Rall [29] used the cable equation with axially-variant parameters to simulate changes in the action potential due to nonuniformities such as tapering axons or branches. Rall [62] - [64] has used the core-conductor model with variable membrane conductance to simulate synapses and the passive spread of potential along dendritic trees.

Cable theory yields the transmembrane potential and the potential at either side of the membrane. Attempts have been made to describe the potential field throughout the system by extensions of cable theory (Lorente de No [48]); but the model has been indicated as inaccurate (Clark and Plonsey [8], Rall [65]), particularly in the extracellular region. Other drawbacks have been noted from its one-dimensionality (Clark and Plonsey [8], Eisenberg and Johnson [20]). These inaccuracies were pointed out by comparisons to solutions resulting from studies of a more recent class of models in two and three dimensions. These include the work of Clark and Plonsey [8]-[10] for the two-dimensional intracellular and extracellular fields and currents due to a specified transmembrane potential distribution along a membrane cylinder[1]. Eisenberg and Johnson [20] present a model that yeilds the steady-state intracellular potential distribution in three dimensions from a source current injected by point electrodes. Hellerstein's

---

[1] Rotational symmetry about the cylinder's axis is assumed. This is the case for all of the two-dimensional models.

[30] work gives a two-dimensional model for fields and currents in the intracellular and extracellular regions of a membrane cylinder subjected to a step function in current applied at one side of the membrane and removed on the other.

Klee and Plonsey [43] and [44] formulate an integral equation approach for axially symmetric cells and carry out solutions for the potential distribution resulting from the interaction of a static extracellular electric field and a high conductivity "hole" in a spherical membrane (see also Klee [42] for a model of static electrotonus with a similar source and a variety of cellular geometries). Finally, Rall [65] presents a passive, three-dimensional solution for the time-dependent relaxation of a specified transmembrane potential distribution. These models share the characteristic of being solutions for the electrical response of systems whose geometry represents some portion of neural structure.

The problem studied in this report is an extension of these latter investigations. It may be described as a solution for the electric potentials, fields, and currents in and about a membrane cylinder representing a nerve axon or dendrite. The response sought is for both the passive case of subthreshold stimuli impressed via electrodes and the active case of ion-selective changes in the membrane's conductivity. The model is built from the cellular geometry, the macroscopic properties of the cellular media, and equations describing the interaction of electric fields and volume-conductors. The interest behind its development was a desire to formulate an electric field description for general neural response based upon the known physical structure and composition (ionic

concentrations, macroscopic physical parameters, etc.) of the neuron.

The model is perhaps best described by outlining its presentation and the methods used in the solutions. Chapter 2 is primarily concerned with developing a general set of equations and associated boundary conditions for volume-conductors from Boltzmann's equation and Maxwell's equations. Included is a derivation of the Goldman equation for resting transmembrane potential in cylindrical coordinates. Chapters 3 and 4 solve for and present the response of a three-region model to subthreshold impressed (electrode-supplied) stimuli. Chapter 3 finds the steady-state response in terms of the fields and currents in the membrane, cell interior, and extracellular medium by means of the Fourier exponential transform. The transform is applied to the axial variable and the inverse transform is found by numerical techniques using the digital computer. Chapter 4 extends these solutions to time-dependent stimuli by use of the Laplace transform (on the time variable) and analytical inversions back to the time domain. Interesting features of these solutions are that the electrodes are taken as finite-sized structures, the response to an extracellular stimulating electrode is shown to be quite different than that for an internal stimulus, and a simulation of a myelinated axon is carried out.

Chapter 5 reduces the problem to two regions (intracellular and extracellular) by means of a transmembrane boundary condition that incorporates the Nernst potentials and individual ions' membrane conductances. The electrotonus problem of the previous two chapters is solved in this reduced system, giving a simpler model for this

response when specification of the membrane fields and currents is not required. This model is then extended to predict the response due to time and spatially-dependent changes in the conductance of the membrane to one or more ion species. Simulations of excitatory and inhibitory postsynaptic potentials are presented to illustrate features of the model. As in Chapters 3 and 4, the Fourier and Laplace transforms with numerical and analytical inversions provide the mathematical means for obtaining the solutions.

The result of this research is a model that is far more general in many ways than those of the previous investigators. However, these models in the available literature were of assistance in the formulation of the present work and provided verification of the results of this report in special cases. The contrasts between the present and previous investigations can be summarized as follows.

i) The steady-state and time dependent passive responses in the present report are due to impressed currents supplied via electrodes of finite dimension. Clark and Plonsey [8] - [10] and Rall [65] require specification of the transmembrane potential distribution. Eisenberg and Johnson [20] use point source electrodes and obtain only steady-state results. Hellerstein's [30] model specifies infinitely narrow electrodes; with a current source at one side and a current sink on the other side of the membrane.

ii) The present model obtains the fields within the membrane for the passive response and allows the membrane to have finite thickness (and verifies the necessary assumptions) when the fields

are not obtained in the membrane. All previous field solutions assume the membrane as infinitely thin. Most are for only intracellular and extracellular fields, with Eisenberg and Johnson [20] solving only an intracellular problem.

iii) This model is the first field approach to explicitly include the ionic concentration gradients across the membrane, the individual ionic conductances in the membrane, and the ability to simulate time-dependent active phenomena by specification of spatially and time varying ion-selective conductance functions. Klee and Plonsey's [43] and [44] use of a static electric field and a finite size "hole" in the membrane is the only solution at all similar. They used integral equations and obtained a steady-state response. Other models (Clark and Plonsey [8] - [10]) simulate active phenomena by specification of the transmembrane potential distribution at the membrane and cannot solve for this transmembrane potential as due to conductance changes.

iv) The present report formulates its solutions with the exponential Fourier transform, allowing the use of non-axially symmetric impressed stimuli and conductance perturbations. Although all responses presented are for symmetric stimuli, the solutions are valid for the non-symmetric case and only require the Fourier transform of the desired stimulus or conductance function. Eisenberg and Johnson [20] and Hellerstein [30] have infinitely small electrodes that are inherently symmetric; Klee and Plonsey [43] and [44] use a rotationally symmetric high conductance patch on a spherical cell.

v) The cellular parameters in this report are all specified in terms of bulk parameters of the various media. This follows from a traditional electric field approach where conductivities, electric permittivities, magnetic permeabilities, etc. describe the properties of the medium rather than using resistances (conductances), capacitances, etc. that depend upon both the medium and its geometry. Any conductances or capacitances used are derived in terms of the properties of the medium and geometries of the system. This allows the model to indicate the effects of changing any of the properties of the medium in any region (intracellular, extracellular, or membrane). Also, the common assumption of the intracellular and extracellular media having the same conductivities is not used, as in Hellerstein [20], Klee [42], or Klee and Plonsey [43] and [44].

Thus the model of the present report allows an investigator to simulate a far greater variety of bioelectric phenomena and observe the effects of a wider range of parameter alterations and stimuli than the previously available solutions. Though only a limited number of responses are presented, nearly any time or spatially dependent impressed stimulus may be handled by the techniques presented and essentially any time course of conductance changes can be used to obtain the fields and currents throughout the entire system.

CHAPTER 2

DEVELOPMENT OF THE BASIC EQUATION SET

This chapter is concerned with the development of fundamental equations, boundary conditions, and resting state results that will be used repeatedly in later chapters. Section 2.1 concerns the basic equations for the interior of volume regions. Section 2.2 develops the boundary conditions. Finally, Section 2.3 uses the previous work to obtain a few steady-state results in cylindrical coordinates.

2.1. Basic Equations for Interior Volume Regions

2.1.1. Ion Transport Equations and Maxwell's Equations

The system under study involves the interaction of electric field and diffusion effects on ions in an aqueous solution. The logical starting point is with Boltzmann's equation (describing ionic motion) and Maxwell's equations (for electromagnetic field description). The development of a useable equation set will then follow that carried out in plasma (ionized gas) problems. The equations will be formulated in terms of a dependence on concentrations (moles/m^3), as is the usual practice in physiology, rather than use number density (ions/m^3) as commonly seen in physics and

engineering.[1] Units otherwise will be standard MKSA.

The intracellular and extracellular compartments that comprise the system are composed of multi-ionic fluids in which the solvent is water. As the motion of individual ions is not of concern, it is appropriate to use the first two moments of Boltzmann's equation to characterize their macroscopic (or average) properties of density and velocity (see Tanenbaum [75]). For each ion species "i", the time varying transport equations that describe these quantities are

$$\frac{\partial n_i(\vec{r},t)}{\partial t} + \nabla \cdot [n_i(\vec{r},t)\vec{v}_i(\vec{r},t)] = 0 \tag{2.1}$$

$$\frac{\partial \vec{v}_i(\vec{r},t)}{\partial t} + [\vec{v}_i(\vec{r},t)\cdot\nabla]\vec{v}_i(\vec{r},t) = \frac{q_i}{m_i}[\vec{E}(\vec{r},t) + \vec{v}_i(\vec{r},t) \times \vec{B}(\vec{r},t)]$$

$$- \frac{kT_i}{m_i n_i(\vec{r},t)} \nabla n_i(\vec{r},t) - \nabla \phi_i(\vec{r},t) + \frac{1}{m_i n_i(\vec{r},t)} \vec{P}_i(\vec{r},t) \tag{2.2}$$

where

$n_i(\vec{r},t)$ = number density of the ith ion species (ions/m^3)

$\vec{v}_i(\vec{r},t)$ = average velocity of the ith ion species (m/sec)

q_i = effective charge of the ith ion species (coulombs)

m_i = effective mass of the ith ion species (kg)

---

[1] Actually concentrations are usually given in the literature in terms of m Moles/liter or μ Moles/mℓ. However, there is no need to convert units as moles/m^3 = m Moles/liter = μ Moles/mℓ.

T_i = temperature of the ith ion species (°K)

k = Boltzmann's constant (1.38×10^{-23} joules/°K)

$\phi_i(\vec{r},t)$ = gravitational potential of the ith ion species (m^2/sec^2)

$\vec{E}(\vec{r},t)$ = electric field with which the ions interact (volts/m)

$\vec{B}(\vec{r},t)$ = magnetic induction with which the ions interact ($webers/m^2$)

$\vec{P}_i(\vec{r},t)$ = time rate of increase of momentum per unit volume of the ith ion species due to effective collision or viscous damping forces from interaction with neutral H_2O molecules (kg/m^2 sec).

The desired forms of these equations will relate concentrations to electric current densities. The concentration of the ith ion species is defined as

$$C_i(\vec{r},t) = n_i(\vec{r},t)/L \quad moles/m^3 \tag{2.3}$$

where L = Avogadro's number (6.02×10^{23} ions/mole). The current due to the motion of the ith ion species is identified as[1]

$$\vec{J}_i(\vec{r},t) = z_i F\, C_i(\vec{r},t)\vec{v}_i(\vec{r},t) \quad amps/m^2 \tag{2.4}$$

where z_i = valence of the ith ion species (signed) and F = Faraday's constant (9.65×10^4 coulombs/mole). Thus applying definitions (2.3) and (2.4) to equation (2.1) (by multiplying both

---

[1] Note that z_iF is the effective charge of the ith ion species (coulombs/mole) when concentration is in $moles/m^3$. The particle flux density, $\vec{J}_i = C_i\vec{v}_i$ ($moles/m^2$ sec), is commonly used (Plonsey [60]) for characterizing ionic motion. It follows then that $\vec{J}_i = q_i\vec{J}_i$ in $amps/m^2$.

sides by $z_i F/L$) yields

$$z_i F \frac{\partial C_i(\vec{r},t)}{\partial t} + \nabla \cdot \vec{J}_i(\vec{r},t) = 0 \ . \tag{2.5}$$

Equation (2.5) is a continuity equation relating charge density ($z_i F\ C_i$) to current ($\vec{J}_i$) for each ion species.

A similar manipulation is performed on equation (2.2), but several assumptions appropriate for physiological systems are made to simplify its form. First consider the collision term containing $\vec{P}_i$. By definition

$$\vec{P}_i = -n_i \frac{\partial}{\partial t} (m_i \vec{v}_i)\Big|_{\text{viscous}} \ . \tag{2.6}$$

The viscous damping force, $\frac{\partial}{\partial t} (m_i \vec{v}_i)\Big|_{\text{viscous}}$ is given by Stoke's law (see Kortum [45]) as

$$(\vec{F}_\eta)_i = R_i \vec{v}_i \tag{2.7}$$

where $(\vec{F}\eta)_i$ is the viscous damping force and R_i is the viscous resistance coefficient (η refers to viscosity). $R_i(\vec{r})$ is related to the electric mobility[1] of the ith ion species, $u_i(\vec{r})$, through

$$u_i(\vec{r}) = \frac{|q_i|}{R_i(\vec{r})} \ \text{m}^2/\text{volt sec} \ . \tag{2.8}$$

Thus applying equations (2.7) and (2.8) to definition (2.6); the expression for $\vec{P}_i$ becomes

---

[1] $\vec{v}_i = u_i \vec{E}$ defines the electric mobility, u_i, of positive ions. See Plonsey [60]; Kortum [45].

$$\vec{P}_i = -n_i \frac{\partial}{\partial t} (m_i \vec{v}_i)\Big|_{viscous} = -n_i (\vec{F}_\eta)_i = \frac{-n_i |q_i|}{u_i} \vec{v}_i \ . \qquad (2.9)$$

Noting that

$$q_i = z_i e \qquad \text{coulombs/ion} \qquad (2.10)$$

is the effective charge carried by an ion of species "i" with valance z_i (e = absolute value of electronic charge = 1.6×10^{-19} coulombs), then the last term in equation (2.2) has the form

$$\frac{1}{n_i m_i} \vec{P}_i = \frac{-|z_i| e}{m_i u_i} \vec{v}_i \ . \qquad (2.11)$$

Further appropriate assumptions for ions in an aqueous solution are made as follows.

i) All ions are at the same temperature, so that $T_i = T$ (°K).

ii) Gravitational forces are negligible such that $\nabla \phi_i \doteq 0$.

iii) $\vec{v}_i(\vec{r},t)/c << 1$ (where c = speed of light) is assumed; the force due to magnetic induction ($\vec{B}$) is far smaller than than for the electric field (Tanenbaum [75]). This yields $\vec{v}_i \times \vec{B} \doteq 0$.

iv) As the ions are in a state of near continuous collision with the solvent, only small perturbations from the resting state, equilibrium condition of $\vec{v}_i(\vec{r},t) = 0$ are assumed (see Tanenbaum [75], Kortum [45]). Then $(\vec{v}_i \cdot \nabla)\vec{v}_i$ is a negligible second order term and can be set to zero.

With these assumptions, equation (2.2) reduces to

$$\frac{\partial \vec{v}_i}{\partial t} + \frac{|z_i| e}{m_i u_i} \vec{v}_i = \frac{z_i e}{m_i} \vec{E} - \frac{kT}{n_i m_i} \nabla n_i \ . \qquad (2.12)$$

Multiplying by $C_i = n_i/L$ (definition (2.3)) and applying assumption (iv) ($\vec{v}_i$ small perturbation from zero) leads to:

$$C_i \frac{\partial \vec{v}_i}{\partial t} + \frac{|z_i|e}{m_i u_i} (C_i \vec{v}_i) = - \frac{kT}{m_i} [\nabla C_i - \frac{z_i C_i e}{kT} \vec{E}]$$

$$\frac{\partial (C_i \vec{v}_i)}{\partial t} = C_i \frac{\partial \vec{v}_i}{\partial t} + \vec{v}_i \frac{\partial C_i}{\partial t} \doteq C_i \frac{\partial \vec{v}_i}{\partial t} \qquad \text{(assumption (iv))}$$

$$\frac{\partial (C_i \vec{v}_i)}{\partial t} + \frac{|z_i|e}{m_i u_i} (C_i \vec{v}) = - \frac{kT}{m_i} [\nabla C_i - \frac{z_i C_i e}{kT} \vec{E}] \; . \qquad (2.13)$$

With definition (2.4) and noting that $e/k = F/R$, where R is the gas constant (8.31 joules/mole °K), the final form for the second moment equation is

$$\frac{\partial \vec{J}_i}{\partial t} + \frac{|z_i|e}{m_i u_i} \vec{J}_i = - \frac{z_i F \; kT}{m_i} [\nabla C_i - \frac{z_i C_i F}{RT} \vec{E}] \; . \qquad (2.14)$$

Equation (2.14) is a momentum transfer equation, relating an increase in momentum due to collisions, concentration gradients, and electric field forces. It is also a generalized Nernst-Planck equation, as it reduces to the standard Nernst-Planck equation (commonly used in electrophysiology and the study of bioelectric phenomena) in static or quasi-static conditions where $\frac{\partial}{\partial t} \vec{J}_i \to 0$. Along with equation (2.5), it is coupled to Maxwell's equations for the description of electric and magnetic fields due to electric charges and currents. The next step is to express Maxwell's equations in forms appropriate for the electric source terms in ionic fluids, i.e. C_i and $\vec{J}_i$.

Maxwell's equations for the electromagnetic field in a linear, homogeneous, isotropic medium are

$$\nabla \cdot \vec{E}(\vec{r},t) = \rho(\vec{r},t)/\varepsilon \tag{2.15}$$

$$\nabla \times \vec{E}(\vec{r},t) = -\frac{\partial \vec{B}(\vec{r},t)}{\partial t} \tag{2.16}$$

$$\nabla \times \vec{B}(\vec{r},t) = \mu \vec{J}(\vec{r},t) + \mu\varepsilon \frac{\partial \vec{E}(\vec{r},t)}{\partial t} \tag{2.17}$$

$$\nabla \cdot \vec{B}(\vec{r},t) = 0 \tag{2.18}$$

where μ = permeability of the medium (henrys/m) and ε = permittivity of the medium (farads/m). The medium is to be regarded as that in which the sources are immersed.

In equation (2.15), ρ = charge density (coulombs/m^3) and describes all the free charged particles in the system. It can be expressed as

$$\rho(\vec{r},t) = \rho_s(\vec{r},t) + e \sum_i z_i n_i(\vec{r},t) \tag{2.19}$$

where ρ_s is an externally applied charge density (stimulus) and the second term is a sum over all ion species "i". Applying $C_i = n_i/L$ and $F = eL$, relation (2.19) becomes

$$\rho = \rho_s + F \sum_i z_i C_i \ . \tag{2.20}$$

Maxwell equation (2.15) then has the form

$$\nabla \cdot \vec{E} = 1/\varepsilon \left[\rho_s + F \sum_i z_i C_i\right] \ . \tag{2.21}$$

$\vec{J}(\vec{r},t)$ in equation (2.17) is expanded in a similar manner as

$$\vec{J}(\vec{r},t) = \vec{J}_s(\vec{r},t) + \sum_i \vec{J}_i \tag{2.22}$$

where $\vec{J}_s$ is an externally applied current density (amps/m^2) and the $\vec{J}_i$ are defined in equation (2.4). In biological systems, magnetization effects are not present, so that $\mu = \mu_o$ where μ_o is the permeability of free space ($4\pi \times 10^{-7}$ henrys/m). With these definitions, Maxwell equation (2.17) has the form

$$\nabla \times \vec{B} = \mu_o[\vec{J}_s + \sum_i \vec{J}_i] + \mu_o \varepsilon \frac{\partial \vec{E}}{\partial t} . \tag{2.23}$$

A continuity equation relating total charge to total current can be obtained by taking the divergence of equation (2.23).

$$\nabla \cdot (\nabla \times \vec{B}) = 0 = \mu_o[\nabla \cdot \vec{J}_s + \sum_i \nabla \cdot \vec{J}_i] + \mu_o \varepsilon \frac{\partial(\nabla \cdot \vec{E})}{\partial t} . \tag{2.24}$$

Applying equation (2.21) for $\nabla \cdot \vec{E}$ yields

$$[\nabla \cdot \vec{J}_s + \sum_i \nabla \cdot \vec{J}_i] + \frac{\partial}{\partial t}[\rho_s + F \sum_i z_i C_i] = 0 . \tag{2.25}$$

Equation (2.25) is equivalent to applying the expansions for ρ and $\vec{J}$ (relations (2.20) and (2.22)) to the continuity equation of electromagnetics. As the externally applied charge and current densities must obey conservation of charge (these sources being separate from the ions in the system), they are related in a separate continuity equation as

$$\nabla \cdot \vec{J}_s + \frac{\partial p_s}{\partial t} = 0 . \tag{2.26}$$

Collecting the equations that describe the motions of ions in the system (via the interaction of electromagnetic forces and viscous collision forces of the H_2O medium) gives:

$$z_i F \frac{\partial C_i(\vec{r},t)}{\partial t} + \nabla \cdot \vec{J}_i(\vec{r},t) = 0 \tag{2.5}$$

$$\frac{\partial \vec{J}_i(\vec{r},t)}{\partial t} + \frac{|z_i| e}{m_i u_i(\vec{r})} \vec{J}_i(\vec{r},t) = - \frac{z_i F\, kT}{m_i} [\nabla C_i(\vec{r},t) - \frac{z_i F\, C_i(\vec{r},t)}{RT} \vec{E}(\vec{r},t)] \tag{2.14}$$

$$\nabla \cdot \vec{E}(\vec{r},t) = 1/\varepsilon \, [\rho_s(\vec{r},t) + F \sum_i z_i C_i(\vec{r},t)] \tag{2.21}$$

$$\nabla \times \vec{E}(\vec{r},t) = - \frac{\partial \vec{B}(\vec{r},t)}{\partial t} \tag{2.16}$$

$$\nabla \times \vec{B}(\vec{r},t) = \mu_o [\vec{J}_s(\vec{r},t) + \sum_i \vec{J}_i(\vec{r},t)] + \mu_o \varepsilon \frac{\partial \vec{E}(\vec{r},t)}{\partial t} \tag{2.23}$$

$$\nabla \cdot \vec{B}(\vec{r},t) = 0 \tag{2.18}$$

$$\nabla \cdot \vec{J}_s(\vec{r},t) = \frac{\partial \rho_s(\vec{r},t)}{\partial t} \, . \tag{2.26}$$

The assumptions so far have included:

i) no gravitational effects,

ii) $\vec{v}_i$ a small perturbation from $\vec{v}_i = 0$ (resting condition for average velocity),

iii) $\vec{v}_i << c$ (follows from ii) above), and

iv) $\vec{P}_i$ term is due to viscous "collisions" between ions and H_2O molecules.

2.1.2. Ion-Acoustic Phenomena in Physiological Fluids

The basic set of equations developed in the last section are essentially the same as those describing a gaseous plasma with the exception of the relative importance of the term due to collisions with neutral particles (see Tanenbaum [75] or Schmidt [72]). Since a neuron exhibits a propagated event in the action potential, it is possible that there is a coupling between the nerve impulse and a wave excited in the "plasma" represented by the ions in the cellular fluids. As the assumption has been made that magnetic forces do not significantly affect ion motions in a physiological fluid, the equations developed in Section 2.1.1 will not describe an electromagnetic wave in the system. This is logical and necessary, as EM waves propagate near (or at) the speed of light, while the action potential travels at a velocity on the order of 100 m/sec. However, a compression wave can also be excited in a plasma. It consists of electric field and diffusion effects interacting to produce a wave phenomena, and bears the descriptive name of ion-acoustic wave. Most importantly, this ion-acoustic wave has a relatively low propagation velocity (Tanenbaum [75]). This section will examine the likelihood of such an event occurring in a physiological system.

Consider first the steady state, without any stimulus applied to excite the ions. The equilibrium conditions (denoted by subscript "o") are:

$$C_i(\vec{r},t) = C_{io} \quad \text{(a non zero constant)}, \tag{2.27}$$

$$\vec{J}_i(\vec{r},t) = \vec{J}_{io} = 0 \quad \text{(as average velocity = 0, see assumptions in section 2.1.1)}, \tag{2.28}$$

$$\sum_i z_i C_{io} = 0 \qquad \text{(electroneutrality)}, \tag{2.29}$$

$$\vec{E}(\vec{r},t) = \vec{E}_o = 0 \ , \tag{2.30}$$

$$\vec{B}(\vec{r},t) = \vec{B}_o = 0 \quad \text{(since net charges and currents are zero)}. \tag{2.31}$$

Note that relations (2.27) - (2.31) apply only to a volume of ionic fluid (i.e., the intracellular or extracellular spaces) and do not account for boundary effects or conditions inside of a cell membrane. Electroneutrality (equation (2.29)), applies only for distances on the order of (or greater than) the Debye shielding distance, R_m. (Electroneutrality is thus a macroscopic condition, see Tanenbaum [75].) Since R_m in a physiological system is small compared to the dimensions commonly found in such systems, condition (2.29) is easily satisfied in the problem under consideration. For example, $R_m \doteq 10$ Å for the dominant ion species in the interior or exterior of a neuron, while the thickness of a cell membrane (the smallest dimension in the system under study) is on the order of 100 Å. (This is discussed in greater detail in Plonsey [60], Chapter 3.)

The system is excited by either an external charge or current density, $\rho_s(\vec{r},t)$ and $\vec{J}_s(\vec{r},t)$ respectively. Subsequent to the stimulus, the system is perturbed from its resting state. These perturbed quantities in the system are described using a small signal analysis[1] as:

---

[1] Essentially a first term Taylor expansion about the resting condition.

$$C_i(\vec{r},t) = C_{io} + C_i'(\vec{r},t) \quad (\text{where } |C_i'| << C_{io}), \tag{2.32}$$

$$\vec{J}_i(\vec{r},t) = \vec{J}_{io} + \vec{J}_i'(\vec{r},t) = \vec{J}_i'(\vec{r},t) \quad (\text{by equation (2.28)}), \tag{2.33}$$

$$\vec{E}(\vec{r},t) = \vec{E}_o + \vec{E}'(\vec{r},t) = \vec{E}'(\vec{r},t) \quad (\text{by equation (2.30)}), \tag{2.34}$$

$$\vec{B}(\vec{r},t) = \vec{B}_o + \vec{B}'(\vec{r},t) = \vec{B}'(\vec{r},t) \quad (\text{by equation (2.31)}) \tag{2.35}$$

where the primed functions represent the deviations from the steady-state resting condition ("o") values. Note that the variation of the concentration of any ion species from its resting value is assumed small. It is emphasized that the condition (2.30), $\vec{E}_o = 0$, applies only in the intracellular and extracellular regions of a resting neuron. $\vec{E}_o \neq 0$ in the cell membrane, even in the resting state.

Applying the small signal expansions (2.32) - (2.35) to the equation set developed in Section 2.1.1 yields

$$z_i F \frac{\partial C_i'}{\partial t} + \nabla \cdot \vec{J}_i' = 0 , \tag{2.36}$$

$$\frac{\partial \vec{J}_i'}{\partial t} + \nu_i \vec{J}_i' = \frac{-z_i F\, kT}{m_i} \left(\nabla C_i' - \frac{z_i F}{RT} C_{io} \vec{E}'\right), \tag{2.37}$$

$$\nabla \cdot \vec{E}' = 1/\varepsilon \left[\rho_s + F \sum_i z_i C_i'\right] , \tag{2.38}$$

$$\nabla \times \vec{E}' = - \frac{\partial \vec{B}'}{\partial t} , \tag{2.39}$$

$$\nabla \times \vec{B}' = \mu_o [\vec{J}_s + \sum_i \vec{J}_i'] + \mu_o \varepsilon \frac{\partial \vec{E}'}{\partial t} , \tag{2.40}$$

$$\nabla \cdot \vec{B}' = 0 . \tag{2.41}$$

In equation (2.39), an "effective" collision frequency has been

defined as[1]:

$$\nu_i = \frac{|z_i|e}{m_i u_i} \quad (\text{sec})^{-1} . \tag{2.42}$$

ν_i represents the viscous interaction of ions with the H_2O molecules of the solvent. It is an "effective" collision frequency since ions in water are in a state of essentially continuous contact with the solvent (Tanenbaum [75] discusses collisions in a plasma, Kortum [45] gives conditions on ions in fluids). The second order term, $C_i'\vec{E}'$, has been dropped in equation (2.37), and the electroneutrality condition (2.29) has been applied in equation (2.38).

A wave equation for $C_i'(\vec{r},t)$ can be developed as follows. Taking the divergence of equation (2.37) gives

$$\frac{\partial}{\partial t}(\nabla \cdot \vec{J}_i') + \nu_i(\nabla \cdot \vec{J}_i') = \frac{-z_i F\ kT}{m_i}\left[\nabla^2 C_i' - \frac{z_i F}{RT} C_{io}(\nabla \cdot \vec{E}')\right] . \tag{2.43}$$

Applying the ion conservation relation (2.36) for $\nabla \cdot \vec{J}'$ and Maxwell equation (2.38) for $\nabla \cdot \vec{E}'$ leads to

$$\frac{z_i F\ kT}{m_i}\nabla^2 C_i' - z_i F\ \nu_i \frac{\partial C_i'}{\partial t} - z_i F \frac{\partial^2 C_i'}{\partial t^2} - \frac{k\ z_i^2 F^3}{m_i R\ \varepsilon} C_{io} \sum_j z_j C_j' = \frac{k z_i^2 F^2}{m_i R\ \varepsilon} C_{io}\ \rho_s . \tag{2.44}$$

Canceling the common $z_i F$ factor and defining two appropriate

---

[1] The electric mobility, u_i is assumed constant within the intracellular and extracellular volume conductors.

constants for the ith ion species (see Tanenbaum [75]) as

$$v_{it}^2 = \frac{k T_i}{m_i} = [\text{ion thermal velocity, (m/sec)}]^2 \tag{2.45}$$

$$\omega_{ip}^2 = \frac{kz_i^2F^2}{m_i R \varepsilon} C_{io} = \frac{z_i^2 e^2 n_{io}}{m_i \varepsilon} = [\text{ion resonance frequency, (sec)}^{-1}]^2 \tag{2.46}$$

then equation (2.44) becomes

$$[\nabla^2 - \frac{\nu_i}{v_{it}^2}\frac{\partial}{\partial t} - \frac{1}{v_{it}^2}\frac{\partial^2}{\partial t^2}]C_i' - \frac{\omega_{ip}^2}{z_i v_{it}^2}\sum_j z_j C_j' = \frac{\omega_{ip}^2}{z_i F v_{it}^2}\rho_s \ . \tag{2.47}$$

Each ion species in the multi-ion physiological fluid will satisfy an equation having the form of equation (2.47). These equations are a system of coupled wave equations for the concentration perturbations of the individual ion species. The solution of equation (2.47) is that of a damped wave, characterized by an electric field oriented in the direction of propagation (longitudinal ion-acoustic wave, Tanenbaum [75]). The propagation velocity will depend upon the coupling between ion species, but is roughly equal to the ion thermal velocity v_{it}.

An examination of the possible magnitudes for v_{it} encourages the notion that an ion-acoustic wave could be coupled to the action potential. Katz [40] gives typical values for the parameters involved as represented in Table (2.1).

Table (2.1)

Parameters for Ions in a Physiological Fluid

Ion	Valence (z_i)	Calculated Hydration Numbers	Absolute Mobility (u_i) in H_2O (μ/sec)/(volt/cm)	Atomic Weight (grams/mole)
Na^+	+1	4.5	5.2	23.00
K^+	+1	2.9	7.64	39.10
Cl^-	-1	2.9	7.91	35.46

To calculate the ion thermal velocity of an ion; the equivalent mass is needed. The equivalent mass of an ion is the mass of the ion itself augmented by the masses of the water molecules bound to the ion by hydration forces (see Lehninger [46], Katz [40]). Thus m_i for the three ions would be (atomic weight of H_2O = 18.02 grams/mole):

$$m_{Na^+} = (23.00 + 4.5 \times 18.02)/6.02 \times 10^{23} \left(\frac{\text{grams}}{\text{ion}}\right) \times 10^{-3} \left(\frac{\text{kg}}{\text{gram}}\right)$$

$$= 1.73 \times 10^{-25} \frac{\text{kg}}{\text{ion}} \qquad (2.48)$$

$$m_{K^+} = [(39.10 + 2.9 \times 18.02)/6.02 \times 10^{23}] \times 10^{-3} \frac{\text{kg}}{\text{ion}}$$

$$= 1.52 \times 10^{-25} \frac{\text{kg}}{\text{ion}} \qquad (2.49)$$

$$m_{Cl^-} = 1.46 \times 10^{-25} \frac{\text{kg}}{\text{ion}} \; . \qquad (2.50)$$

Using these calculated masses, the ion thermal velocities expected in the intracellular and extracellular regions would be (at T = 37°C; 310°K)

$$v^2_{Na^+} = \frac{310°K \times 1.38 \times 10^{-23} \text{ joules/°K-ion}}{1.73 \times 10^{-25} \text{ kg/ion}}$$

$$= 2.47 \times 10^4 \text{ m}^2/\text{sec}^2$$

$$v_{Na^+} = 1.57 \times 10^2 \text{ m/sec} \tag{2.51}$$

$$v_{K^+} = 1.68 \times 10^2 \text{ m/sec} \tag{2.52}$$

$$v_{Cl^-} = 1.71 \times 10^2 \text{ m/sec} \quad . \tag{2.53}$$

An order of magnitude of 100 m/sec is within the observed range of action potential propagation velocities[1] (see Stevens [74], Plonsey [60]).

The term $\frac{\nu_i}{v^2_{it}} \frac{\partial}{\partial t}$ in equation (2.47) represents losses due to collisions (this term's origin was the $\vec{P}_i$ term in equation (2.2)). Thus the solutions for C'_i can be expected to be in the form of damped waves, the losses coming from the ν_i term. If these waves are to be representative of the action potential in a neuron, this loss term must be canceled by some source ($\rho_s(\vec{r},t)$) as the action potential propagates without degeneration. This ρ_s would represent the experimentally observed ionic currents across the cell membrane, upon which the Hodgkin and Huxley model is based (Hodgkin and Huxley [34] - [37]). Identification of the nature of the source necessary to give an action potential waveform might arise from a solution of equation (2.47). Unfortunately,

---

[1] The term denoting propagation velocity used by physiologists is "conduction velocity", referring to the velocity at which a nerve 'conducts' an impulse. The range of observed conduction velocities is ~ 0.1 to 100 m/sec.

this does not appear to be the case, as some simple solutions of equation (2.47) indicate an ion-acoustic wave is unlikely as an explanation of the action potential.

To illustrate the above observation, consider the case of a single ion species "i" with $z_i = 1$ in an infinite, homogeneous, isotropic aqueous solution. As any spatial direction is equivalent, only one dimension will be considered (i.e., spatial variations along the x-axis). Thus ∇^2 reduces to $\frac{\partial^2}{\partial x^2}$ and the system of equations represented by equation (2.47) reduces to the single relation

$$[\frac{\partial^2}{\partial x^2} - \frac{\nu}{v_t^2}\frac{\partial}{\partial t} - \frac{1}{v_t^2}\frac{\partial^2}{\partial t^2} - \frac{\omega_p^2}{v_t^2}]C' = \frac{\omega_p^2}{Fv_t^2}\rho_s \quad [1] \quad . \tag{2.54}$$

This is an inhomogeneous Klein-Gordon wave equation for the perturbation $C'(\vec{r},t)$ of the concentration of the ions of species "i" (see Morse and Feshback [49]). In effect, the assumptions involved in using equation (2.54) to describe possible events in an axon are:

i) the intracellular region can be approximated by a one dimensional model,

ii) an ion-acoustic wave involving only a single ion species is excited, and

iii) membrane effects (boundary conditions) are ignored.

Consider an impulse stimulus of the form $\rho_s = a\delta(x)\delta(t)$ (i.e., a spike at $x = 0$ and $t = 0$). The source term of equation

---

[1] The i and j subscripts have been dropped as only one ion species is assumed involved.

(2.54) then becomes

$$\frac{\omega_p^2}{Fv_t^2}\rho_s(x,t) = \frac{\omega_p^2 a}{Fv_t^2}\delta(x)\delta(t)$$

$$= A\delta(x)\delta(t) \qquad (2.55)$$

where $A = \frac{\omega_p a}{Fv_t^2}$ = constant.

Also assume for now that, by some action at the membrane, the $\frac{\nu}{v_t^2}\frac{\partial}{\partial t}$ damping term is canceled so that the wave will propagate without losses[1]. For this simplified case, equation (2.54) reduces to

$$[\frac{\partial}{\partial x^2} - \frac{1}{v_t^2}\frac{\partial^2}{\partial t^2} - \frac{\omega_p^2}{v_t^2}]C' = A\delta(x)\delta(t) \ . \qquad (2.56)$$

To solve the partial differential equation (2.56), apply the Laplace transform on the time variable t as follows:

$$\mathcal{L}[C'(x,t)] = \overline{C}'(x,s) = \int_o^\infty C'(x,t)e^{-st}dt \qquad (2.57)$$

$$\mathcal{L}[A\delta(x)\delta(t)] = A\delta(x) \qquad (2.58)$$

$$\mathcal{L}[\frac{\partial^2}{\partial t^2}C'(x,t)] = s^2\overline{C}'(x,s) \ . \qquad (2.59)$$

Note that relation (2.59) assumes $C'(x,0) = \frac{\partial}{\partial t}C'(x,0) = 0$ (system at rest at $t = 0$). Applying the transform to equation (2.56) and using the relations (2.57) - (2.59) yields

---

[1] This might be due to an additional "traveling" source term at the membrane, maintained by an influx of N_a^+ ions and an efflux of K^+ ions. Strong experimental evidence shows this to be the case for action potential propagation (Katz [40], Plonsey [60]).

$$\left[\frac{\partial^2}{\partial x^2} - \frac{s^2}{v_t^2} - \frac{\omega_p^2}{v_t^2}\right]\bar{C}'(x,s) = A\delta(x) \quad . \tag{2.60}$$

Defining β^2 as

$$\beta^2 = \frac{s^2}{v_t^2} + \frac{\omega_p^2}{v_t^2} \tag{2.61}$$

yields

$$\left[\frac{\partial^2}{\partial x^2} - \beta^2\right]\bar{C}'(x,s) = A\delta(x) \quad . \tag{2.62}$$

Equation (2.62) has a general solution of the form

$$\bar{C}'(x,s) = K_1(s)e^{+\beta|x|} + K_2(s)e^{-\beta|x|} \tag{2.63}$$

where K_1 and K_2 are to be determined by matching to the source term and boundary conditions. As solutions must be finite for all space and β is a positive constant (for fixed s), $K_1 = 0$ is determined by considering $x \to \infty$. Substituting solution (2.63) back into equation (2.62) gives $K_2 = \frac{A}{2\beta}$ such that

$$\begin{aligned}\bar{C}'(x,s) &= \frac{A}{2\beta}\, e^{-\beta|x|} \\ &= \frac{A\, v_t}{2\sqrt{s^2 + \omega_p^2}}\, e^{-\sqrt{s^2 + \omega_p^2}\,|x|/v_t} \quad .\end{aligned} \tag{2.64}$$

By use of a table of Laplace transforms[1], the time dependent solution of equation (2.56) is obtained as

---

[1] See Churchill [7], a good reference for solutions of differential equations using a wide variety of transform techniques.

$$C'(x,t) = A \frac{v_t}{2} U(t - x/v_t) J_o(\omega_p \sqrt{t^2 - (x/v_t)^2}). \qquad (2.65)$$

This solution holds for $x \geq 0$; where $U(\cdot)$ is the unit step function, and $J_o(\cdot)$ is the zero order Bessel function of the first kind.

The solution (2.65) has the nature of an event that moves in the $+x$ direction with time, as seen in Figure 2.1. It is noted that the leading edge of the "wave"[1] propagates at a velocity of v_t (this is a result of the unit step function, $U(t - x/v_t)$). The "waveform" undergoes a marked distortion as it travels, as is seen by comparing Figure 2.1(a) and (b). This is a result of the $\sqrt{t^2 - (x/v_t)^2}$ argument of the Bessel function introducing a non-linearity into the linked time and space dependences. Figure 2.1(c) is a graph of solution (2.65) versus time, the more traditional method of plotting active events of an axon. The solution shown in this form bears some resemblance to the waveform of an action potential, and since field quantities (such as potential) reflect the nature of their sources (C' in this case), the solution appears encouraging.

The shortcoming of this approach is evident when the damping term is included. This is seen in the case of a myelinated axon Many of the axons in mammalian nervous systems have a periodically interrupted insulating covering referred to as the myelin sheath. This myelin sheath is formed by neuroglial cells (Schwann cells in

---

[1] A propagating wave has a time and space dependence linked in the form of $(t - x/v)$. Solution (2.65) is not in the form of a true wave as this is not the case for the argument of J_o.

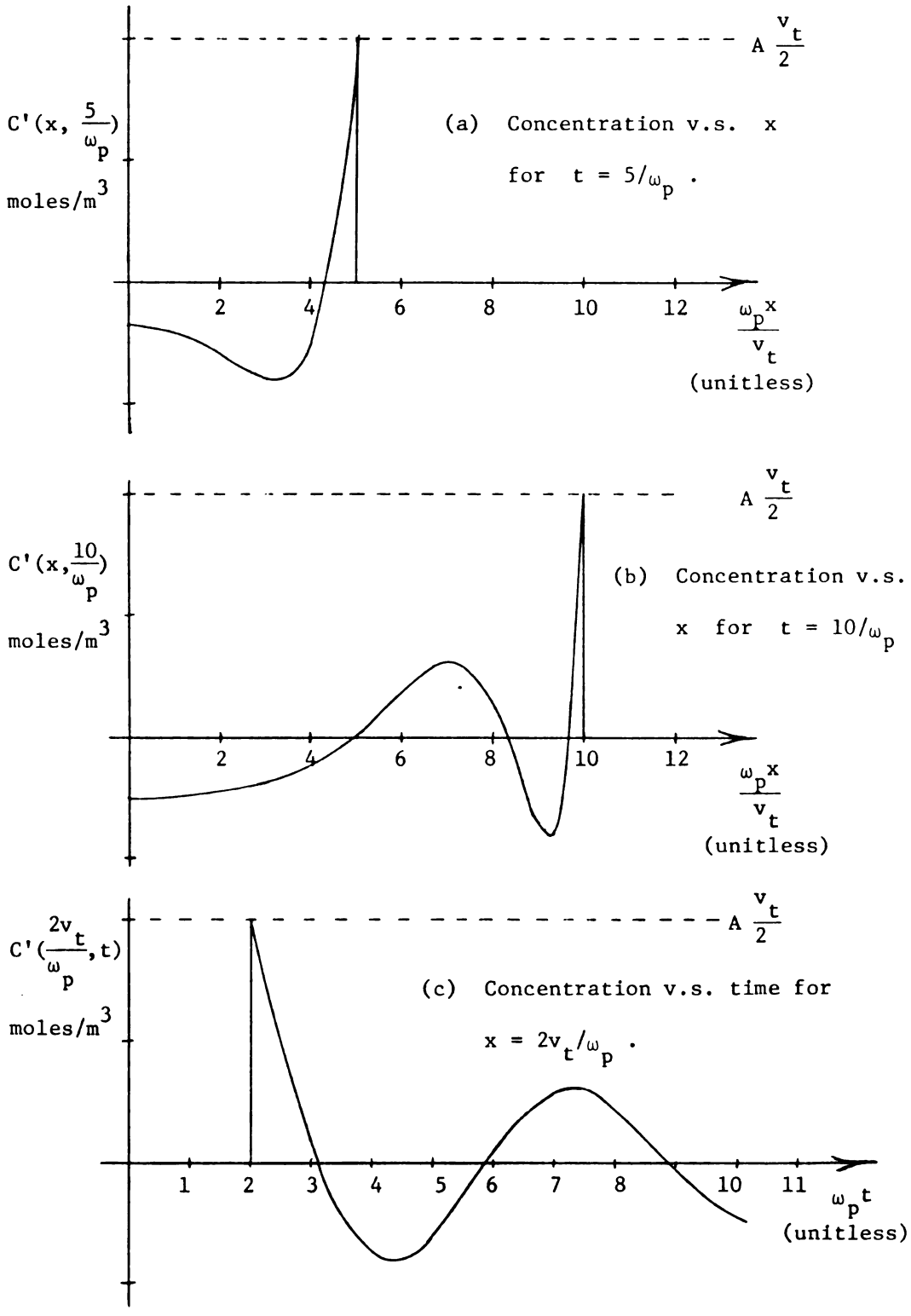

FIGURE 2.1

Concentration "Wave" Solution from Equation (2.65)

the peripheral nerves) tightly wrapping several layers of their membrane around the axon. The covering is interrupted at approximately 1 mm intervals, forming gaps known as the nodes of Ranvier (see Figure 2.2). The myelin effectively blocks the flow of source currents through the membrane, allowing the action potential to be generated only at the nodes. Between nodes, a passive spread of potential occurs. Nerve impulse conduction in a myelinated axon is said to be saltatory; the action potential "jumping" from one node to the next. A conduction "jump" is possible from node A to node B (Figure 2.2) only if the passive spread of potential from the impulse at node A is above the threshold for generation of a new action potential when it reaches B.[1]

For a myelinated axon, there cannot be any source term (ρ_s) from the membrane, to cancel the effects of the damping term in regions where currents through the membrane are blocked by the myelin sheath. If an ion-acoustic wave is to propagate in such a situation, it would have to travel from one node to the next with a small enough attenuation (from the damping term) to allow an above threshold depolarization of the neuronal membrane at the latter node[2]. To consider this situation, equation (2.54) must be solved with the damping term present.

---

1 References for the physiology of myelinated axons and saltatory conduction include Eccles [17] and [19], Ganong [27], Katz [40], Ochs [54], Ruch and Patton [70], and Stevens [74].

2 An above threshold transmembrane potential will allow the action potential to be regenerated at that point.

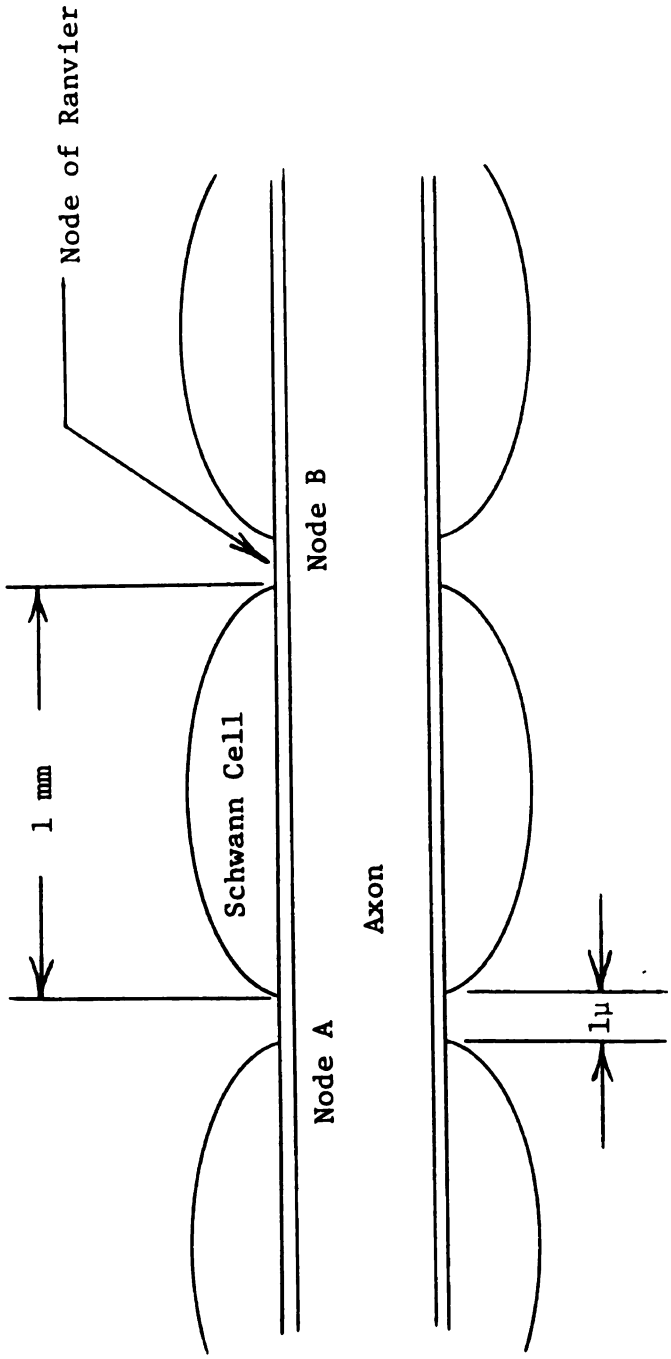

FIGURE 2.2

Myelinated Axon

Proceeding as before, the Laplace transform on time of wave equation (2.54) with the source as given in expression (2.55) yields

$$[\frac{\partial^2}{\partial x^2} - \frac{s^2}{v_t^2} - \frac{\nu s}{v_t^2} - \frac{\omega_p^2}{v_t^2}]\bar{C}'(x,s) = A\delta(x) \quad . \tag{2.66}$$

Defining β^2 as

$$\beta^2 = \frac{1}{v_t^2}[s^2 + \nu s + \omega_p^2] \tag{2.67}$$

results in equation (2.66) having the same form as equation (2.62). The solution (2.64) thus applies to this case, with β as redefined in relation (2.67). This gives the solution of equation (2.66) as

$$\bar{C}'(x,s) = \frac{A\, v_t}{2\sqrt{s^2 + \nu s + \omega_p^2}}\, e^{-\sqrt{s^2 + \nu s + \omega_p^2}\,|x|/v_t} \quad . \tag{2.68}$$

The inversion of transform domain solution (2.68) back to the time domain is performed using the change of variable of $\check{s}$ where

$$\check{s} = s + \frac{\nu}{2} \quad \Rightarrow \quad s = \check{s} - \frac{\nu}{2} \tag{2.69}$$

giving

$$(\check{s})^2 = s^2 + s\nu + \frac{\nu^2}{4} \quad \Rightarrow \quad s^2 + \nu s = (\check{s})^2 - \frac{\nu^2}{4} \quad . \tag{2.70}$$

Then $\bar{C}'(x,\check{s})$ is

$$\bar{C}'(x,\check{s}) = \frac{A\, v_t}{2\sqrt{(\check{s})^2 + (\omega_p^2 - \nu^2/4)}}\, e^{-\sqrt{(\check{s})^2 + \omega_p^2 - \nu^2/4}\,|x|/v_t} \quad . \tag{2.71}$$

The inverse is then found (by definition, see Churchill [7]) as

$$C'(x,t) = \frac{1}{2\pi j}\int_{\gamma-j\infty}^{\gamma+j\infty} \bar{C}'(x,s)e^{ts}ds$$

$$= \frac{1}{2\pi j}\int_{\gamma+\nu/2-j\infty}^{\gamma+\nu/2+j\infty} \bar{C}'(x,\check{s})e^{t(\check{s}-\nu/2)}d\check{s}$$

$$= e^{-\nu t/2}\left[\frac{1}{2\pi j}\int_{\tilde{\gamma}-j\infty}^{\tilde{\gamma}+j\infty} \bar{C}'(x,\check{s})e^{t\check{s}}d\check{s}\right] \quad . \tag{2.72}$$

Since the integral in relation (2.72) is now the same as that defining the inverse Laplace transform of the previous solution (2.64), but with ω_p^2 replaced by the constant $(\omega_p^2 - \nu^2/4)$, the solution for this case is

$$C'(x,t) = e^{-\nu t/2}\left[\frac{Av_t}{2}\, U(t - \frac{x}{v_t})J_o\left(\sqrt{(\omega_p^2 - \frac{\nu^2}{4})[t^2 - (x/v_t)^2]}\right)\right] \quad . \tag{2.73}$$

The inversion assumes that the factor $(\omega_p^2 - \nu^2/4)$ is a positive number. For the case where $(\omega_p^2 - \nu^2/4)$ is negative, the Bessel function $J_o(\cdot)$ becomes the modified Bessel function $I_o(\cdot)$ (see Churchill [7]). Calculation of ω_p and ν for representative parameters for ions in a typical neuron will indicate which form is appropriate. From Katz [40], the concentration of K^+ ions in the intracellular space of a squid axon is 400 m Moles/liter. With this concentration, the effective mass of K^+ ions as given in equation (2.49), the mobility of K^+ ions from Table 2.1, and $\varepsilon = 80\varepsilon_0$ (for H_20); ω_p and ν for potassium ions are then calculated as follows:

$$\nu_{K^+} = \frac{|z_{K^+}|e}{m_{K^+} u_{K^+}} \qquad \text{(from definition (2.42))}$$

$$= \frac{1.6 \times 10^{-19} \text{ coulombs/ion}}{(1.52 \times 10^{-25} \text{ kg/ion})(7.64 \ \mu\text{/sec/volt/cm})}$$

$$(\mu\text{/sec/volt/cm}) = 10^{-8} \text{ m}^2\text{/volt-sec}$$

$$\frac{\text{coulombs}}{\text{kg}} \times \frac{\text{volt-sec}}{\text{m}^2} = \frac{1}{\text{sec}}$$

$$\nu_{K^+} = 1.38 \times 10^{13} \text{ sec}^{-1} \tag{2.74}$$

$$\omega^2_{K^+p} = \frac{k z^2_{K^+} F^2}{m_{K^+} R \varepsilon} C_{K^+o} \qquad \text{(from definition (2.46))}$$

$$\omega^2_{K^+p} = \frac{(1.38\times10^{-23} \text{ joules/°K})(9.65\times10^{4} \text{ coulombs/mole})^2 (400 \ \frac{\text{m moles}}{\text{liter}})}{(1.52\times10^{-25} \text{ kg/ion})(8.31 \text{ joules/mole °K})(80\times8.85\times10^{-12} \ \frac{\text{farad}}{\text{m}})}$$

$$\text{m Moles/liter} = \text{Moles/m}^3$$

$$\omega^2_{K^+p} = 5.75 \times 10^{22} \text{ sec}^{-2} \tag{2.75}$$

$$\omega_{K^+p} = 2.40 \times 10^{11} \text{ sec}^{-1} . \tag{2.76}$$

The determining factor for this case is then

$$\omega^2_{K^+p} - \frac{\nu^2_{K^+}}{4} = (5.75 \times 10^{22} - 4.76 \times 10^{25}) \text{sec}^{-2} \doteq -4.76 \times 10^{25} .$$

Since the result is negative, the correct functional form is $I_o(\cdot)$ in solution (2.73). The factor $(\omega_p^2 - \nu^2/4)$ is again negative for K^+ ions in the extracellular region; and for Na^+

and Cl^- ions in both the intracellular and extracellular regions (using values for parameters from Katz [40]). Thus, for all ion species, the waveform changes from that in Figure (2.1) to an attenuated cut-off form in the presence of the damping term. This attenuation, due to viscous collisions, occurs very quickly in both time and space. Time domain damping is evident in solution (2.73) in the $\exp[-\nu t/2]$ factor. The time constant (τ) for an e^{-1} drop is apparent as

$$\tau = 2/\nu \ . \tag{2.77}$$

Using the collision frequency for K^+ ions calculated in equation (2.74), this becomes

$$\begin{aligned} \tau &= 2/(1.38 \times 10^{13}) \text{ sec} \\ &= 1.45 \times 10^{-13} \text{ sec} \ . \end{aligned} \tag{2.78}$$

As K^+ ions exhibit an ion-acoustic wave propagation velocity on the order of $v_{K^+} = 1.68 \times 10^2$ m/sec (relation (2.52)), the distance (λ) traversed by such a disturbance before an e^{-1} decay in magnitude is just

$$\begin{aligned} \lambda &= \tau \, v_{K^+} \\ &= 1.45 \times 10^{-13} \times 168 \text{ m} \\ &= 2.44 \times 10^{-11} \text{ m} \\ &= 0.244 \text{ Å} \ . \end{aligned} \tag{2.79}$$

This result is significant, as a propagation distance of less than a quarter angstrom is far too small to suppose that the

concentration wave could travel in any fashion between nodes (about 1 mm) in a myelinated axon.

The development described above was for an impulse stimulus. It may be argued that the action potential as a finite-time event would display a different effect. This does not appear to be the case. A solution of equation (2.54) with a step function stimulus in time, located at one point $x = 0$ reveals little change in result (2.79). In this case[1], the source term is

$$\frac{\omega_p^2}{Fv_t^2}\rho_s(x,t) = A\delta(x)\,U(t)\ , \tag{2.80}$$

where $U(t)$ is a unit step in time, initiated at $t = 0$. The Laplace transform on the time variable of the wave equation with dissipation is then

$$[\frac{\partial^2}{\partial x^2} - \frac{s^2}{v_t^2} - \frac{\nu s}{v_t^2} - \frac{\omega_p^2}{v_t^2}]\bar{C}'(x,s) = \frac{A}{s}\,\delta(x)\ . \tag{2.81}$$

With β^2 defined as in equation (2.67), the wave equation becomes

$$[\frac{\partial^2}{\partial x^2} - \beta^2]\bar{C}'(x,s) = \frac{A}{s}\,\delta(x)\quad . \tag{2.82}$$

The solution of equation (2.82) is the same as in result (2.68), with the exception of $A \to A/s$:

---

[1] A step function in time was chosen as being the opposite extreme from an infinitely brief pulse. The solution will indicate the extent of the stimulus' effect in the steady state.

$$\bar{C}'(x,s) = \frac{A\, v_t}{2s\sqrt{s^2 + \nu s + \omega_p^2}}\, e^{-\sqrt{s^2 + \nu s + \omega_p^2}\,|x|/v_t} . \qquad (2.83)$$

It is not necessary to invert transform domain solution (2.83), as the behavior in the steady state (at $t \to \infty$) can be obtained via the final-value theorem for Laplace transforms (see Churchill [7]). This theorem states that

$$\lim_{t\to\infty} F(t) = \lim_{s\to 0} s\, f(s) \qquad (2.84)$$

where $f(s) = \mathcal{L}\{F(t)\}$.

Applying theorem (2.84) to the solution (2.83) yields

$$C'(x,\ t \to \infty) = \frac{A\, v_t}{2\,\omega_p}\, e^{-\omega_p |x|/v_t} . \qquad (2.85)$$

For this case, there is a space constant (λ) for an e^{-1} decay of the solution from its value at $x = 0$ of

$$\lambda = v_t/\omega_p . \qquad (2.86)$$

For K^+ ions, using the values for v_{K^+} and ω_{K^+p} previously calculated, this length constant is

$$\lambda = \frac{168 \text{ m/sec}}{2.4 \times 10^{11} \text{ 1/sec}} = 7.0 \times 10^{-10} \text{ m}$$

$$= 7.0 \text{ Å} . \qquad (2.87)$$

This length remains far too small for any effect at one node to reach a subsequent node in a myelinated axon. For any signficant ion species, the result remains essentially the same over the range of parameters typical for a squid axon.

The conclusion that can be drawn from these simple solutions is that there is little likelihood that the excitation of an ion-acoustic wave is the basis for action potential conduction. The results of this section can be summarized by the observation that the collisions in the system vastly overwhelm relaxation effects. The collision frequencies are on the order of 10^{13} per second, giving time constants for the response to field changes on the order of 10^{-13} seconds. Since this study uses a macroscopic approach to model phenomena that have time constants on the order of 10^{-4} seconds (Plonsey [60]), the effects considered in this section due to ion-acoustic waves being excited in a plasma are insignificant. This allows further simplification of the basic equations describing the system.

2.1.3. Reduction of Basic Equations to Quasi-Static Form

The coupled wave equations (2.47) of the last section were derived from the momentum transfer equation (2.14). The propagation term $(\partial^2/\partial t^2)$ had its origins in the $\frac{\partial}{\partial t}\vec{J}_i$ term of transport equation (2.14); the damping term $(\frac{\partial}{\partial t})$ arose from the $\frac{|z_i|e}{m_i u_i}\vec{J}_i$ term. The previous section demonstrated that the loss term far exceeds the term for propagation effects. In terms of equation (2.14), this indicates the $\frac{\partial}{\partial t}\vec{J}_i$ term is negligible with respect to $\frac{|z_i|e}{m_i u_i}\vec{J}_i$.

The conclusion above is strengthened by considering these terms directly. For K^+ ions, the collision term is

$$\frac{|z_{K^+}|e}{m_{K^+}u_{K^+}}\vec{J}_{K^+} = \nu_{K^+}\vec{J}_{K^+} = 1.38 \times 10^{13}\vec{J}_{K^+} \quad \text{sec}^{-1} \tag{2.88}$$

using result (2.74). The ionic current would thus have to possess a time rate of change on the order of 10^{13} sec^{-1} for the propagation term to compare with the collision term. The highest observed frequency component in the system is the rising phase of the action potential, on the order of 10^4 sec^{-1} (from Plonsey [60]). It is apparent that the time derivative term in equation (2.14) can be dropped, simplifying the transport equation to

$$\vec{J}_i(\vec{r},t) = \frac{-z_i u_i RT}{|z_i|}\left[\nabla C_i(\vec{r},t) - \frac{z_i F\, C_i(\vec{r},t)}{RT}\vec{E}(\vec{r},t)\right] . \tag{2.89}$$

Equation (2.89) is the well known Nernst-Planck equation, widely used in electrophysiology (see Plonsey [60]). It relates

current flow in an aqueous solution of ions to two effects: diffusion due to concentration gradients (∇C_i) and drift due to electric field (electric potential gradients). It is emphasized that this current results from a physical motion of ions and does not contain any polarization (displacement) current effects.

The system of equations developed in Section 2.1.1 can be further simplified by an appropriate quasi-static approximation[1]. In general, a conductor is described by a conductivity, σ(mhos/m), and a dielectric permittivity, ε(farads/m). The total current density in the conductor is due to both conduction ($\sigma \vec{E}$) and displacement ($\varepsilon \frac{\partial \vec{E}}{\partial t}$) currents. In the case of biological media, the displacement current is small compared to the conduction current, for frequencies up to 10 KHz. This is expressed in the Fourier transform frequency domain as $\frac{\omega\varepsilon}{\sigma} << 1$. Currents maintained by electric fields will therefore be considered the result of conduction only, and the biological media will be considered purely resistive. In this situation, the total current due to an electric field is

$$\vec{J}(\vec{r},t) = \sigma(\vec{r},t)\ \vec{E}(\vec{r},t)\ . \tag{2.90}$$

By comparison with equation (2.89), the conductivity of any ion species is then given as

$$\sigma_i(\vec{r},t) = |z_i| F\ u_i(\vec{r}) C_i(\vec{r},t) \tag{2.91}$$

---

[1] This formulation is widely used in electrophysiology. Plonsey [60] or Plonsey and Heppner [61] contains an expanded development of the details.

with the total conductivity for the medium being the sum over all charge carriers in the system:

$$\sigma(\vec{r},t) = \sum_i \sigma_i(\vec{r},t) = \sum_i |z_i| F u_i(\vec{r}) C_i(\vec{r},t) \quad . \tag{2.92}$$

This approximation neglects capacitive effects within the volume conductor. Thus any capacitance seen in the system will be due to the dielectric discontinuity at the boundary between two regions of different permittivity.

A further consequence of the quasi-static approximation is to neglect the induction component of the electric field. The relationships between the electromagnetic potential functions ($\phi(\vec{r},t)$ and $\vec{A}(\vec{r},t)$) and the electric and magnetic fields are:

$$\vec{B}(\vec{r},t) = \nabla \times \vec{A}(\vec{r},t) \tag{2.93}$$

$$\vec{E}(\vec{r},t) = -\nabla\phi(\vec{r},t) - \frac{\partial \vec{A}(\vec{r},t)}{\partial t} \quad . \tag{2.94}$$

At the frequencies observed in naturally occurring bioelectric phenomena, $|\omega\vec{A}| << |\nabla\phi|$ for typical biological media, sources, and distances (see Plonsey [60]). Accordingly, the induction component of $\vec{E}$ (due to $\frac{\partial}{\partial t}\vec{A}$) may be dropped, leaving expression (2.94) as

$$\vec{E}(\vec{r},t) = -\nabla\phi(\vec{r},t) \quad . \tag{2.95}$$

Since the magnetic field does not appear in the continuity equation or the Nernst-Planck equation, and the vector potential will not be used to calculate $\vec{E}$, both $\vec{A}$ and $\vec{B}$ need not be considered further for problems involving natural bioelectric events.

With the quasi-static approximation, the basic system of equations may be summarized as:

$$z_i F \frac{\partial C_i(\vec{r},t)}{\partial t} + \nabla \cdot \vec{J}_i(\vec{r},t) = 0 \tag{2.96}$$

$$\vec{J}_i(\vec{r},t) = \frac{-z_i u_i(\vec{r}) RT}{|z_i|} \nabla C_i(\vec{r},t) + \sigma_i(\vec{r},t)\vec{E}(\vec{r},t) \tag{2.97}$$

$$\sigma_i(\vec{r},t) = |z_i| F\, u_i(\vec{r}) C_i(\vec{r},t) \tag{2.98}$$

$$\nabla \cdot \vec{E}(\vec{r},t) = 1/\varepsilon [\rho_s(\vec{r},t) + F \sum_i z_i C_i(\vec{r},t)] \tag{2.99}$$

$$\vec{E}(\vec{r},t) = -\nabla\Phi(\vec{r},t) \ . \tag{2.100}$$

The electric field described by the above set of equations is irrotational such that $\nabla \times \vec{E} = 0$ (see King [41]). The aqueous ion transport (plasma) development of Section 2.1.2 could have been carried out using the quasi-static approximation, since the $\vec{E}$ field of an ion-acoustic wave satisfies $\nabla \times \vec{E} = 0$ (see Tanenbaum [75]). The system of equations (2.96) - (2.100) will be used as the basic set of equations for the remainder of this study.

A somewhat useful definition can be applied in connection with equation (2.97). The current due to concentration gradients can be considered as that maintained by an "impressed" electric field[1]. With this definition equation (2.97) can be written as

$$\vec{J}_i(\vec{r},t) = \sigma_i(\vec{r},t)(\vec{E}(\vec{r},t) + \vec{E}_i^e(\vec{r},t)) \tag{2.101}$$

---

[1] This follows the technique used to handle effective fields, such as seen in representing the chemical forces in a common battery. See King [41].

where the impressed electric field $\vec{E}_i^e$ is defined as

$$\vec{E}_i^e = \frac{-RT}{z_i F} \frac{\nabla C_i(\vec{r},t)}{C_i(\vec{r},t)} \quad . \tag{2.102}$$

The impressed field $\vec{E}_i^e$ is maintained by ionic concentration gradients, and can be expressed as the gradient of an equivalent concentration potential (the Nernst potential). This will be demonstrated in Section 2.2.2. The field $\vec{E}$ in equation (2.101) is the coulomb electric field maintained by charges in the system, and is expressed as the gradient of the electric scalar potential (equation (2.100)). Thus the electric field $\vec{E}$ will henceforth be referred to as the coulomb field. Equation (2.101) will be useful in developing an equivalent circuit for a biological membrane (Section 2.2.2).

2.2. Boundary Conditions for Bioelectric Fields and Potentials

2.2.1. Boundary Conditions at an Interface Surface

The equations developed in Section 2.1 apply only at interior points in a volume region of a biological medium. Any useful problem will involve two or more volume conductor regions separated by interface surfaces. Boundary conditions that relate field quantities across these interfaces must be developed. The relations obtained in this section will apply to this situation. Along with equations (2.96) - (2.100), they form the complete system of equations necessary to solve a large class of bioelectric field problems.

With the geometry as shown in Figure 2.3, the boundary conditions that apply to a general EM field problem are:

$$\hat{t} \cdot (\vec{E}_2(\vec{r},t) - \vec{E}_1(\vec{r},t)) = 0 \tag{2.103}$$

$$\hat{n} \cdot (\vec{J}_2(\vec{r},t) - \vec{J}_1(\vec{r},t)) = - \frac{\partial \eta(\vec{r},t)}{\partial t} \tag{2.104}$$

$$\hat{n} \cdot (\varepsilon_2 \vec{E}_2(\vec{r},t) - \varepsilon_1 \vec{E}_1(\vec{r},t)) = \eta(\vec{r},t) \tag{2.105}$$

where all quantities are evaluated at the boundary surface, and

$\eta(\vec{r},t)$ = surface charge on the interface (coulombs/m^2);

$\hat{t}$ = unit vector tangential to the boundary surface;

$\hat{n}$ = unit vector normal to the boundary surface, with direction defined as from region (1) into region (2).

Boundary condition (2.103) is derived from Maxwell equation (2.16) (for $\nabla \times \vec{E}$) via Stoke's theorem applied on a differentially small closed contour traversing both regions. In a similar manner,

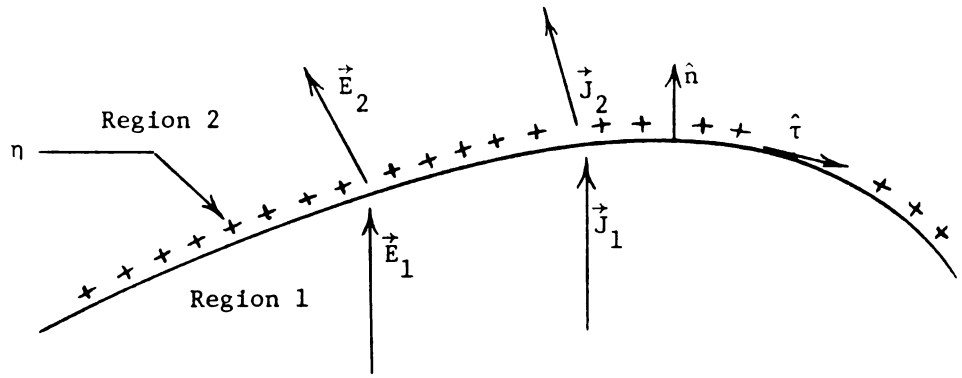

FIGURE 2.3

Geometry for General Boundary Conditions

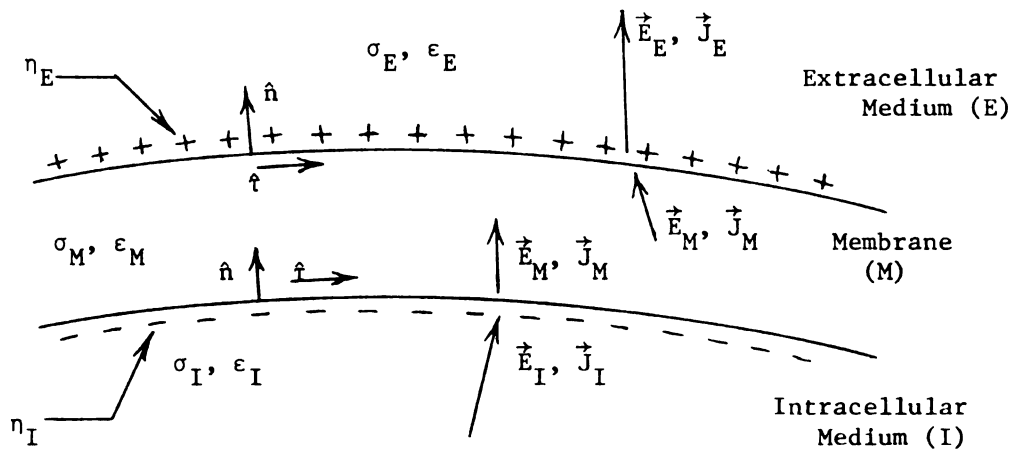

FIGURE 2.4

Geometry for Boundary Conditions at Cell Membrane Interfaces

boundary conditions (2.104) and (2.105) are obtained from the divergence of Maxwell equation (2.17) (for $\nabla \times \vec{B}$) and the continuity equation (2.26) by applying the divergence theorem to a small pillbox bisected by the interface. It is noted that these boundary conditions apply to any general EM field problem as they are derived from Maxwell's equations with no assumptions[1].

An alternate form of boundary condition (2.103) is given by King [41] as

$$\Phi_2(\vec{r},t) - \Phi_1(\vec{r},t) = 0 \ . \tag{2.106}$$

This condition states that the scalar potential for electric field is continuous across the boundary, and it holds only if a surface density of polarization (dipole layer of charge) is not present. So long as a single interface between two regions is considered, this problem will not arise (see King [41], Chapter 3). For the case in Section 2.2.2 where the cell membrane is taken to be infinitely thin, boundary condition (2.106) will not apply as the internal and external surface charge densities on the membrane will then represent a surface density of polarization[2].

---

[1] Details of the derivations may be found in any basic electromagnetics text. Two such references are King [41] and Ramo, Whinnery, and Van Duzer [67]. These boundary conditions are applicable to the quasi-static approximation with no alterations.

[2] In this case there will be a finite jump in potential across the (infinitely thin) membrane, i.e. the transmembrane potential. The cell membrane is perhaps the closest approximation known of a surface density of polarization.

From equations (2.104) and (2.105) it is clear that the normal component of current crossing a boundary will be discontinuous only with time-dependent changes in the surface charge density. This charge density is related to any discontinuity of normal electric displacement $(\vec{D} = \varepsilon\vec{E})$ at the interface. Note that the normal component of $\vec{E}$ can have a large discontinuity even in the absence of surface charge if $\varepsilon_1 \neq \varepsilon_2$.

Now consider the application of these boundary conditions to membrane interfaces existing in a general biological cell. The appropriate geometry is illustrated in Figure 2.4. The surface charges shown in the figure reflect the nature of observed surface charges in resting neurons (see Plonsey [60]), but in the following development they will be handled in a general fashion and their sign and magnitude determined by the fields and currents associated with them. At the interface separating the intracellular space and the membrane, equations (2.104) - (2.106) become[1]

$$\Phi_M = \Phi_I \tag{2.107}$$

$$\hat{n} \cdot (\vec{J}_M - \vec{J}_I) = - \frac{\partial \eta_I}{\partial t} \tag{2.108}$$

$$\hat{n} \cdot (\varepsilon_M \vec{E}_M - \varepsilon_I \vec{E}_I) = \eta_I \ . \tag{2.109}$$

Likewise at the membrane-extracellular spaces interface, the boundary conditions are

---

[1] The boundary condition (2.106) for continuity of scalar potential will be used rather than its alternate form, relation (2.103) for the continuity of tangential $\vec{E}$ field. This proves to be more convenient for most bioelectric field solutions.

$$\Phi_E = \Phi_M \tag{2.110}$$

$$\hat{n} \cdot (\vec{J}_E - \vec{J}_M) = - \frac{\partial \eta_E}{\partial t} \tag{2.111}$$

$$\hat{n} \cdot (\epsilon_E \vec{E}_E - \epsilon_M \vec{E}_M) = \eta_E \ . \tag{2.112}$$

Equations (2.109) and (2.112) may be combined with relations (2.108) and (2.111) to eliminate the surface charge densities as

$$\hat{n} \cdot (\vec{J}_M - \vec{J}_I) = \hat{n} \cdot [\frac{\partial}{\partial t} (\epsilon_I \vec{E}_I - \epsilon_M \vec{E}_M)] \tag{2.113}$$

$$\hat{n} \cdot (\vec{J}_E - \vec{J}_M) = \hat{n} \cdot [\frac{\partial}{\partial t} (\epsilon_M \vec{E}_M - \epsilon_E \vec{E}_E)] \ . \tag{2.114}$$

The boundary conditions (2.113) and (2.114) may be expanded by considering the current density in each region. By the results of Section 2.1.2, a perturbation in $C_i(\vec{r},t)$ for any ion species will decay to the steady-state concentration with space constants on the order of angstroms, and time constants on the order of 10^{-13} seconds[1]. For a macroscopic investigation of bulk phenomena with frequency spectra below 10 KHz, any perturbation in $C_i(\vec{r},t)$ from steady-state levels can thus be ignored to a very good approximation. With this assumption, the ∇C_i term in the Nernst-Planck equation (2.97) vanishes in the intracellular and extracellular spaces. The total current densities in those media then become

$$\vec{J}_I(\vec{r},t) = \sum_i \vec{J}_{Ii}(\vec{r},t) = \sum_i \sigma_{Ii} \vec{E}_I(\vec{r},t) = \sigma_I \vec{E}_I(\vec{r},t) \tag{2.115}$$

---

[1] This result is also stated in Kortum [45].

$$\vec{J}_E(\vec{r},t) = \sum_i \vec{J}_{Ei}(\vec{r},t) = \sum_i \sigma_{Ei}\vec{E}_E(\vec{r},t) = \sigma_E\vec{E}_E(\vec{r},t) \qquad (2.116)$$

where the sum is over all significant ion species "i" and $\vec{E}$ is the coulomb field. Note that the conductivities (defined in expressions (2.91) and (2.92)) are now taken to be constant, in keeping with the assumption of $\nabla C_i = 0$ in these regions (and the previous assumption applied in Section 2.1.3 that time changes in C_i are insignificant: $\frac{\partial}{\partial t} C_i \doteq 0$). The current densities in these media are thus considered totally resistive; driven by electric fields only and characterized by a conductivity which is the sum of the individual conductivities contributed by each ion species (charge carrier).

The current density in the cell membrane requires a different treatment. As above, perturbations from the steady-state resting condition will be considered negligible, following the conclusions of Sections 2.1.2 and 2.1.3. However, even in the resting state, ∇C_i is non-zero in the membrane. With the condition on ion species "i" that $C_{Ii} \neq C_{Ei}$ (resting state concentrations, now assumed to be constants over these regions), there will exist a concentration gradient across the cell membrane. If the membrane conductivity for each such ion species is non-zero, C_{Mi} will be a continuous function of space inside the membrane. Furthermore, if σ_{Mi} is a function of time or position[1], C_{Mi} will also vary with time or position. Thus current flow in the membrane is characterized as

---

[1] The word 'position' is used here in the sense of a location along the cell's surface and not in the sense of a space variable normal to the membrane. For a cylindrical cell centered on the z axis of cylindrical polar coordinates, this would refer to a variation in z or ϕ, but not in r (the radial coordinate).

$$\vec{J}_M(\vec{r},t) = \sum_i \vec{J}_{Mi}(\vec{r},t)$$

$$= \sum_i \left[\frac{-z_i u_i(\vec{r})RT}{|z_i|} \nabla C_{Mi}(\vec{r},t) + \sigma_{Mi}(\vec{r},t)\vec{E}_M(\vec{r},t)\right] . \qquad (2.117)$$

With definitions (2.115) - (2.117), the boundary conditions (2.113) and (2.114) become

$$\hat{n} \cdot \left[\sum_i \left(\frac{-z_i u_i RT}{|z_i|} \nabla C_{Mi} + \sigma_{Mi}\vec{E}_M\right) + \varepsilon_M \frac{\partial}{\partial t}\vec{E}_M - \sigma_I \vec{E}_I - \varepsilon_I \frac{\partial}{\partial t}\vec{E}_I\right] = 0 \qquad (2.118)$$

$$\hat{n} \cdot \left[\sigma_E \vec{E}_E + \varepsilon_E \frac{\partial}{\partial t}\vec{E}_E - \sum_i \left(\frac{-z_i u_i RT}{|z_i|} \nabla C_{Mi} + \sigma_{Mi}\vec{E}_M\right) - \varepsilon_M \frac{\partial}{\partial t}\vec{E}_M\right] = 0 \qquad (2.119)$$

The functional dependence of the concentrations may be summarized with

$$C_{Ii}(\vec{r},t) \doteq C_{Ii} = \text{(constant)} \qquad (2.120)$$

$$C_{Ei}(\vec{r},t) \doteq C_{Ei} = \text{(constant)} \qquad (2.121)$$

$$C_{Mi}(\vec{r},t) = \text{space and time dependent}^1 . \qquad (2.122)$$

In terms of the impressed field quantities defined in Section 2.1.3, the membrane current is given by

$$\vec{J}_M(\vec{r},t) = \sum_i \sigma_{Mi}(\vec{r},t)[\vec{E}_M(\vec{r},t) + \vec{E}^e_{Mi}(\vec{r},t)] \qquad (2.123)$$

---

[1] Implicit in assumptions (2.120) and (2.121) is the hypothesis that ion movements across the membrane (in the form of ionic currents) do not occur in sufficient magnitude to disturb the steady state concentration profiles. Katz [40] indicates this to be an appropriate assumption even in the case of an action potential.

where

$$\vec{E}^{e}_{Mi} = - \frac{RT}{z_i F} \frac{\nabla C_{Mi}(\vec{r},t)}{C_{Mi}(\vec{r},t)} \quad . \tag{2.124}$$

$\vec{E}^{e}_{Mi}$ is the impressed (equivalent) electric field maintained by the concentration gradient of the ith ion species. With this definition, the boundary conditions (2.118) and (2.119) are rewritten as

$$\hat{n} \cdot [\sum_i \sigma_{Mi}(\vec{E}_M + \vec{E}^{e}_{Mi}) + \varepsilon_M \frac{\partial}{\partial t} \vec{E}_M - \sigma_I \vec{E}_I - \varepsilon_I \frac{\partial}{\partial t} \vec{E}_I] = 0 \tag{2.125}$$

$$\hat{n} \cdot [\sigma_E \vec{E}_E + \varepsilon_E \frac{\partial}{\partial t} \vec{E}_E - \sum_i \sigma_{Mi}(\vec{E}_M + \vec{E}^{e}_{Mi}) - \varepsilon_M \frac{\partial}{\partial t} \vec{E}_M] = 0 \quad . \tag{2.126}$$

The relations (2.107), (2.110), (2.118), and (2.119) form the complete set of boundary conditions necessary for the solution of electric field problems in biological cells. They are applicable to both time-dependent and quasi-static phenomena as they were developed directly from Maxwell's equations. Expressions (2.125) and (2.126) are alternate forms of equations (2.118) and (2.119) and will be used in the next section. It is emphasized that the relationships in this section are valid only when the field quantities they contain are evaluated at the appropriate interface.

2.2.2. Boundary Conditions Describing the Cell Membrane

In many investigations, to reduce the complexity of resulting solutions, the neuronal membrane is modeled as infinitely thin[1]. Since its thickness is on the order of 100 Å (Eccles [17]), this assumption is normally valid and very useful. The major difficulty encountered in considering the membrane as a single surface involves relating field quantities (such as potential, current, and electric field) across the boundary that it forms. To accomplish this, these field quantities in the boundary conditions of the previous section must be integrated across the membrane.

Consider the membrane geometry as depicted in Figure 2.5. If it is possible to relate the field parameters defined on the interior membrane surface at (b) to those on the exterior surface at (a), then the intracellular and extracellular field solutions may be obtained without solving the problem inside the membrane. From Section 2.1.3, the current density inside the membrane due to the ith ion species is

$$\vec{J}_{Mi}(\vec{r},t) = \sigma_{Mi}(\vec{r},t)[\vec{E}_M(\vec{r},t) + \vec{E}^e_{Mi}(\vec{r},t)] \tag{2.127}$$

where

$$\sigma_{Mi}(\vec{r},t) = |z_i| F\, u_{Mi}(\vec{r}) C_{Mi}(\vec{r},t) \quad . \tag{2.128}$$

---

[1] This is the case in work done by Eisenberg and Johnson [20], Hellerstein [30], and Rall [65]. This assumption is also implicit in the core conductor model (Plonsey [60]).

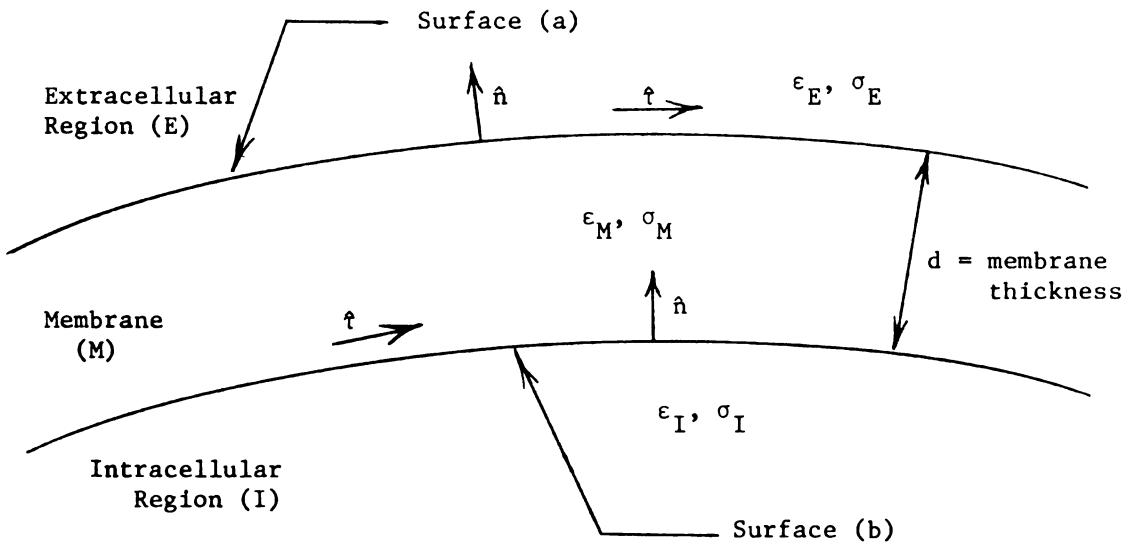

FIGURE 2.5

Geometry for Trans-Membrane Boundary Conditions

The (negative) line integral from the surface at (a) to the surface at (b) (S_a and S_b respectively) of equation (2.127) is taken as

$$-\int_{S_a}^{S_b} \frac{\vec{J}_{Mi}(\vec{r},t)}{\sigma_{Mi}(\vec{r},t)} \cdot d\vec{\ell} = -\int_{S_a}^{S_b} [\vec{E}_M(\vec{r},t) + \vec{E}^e_{Mi}(\vec{r},t)] \cdot d\vec{\ell} \qquad (2.129)$$

where $d\vec{\ell} = \hat{n}d\ell$. Applying the mean-value theorem for integrals (Olmsted [58]) gives

$$\hat{n} \cdot \vec{J}_{Mi}(\vec{r}^*,t) \int_{S_a}^{S_b} \frac{d\ell}{\sigma_{Mi}(\vec{r},t)} = -\int_{S_a}^{S_b} \vec{E}_M \cdot d\vec{\ell} - \int_{S_a}^{S_b} \vec{E}^e_{Mi} \cdot d\vec{\ell} \qquad (2.130)$$

where $\vec{r}^*$ specifies some point between S_a and S_b on the path of integration. The conductance of the ith ion species is now defined as[1]

$$g_i(\vec{r}_\tau,t) = [\int_{S_a}^{S_b} \frac{d\ell}{\sigma_{Mi}(\vec{r},t)}]^{-1} \ (\text{mhos/m}^2) \qquad (2.131)$$

where $\vec{r}_\tau$ is a two-dimensional position vector (one dimension, that normal to the membrane interfaces, having been integrated out). Vector $\vec{r}_\tau$ may be defined in terms of the position vector $\vec{r}$ as follows:

$$\vec{r} = \vec{r}_\tau + \hat{n}s \qquad (2.132)$$

---

[1] This definition follows Stevens [74], Chapter 10 or Finkelstein and Mauro [23]. The intent is to remove (via integration) parameters that are defined inside the membrane. The membrane is so very thin that macroscopic definitions tend to lose their meaning, and it is experimentally easier to measure quantities across the membrane (such as conductance) than quantities within the membrane (such as conductivity).

$\vec{r}_\tau$ = vector from origin to inner surface of membrane,

s = normal distance into membrane; $0 \leq s \leq d$, where

d = membrane thickness.

For example, in terms of cylindrical polar coordinates, with the z axis as the center of a cylindrical cell and radial distance $r = b$ to the inner membrane interface (see Figure 2.7 of Section 2.3), $\vec{r}_\tau = \hat{r}b + \hat{z}z$.

Now one of two assumptions is invoked. It is assumed that either:

i) The membrane is effectively infinitely thin, so that whatever current enters the membrane normally (perpendicular to) on one side emerges directly opposite (still in the $\hat{n}$ direction) on the other side. This is equivalent to neglecting the tangential component of current in the membrane.

ii) The membrane is anisotropic so that no current can flow in a direction tangential to the membrane's surface. Conduction through the membrane is often considered to be the result of ions confined to specific channels (pores) (see Katz [40], Plonsey [60], or Ruch and Patton [70]). This is a physical constraint that forces the $\hat{t}$ components of membrane current density to be zero.

With either assumption, the normal ($\hat{n}$) component of membrane current is the <u>only</u> component. As a result the current density must be a

constant across the membrane[1]. This gives

$$\hat{n} \cdot \vec{J}_{Mi}(\vec{r}^{*},t) = J_{Mi}(\vec{r}_{\tau},t) \tag{2.133}$$

where J_{Mi} is the magnitude of the normal current density[2] at location $\vec{r}_{\tau}$. With relation (2.133) and definition (2.131), equation (2.130) becomes

$$J_{Mi}(\vec{r}_{\tau},t) = g_i(\vec{r}_{\tau},t)\left[-\int_{S_a}^{S_b} \vec{E}_M \cdot d\vec{\ell} - \int_{S_a}^{S_b} \vec{E}^{e}_{Mi} \cdot d\vec{\ell}\right] . \tag{2.134}$$

For quasi-static conditions, the potential difference between two points (1) and (2) is defined as[3]

$$V_{12} = \Phi_1 - \Phi_2 = -\int_2^1 \vec{E} \cdot d\vec{\ell} . \tag{2.135}$$

Applying this definition to the first term on the right-hand-side of equation (2.134) yields

$$V_m = \Phi_M|_{S_b} - \Phi_M|_{S_a} = -\int_{S_a}^{S_b} \vec{E}_M \cdot d\ell \tag{2.136}$$

---

[1] For current density to be constant for the case of assumption ii) requires the additional constraint that any curvature of the membrane is small with respect to the membrane's thickness so that the membrane may be considered as planar. This is discussed at the end of Section 2.3 for a cylindrical cell.

[2] It is emphasized that $\hat{n}\, J_{Mi}$ represents the only component of current density in the membrane. This gives J_{Mi} as the magnitude of the total current density.

[3] See Ramo, Whinnery, and Van Duzer [67]. Static or quasi-static conditions are necessary so that voltage (V_{12}) is synonymous with scalar potential difference.

where Φ_M is the scalar potential in the membrane and V_m is defined as the transmembrane potential. By use of boundary conditions (2.107) and (2.110) (potential is continuous across an interface) the scalar potentials in equation (2.136) become

$$\Phi_M|_{S_b} = \Phi_I|_{S_b} = \Phi_I(\vec{r}_\tau, t) \quad \ldots \text{ the scalar potential at point } (\vec{r}_\tau) \tag{2.137}$$

$$\Phi_M|_{S_a} = \Phi_E|_{S_a} = \Phi_E(\vec{r}_\tau + \hat{n}d, t) \quad \ldots \text{ the scalar potential at point } (\vec{r}_\tau + \hat{n}d) \; . \tag{2.138}$$

This gives the transmembrane potential as[1]

$$V_m(\vec{r}, t) = \Phi_I(\vec{r}_\tau, t) - \Phi_E(\vec{r}_\tau + \hat{n}d, t) \; . \tag{2.139}$$

Similarly, an effective potential difference across the membrane maintained by the impressed field may be defined with

$$V^e_{mi}(\vec{r}, t) = -\int_{S_a}^{S_b} \vec{E}^e_{Mi}(\vec{r}, t) \cdot d\vec{\ell} \; . \tag{2.140}$$

This equivalent voltage may be further identified by expressing $\vec{E}^e_{Mi}$ in terms of its definition (2.102):

---

[1] This follows the convention of physiologists to define V_m as the intracellular minus the extracellular potential. Also note the position vector $\vec{r}$ for V_m is variable only in two dimensions as V_m is defined across the membrane.

$$V_{mi}^{e} = -\int_{S_a}^{S_b} \vec{E}_{Mi}^{e} \cdot d\vec{\ell} = -\int_{S_a}^{S_b} \left(-\frac{RT}{z_i F} \frac{\nabla C_{Mi}}{C_{Mi}}\right) \cdot d\vec{\ell}$$

$$= \frac{RT}{z_i F} \int_{S_a}^{S_b} \frac{1}{C_{Mi}} \frac{\partial C_{Mi}}{\partial \ell} \, d\ell \quad \left(\text{as } d\vec{\ell} \cdot \nabla = \frac{\partial}{\partial \ell}\right)$$

$$= \frac{RT}{z_i F} \int_{S_a}^{S_b} \frac{\partial C_{Mi}}{C_{Mi}}$$

$$= \frac{RT}{z_i F} \ln \frac{[C_{Mi}]_b}{[C_{Mi}]_a} \tag{2.141}$$

where $[C_{Mi}]_b$ and $[C_{Mi}]_a$ are the concentrations of ions of species "i" just inside the membrane at surfaces S_b and S_a respectively.

Assuming that the concentration of the ith ion species just inside the membrane interface is related to the concentration just outside the membrane by a constant partition coefficient β_i (see Plonsey [60]) gives

$$[C_{Mi}]_b = \beta_i [C_{Ii}]_b = (\text{constant}^{1}) \tag{2.142}$$

$$[C_{Mi}]_a = \beta_i [C_{Ei}]_a = (\text{constant}^{1}) \, . \tag{2.143}$$

Then expression (2.137) for the equivalent potential becomes

$$V_{mi}^{e} = \frac{RT}{z_i F} \ln \frac{\beta_i [C_{Ii}]_b}{\beta_i [C_{Ei}]_a} = \frac{RT}{z_i F} \ln \frac{[C_{Ii}]_b}{[C_{Ei}]_a} = (\text{constant}). \tag{2.144}$$

From equation (2.144), V_{mi}^{e} may be identified as equivalent to the

---

[1] As C_{Ii} and C_{Ei} have been assumed constant in Section 2.2.1.

Nernst potential for the ith ion species. The Nernst potential is defined as the equilibrium transmembrane potential required to result in a drift current which just balances the diffusion current due to an ionic concentration gradient[1]. From Plonsey [60], the Nernst potential of the ith ion species is

$$V_i^e = - \frac{RT}{z_i F} \ell n \frac{[C_{Ii}]_b}{[C_{Ei}]_a} \quad . \tag{2.145}$$

By comparison with result (2.144), it is evident that

$$-V_{mi}^e = V_i^e \quad . \tag{2.146}$$

With definitions (2.136), (2.140), and (2.146), equation (2.130) can be expressed as

$$J_{Mi}(\vec{r}_\tau, t) = g_i(\vec{r}_\tau, t)(V_m(\vec{r},t) - V_i^e) \quad . \tag{2.147}$$

Equation (2.147) relates the normal current density (assumed to be the total current density) of the ith ion species within the membrane to a conductance multiplying the difference between the voltage due to the coulomb field and a constant Nernst potential. The total current density through the membrane is then the sum over all contributing ion species:

$$\begin{aligned} J_M(\vec{r}_\tau,t) &= \sum_i J_{Mi}(\vec{r}_\tau,t) \\ &= \sum_i g_i(\vec{r}_\tau,t)(V_m(\vec{r},t) - V_i^e) \quad . \end{aligned} \tag{2.148}$$

---

[1] The Nernst potential may be derived by setting $\vec{J}_i = 0$ in the Nernst-Planck equation, integrating from S_a to S_b, and applying

Now consider boundary conditions (2.125) and (2.126). The membrane current density, used in each expression, is given by equation (2.123) as

$$\vec{J}_M = \sum_i \sigma_{Mi}(\vec{E}_M + \vec{E}^e_{Mi}) \ , \tag{2.123}$$

evaluated at the appropriate interface. By use of result (2.148), this current density may be replaced in both boundary conditions with

$$\vec{J}_M = \sum_i g_i(V_m - V^e_i)\hat{n} \ , \tag{2.149}$$

which is invariant across the membrane and thus the same at either interface. The boundary conditions then become

$$\sum_i g_i(V_m - V^e_i) + \hat{n}\cdot[\varepsilon_M \frac{\partial}{\partial t}\vec{E}_M - \varepsilon_I \frac{\partial}{\partial t}\vec{E}_I - \sigma_I\vec{E}_I] = 0 \tag{2.150}$$

$$\hat{n}\cdot[\sigma_E\vec{E}_E + \varepsilon_E \frac{\partial}{\partial t}\vec{E}_E - \varepsilon_M \frac{\partial}{\partial t}\vec{E}_M] - \sum_i g_i(V_m - V^e_i) = 0 \ . \tag{2.151}$$

The $\varepsilon \frac{\partial}{\partial t}\vec{E}$ terms in the preceeding expressions give rise to a membrane capacitance. $\varepsilon\vec{E}$ at the interface of each region is related to surface charge density as seen in boundary conditions (2.109) and (2.112) of Section 2.2.1:

$$\hat{n} \cdot (\varepsilon_M\vec{E}_M - \varepsilon_I\vec{E}_I) = \eta_I \tag{2.109}$$

$$\hat{n} \cdot (\varepsilon_E\vec{E}_E - \varepsilon_M\vec{E}_M) = \eta_E \ . \tag{2.112}$$

The normal component of $\vec{E}_M$ will be approximated as being a

constant across the membrane[1], giving the result

$$\hat{n} \cdot \vec{E}_M = \frac{V_m}{d} \tag{2.152}$$

where V_m is the transmembrane potential (see definition (2.139)) and d is the membrane thickness. As the cell membrane is on the order of 100 $\mathring{A}$ thick, and the potential across the membrane of a neuron at rest is on the order of 0.01 volts, the magnitude of $\hat{n} \cdot \vec{E}_M$ is on the order of 0.01 volts/100 $\mathring{A}$ = 10^6 volts/meter. With such an immense field strength, variations from the constant-field condition would have to be enormous to be a significant deviation from approximation (2.152). Accepting relation (2.152) as a valid approximation, and taking the time derivative of equations (2.109) and (2.112) yields

$$\varepsilon_M/d \frac{\partial}{\partial t} V_m - \varepsilon_I \hat{n} \cdot \frac{\partial}{\partial t} \vec{E}_I \doteq \frac{\partial}{\partial t} \eta_I \tag{2.153}$$

$$\varepsilon_E \hat{n} \cdot \frac{\partial}{\partial t} \vec{E}_E - \varepsilon_M/d \frac{\partial}{\partial t} V_m \doteq \frac{\partial}{\partial t} \eta_E \cdot \tag{2.154}$$

With V_m being defined via a line integral of $\vec{E}_M$ across the membrane, it is expected that $\hat{n} \cdot \frac{\partial}{\partial t} \vec{E}_M = \frac{\partial}{\partial t} V_m/d$ would have the same order of magnitude as $\hat{n} \cdot \frac{\partial}{\partial t} \vec{E}_I$ or $\hat{n} \cdot \frac{\partial}{\partial t} \vec{E}_E$ (as time rate of changes of fields on either side of the membrane interfaces should be similar). This gives

$$\varepsilon_M/d \frac{\partial}{\partial t} V_m >> \varepsilon_I \hat{n} \cdot \frac{\partial}{\partial t} \vec{E}_I \tag{2.155}$$

---

[1] The constant-field approximation has been widely used in membrane electrophysiology, and has given results in good agreement with experimental observations. See Plonsey [60] for further discussion.

$$\varepsilon_M/d \frac{\partial}{\partial t} V_m >> \varepsilon_E \hat{n} \cdot \frac{\partial}{\partial t} \vec{E}_E , \tag{2.156}$$

since for a typical cell ε_M is approximately $6\varepsilon_o$; ε_I and ε_E are approximately $80\varepsilon_o$ (the value for H_2O); and with $d = 100$ Å, ε_M/d is on the order of 10^7 times larger than ε_I or ε_E (values from Katz [40]). Thus expressions (2.153) and (2.154) to a very good approximation are

$$\varepsilon_M/d \frac{\partial}{\partial t} V_m \doteq \frac{\partial}{\partial t} \eta_I \tag{2.157}$$

$$\varepsilon_M/d \frac{\partial}{\partial t} V_m \doteq - \frac{\partial}{\partial t} \eta_E \tag{2.158}$$

with the further result that

$$\frac{\partial}{\partial t} \eta_I \doteq - \frac{\partial}{\partial t} \eta_E . \tag{2.159}$$

The relationship between a current, voltage, and capacitance is $I = C \frac{\partial}{\partial t} V$. Noting that the time derivative of a (surface) charge density yields a current density gives rise to the definition

$$C_m = \varepsilon_M/d \quad (\text{farads/m}^2) , \tag{2.160}$$

so that

$$C_m \frac{\partial}{\partial t} V_m \doteq \frac{\partial}{\partial t} \eta_I \doteq - \frac{\partial}{\partial t} \eta_E \tag{2.161}$$

where C_m is defined as the membrane capacitance per unit area.

With the time derivative of boundary conditions (2.109) and (2.112), expressions (2.150) and (2.151) now become

$$\sum_i g_i(V_m - V_i^e) - \sigma_I \hat{n} \cdot \vec{E}_I + \frac{\partial}{\partial t} \eta_I = 0 \tag{2.162}$$

$$\sigma_E \hat{n} \cdot \vec{E}_E + \frac{\partial}{\partial t} \eta_E - \sum_i g_i(V_m - V_i^e) = 0 \ . \qquad (2.163)$$

Denoting the $\hat{n}$ component of a vector with the subscript n and applying expression (2.161) gives the final boundary conditions across the membrane as

$$\sum_i g_i(V_m - V_i^e) + C_m \frac{\partial}{\partial t} V_m - \sigma_I E_{In} = 0 \qquad (2.164)$$

$$\sigma_E E_{En} - \sum_i g_i(V_m - V_i^e) - C_m \frac{\partial}{\partial t} V_m = 0 \ . \qquad (2.165)$$

The capacitance term in the above expressions arises from the effects of displacement (polarization) current within the membrane. As noted in Section 2.1.3, displacement currents can be ignored in the intracellular and extracellular volume conductors as the conductivity in those regions is large with respect to polarization effects for the frequency spectra of natural bioelectric phenomena. This is not the case in the membrane as its conductivity is far smaller[1]. Thus at the boundaries of the membrane, dielectric effects become apparent in the form of surface charges and related capacitance. The net effect of the approximations involved in expressions (2.157) and (2.158) is that the displacement currents in the intracellular and extracellular regions may be ignored, while displacement current in the membrane is significant.

Boundary conditions (2.164) and (2.165) describe the normal current density ($\sigma \vec{E}_n$) at the interior or exterior membrane surface

---

[1] The membrane is in fact a very good dielectric, maintaining a field on the order of 10^6 volts/meter in the resting state. This compares with a breakdown field strength of 3×10^6 volts/meter for air.

as due to a capacitive current and drift current driven by the transmembrane potential and the (constant) Nernst potentials of the ions. Adding these boundary conditions yields the relationship between normal current densities across the membrane as

$$\sigma_E E_{En} - \sigma_I E_{In} = 0 \ . \tag{2.166}$$

Equation (2.166) reiterates the major assumption of this section that membrane current has only a constant, normal component. The net result as seen in expression (2.166) is that any current that enters the membrane at one point emerges from the membrane directly opposite its entry point on the other side.

The desired boundary conditions are displayed in equations (2.164) - (2.166). They can be summarized with

$$\sigma_E E_{En} = \sigma_I E_{In} = C_m \frac{\partial V_m}{\partial t} + \sum_i g_i (V_m - V_i^e) \ , \tag{2.167}$$

which is essentially the same result as used by Hodgkin and Huxley [37] in their classic development. Equation (2.167) describes a useful equivalent circuit for the membrane in per-unit-area parameters. Following Hodgkin and Huxley, Na^+ and K^+ are taken as the only two ion species with variable conductivities. All other ion species are lumped into a single "leakage" conductance (g_ℓ) and Nernst potential (V_ℓ^e). This gives

$$\sigma_E E_{En} = \sigma_I E_{In} = C_m \frac{\partial V_m}{\partial t} + g_{Na^+}(V_m - V^e_{Na^+}) + g_{K^+}(V_m - V^e_{K^+})$$

$$+ g_\ell (V_m - V_\ell^e) \ . \tag{2.168}$$

Expression (2.168) defines the equivalent circuit configuration as shown in Figure 2.6. Note that the sign conventions have been followed of $\hat{n}$ being directed outward from the cell interior and all voltages defined as intracellular with respect to extracellular potential. The series of papers by Hodgkin and Huxley ([34] - [37]) derived this equivalent circuit and obtained the functional dependence of g_{Na^+} and g_{K^+} via experimental observations. The material presented in this section indicates the procedure and assumptions necessary to arrive at their result from an EM field approach, and defines the conductances in terms of membrane conductivity[1].

---

[1] See also Finkelstein and Mauro [23] for a discussion of equivalent circuit derivations and definitions of parameters for several different circuit descriptions of the membrane.

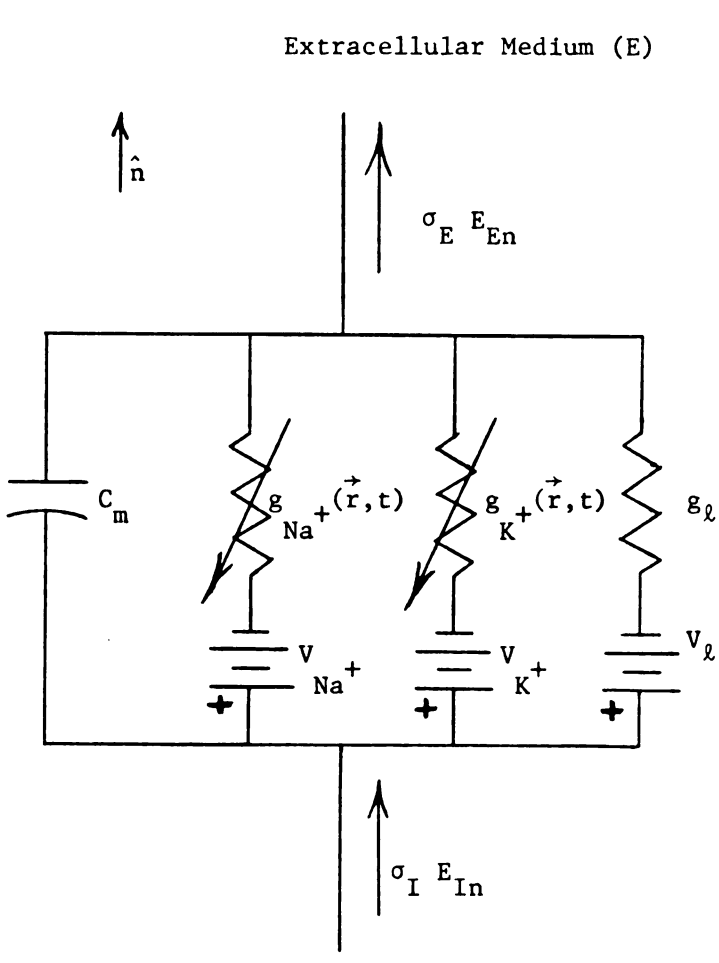

FIGURE 2.6

Equivalent Circuit for a Unit Area of Membrane

2.3. Constant-Field Membrane Model in Cylindrical Coordinates

This section will derive a few basic results for a membrane of cylindrical geometry. The structure modeled will consist of a nerve axon (or dendrite) in its resting condition. The geometry is outlined in Figure 2.7. The structure is assumed to be rotationally symmetric about the z axis, so that all physical quantities will be independent of ϕ. The internal radius is b, external radius is a, and the membrane thickness is then $a-b = d$. From result (2.101), the current due to any ion species is given as

$$\vec{J}_i = \sigma_i(\vec{E}_i^e + \vec{E}) \tag{2.101}$$

where

$$\sigma_i = |z_i| F u_i C_i \tag{2.91}$$

$$\vec{E}_i^e = - \frac{RT}{z_i F} \frac{\nabla C_i}{C_i} \tag{2.102}$$

$$\vec{E} = -\nabla \Phi \ . \tag{2.100}$$

Within any volume region (E, M, or I) electroneutrality is assumed, such that

$$\sum_i z_i C_i = 0 \ . \tag{2.169}$$

In the intracellular (I) and extracellular (E) regions, this condition will be satisfied in the resting state for macroscopic distances greater than the Debye shielding distance (about 10 Å, see Section 2.1.2 or Plonsey [60]). In the membrane (M), it will

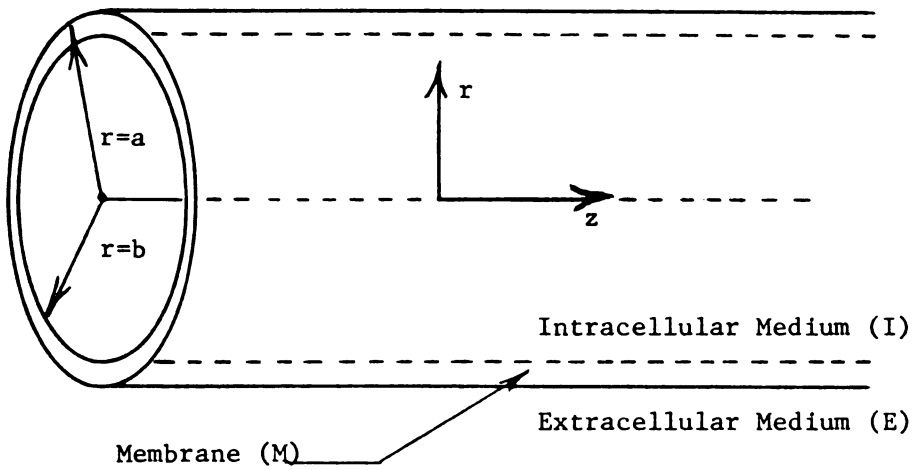

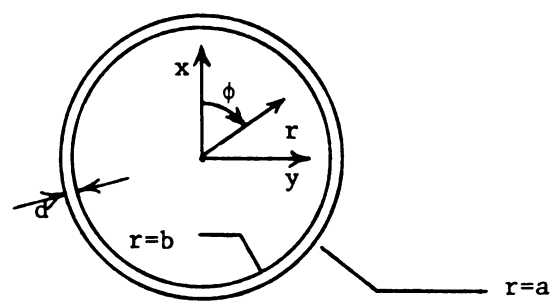

a-b = d

FIGURE 2.7

Cylindrical Geometry for a Nerve Axon or Dendrite

be assumed that condition (2.169) is satisfied, though it is noted that macroscopic conditions are not well defined in a structure that can be as small as 50 Å thick[1]. With no externally applied sources, the divergence equation for $\vec{E}$ (2.99) reduces to

$$\nabla \cdot \vec{E}(r,z,t) = 0 \quad \text{(in E,M, or I)}. \tag{2.170}$$

In the resting state, the transmembrane potential is longitudinally invariant, with the result that fields and currents have neither $\hat{z}$ components nor z dependence. Thus in cylindrical coordinates equation (2.170) becomes

$$\nabla \cdot \vec{E}(r) = \frac{1}{r} \frac{\partial}{\partial r} [r\, E_r(r)] = 0 \ . \tag{2.171}$$

Now it is possible to proceed to solve for $\vec{E}_M(r) = \hat{r}\, E_{Mr}(r)$, the field in the membrane. By equation (2.171) $(r\, E_{Mr}) = K =$ (constant), giving

$$E_{Mr} = \frac{K}{r} \ . \tag{2.172}$$

Applying the definition of V_m from equation (2.139) yields[2]

$$\begin{aligned} V_m &= \Phi_I(b) - \Phi_E(a) = -\int_a^b E_{Mr}(r)dr \\ &= -\int_a^b \frac{K}{r}\, dr \\ &= -K\ \ell n \frac{b}{a} \ . \end{aligned} \tag{2.173}$$

---

[1] Many authors describing microscopic conditions within the membrane use a fixed-charge model (Plonsey [60], Offner [57]). The assumption applied here is that any fixed charges inside the membrane are canceled in a macroscopic sense by mobile ions of the opposite sign.

[2] Note that V_m (in the resting condition) is a constant, and $\vec{E}_M$ is only a function of r. Time dependence is dropped as the system is assumed time invariant in the resting state.

This defines K as

$$K = \frac{V_m}{\ell n\ a/b} \ . \tag{2.174}$$

Thus in the resting state, the electric field in the membrane is

$$E_{Mr}(r) = \frac{V_m}{r\ \ell n\ \ a/b} \ . \tag{2.175}$$

With $a >> d = a-b$ (axon radii range from 1μ to 1 mm, while d is in the range of 50 to 150 Å), a series expansion can be applied to $\ell n\ a/b$ giving

$$\ell n\ a/b = \ell n \frac{a}{a-d} \doteq \frac{d}{a-d} \ . \tag{2.176}$$

Realizing that, for points interior to the membrane, r is restricted to $a-d < r < a$, the result follows that $r\ \ell n\ a/b \doteq \frac{rd}{a-d} \doteq d$. Equation (2.175) then reduces to

$$E_{Mr}(r) \doteq \frac{V_m}{d} = (\text{constant}) \ . \tag{2.177}$$

Equation (2.177) indicates that to a very good approximation the electric field in the membrane will be constant. A constant-field assumption is widely used in membrane biophysics problems and it will hold for cylindrical coordinates so long as $d << a$. In the steady-state resting condition, no net charge is transferred across the membrane. The result of this, in all three compartments (E,M,I), is that

$$\vec{J} = \sum_i \vec{J}_i \equiv 0 \ . \tag{2.178}$$

By use of relations (2.115) and (2.116), the electric fields in the interior and exterior regions may be found as

$$\vec{J}_I = \sigma_I \vec{E}_I = 0 \Rightarrow \vec{E}_I = 0 , \tag{2.179}$$

$$\vec{J}_E = \sigma_E \vec{E}_E = 0 \Rightarrow \vec{E}_E = 0 . \tag{2.180}$$

The electric field for all space can now be summarized with

$$\begin{aligned} \vec{E}_I &= 0 && 0 < r < b \\ \vec{E}_M &= \frac{V_m}{r \, \ell n \, a/b} \hat{r} && b < r < a \\ \vec{E}_E &= 0 && a < r \quad . \end{aligned} \tag{2.181}$$

By equation (2.100), this implies

$$\begin{aligned} \Phi_I(\vec{r}) &= (\text{constant}) \\ \Phi_M(\vec{r}) &= f(r) \\ \Phi_E(\vec{r}) &= (\text{constant}) . \end{aligned} \tag{2.182}$$

Since Φ_E = (constant) and the potential at $r \to \infty$ is required to be zero (by definition), $\Phi_E = 0$. Applying the definition of transmembrane potential gives $V_m = \Phi_I(b) = \Phi_I(\vec{r})$. Then by use of $\vec{E} = -\nabla \Phi$, and integrating for $\Phi_M(\vec{r})$ (applying the boundary condition requiring the continuity of potential at interfaces) gives

$$\begin{aligned} \Phi_I &= V_m \\ \Phi_M &= V_m \left(1 - \frac{\ell n \; r/b}{\ell n \; a/b}\right) \\ \Phi_E &= 0 . \end{aligned} \tag{2.183}$$

The final consideration is to evaluate V_m. Due to the longitudinal invariance, the condition $J_{zi} = 0$ holds in all compartments for all ion species "i". In the steady state, the continuity equation (2.96) reduces (in the membrane) to

$$\frac{1}{r}\frac{\partial}{\partial r}\left(r\, J_{Mri}(r)\right) = 0 \ . \tag{2.184}$$

This indicates that

$$r\, J_{Mri}(r) = (\text{constant}) \ . \tag{2.185}$$

Applying the conditions of longitudinal invariance, no $\hat{z}$ component of membrane current density, and rotational symmetry to the Nernst-Planck equation (2.97) gives

$$J_{Mri}(r) = \frac{-z_i u_{Mi}(r) RT}{|z_i|}\frac{\partial C_{Mi}(r)}{\partial r} + |z_i| F u_{Mi}(r) C_{Mi}(r) E_{Mr}(r). \tag{2.186}$$

The assumption is now made that $u_{Mi}(r)$ (the mobility of the ith ion species within the membrane) is a constant[1]. With this and the solution (2.181) for E_{Mr}, equation (2.186) can be expressed as

$$J_{Mri}(r) = \frac{-z_i u_{Mi} RT}{|z_i|}\frac{\partial C_{Mi}(r)}{\partial r} + |z_i| F u_{Mi} C_{Mi}(r)\left[\frac{V_m}{r\, \ell n\ a/b}\right], \tag{2.187}$$

or

$$\frac{\partial C_{Mi}}{\partial r} - \frac{z_i F\, V_m}{RT\ \ell n\ a/b}\frac{C_{Mi}}{r} = \frac{-z_i\, J_{Mri}}{|z_i| u_{Mi}\, RT} \ . \tag{2.188}$$

The first-order differential equation (2.188) is easily solved in the form

---

[1] This assumption is necessary in the development of the Goldman equation (see Plonsey [60]). It implies that the membrane is considered homogeneous as well as uniform.

$$C_{Mi}(r) = C^{c}_{Mi}(r) + C^{p}_{Mi}(r) \tag{2.189}$$

where $C^{p}_{Mi}(r)$ = the particular integral,

and $C^{c}_{Mi}(r)$ = the complementary function.

By inspection, the particular integral is found as

$$C^{p}_{Mi} = \frac{r\, J_{Mri}(r)\ \ell n\ a/b}{|z_i| F\, u_{Mi}\, V_m} \tag{2.190}$$

since by result (2.185), $r\, J_{Mri}(r)$ is a constant. The homogeneous equation is integrated to yield the complementary function as

$$C^{c}_{Mi}(r) = A\, r^{(\frac{z_i V_m F}{RT\ \ell n\ a/b})} = A \exp[\frac{z_i F V_m\ \ell n\ r}{RT\ \ell n\ a/b}] \tag{2.191}$$

where A = constant of integration.

Thus the complete solution takes the form

$$C_{Mi}(r) = A \exp\,[\frac{z_i F V_m\ \ell n\ r}{RT\ \ell n\ a/b}] + \frac{r\, J_{Mri}(r)\ \ell n\ a/b}{|z_i| F\, u_{Mi}\, V_m}\ . \tag{2.192}$$

The constant of integration (A) is found by evaluating equation (2.192) at r = b:

$$C_{Mi}(b) = A \exp\,[\frac{z_i F V_m\ \ell n\ b}{RT\ \ell n\ a/b}] + \frac{b\, J_{Mri}(b)\ \ell n\ a/b}{|z_i| F\, u_{Mi} V_m}\ . \tag{2.193}$$

This gives integration constant A as

$$A = [C_{Mi}(b) - \frac{b\, J_{Mri}(b)\ \ell n\ a/b}{|z_i| F\, u_{Mi} V_m}] \exp\,[\frac{-z_i F V_m\ \ell n\ b}{RT\ \ell n\ a/b}]\ . \tag{2.194}$$

With definition (2.194), the concentration of the ith ion species at any point r in the membrane is

$$C_{Mi}(r) = [C_{Mi}(b) - \frac{b\ J_{Mri}(b)\ \ell n\ a/b}{|z_i| F\ u_{Mi} V_m}] \exp[\frac{z_i F\ V_m\ \ell n\ r/b}{RT\ \ell n\ a/b}]$$

$$+ \frac{r\ J_{Mri}(r)\ \ell n\ a/b}{|z_i| F\ u_{Mi}\ V_m} \ . \qquad (2.195)$$

Now expression (2.195) is evaluated at $r = a$ and it is noted (by result (2.185)) that $r\ J_{Mri}(r) = (\text{constant}) = b\ J_{Mri}(b) = a\ J_{Mri}(a)$ to obtain

$$r\ J_{Mri}(r) = \frac{|z_i| F\ u_{Mi} V_m}{\ell n\ a/b} \left[\frac{C_{Mi}(a) - C_{Mi}(b)\exp(\frac{z_i F\ V_m}{RT})}{1 - \exp(\frac{z_i F\ V_m}{RT})}\right] . \qquad (2.196)$$

By the assumptions described in the previous section regarding the partition coefficient β (equations (2.142) and (2.143)),

$$J_{Mri}(r) = \frac{|z_i| F\ u_{Mi} V_m}{r\ \ell n\ a/b}\ \beta_i \left[\frac{C_{Ei} - C_{Ii}\ \exp(\frac{z_i F\ V_m}{RT})}{1 - \exp(\frac{z_i F\ V_m}{RT})}\right] , \qquad (2.197)$$

where C_{Ei} and C_{Ii} are the (constant) extracellular and intracellular concentrations of the ith ion species. Defining a permeability coefficient for the ith ion species as

$$P_i = \frac{u_i RT}{|z_i| F\ d}\ \beta_i \quad (\text{m/sec}) \qquad (2.198)$$

and substituting these last two expressions into the steady-state electroneutrality condition (2.178) leads to

$$0 = \sum_i \vec{J}_{Mi} = \sum_i \frac{P_i |z_i|^2 F^2 V_m d}{r\ RT\ \ell n\ a/b} \left[\frac{C_{Ei} - C_{Ii}\ \exp(\frac{z_i F\ V_m}{RT})}{1 - \exp(\frac{z_i F\ V_m}{RT})}\right] \tag{2.199}$$

since $\vec{J}_{Mi}$ has only an $\hat{r}$ component.

To obtain a final result, the three ion species (sodium, potassium, and chloride) that are the charge carriers within the membrane are explicitly inserted into constraint (2.199), and the equation is rearranged to determine V_m:

$$0 = \frac{V_m d\ F^2}{r\ RT\ \ell n\ a/b} \sum_i |z_i|^2 P_i \left[\frac{C_{Ei} - C_{Ii}\ \exp(\frac{z_i F\ V_m}{RT})}{1 - \exp(\frac{z_i F\ V_m}{RT})}\right] \tag{2.200}$$

$$0 = P_{Na^+}\{\frac{[C_{Na^+}]_E - [C_{Na^+}]_I \exp(F\ V_m/RT)}{1 - \exp(F\ V_m/RT)}\} + P_{K^+}\{\frac{[C_{K^+}]_E - [C_{K^+}]_I \exp(FV_m/RT)}{1 - \exp(F\ V_m/RT)}\}$$

$$+ P_{Cl^-}\{\frac{[C_{Cl^-}]_E \exp(F\ V_m/RT) - [C_{Cl^-}]_I}{1 - \exp\ (F\ V_m/RT)}\} \tag{2.201}$$

$$\exp(F\ V_m/RT) = \frac{P_{Na^+}[C_{Na^+}]_E + P_{K^+}[C_{K^+}]_E + P_{Cl^-}[C_{Cl^-}]_I}{P_{Na^+}[C_{Na^+}]_I + P_{K^+}[C_{K^+}]_I + P_{Cl^-}[C_{Cl^-}]_E} \tag{2.202}$$

$$V_m = \frac{RT}{F}\ \ell n\ \frac{P_{Na^+}[C_{Na^+}]_E + P_{K^+}[C_{K^+}]_E + P_{Cl^-}[C_{Cl^-}]_I}{P_{Na^+}[C_{Na^+}]_I + P_{K^+}[C_{K^+}]_I + P_{Cl^-}[C_{Cl^-}]_E}\ . \tag{2.203}$$

This result for V_m is the well known Goldman equation for transmembrane potential (see Plonsey [60]).

The results of this section are summarized as follows. For a membrane described by cylindrical coordinates in its steady

state resting condition, the fields, currents, and potentials are given as

i) $\vec{E}_I = \vec{E}_E = \vec{J}_I = \vec{J}_E = 0$.

ii) $\vec{J}_{Mi} = \hat{r}\, J_{Mri}(r)$; $\vec{E}_M = \hat{r}\, E_{Mr}(r)$,

iii) $r\, E_{Mr}(r) = \text{(constant)}$; $r\, J_{Mr}(r) = \text{(constant)}$, and

iv) the Goldman equation (for V_m) holds.

These results are contrasted to the usual constant-field development where the problem is solved with a planar membrane in rectangular coordinates, resulting in $\vec{J}_{Mi}$ and $\vec{E}_M$ both being constants (see Plonsey [60]). With the condition of $a >> d$, the cylindrical $\vec{E}_M$ and $\vec{J}_{Mi}$ approach the situation of the rectangular solutions as being approximately constant. In either case, the Goldman equation is exactly the same for either a planar or cylindrical membrane.

CHAPTER 3

STEADY-STATE ELECTROTONUS

This chapter is concerned with developing a solution for electric field quantities in and about an axon or dendrite that has been subjected to a constant, maintained stimulus long enough for transients to damp out. The solution is found for three volume conductor compartments (intracellular, extracellular and membrane), so that the effect of allowing membrane current to have a longitudinal component can be examined (as compared to solutions in Chapter 5 where $\vec{J}_M$ is allowed only a normal component). The first section of this chapter is a statement of the problem and assumptions. Sections 3.2 and 3.3 carry out the solution using the Fourier transform and numerical inversions for a variety of stimulating electrodes. Included in the last section are plots of potential as functions of r and z, and a calculation of membrane capacitance from surface charge and transmembrane potential.

3.1 Statement of the Problem

The model under consideration is that of a cylindrical cellular structure, such as an axon or a dendrite. In the last chapter (Section 2.3), a simple solution for the resting potential in cylindrical geometry was carried out. This chapter considers perturbations from that solution caused by a steady, subthreshold

stimulus of an infinite duration. This type of source yields two simplifications to the problem. The first is that in the steady state all quantities will be time independent (the stimulus being maintained long enough for transients to end), allowing all time derivatives to be set to zero. The second simplification is that, for a subthreshold stimulus, active events (the action potential) are not excited and the membrane parameters may be taken as remaining at their resting-condition values. Physiologists label this type of situation as steady-state electrotonus (see Plonsey [60], Ochs [54]).

The geometry to be used is illustrated in Figure 3.1. The coordinates are cylindrical polar (r,ϕ, z), with the z axis aligned with the central axis of the membrane cylinder. The cellular structure is assumed to be uniform in the $\hat{z}$ direction with inner and outer radii of $r = b$ and $r = a$ respectively. This gives the membrane thickness as $d = a - b$. The three compartments, separated by the membrane interfaces, are the intracellular (I) for $0 \leq r \leq b$, the extracellular (E) for $r \geq a$, and the membrane (M) for $b < r < a$.

The length of the cylindrical cell is taken to be infinite in both the $\pm \hat{z}$ directions. Rall [65] demonstrates that the electrical behavior of a finite cell and an infinite cell are essentially the same if the finite cylinder is longer than a few length constants, λ.[1] This conclusion is also

---

[1] The length constant λ is defined as the longitudinal distance required for an electrotonic perturbation in V_m to decay by e^{-1}.

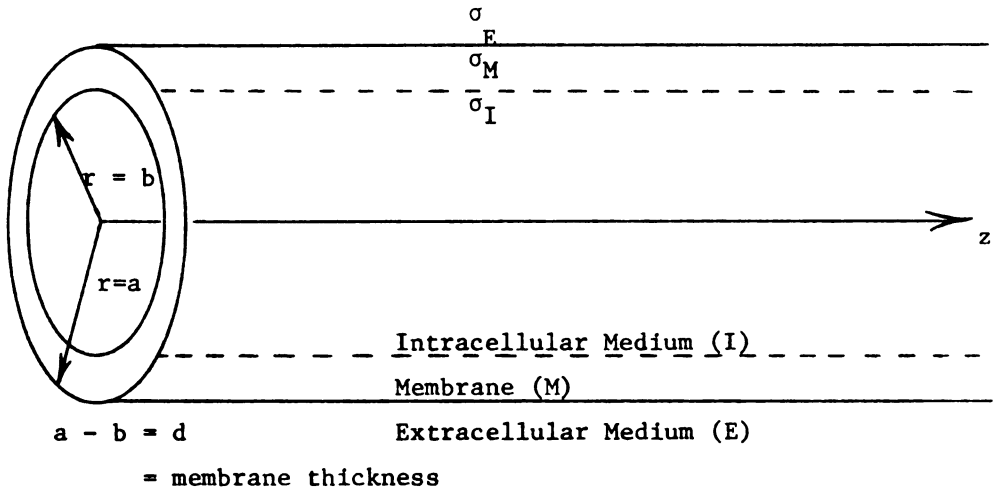

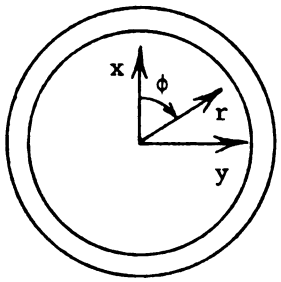

FIGURE 3.1

Geometry for a Cylindrical Cell

supported by Eisenberg and Johnson [20]; and a similar result is given by Klee [42] for cells that are long with respect to their radius. Thus solutions for an infinitely long structure hold for a large class of real axons and dendrites.

Another idealization of the geometry is to assume that all quantities in the system are rotationally symmetric about the z axis. This condition is met if all stimuli are supplied via electrodes having rotational symmetry[1] (i.e., ring electrodes centered on the z axis). This assumption serves to reduce the problem to one involving only two spatial coordinates: r and z. If these sources are further constrained to be applied only at the membrane interface boundaries, then the source terms for the volume conductor regions ($\vec{J}_s$ and ρ_s) can be set to zero in the equations developed in Section 2.1.3. The stimuli are then applied in the boundary conditions. This technique is similar to that used in separation of variables solutions (see Arfken [2]), and was utilized by Hellerstein [30] in his electrotonus development[2].

Now consider the fields and currents in the intracellular and extracellular regions. With the appropriate assumptions[3] that

---

[1] The work of Eisenberg and Johnson [20] on steady-state electrotonus in three dimensions (r,ϕ,z) with point electrodes indicates that perturbations from rotational symmetry are insignificant for axial distances from the source electrode greater than the axon diameter. Thus even non-rotationally symmetric stimuli will yield results similar to those presented here for such distances.

[2] Hellerstein [30] chose the limited case of currents and charges being supplied by a source on one side of the membrane and absorbed by a sink directly opposite on the other side of the membrane. The case presented here is more general.

[3] See Chapter 2, Sections 2.1.3 and 2.2.1.

the cell interior and exterior are described by simple, linear, homogeneous, and electroneutral media[1], then the volume conductor equations are given as:

$$\vec{J}_I(r,z) = \sigma_I \vec{E}_I(r,z) \tag{3.1}$$

$$\vec{J}_E(r,z) = \sigma_E \vec{E}_E(r,z) \tag{3.2}$$

$$\sigma_I = \sum_i \sigma_{Ii} = \sum_i |z_i| F\, u_{Ii} C_{Ii} \tag{3.3}$$

$$\sigma_E = \sum_i \sigma_{Ei} = \sum_i |z_i| F\, u_{Ei} C_{Ei} \tag{3.4}$$

$$\nabla^2 \phi_I(r,z) = 0 \tag{3.5}$$

$$\nabla^2 \phi_E(r,z) = 0 \tag{3.6}$$

$$\vec{E}_I(r,z) = -\nabla \phi_I(r,z) \tag{3.7}$$

$$\vec{E}_E(r,z) = -\nabla \phi_E(r,z) \ . \tag{3.8}$$

The membrane exhibits a more complicated behavior. As noted in the introduction to this chapter, the solution will be carried out for fields and currents within the membrane. The primary reason for this is to check on the assumption required to obtain the boundary conditions in Section 2.2.2; i.e., that membrane currents have only a normal ($\hat{r}$) component. In this chapter and the

---

[1] This implies that u_{Ii}, u_{Ei}, C_{Ii}, and C_{Ei} are all constants, see Section 2.2.1.

next, the membrane will be considered a homogeneous and isotropic medium, allowing currents in the tangential ($\hat{z}$) as well as radial direction. Other advantages to solving the three compartment system (as opposed to integrating the membrane out of the problem as is done in Section 2.2.2 and Chapter 5) is that it enables modeling of fields within the myelin sheath (see Chapter 4) and it allows a direct calculation for membrane capacitance (see Section 3.3.4).

The equation that describes current density within the membrane is given in Section 2.2.1 as

$$\vec{J}_M(r,z) = \sum_i \left[\frac{-z_i u_i(r) RT}{|z_i|} \nabla C_{Mi}(r,z) + \sigma_{Mi}(r,z)\vec{E}_M(r,z)\right] \quad , \qquad (3.9)$$

where rotational symmetry, steady-state conditions, and uniformity of the membrane in the $\hat{z}$ direction have been assumed. The concentration profiles and mobilities of each ion species "i" are now assumed to remain at their resting (no stimulus) condition values, giving

$$\vec{J}_M(r,z) = \sum_i \left[\frac{-z_i u_i RT}{|z_i|} \nabla C_{Mi}(r) + \sigma_{Mi}(r)\vec{E}_M(r,z)\right] \quad , \qquad (3.10)$$

where u_i has been taken as constant (as in Section 2.3) and $C_{Mi}(r)$ is given by solution (2.195) of Section 2.3. The $\nabla C_{Mi}(r)$ terms in equation (3.10) are the source of the resting transmembrane potential. If the coulomb field $\vec{E}_M$ is expanded via a small signal analysis into

$$\vec{E}_M(r,z) = \vec{E}_{Mo}(r) + \vec{E}'_M(r,z), \tag{3.11}$$

where $\vec{E}_{Mo}$ is the resting condition field and $\vec{E}'_M$ is the perturbation, then equation (3.10) becomes

$$\vec{J}_M(r,z) = \sum_i \left[\frac{-z_i u_i RT}{|z_i|} \nabla C_{Mi}(r) + \sigma_{Mi}(r)\vec{E}_{Mo}(r)\right] + \sum_i \sigma_{Mi}(r)\vec{E}'_M(r,z). \tag{3.12}$$

The first summation on the right hand side of equation (3.12) is just the membrane current in the resting state, and this (by steady-state considerations, see Section 2.3) must be zero[1]. Thus the current density within the membrane is

$$\vec{J}_M(r,z) = \sigma_M(r)\vec{E}'_M(r,z) \ , \tag{3.13}$$

where

$$\sigma_M(r) = \sum_i \sigma_{Mi}(r) \ . \tag{3.14}$$

A major assumption is now applied. The total conductivity (σ_M) will be taken as a constant. While the conductivities of the individual ion species (σ_{Mi}) are clearly non-constant in at least the radial direction (see Section 2.3), the sum of individual ionic current densities at any point in the system must be zero to satisfy steady-state and electroneutrality conditions. With a constant-field membrane, this implies that σ_M is a

---

[1] The field, $\vec{E}_{Mo}$, is just that maintained by the concentration gradients so that their net effect on total current flow is zero.

constant[1]. Using this assumption, the equations describing the perturbations from the resting state within the membrane are

$$\vec{J}_M = \sigma_M \vec{E}'_M \ (r,z) \tag{3.15}$$

$$\nabla^2 \Phi'_M = 0 \tag{3.16}$$

$$\vec{E}'_M = -\nabla \Phi'_M \tag{3.17}$$

where the prime denotes that the quantity is a change from the resting value, and macroscopic electroneutrality has been assumed[2]. As the conductivity is (for now) assumed invariant, it may be expressed in terms of the total conductance (g_m) across the membrane as

$$\sigma_M = g_m d \quad \text{mhos/m} \ . \tag{3.18}$$

The electric field and potential in the cell interior and exterior may similarly be expanded into a resting condition component (subscript "o") and a perturbation (primed quantity). Applying the results of Section 2.3, these quantities become

$$\vec{E}_E(r,z) = \vec{E}_{Eo} + \vec{E}'_E(r,z) = \vec{E}'_E(r,z) \tag{3.19}$$

---

[1] Otherwise there will be a build up of charge within the membrane.

[2] Some authors (see Offner [56], [57]) postulate a given mobility and/or conductivity function within the membrane and carry out one dimensional solutions in the resting state. This type of solution is close to a microscopic approach, and is not the class of problem being considered here.

$$\vec{E}_I(r,z) = \vec{E}_{Io} + \vec{E}'_I(r,z) = \vec{E}'_I(r,z) \tag{3.20}$$

$$\Phi_E(r,z) = \Phi_{Eo} + \Phi'_E(r,z) = \Phi'_E(r,z) \tag{3.21}$$

$$\Phi_I(r,z) = \Phi_{Io} + \Phi'_I(r,z) = V_r + \Phi'_I(r,z) \tag{3.22}$$

where V_r is the resting potential across the membrane. By linear superposition, the problem may be solved using equations (3.1) - (3.8) and (3.15) - (3.18) for $\vec{E}'$ and Φ' in each region, and the total electric field and potential recovered by combining the resting condition results with the perturbation solutions.

To completely specify the problem, the boundary conditions at the membrane interfaces must be given. From Section 2.2.1, the potential across these surfaces is continuous as

$$\Phi_E(a,z) = \Phi'_M(a,z) \quad (r = a) \tag{3.23}$$

$$\Phi'_I(b,z) = \Phi'_M(b,z) \quad (r = b) \tag{3.24}$$

where the perturbations in potential have been used (by linear superposition, they must satisfy the boundary conditions) and $\Phi_E = \Phi'_E$ has been applied.

The boundary conditions on normal ($\hat{r}$) current densities are complicated by the inclusion of the source terms. The electrodes are assumed to be ring structures that cause a rotationally symmetric discontinuity in normal current density across the interface. The stimulus for the problem is thus

a current source or sink just at the membrane surfaces that affects only the normal component of current at the electrode location[1]. With this source term and steady-state conditions ($\frac{\partial}{\partial t} \to 0$), these boundary conditions are (from expressions (2.113) and (2.114), Chapter 2)

$$J_{Er}(a,z) - J_{Mr}(a,z) = J_E^s(z) \tag{3.25}$$

$$J_{Mr}(b,z) - J_{Ir}(b,z) = J_I^s(z) \tag{3.26}$$

where J_E^s and J_I^s are the external and internal stimulus current densities. Applying equations (3.1), (3.2), and (3.13) for current densities, and relations (3.19) and (3.20) for perturbations of $\vec{E}_I$ and $\vec{E}_E$ leads to

$$\sigma_E E_{Er}(a,z) - \sigma_M E'_{Mr}(a,z) = J_E^s(z) \tag{3.27}$$

$$\sigma_M E'_{Mr}(b,z) - \sigma_I E_{Ir}(b,z) = J_I^s(z) \ . \tag{3.28}$$

The total problem is now specified, given the source current densities J_E^s and J_I^s. The defining equations can be summarized as

$$\nabla^2 \begin{Bmatrix} \Phi'_I(r,z) \\ \Phi'_M(r,z) \\ \Phi_E(r,z) \end{Bmatrix} = 0 \tag{3.29}$$

---

[1] The geometry and physical realization of this type of source is discussed in Section 3.2.2.

where

$$\begin{Bmatrix} \vec{E}_I(r,z) \\ \vec{E}'_M(r,z) \\ \vec{E}_E(r,z) \end{Bmatrix} = -\nabla \begin{Bmatrix} \Phi'_I(r,z) \\ \Phi'_M(r,z) \\ \Phi_E(r,z) \end{Bmatrix} \tag{3.30}$$

With boundary conditions (3.23), (3.24), (3.27), and (3.28), they form the complete set of equations to be solved in the next section.

3.2. Steady-State Electrotonic Solution in Fourier Domain

3.2.1. General Fourier Transform Solution

Several techniques might be utilized to solve the problem described in Section 3.1. These methods include separation of variables, development of a Green's function, and Fourier transform. Of these three, the Fourier transform approach proves to be the simplest and most direct. Hellerstein [30] and Clark and Plonsey [8] have used this technique on similar problems involving two volume conductor regions.

The exponential Fourier transform of a function $F(x)$ is defined with[1]

$$\mathcal{F}_k\{F(x)\} = \bar{F}(k) = \int_{-\infty}^{\infty} F(x)e^{-jkx}\,dx \tag{3.31}$$

$$F(x) = \mathcal{F}_k^{-1}\{\bar{F}(k)\} = \frac{1}{2\pi}\int_{-\infty}^{\infty} \bar{F}(k)e^{jkx}\,dk\ . \tag{3.32}$$

Derivatives with respect to the variable x are transformed as

$$\mathcal{F}_k\{\frac{\partial^n F(x)}{\partial x^n}\} = (jk)^n\bar{F}(k)\ . \tag{3.33}$$

This transform will be applied on the spatial variable z in solving the problem described in the previous section.

The equations (3.29) for the potential in each of the three compartments are all identical. Thus only one representative equation need be solved. This equation is just Laplace's equation:

---

[1] See Erdélyi et al. [21] or Churchill [7] for definitions, properties , and tables of Fourier transforms.

$$\nabla^2\Phi(r,z) = 0 \tag{3.34}$$

where Φ can represent the intracellular, membrane, or extracellular potential. Expanding the operator ∇^2 in cylindrical coordinates leads to

$$\frac{1}{r}\frac{\partial}{\partial r}\left[r\frac{\partial\Phi(r,z)}{\partial r}\right] + \frac{\partial^2\Phi(r,z)}{\partial z^2} = 0 \ . \tag{3.35}$$

Taking the Fourier transform of equation (3.35) and applying property (3.33) yields

$$\frac{\partial^2}{\partial r^2}\bar{\Phi}(r,k) + \frac{1}{r}\frac{\partial}{\partial r}\bar{\Phi}(r,k) - k^2\bar{\Phi}(r,k) = 0 \ , \tag{3.36}$$

a second order, ordinary differential equation.

Equation (3.36) has the general solution

$$\bar{\Phi}(r,k) = C_1(k)I_o(kr) + C_2(k)K_o(kr) \ , \tag{3.37}$$

where $I_o(\cdot)$ and $K_o(\cdot)$ are the zero-order modified Bessel functions[1]. $C_1(k)$ and $C_2(k)$ are the integration constants to be determined by the boundary conditions. The functions $I_o(x)$ and $K_o(x)$ have the properties that

$$\lim_{x\to\infty} I_o(x) = \infty \tag{3.38}$$

---

[1] See Abramowitz and Stegun [1] or Arfken [2] for reference to the modified Bessel functions and their defining equation.

$$\lim_{x \to o} K_o(x) = \infty \ . \tag{3.39}$$

Since on physical grounds the potential is required to be finite at $r = 0$ and $r = \infty$, the intracellular potential must have $C_2(k) = 0$ (as $r = 0 \in [0,b]$) and the extracellular case requires $C_1(k) = 0$ (as $r = \infty \in [a, \infty)$). Thus the potential for each of the three compartments may be expressed as

$$\bar{\Phi}'_I(r,k) = A(k)I_o(kr) \tag{3.40}$$

$$\bar{\Phi}'_M(r,k) = B(k)I_o(kr) + C(k)K_o(kr) \tag{3.41}$$

$$\bar{\Phi}_E(r,k) = D(k)K_o(kr) \tag{3.42}$$

where A, B, C, and D are to be determined via the boundary conditions at the membrane.

Taking the Fourier transform of boundary conditions (3.23), (3.24), (3.27), and (3.28) leads to

$$\bar{\Phi}_E(a,k) = \bar{\Phi}'_M(a,k) \tag{3.43}$$

$$\bar{\Phi}'_I(b,k) = \bar{\Phi}'_M(b,k) \tag{3.44}$$

$$\sigma_E \bar{E}_{Er}(a,k) - \sigma_M \bar{E}'_{Mr}(a,k) = \bar{J}^s_E(k) \tag{3.45}$$

$$\sigma_M \bar{E}'_{Mr}(b,k) - \sigma_I \bar{E}_{Ir}(b,k) = \bar{J}^s_I(k) \tag{3.46}$$

where $\bar{J}_E^s(k)$ and $\bar{J}_I^s(k)$ are the transforms of the source current densities (and will be specified in the next section). Boundary conditions (3.45) and (3.46) may be expressed in terms of potential by means of equations (3.30) as

$$\sigma_M \frac{\partial}{\partial r} \bar{\Phi}_M'(a,k) - \sigma_E \frac{\partial}{\partial r} \bar{\Phi}_E(a,k) = \bar{J}_E^s(k) \tag{3.47}$$

$$\sigma_I \frac{\partial}{\partial r} \bar{\Phi}_I'(b,k) - \sigma_M \frac{\partial}{\partial r} \bar{\Phi}_M'(b,k) = \bar{J}_I^s(k) \ . \tag{3.48}$$

Now the constants A(k), B(k), C(k), and D(k) are determined by applying the above boundary conditions. Substituting equations (3.40) - (3.42) into relations (3.43) and (3.44) yields

$$D(k) = B(k) \frac{I_o(ka)}{K_o(ka)} + C(k) \tag{3.49}$$

$$A(k) = B(k) + C(k) \frac{K_o(kb)}{I_o(kb)} \ . \tag{3.50}$$

Similarly, boundary conditions (3.47) and (3.48) give

$$k\sigma_M[B(k)I_1(ka) - C(k)K_1(ka)] + k\sigma_E D(k)K_1(ka) = \bar{J}_E^s(k) \tag{3.51}$$

$$k\sigma_I A(k)I_1(kb) - k\sigma_M[B(k)I_1(kb) - C(k)K_1(kb)] = \bar{J}_I^s(k) \tag{3.52}$$

where the properties $\frac{\partial}{\partial x} I_o(x) = I_1(x)$ and $\frac{\partial}{\partial x} K_o(x) = -K_1(x)$ have been applied (see Abramowitz and Stegun [1]). Rearranging equations (3.51) and (3.52) obtains

$$D = \frac{\overline{J}_E^s}{k\sigma_E K_1(ka)} + \frac{\sigma_M}{\sigma_E}\left[C - B\,\frac{I_1(ka)}{K_1(ka)}\right] \tag{3.53}$$

$$A = \frac{\overline{J}_I^s}{k\sigma_I I_1(kb)} + \frac{\sigma_M}{\sigma_I}\left[B - C\,\frac{K_1(kb)}{I_1(kb)}\right] . \tag{3.54}$$

Equations (3.49), (3.50), (3.53) and (3.54) are combined to find the constants A through D. Substituting relation (3.53) into equation (3.49) leads to

$$(\sigma_E - \sigma_M)C = \frac{\overline{J}_E^s}{k\,K_1(ka)} - \left[\sigma_E\,\frac{I_o(ka)}{K_o(ka)} + \sigma_M\,\frac{I_1(ka)}{K_1(ka)}\right]B . \tag{3.55}$$

Likewise, equations (3.50) and (3.54) yield

$$(\sigma_I - \sigma_M)B = \frac{\overline{J}_I^s}{k\,I_1(kb)} - \left[\sigma_I\,\frac{K_o(kb)}{I_o(kb)} + \sigma_M\,\frac{K_1(kb)}{I_1(kb)}\right]C . \tag{3.56}$$

Combining equations (3.55) and (3.56) gives C(k) as

$$C(k) = \frac{(\sigma_I - \sigma_M)\overline{J}_E^s(k)}{k\,K_1(ka)F(k)} - \frac{\overline{J}_I^s(k)}{k\,I_1(kb)F(k)}\left[\sigma_E\,\frac{I_o(ka)}{K_o(ka)} + \sigma_M\,\frac{I_1(ka)}{K_1(ka)}\right], \tag{3.57}$$

where F(k) is defined by

$$F(k) = \left[(\sigma_I - \sigma_M)(\sigma_E - \sigma_M) - \left(\sigma_I\,\frac{K_o(kb)}{I_o(kb)} + \sigma_M\,\frac{K_1(kb)}{I_1(kb)}\right)\left(\sigma_E\,\frac{I_o(ka)}{K_o(ka)} + \sigma_M\,\frac{I_1(ka)}{K_1(ka)}\right)\right] . \tag{3.58}$$

Using relation (3.57) in equation (3.56) then obtains

$$B(k) = \frac{-\overline{J}_E^s(k)}{k\, K_1(ka)F(k)} \left[\sigma_I \frac{K_o(kb)}{I_o(kb)} + \sigma_M \frac{K_1(kb)}{I_1(kb)}\right] + \frac{(\sigma_E - \sigma_M)\overline{J}_I^s(k)}{k\, I_1(kb)F(k)} \quad (3.59)$$

Finally, with equations (3.57) and (3.59), A(k) and D(k) are found from relations (3.54) and (3.53) as

$$A(k) = \frac{-\sigma_M \overline{J}_E^s(k)}{k^2 b\, I_o(kb)I_1(kb)K_1(ka)F(k)} + \frac{\overline{J}_I^s(k)}{k\, I_1(kb)F(k)} \left[(\sigma_E - \sigma_M) - \frac{K_o(kb)}{I_o(kb)} \left(\sigma_E \frac{I_o(ka)}{K_o(ka)} + \sigma_M \frac{I_1(ka)}{K_1(ka)}\right)\right] \quad (3.60)$$

$$D(k) = \frac{\overline{J}_E^s(k)}{k\, K_1(ka)F(k)} \left[(\sigma_I - \sigma_M) - \frac{I_o(ka)}{K_o(ka)} \left(\sigma_I \frac{K_o(kb)}{I_o(kb)} + \sigma_M \frac{K_1(kb)}{I_1(kb)}\right)\right] - \frac{\sigma_M \overline{J}_I^s(k)}{k^2 a\, I_1(kb)K_o(ka)K_1(ka)F(k)} \quad (3.61)$$

where the property $1/x = I_o(x)K_1(x) + I_1(x)K_o(x)$ has been utilized (Abramowitz and Stegun [1]).

With the constants A through D given above, the potential in each compartment is found by taking the inverse Fourier transforms of each potential:

$$\phi_I'(r,z) = \frac{1}{2\pi} \int_{-\infty}^{\infty} A(k) I_o(kr) e^{jkz} dk \quad (3.62)$$

$$\phi'_M(r,z) = \frac{1}{2\pi} \int_{-\infty}^{\infty} [B(k)I_o(kr) + C(k)K_o(kr)]e^{jkz}dk \qquad (3.63)$$

$$\phi_E(r,z) = \frac{1}{2\pi} \int_{-\infty}^{\infty} D(k)K_o(kr)e^{jkz}dk \ . \qquad (3.64)$$

As the expressions in transform (k) space are quite complicated, it is not possible to invert these solutions analytically[1]. The only recourse is to use a digital computer and perform the inversions numerically. This is carried out in Section 3.3. However, first the source current densities $\overline{J}_I^s(k)$ and $\overline{J}_E^s(k)$ and the electrodes that supply them must be specified, as the exact form of the solution is determined by the stimulus functions.

It is also possible to specify the electric field and current density of each region in transform space. Applying relation (3.30) and property (3.33) to equations (3.62) - (3.64) gives

$$E_{Ir}(r,z) = -\frac{1}{2\pi} \int_{-\infty}^{\infty} k\, A(k)I_1(kr)e^{jkz}dk \qquad (3.65)$$

$$E_{Iz}(r,z) = -\frac{1}{2\pi} \int_{-\infty}^{\infty} jk\, A(k)I_o(kr)e^{jkz}dk \qquad (3.66)$$

$$E'_{Mr}(r,z) = -\frac{1}{2\pi} \int_{-\infty}^{\infty} k[B(k)I_1(kr) - C(k)K_1(kr)]e^{jkz}dk \qquad (3.67)$$

$$E_{Mz}(r,z) = -\frac{1}{2\pi} \int_{-\infty}^{\infty} jk[B(k)I_o(kr) + C(k)K_o(kr)]e^{jkz}dk \qquad (3.68)$$

$$E_{Er}(r,z) = \frac{1}{2\pi} \int_{-\infty}^{\infty} k\, D(k)K_1(kr)e^{jkz}dk \qquad (3.69)$$

---

[1] Hellerstein [30] shows that with a series of approximations, a simpler two-compartment model reduces to the cable equations for electrotonus. These approximations will not apply in the general case (especially near the electrodes) as the integration range is infinite.

$$E_{Ez}(r,z) = -\frac{1}{2\pi}\int_{-\infty}^{\infty} jk\, D(k)K_o(kr)e^{jkz}dk \ . \qquad (3.70)$$

The current density at any point is obtained by multiplying the electric field at that location with the appropriate conductivity for the region. It is easier and more accurate to obtain electric field or current density from equations (3.65) - (3.70) with numerical integration than to use relations (3.62) - (3.64) to first find potential and (numerically) differentiate for electric field. The most commonly specified parameter in neural theory is V_m, the transmembrane potential, so that most results in this present report will be found by inverting equations (3.62) - (3.64) for potential.

3.2.2. Electrodes and Source Current Densities

The solutions of the previous section are for perturbations in potential that arise when an externally supplied source current density is used as a stimulus. The source was handled in a general fashion and was not specified. This section defines the stimuli and the types of electrodes that supply them.

In Section 3.1, the source terms $J_E^s(z)$ and $J_I^s(z)$ were defined in boundary conditions (3.25) and (3.26) as axially symmetric discontinuities in the normal component of current density across either of the membrane interfaces. The symmetry condition requires that the stimulus be applied via a ring structure placed on the membrane surface involved. The best physical realization of this type of source is a flat metallic ring electrode supplying the source current and located at the membrane. This structure is indicated in Figure 3.2 for the extracellular case. The electrode is specified as a flat wire so that it supplies only a normal current density to the membrane interface region of its location. This neglects end effects (at the electrode edges) and assumes the electrode is wide with respect to its thickness[1].

It is recognized that an electrode of this nature would be difficult to realize at the intracellular-membrane interface. As indicated in Section 3.1, the work of Eisenberg and Johnson [20] suggests that the solution will be independent of electrode

---

[1] For a metal that is a good conductor, the $\vec{E}_{tan} \doteq 0$ boundary condition at the surface of the electrode forces the current density to be normal across that interface (see King [41]). A thin flat wire as depicted in Figure 3.2 thus supplies only a radially oriented current density (neglecting the edges).

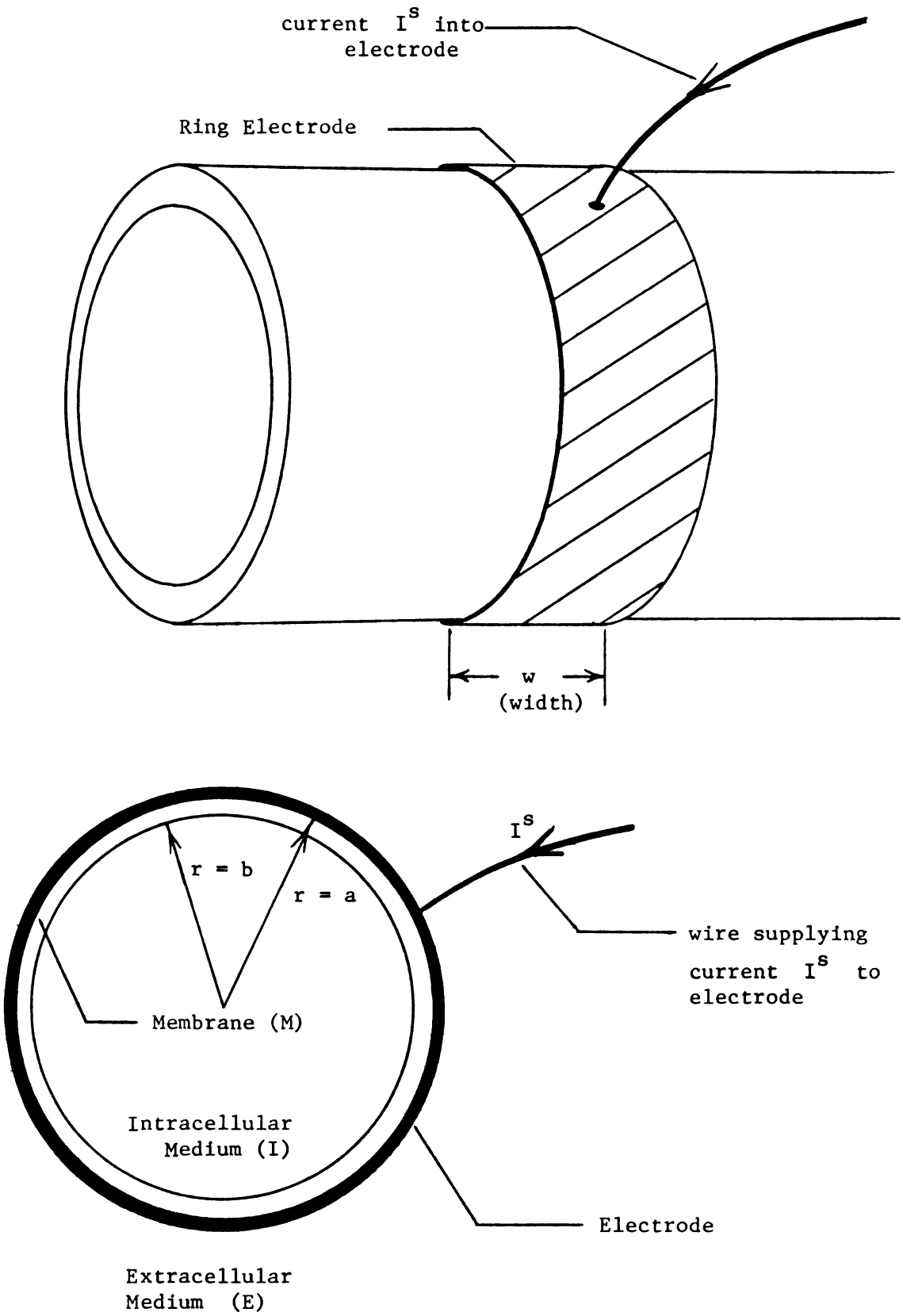

FIGURE 3.2

Extracellular Ring Electrode

geometry for axial distances farther than the cell diameter from the stimulus[1]. Furthermore, if the internal stimulus is supplied via a point electrode (micropipette) located at the cell axis, the response will be the same at a much closer distance to the source. Thus the solution for the change in potential due to an internal ring electrode will be electrode dependent only at points very close to the stimulus. The interior electrode is defined in this manner as this situation is similar to a source supplied by a change in membrane conductance (as seen in the action potential or post synaptic potentials, see Chapter 5).

The source functions in the transform domain are needed to complete the solutions in Section 3.2.1. Assuming that the source current density is uniform (constant) over the surface of the electrode and with the geometry as defined in Figure 3.3, the Fourier transform of either $J_I^s(z)$ or $J_E^s(z)$ is

$$\mathcal{F}_k\{J^s(z)\} = \overline{J}^s(k) = \int_{-\infty}^{\infty} J^s(z)e^{-jkz}dz$$

$$= J^s \int_{-w/2}^{w/2} e^{-jkz}dz$$

$$= \frac{2J^s}{k} \sin(k\, w/2) \qquad (3.71)$$

where $J^s(z)$ represents either $J_I^s(z)$ or $J_E^s(z)$, J^s is defined as the magnitude of the current density, and w is the width of the electrode. This gives the k-space source current densities as

---

[1] Their comparison was to the results for the cable equation that assumes an axially symmetric stimulus often modeled as a ring electrode (see Plonsey [60]).

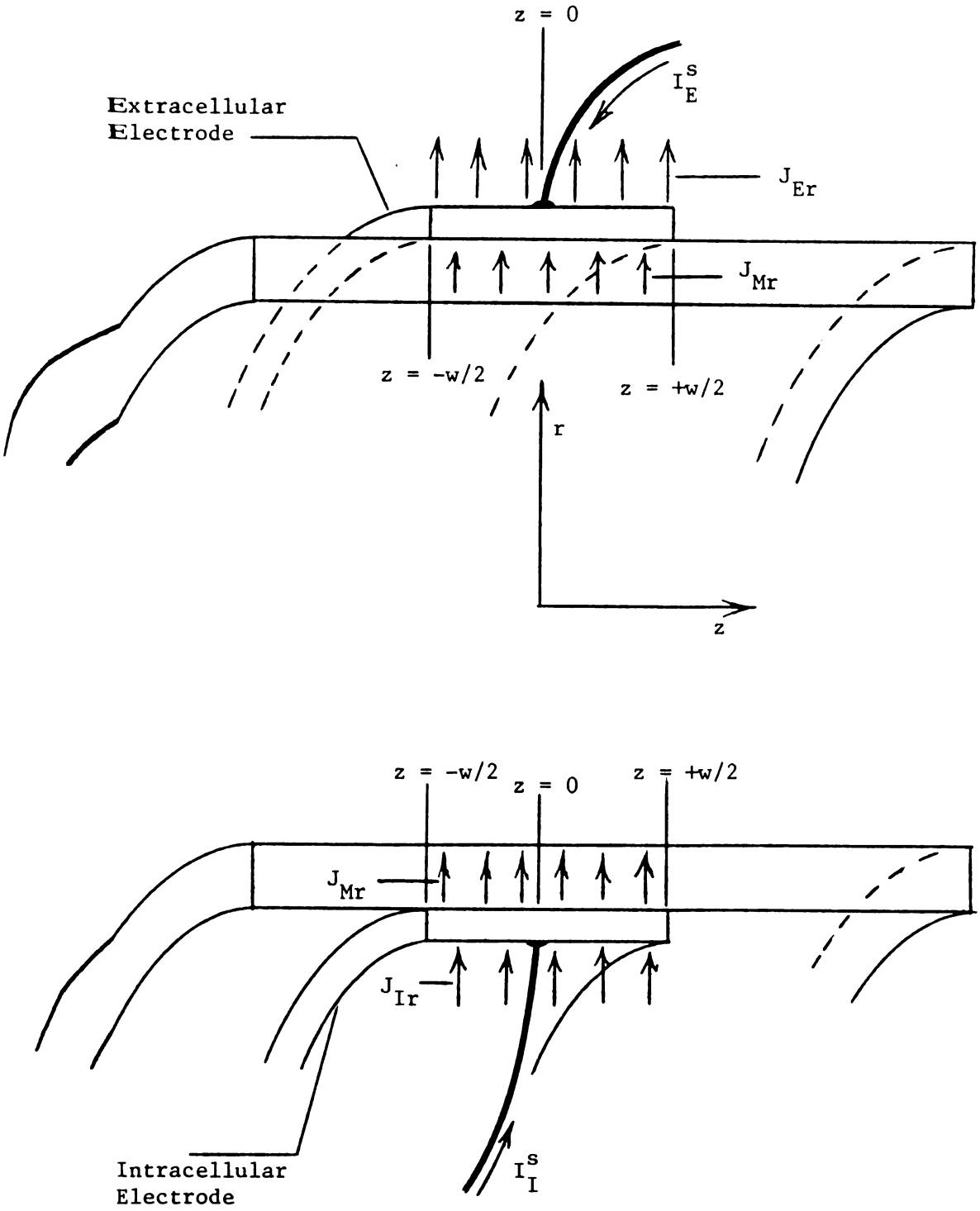

FIGURE 3.3

Cross-Sections of Intracellular and Extracellular Electrode Geometries

$$\overline{J}_I^s(k) = \frac{2J_I^s}{k} \sin(k\,w/2) \tag{3.72}$$

$$\overline{J}_E^s(k) = \frac{2J_E^s}{k} \sin(k\,w/2) \tag{3.73}$$

for an electrode centered on $z = 0$ and supplying a uniform normal current density. If the center of the electrode is not at $z = 0$, the transform domain functions (3.72) and (3.73) must be slightly altered. The Fourier shifting property is defined with

$$\mathcal{F}_k\{F(x + c)\} = \overline{F}(k)e^{jck} \quad (c \text{ real}) \,. \tag{3.74}$$

Applying relationship (3.74) to equations (3.72) and (3.73) for an electrode with center at $z = \ell$ gives

$$\overline{J}_I^s(k) = \frac{2J_I^s}{k} \sin(k\,w/2)e^{-j\ell k} \tag{3.75}$$

$$\overline{J}_E^s(k) = \frac{2J_E^s}{k} \sin(k\,w/2)e^{-j\ell k} \,. \tag{3.76}$$

Thus using linear superposition and relations (3.75) and (3.76) it is possible to construct a source that represents any number of intracellular and/or extracellular stimulating electrodes located at various positions ℓ from $z = 0$.

It remains to define the source magnitudes J_I^s and J_E^s. The stimulating circuit may be modeled as a battery connecting two electrodes; supplying one (a "source" electrode) with a total current I^s and the second (a current "sink") providing the return

path to complete the circuit. If the current I^s is defined as positive when it flows toward the electrode, then the current density magnitudes are

$$J_I^s = \frac{I_I^s}{w2\pi b} \quad \text{amps/m}^2 \tag{3.77}$$

$$J_E^s = \frac{I_E^s}{w2\pi a} \quad \text{amps/m}^2 \tag{3.78}$$

since (for a uniform current density) J^s is just the total current divided by electrode surface area. For the case where J^s is specified, the total current is found as

$$I_I^s = J_I^s \, w2\pi b \quad \text{amps} \tag{3.79}$$

$$I_E^s = J_E^s \, w2\pi a \quad \text{amps} \; . \tag{3.80}$$

That the sign convention implied in relations (3.77) - (3.81) is valid may be demonstrated by considering the definitions (3.25) and (3.26) of J^s as a current density discontinuity at an interface forced by the electrode. Since the membrane has a much lower conductivity than the interior or exterior volume conductors, it may be considered an effective insulator with respect to those regions[1]. A positive I_I^s current will thus result in an inward $(-\hat{r})$ directed electrode current density; a condition satisfied by

---

[1] In fact the membrane is a very good dielectric, as it was demonstrated in Section 2.2.2 that it supports an electric field on the order of 10^6 volts/meter.

boundary condition (3.26) for a positive J_I^s (consider $J_{Ir} - J_{Mr} = -(J_I^s)$, clearly giving a net inward current for $J_I^s > 0$). Similarly an $I_E^s > 0$ gives a net outward current density at the extracellular interface as seen in boundary condition (3.25).

The electrodes used in other authors' solutions have all been infinitely narrow (see Hellerstein [30], Plonsey [60]). This type of electrode is modeled as supplying a source current

$$J^s(z) = J^s\delta(z) \quad \text{amps/m}^2 \tag{3.81}$$

where $\delta(z)$ is the Dirac delta function. While this goemetry simplifies the solutions, it causes a discontinuity in potential, electric field, and current as it postulates an infinite current density at one point $(z = 0)$[1]. Another objection is that a very narrow electrode cannot be expected to deliver only a normal $(\hat{r})$ current density. Despite these difficulties, it is included as a possible source term primarily for comparison to previous work. It may be considered as the limiting case for the finite-width electrode defined in equation (3.71) as $w \to 0$. Taking the Fourier transform of equation (3.81) gives

$$\overline{J}^s(k) = J^s \tag{3.82}$$

where J^s, in terms of the total current I^s supplied to the electrode, is determined as

---

[1] This can be demonstrated in transform space, see Appendix B.

$$J_I^s = \frac{I_I^s}{2\pi b} \quad \text{amps/m} \tag{3.83}$$

$$J_E^s = \frac{I_E^s}{2\pi a} \quad \text{amps/m} \ . \tag{3.84}$$

Note that the delta function has units of 1/meter (Arfken [2]).

It will be easiest to invert the solutions of Section 3.2.1 when only one electrode at the membrane is used. The return path for the current to the generator will then be supplied via an electrode in the extracellular medium at infinity. The validity of this approach is seen by considering one electrode (intracellular or extracellular) centered at $z = 0$ as the current source and a second electrode at $z = +\ell$ on the exterior interface as the current sink. Taking the limit as $\ell \to \infty$, it is apparent from the shifting property (3.76) that the effects due to this electrode will decay to zero as it is moved to infinity[1]. Thus with the source functions as defined in this section the solutions (3.62) - (3.64) yield the perturbation from the resting potential that would be measured between a point electrode at (r,z) and a reference electrode at infinity when the system is stimulated by an electrode centered on $z = 0$ at the membrane[2]. The case of any other current

---

[1] Integration of the sine and cosine terms from $e^{-j\ell k}$ in the inversion yields zero for $\ell \to \infty$ as the sinusoid's period goes to zero (see Arfken [2]).

[2] This situation may be realized in an experimental situation by using a combined reference and current-return electrode in the interstitial fluid (bathing solution about the nerve fiber) at a point away from the stimulus electrode (see Plonsey [60], Taylor [76]).

source and sink electrodes may be handled by linear superposition and shifting the inverted solution (in z-space) to the electrode's location.

3.3. Numerical Inversion of the Fourier-Domain Solution and Results

3.3.1. Methodology of Inversion; Test Data for Axon

The only way to obtain the inverse of the Fourier-domain solutions found in Section 3.2 is to perform the integrations required on a digital computer with numerical techniques. This section discusses briefly the programming involved and also defines the test parameters used for the results presented in the remainder of this chapter.

Equation (3.32) for the inverse Fourier integral can be expanded by means of Euler's formula into two integrals as follows:

$$F(x) = \mathfrak{F}_k^{-1}\{\bar{F}(k)\} = \frac{1}{2\pi}\int_{-\infty}^{\infty}\bar{F}(k)\cos(kx)dk + \frac{j}{2\pi}\int_{-\infty}^{\infty}\bar{F}(k)\sin(kx)dk. \quad (3.85)$$

The solutions for potential (3.62) - (3.64) are all even functions of k when the source terms $J_I^s(k)$ and $J_E^s(k)$ are even functions[1]. For the case of a single stimulating electrode centered on $z = 0$, these source functions are symmetric in k-space (see equations (3.72), (3.73) and (3.82)). Thus the inversion integral reduces to

$$F(x) = \frac{1}{\pi}\int_0^{\infty}\bar{F}(k)\cos(kx)dk \quad (3.86)$$

where $\bar{F}(k)$ is required to be an even function[2].

---

[1] For the mathematical details of this material, refer to Appendix B.

[2] Since $\Phi(r,z)$ is a real function, with the symmetry condition the potential functions and stimulus functions in k-space must be real functions as well. This simplifies the numerical inversions as it is not necessary to use complex variables on the computer.

The inverse transforms as actually programmed on the computer have the form

$$\Phi(r,z) = \frac{1}{\pi}\int_{\delta}^{2\pi/z} \bar{\Phi}(r,k)\cos(kz)dk + \sum_{n=1}^{N} \frac{1}{\pi}\int_{2n\pi/z}^{2(n+1)\pi/z} \bar{\Phi}(r,k)\cos(kz)dk. \tag{3.87}$$

Equation (3.87) embodies two approximations and a strategic choice for segmenting the integration. The approximation is to start the integration at a small number δ instead of at $k = 0$. This is necessary as the integrand diverges as $\ell n(ka)$ for $k \to 0$. Such a curve is integrable analytically, but the computer cannot handle the singularity of the integrand at zero. By choosing δ very close to zero ($\delta = 10^{-9}$ was used in all the numerical results in this thesis) the error becomes vanishingly small.

The second approximation inherent in expression (3.87) is that the upper integration limit has been made finite. Error introduced by this truncation of the infinite integral is insignificant if the cut-off point is high enough[1]. This truncation point is determined in the integration routine by a criterion linked to the segmentation of the integration interval. These sub-intervals are taken as one period (2π radians) of the cosine function and the integration is terminated when the contribution of the $(N + 1)$ segment is minuscule as compared to the total area given by the previous N sub-intervals. By integrating in this piecewise

---

[1] See Appendix B for a complete discussion of error determination, including error bounds for truncation and starting at δ.

fashion, the termination criterion is met when the integrand has either effectively decayed to zero or is essentially constant over the period of the cosine. In the case of the particular functions that arise in the problem under consideration, this method of truncation can be made to give any accuracy desired. The net error from these two approximations (starting at δ, and truncating the infinite upper limit) is easily made negligible (make δ small, chose % of total area very small for cut-off) so that the overall error is determined by the accuracy of the integration routine on any given segment.

For the type of k-space functions encountered in this report, it was found (by trial and error) that the most efficient[1] numerical integration routine is an adaptive Simpson's rule. The theory and algorithm of this process is given in Davis and Rabinowitz [16]. This integrator is adaptive in the sense that it automatically takes smaller steps in the integration process for regions where the integrand has a large slope. Appendix C lists this integration function in Fortran Extended Language as used by the author on a Control Data 6500 computing system[2].

The overall computer program may now be described as follows. First the program reads in the cell parameters (radius, membrane thickness, conductivities, etc.), the stimulus intensity, and the

---

[1] Efficient in the sense of the least computer time involved for a given accuracy. As many numerical inversions were required for the results presented, this became an important factor.

[2] This program is from Davis and Rabinowitz [16], modified for the CDC 6500 computer and has had some minor programming errors removed.

z-points at which the solution is desired. For each position z, the k-space function is integrated by means of the adaptive Simpson's rule function on the interval zero to $2\pi/z$ (if $z = 0$, the interval is determined by the period of the sine function in $J^S(k)$ as $4\pi/w$, see equation (3.71)). This integration process then repeats for successive intervals of $2\pi/z$ width until the truncation criterion is met. For most cases, the functions integrated were $\overline{\Phi}_I(b,k)$ and $\overline{\Phi}_E(a,k)$ so that the transmembrane potential, $V_m(z) = \Phi_I(b,z) - \Phi_E(a,z)$, could be obtained. The integrand is supplied to the program as a separate function called by the Simpson's rule integrator[1].

To simplify comparisons between results, it is appropriate to define a "test axon" consisting of standardized parameters. Variations from this standard normally involve changing only one parameter, allowing the effect to be easily discerned. The largest amount of experimental data and theoretical results are available for the giant axon of Loligo. For the remainder of this chapter and all of the next, this squid axon is used as the "test fiber". A standardized stimulus intensity is also defined in terms of the total current I^S supplied to any electrode.

The parameters for the cell that are necessary to complete the solutions for steady-state electrotonus are σ_I, σ_E, σ_M, a, b, and the stimulus intensity I^S. Katz [40] was used as the reference for the appropriate cell properties, their being found on pp. 46-47. These are given as:

---

[1] For further details on programming, see Appendix C.

$$R_i = \frac{1}{\sigma_I} = 30 \quad \text{ohm-cm}$$

$$R_o = \frac{1}{\sigma_E} = 22 \quad \text{ohm-cm} \tag{3.88}$$

$$R_m = \frac{1}{g_m} = 700 \quad \text{ohm-cm}^2$$

$$a = 250\mu = 0.25 \text{ mm} .$$

Solving for σ_I, σ_E, and σ_M (from equation (3.18) $\sigma_M = g_m d$) with $d = 50$ Å (again from Katz [40]) yields

$$\sigma_I = 3.333 \times 10^{-2} \quad \text{mhos/cm}$$

$$\sigma_E = 4.546 \times 10^{-2} \quad \text{mhos/cm}$$

$$\sigma_M = 7.143 \times 10^{-10} \quad \text{mhos/cm} \tag{3.89}$$

$$a = 0.25 \text{ mm}$$

$$d = 50 \text{ Å}$$

as the "test axon" parameters. The stimulating current standard is taken as 10^{-5} amps, giving about a 40 mv perturbation in the transmembrane potential for the intracellular electrode case. After Section 3.3.3 the electrode width w is taken as 0.5 mm, this being a more realistic and realizable dimension than a narrower wire. Additions to this parameter list (as are necessary for the time varying case, Chapter 4) will be made as needed, and the entire set is listed in Appendix D.

3.3.2. Electrotonic Potential for the Case of an Internal Electrode

This section examines the solutions (3.62) - (3.63) for perturbations in scalar potential caused by a stimulus supplied via an electrode at the interior membrane interface. In all instances, the total current I_I^s into the electrode is held constant at 10^{-5} amps. As the solutions are linear and directly proportional to stimulating current, the result for any other stimulus intensity can be found by multiplying the presented results with the ratio of the new current to 10^{-5} amps. Likewise, the effect of multiple electrodes may be handled by linear superposition.

Nearly all previous models of electrical events associated with neurons have used the transmembrane potential as the end result. Experimentally, this quantity can be measured by the use of an intracellular microelectrode. The perturbation in transmembrane potential from the resting potential is illustrated in Figure 3.4 for the standard axon with a 0.5 mm wide internal stimulating electrode. The curve has a maximum value of 40.5 mV and decays in an exponential fashion for increasing z. The solution is symmetric about $z = 0$. A length constant λ may be found as 5.4 mm for this test axon, λ being defined as the distance required for an e^{-1} decay in the solution from its value at any point. With regard to a cable theory for the same axon, the result (including length constant) is the same to three significant figures for $z > 1$ mm. For regions near the electrode the theories diverge.

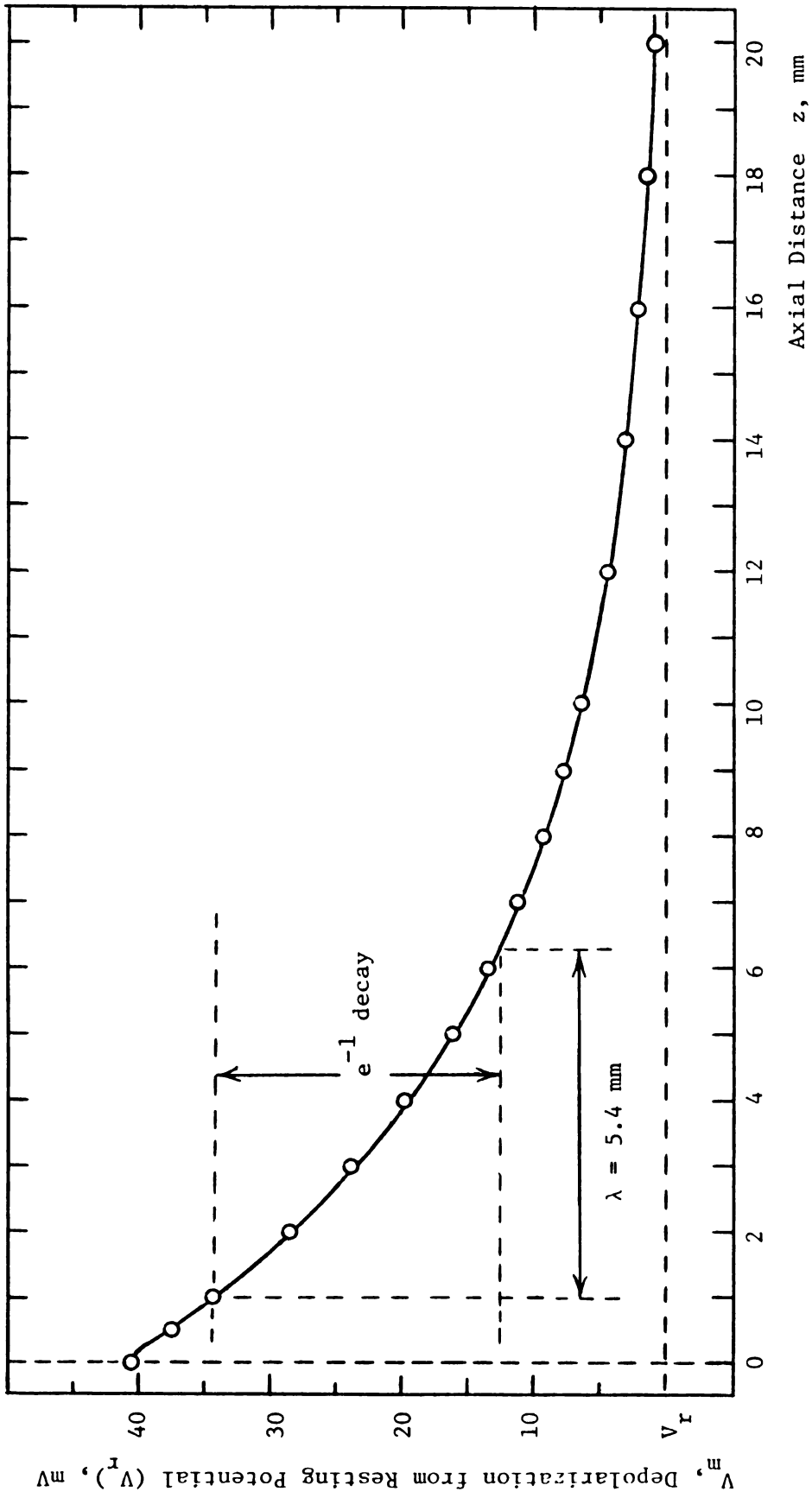

FIGURE 3.4

Transmembrane Potential as a Function of z for a 0.5 mm Wide Internal Electrode

The curve in Figure 3.4 was obtained by inverting solutions (3.62) and (3.64) for $\Phi_I(b,z)$ and $\Phi_E(a,z)$ and using the definition

$$V_m(z) = \Phi_I(b,z) - \Phi_E(a,z) \tag{3.90}$$

to obtain transmembrane potential. In this manner, the model also provides the scalar potential at either side of the membrane. Figure 3.5 is a plot of $\Phi_E(a,z)$ for the same situation as in Figure 3.4. The most apparent feature of this illustration is that the extracellular potential is on the order of 10^3 smaller than the transmembrane potential. For the resolution inherent in the size of these diagrams, this gives Figure 3.4 as also being a plot of $\Phi_I(b,z)$, as for this axon with interior stimulus

$$V_m(z) \doteq \Phi_I(b,z) \ . \tag{3.91}$$

Note that Figure 3.4 gives the perturbation from the resting potential using $\Phi_I = \Phi_I' + V_r$ (see equation (3.22)) while Figure 3.5 plots Φ_E (as $\Phi_E = \Phi_E'$, see equation (3.21)).

Figure 3.5 also indicates that the extracellular potential decays at a slower rate than V_m or Φ_I. The length constant for $\Phi_E(a,z)$ is on the order of 8.5 mm as compared to 5.4 mm for V_m. An extracellular recording electrode would measure Φ_E and thus give a larger length constant than an intracellular recording electrode. Cable theory predicts that Φ_I, Φ_E, and V_m will all decay at the same rate (with length constant λ, see Plonsey [60]).

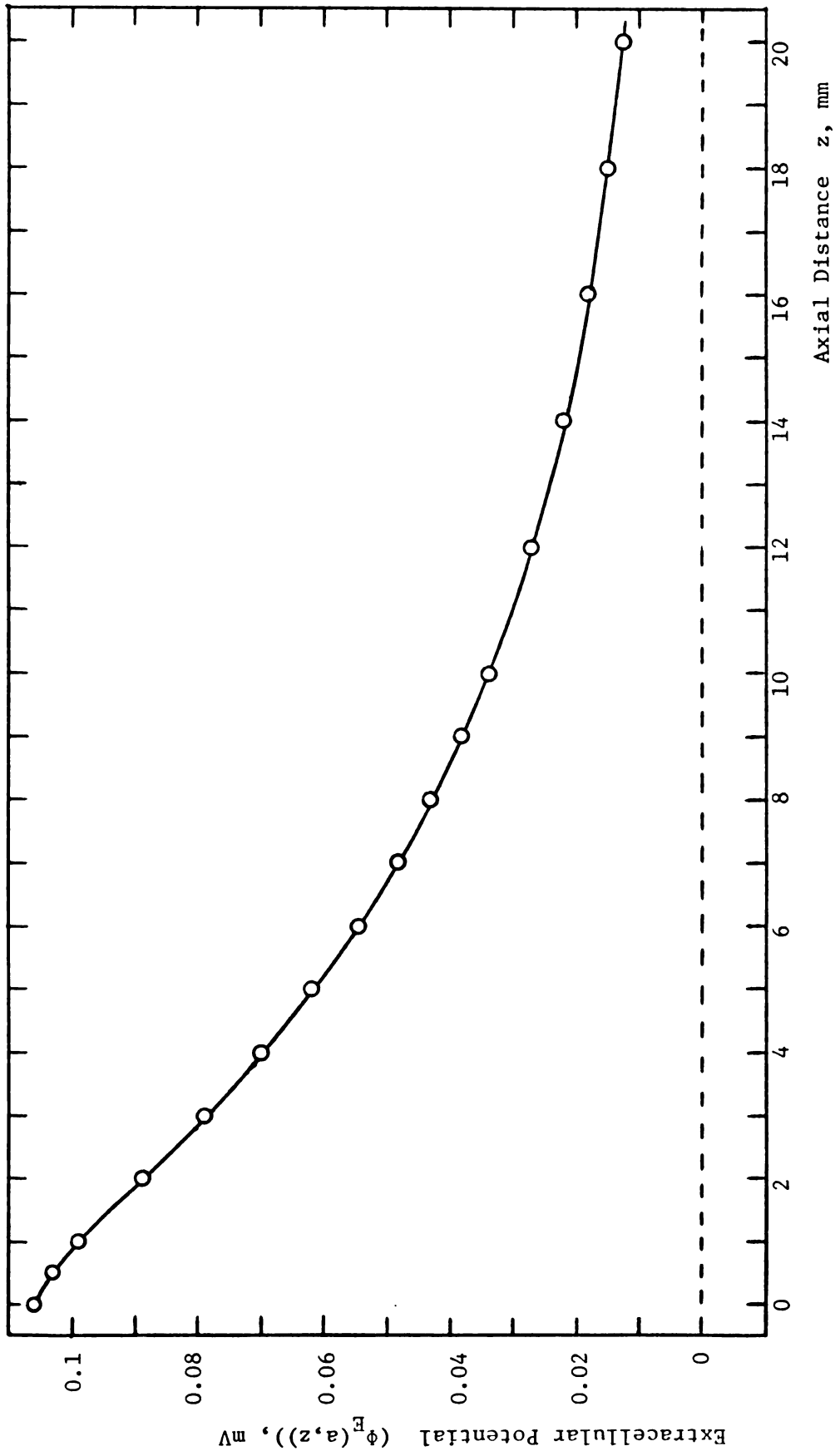

FIGURE 3.5

$\Phi_E(a,z)$ for a 0.5 mm Wide Internal Electrode

The Fourier-transform model shows that the length constant of cable theory will only be correctly measured by means of an intracellular electrode. The two models differ in predicting $\Phi_E(a,z)$ because of an inaccurate assumption in cable theory that the extracellular medium exhibits only axial current flow. This will be further discussed later in this chapter.

An effect seen with this model is that the potential near the electrode varies with the size of the electrode. As is indicated in Figure 3.6, decreasing the width of the electrode causes an increase in V_m at the electrode. This is due to an increase in J_I^s as the surface area of the electrode shrinks ($J_I^s = I_I^s/2\pi bw$, for I_I^s fixed J_I^s increases for decreasing w). As the width of the electrode goes to zero, the potential at the electrode develops a singularity in that it diverges to infinity[1]. This expresses the fact that it would take an infinite potential to drive a finite amount of current (I_I^s) through an electrode of zero surface area. As previous field solutions have all used a delta function type of stimulus, they exhibit this same singularity[2]. Only with a finite width electrode will V_m at $z = 0$ be finite and E_z at $z = 0$ be defined.

Another property of this model as seen in Figure 3.6 is that the potential over the surface of the electrode is nearly

---

[1] What actually happens is that $\Phi_I(b,0) \to \infty$ as $w \to 0$ giving $V_m \doteq \Phi_I \to \infty$. See Appendix B for analytical proof.

[2] Eisenberg and Johnson [20] used point source electrodes (three-dimensional delta functions); Hellerstein [30] used a ring source represented by a delta function in z.

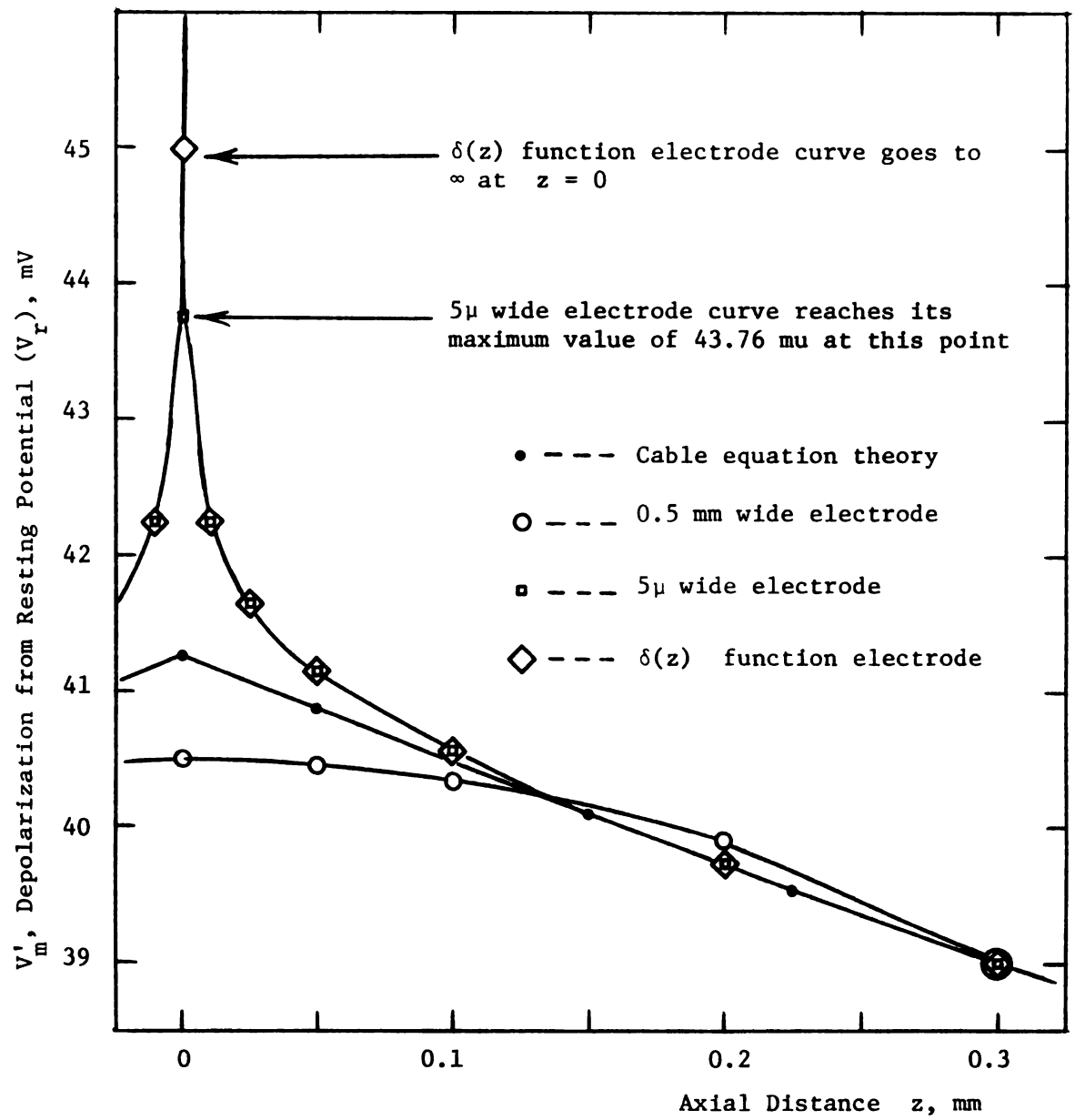

FIGURE 3.6

Transmembrane Potential as a Function of z for Various Electrode Widths, Interior Stimulus

constant. These solutions are for a constant current density supplied by the stimulating electrode over its entire surface. For any near-ideal conductor, the potential should be constant as $\vec{E} \doteq 0$ within the conductor. Thus a constant current density is seen to give essentially the same result as a perfect conductor electrode which would clamp the potential $(\Phi_I(b,z))$ at a constant over its surface area. Note that the potential falls very rapidly beyond the edge of the electrode, as is seen especially in the case of a 5μ wide electrode.

As mentioned above, the transmembrane potential variation predicted by this model matches very closely that predicted by the cable equation. The cable equation is based upon a core-conductor model that represents the nerve fiber as a distributed electrical network. The intracellular and extracellular media are assumed to carry only z-directed currents and are described by resistances per unit length. The membrane connects these two media with a distributed R-C network consisting of a shunt resistance in parallel with a shunt capacitance per unit length[1]. The response of this network to a steady-state current I_o injected into the intracellular region is given by Eisenberg and Johnson [20] as

$$V_m(z) = \frac{I_o}{\pi a}\sqrt{\frac{R_m R_i}{2a}}\, e^{-|z|/\lambda} \qquad (3.92)$$

where $\lambda = \sqrt{\frac{R_m a}{R_i 2}}$, R_m is the resistance per unit area for the

---

[1] See Lorente de No [48] or Plonsey [60] for a complete discussion of cable theory and the core-conductor model. Figure 4.1 in Chapter 4 illustrates the equivalent circuit.

membrane, and R_i is the resistivity of the intracellular medium[1]. As shown in Figure 3.6, the cable equation result diverges from the field solution near the electrode. Core-conductor theory yields a discontinuity in the z-component of electric field at $z = 0$ as the slope in the potential abruptly changes from negative to positive at that point[2]. This is contrasted with the field-solution model that gives $E_z = 0$ at $z = 0$ for a finite-width electrode and a variation in $V_m(0)$ with electrode width. Note that by $z = 0.3$ mm, all cases including cable theory converge to the same curve. For distances greater than 1 mm, the curves match to three significant figures and are exponentially decaying with $\lambda = 5.4$ mm as predicted by the cable equation for this axon (see Figure 3.4).

The steady-state electrotonus solution by Eisenberg and Johnson [20] took the conductivity of the external media as infinitely large. In many instances, the external resistance in the core-conductor network is similarly set to zero. This is because the net extracellular resistance to current flow when the nerve fiber is immersed in a large volume conductor is both very small and difficult to model as a resistor in a network model (see Clark

---

[1] This result is 0.5 times that presented by Eisenberg and Johnson [20] as their model was a semi-infinite axon that allowed current flow only in the +z direction. For an axon infinite in both directions from the stimulus, current flows equally in each direction reducing the solution by 1/2. Also the extracellular region is taken as a perfect conductor due to its large volume (see Plonsey [60], Rall [65]).

[2] The cable equation solution (3.92) uses a delta function stimulus at $z = 0$, giving this effect.

and Plonsey [8], Rall [65]). The effect on V_m of varying σ_E in the Fourier transform solution of this report was seen to be negligible for σ_E in the range of 0.001 mhos/cm to an infinite conductivity. The result of changing σ_E was to alter very slightly the magnitude of $\Phi_I(b,z)$ and it produced a large change in $\Phi_E(a,z)$ (for $\sigma_E = \infty$, $\Phi_E(a,z) = 0$, so percentage-wise the change was very large). However, $\Phi_E(a,z)$ remained far smaller than $\Phi_I(b,z)$ and the variance of each was such that $V_m(z)$ was almost completely unaltered. As an example, for the test axon and standard 0.5 mm internal electrode $\Phi_I(b,0) = 40.569$ mV, $\Phi_E(a,0) = 0.106$ mV and $V_m(0) = 40.464$ mV ($\sigma_E = 0.0455$ mhos/cm). Increasing σ_E to infinity gave $\Phi_I(b,0) = 40.535$ mV, $\Phi_E(a,0) = 0$, and $V_m(0) = \Phi_I(b,0)$. Thus while Φ_E decreased 100%, Φ_I decreased 0.26% and V_m changed only 0.18%.

An advantage of the Fourier transform field solution is that it easily allows examination of the potential at any point in the system, yielding the entire potential field in and about the cell. Figures 3.7 and 3.8 illustrate the z-variation in the perturbation of potential for the center of the cell, midway through the membrane, and at twice and four times the cell's external radius[1]. The radial variation of potential is more clearly seen in Figures 3.9 - 3.11, where the change in potential produced by the stimulus is plotted as a function of r for four values of z ($z = 0$, 1 mm, 5 mm

---

[1] Figure 3.7 gives Φ_I' and Φ_M'. Φ_I is recovered as $\Phi_I = \Phi_I' + V_r$. Also $\Phi_M = \Phi_M' + \Phi_{Mo}$ where Φ_{Mo} is given in Section 2.3.

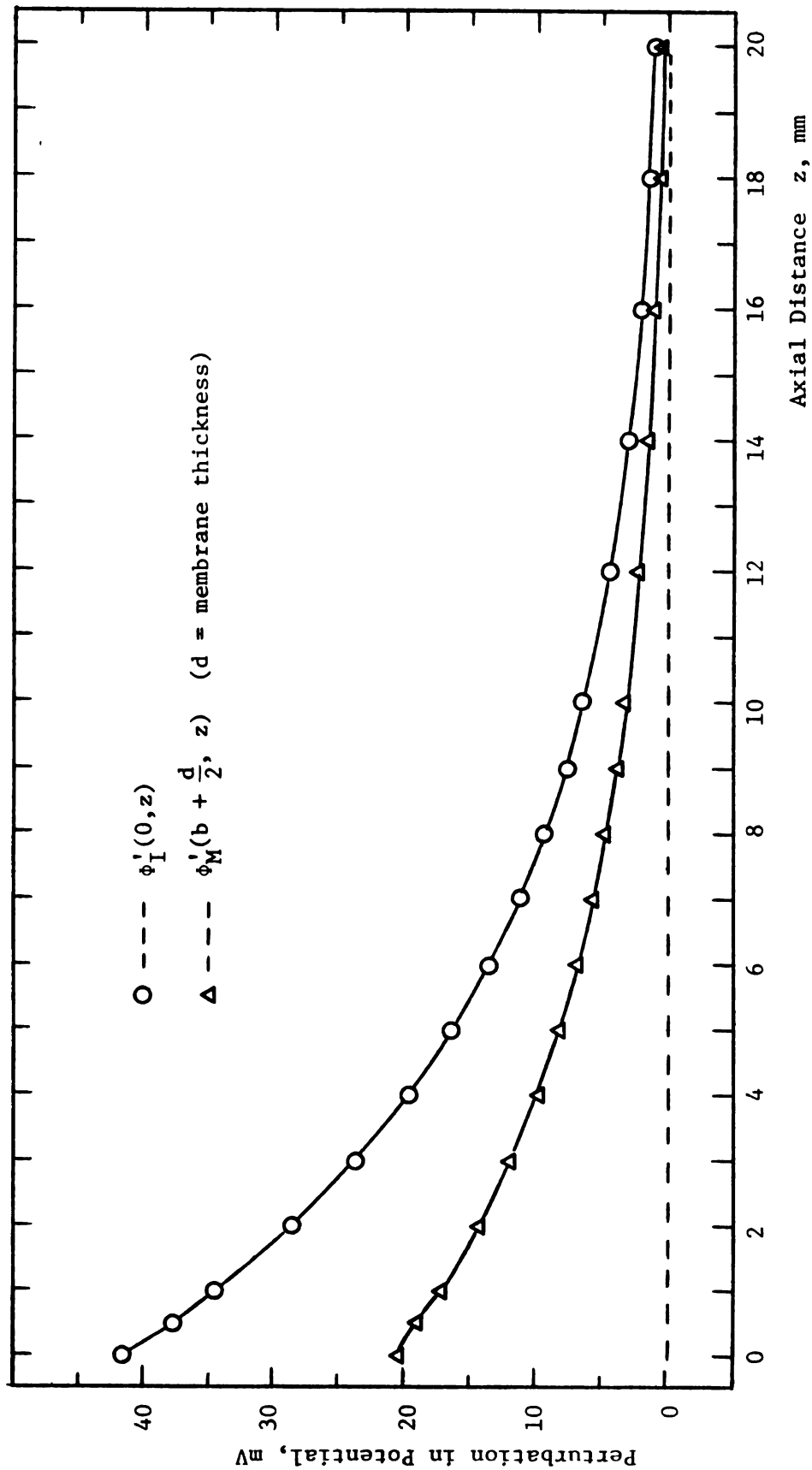

FIGURE 3.7

Potential at the Cell Axis and Mid-Membrane as a Function of z for a 0.5 mm Wide Internal Electrode

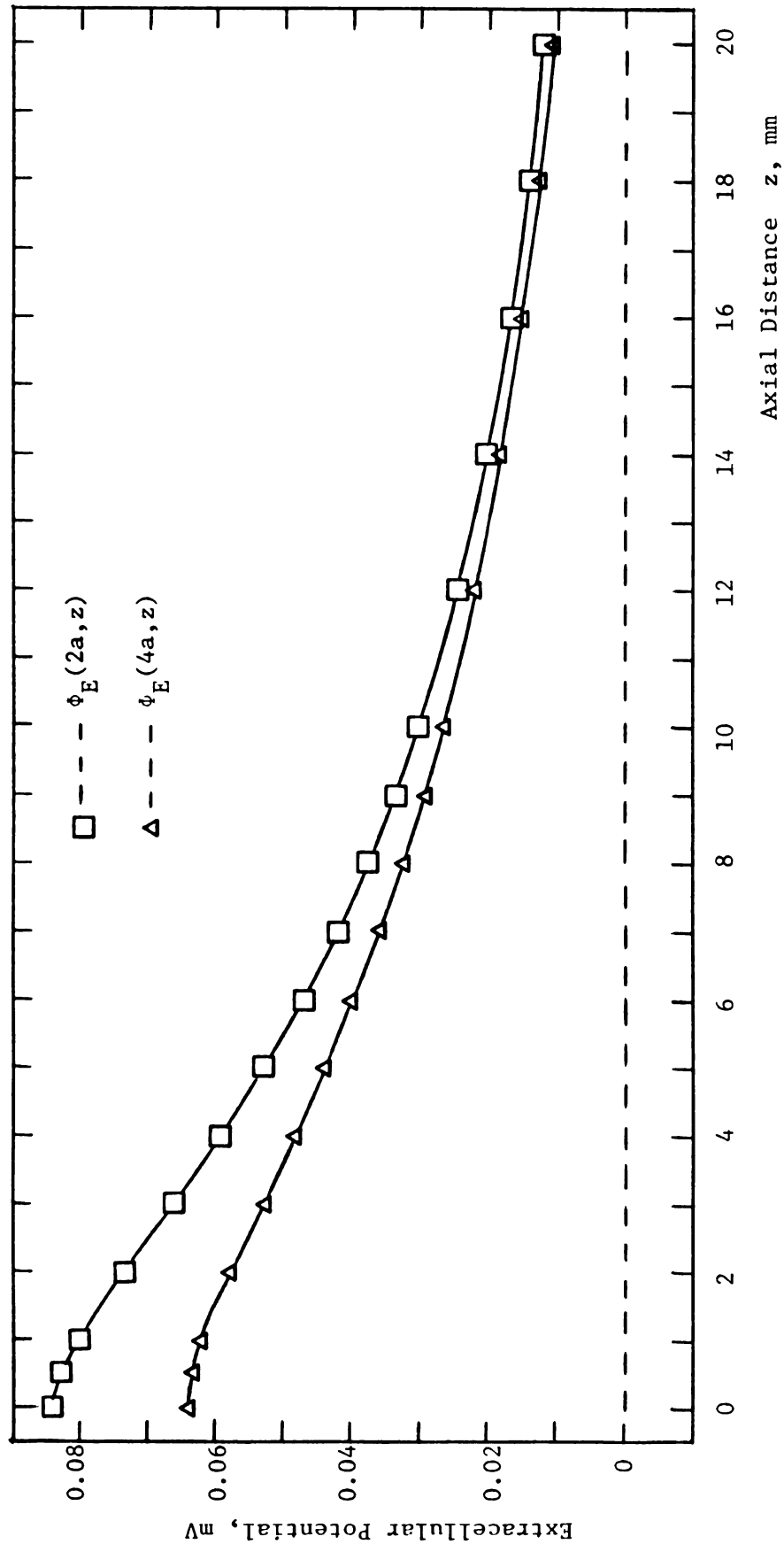

FIGURE 3.8

Extracellular Potential at Twice and Four Times the Cell Radius as a Function of z for a 0.5 mm Wide Internal Electrode

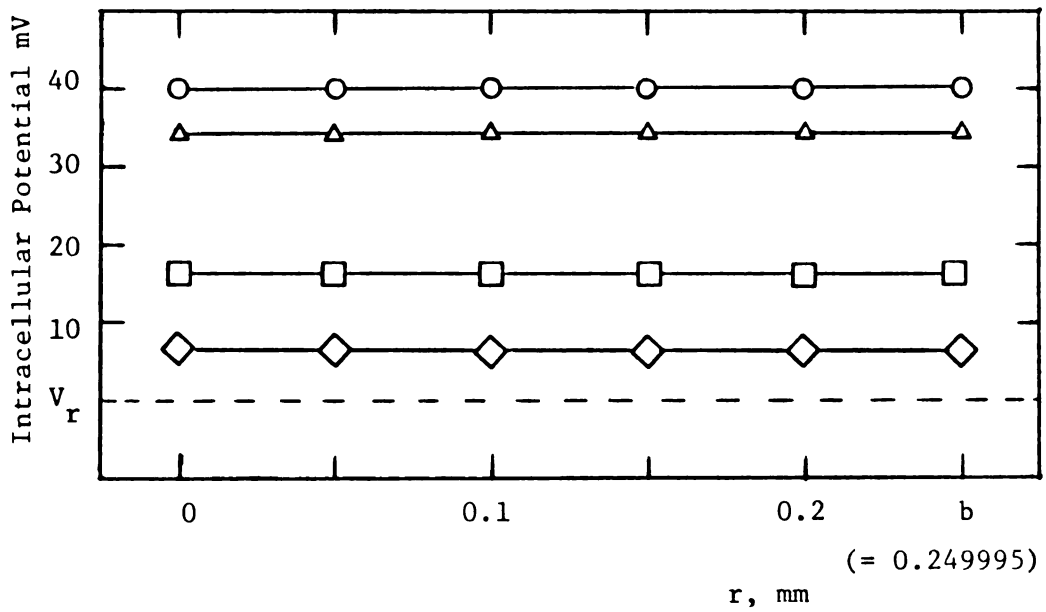

FIGURE 3.9

$\Phi_I(r,z)$ as a Function of r for Various z, 0.5 mm Wide Internal Electrode

KEY

○ --- z = 0

△ --- z = 1 mm

□ --- z = 5 mm

◇ --- z = 10 mm

(Both Graphs)

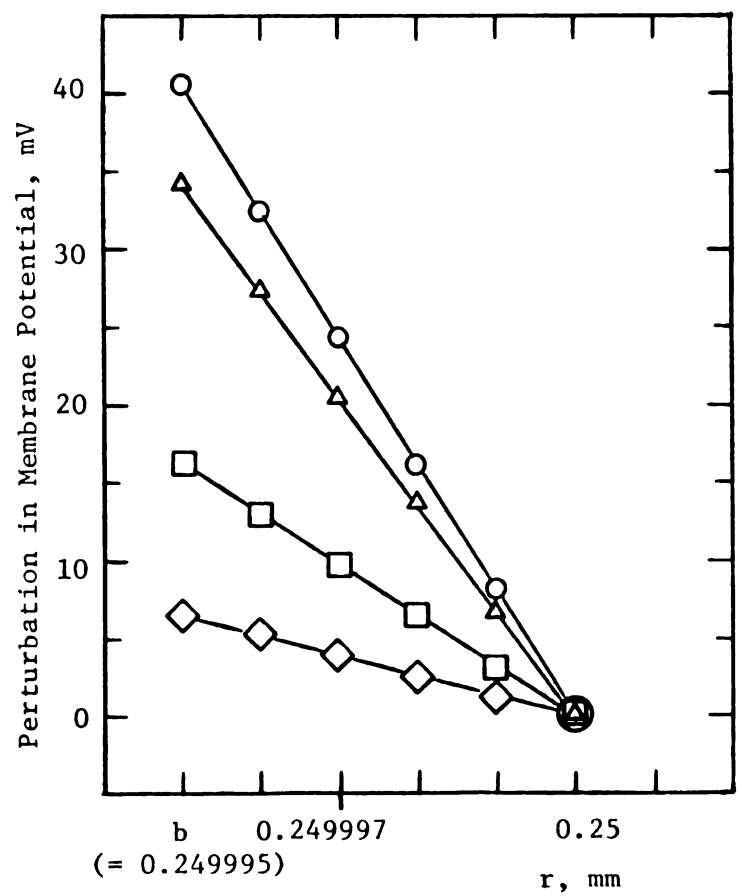

FIGURE 3.10

$\Phi'_M(r,z)$ as a Function of r for Various z, 0.5 mm

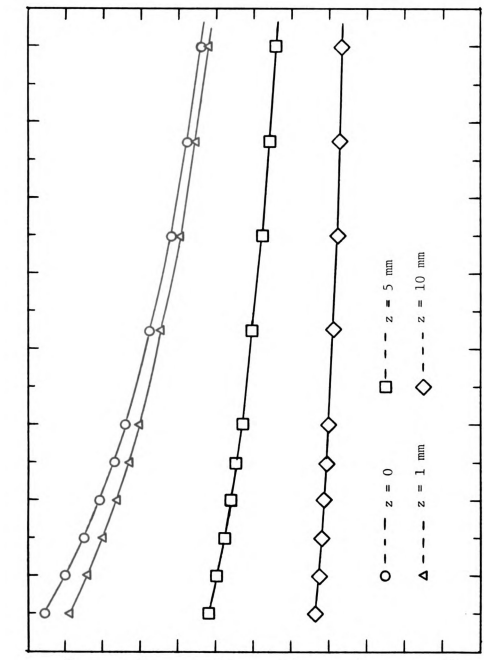

FIGURE 3.11

$\Phi_E(r,z)$ as a Function of r for Various z, 0.5 mm Wide Internal Electrode

and 10 mm). As is seen in Figures 3.7 and 3.9, the potential in the intracellular space is essentially constant in the radial direction ($0 \leq r \leq b$, $b = 0.249995$ mm) and varies exponentially in z. Figures 3.7 and 3.10 indicate the perturbation in membrane potential is linear in r, varying from $\Phi_I(b,z)$ to $\Phi_E(a,z)$ for $b \leq r \leq a$, and is also an exponential function of z. Finally, Figures 3.8 and 3.11 show that $\Phi_E(r,z)$ decreases in a smooth curve for $r \geq a$ and for increasing z. The fact that Φ_E is not a linear function of r or an exponential function of z reiterates the conclusion of Clark and Plonsey [8] that the core-conductor model does not realistically describe the extracellular region. The core-conductor model assumes only z-directed currents in the extracellular space, an assumption poorly met near the electrode where a large gradient of potential in the r-direction clearly exists.

The results of the Fourier transform field solution for the case of an internal stimulating electrode may be summarized as follows.

i) Transmembrane potential varies as a decreasing exponential function of z with magnitudes and length constant well predicted by the simpler cable equation theory. $\Phi_E(a,z)$ decays at a slower rate than predicted by cable theory.

ii) Near the electrode the solution is seen to vary considerably depending upon electrode width. As the electrode surface area goes to zero, Φ_I goes to infinity at the electrode. Cable theory gives a maximum E_z at $z = 0$ while the

field solution for a finite electrode (correctly) gives $E_z = 0$ at this point.

iii) Variation of σ_E produces little effect on V_m or Φ_I but major changes in Φ_E. In all realistic cases $\Phi_I >> \Phi_E$ giving $V_m \doteq \Phi_I(b,z)$.

iv) Radially, Φ_I is constant; Φ_M is a linear function between $\Phi_I(b,z)$ at b and $\Phi_E(a,z)$ at a; and Φ_E decreases to zero along a smooth curve as $r \to \infty$.

3.3.3. Electrotonic Potential for the Case of an External Electrode.

The steady-state perturbations in potential at the membrane of a cylindrical cell subjected to a maintained stimulus supplied via an extracellular ring electrode are illustrated in Figure 3.12. Moving the electrode to the external membrane surface (and maintaining the same stimulus intensity of $I^s = 10^{-5}$ amps) produces a radically different potential field than in the case of an intracellular electrode. The extracellular potential at the membrane ($\Phi_E(a,z)$) now has a sharp peak near the electrode and its magnitude rapidly falls toward zero at points away from the electrode. The intracellular perturbation in potential ($\Phi_I'(b,z)$) decays to zero from its maximum value (at $z = 0$) at a much slower rate than $\Phi_E(a,z)$. Unlike the intracellular stimulus case, these potentials are of the same order of magnitude over most of the axon. As in the previous case of interior stimulus, the potentials are symmetric about $z = 0$.

Because of the large volume of the extracellular medium, the net resistance to currents flowing away from the electrode is much smaller than when the electrode was placed in the cell interior. With an internal electrode, the small intracellular volume (per unit length) and low conductivity membrane presented a relatively high resistance path to currents from the electrode, giving a 40 mV perturbation in potential between the electrode and the reference point at infinity. This potential represents an ohmic effect of the current flow out to infinity. In the present case of an

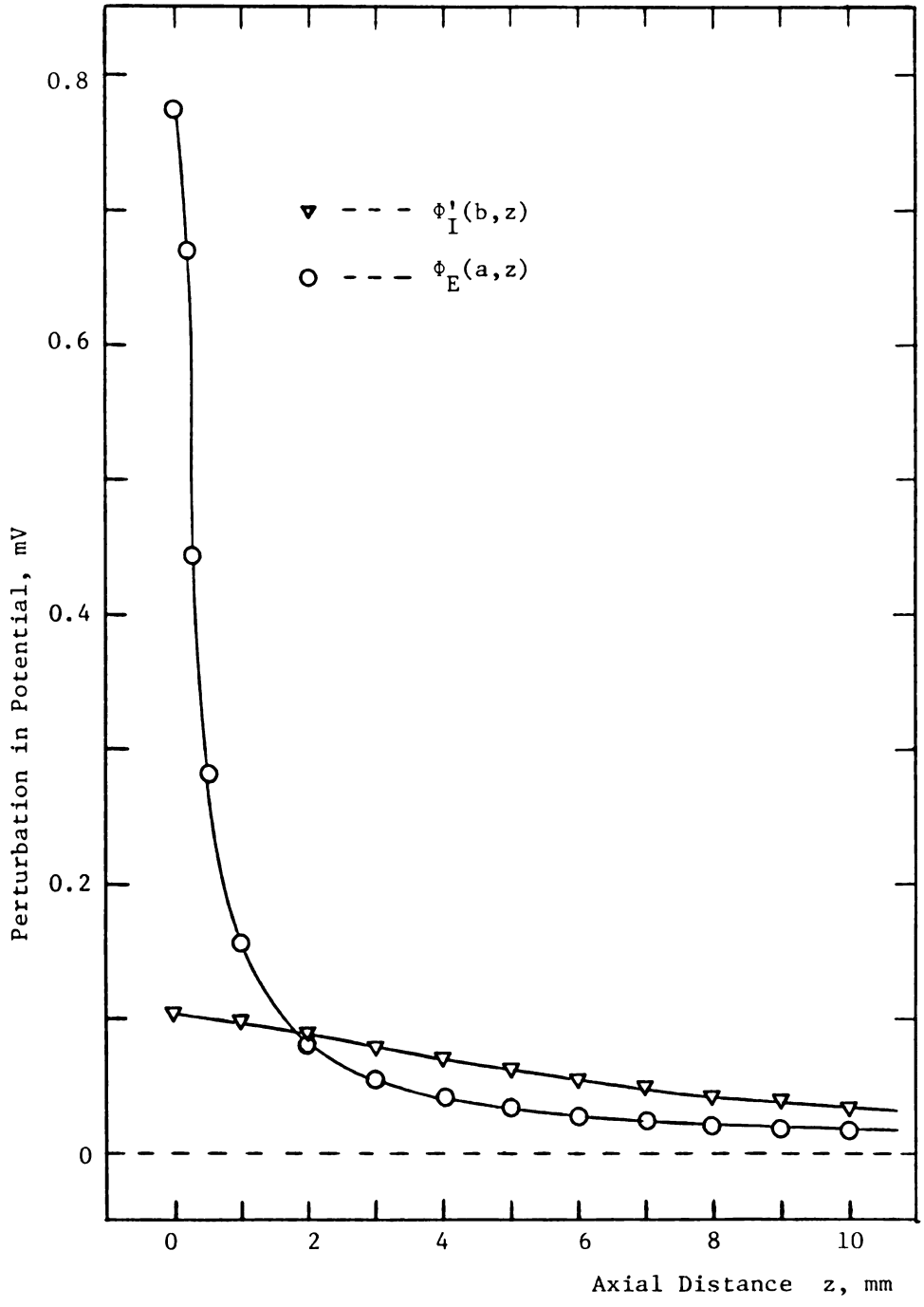

FIGURE 3.12

$\Phi_I'(b,z)$ and $\Phi_E(a,z)$ as Functions of z
for a 0.5 mm Wide External Electrode

external electrode, there is little resistance to current flow between the electrode and infinity. Thus the magnitude of potential is much smaller at the electrode (0.75 mV) and potential decreases very rapidly as the current from the electrode diverges in the large extracellular space.

The intracellular potential is perturbed very slightly by the small amount of current that "leaks" through the low conductivity of the membrane near the electrode. This net addition of positive charge produces a depolarization on the order of 0.1 mV at $z = 0$ and this perturbation decays to zero as the resultant current flows axially down the fiber and leaves through the membrane. Thus, because of the highly resistive nature of the membrane, the intracellular potential perturbation decays to zero at a much slower axial rate than $\Phi_E(a,z)$. Also, this perturbation is almost exactly the same as that seen in $\Phi_E(a,z)$ for an intracellular electrode (compare Figures 3.5 and 3.12).

An effect of the great difference in the axial gradients of Φ_I and Φ_E is that there exists a point at about $z = 2$ mm where $\Phi_I(b,z) = \Phi_E(a,z)$ (see Figure 3.12). Near the electrode Φ_E is larger than Φ_I, but this situation reverses itself for distances greater than 2 mm. This produces a point where the perturbation in transmembrane potential is zero, as seen in Figure 3.13. The definition of transmembrane potential as intracellular minus extracellular potential gives a net hyperpolarization in V_m near the electrode[1]. This hyperpolarization drops to zero at $z = 1.84$ mm

---

[1] The resting transmembrane potential of a neuron is on the order of -60 mV. A decrease in potential thus increases the polarization across the membrane, giving a hyperpolarization.

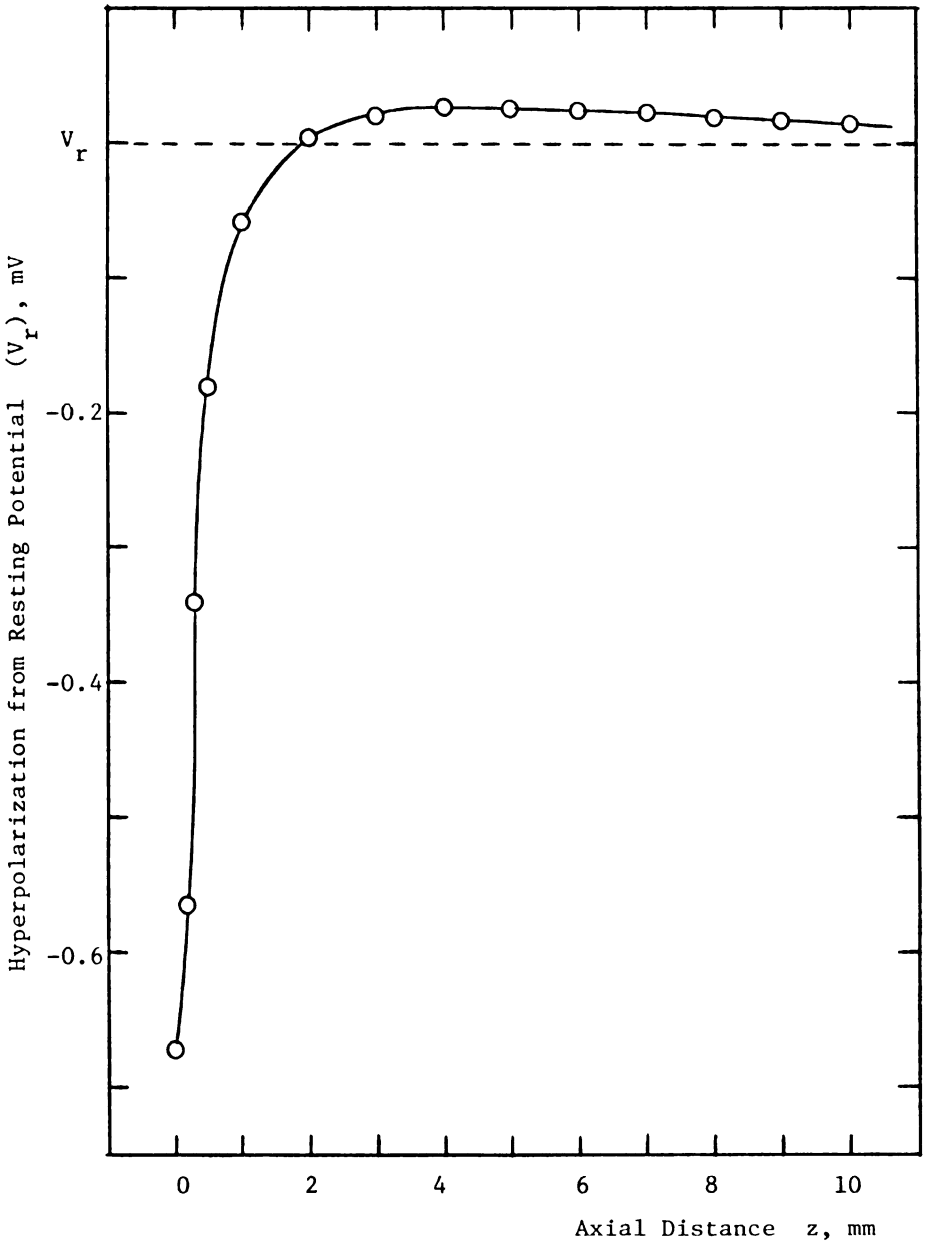

FIGURE 3.13

Transmembrane Potential as a Function of z
for a 0.5 mm Wide External Electrode

and then reverses to become a net depolarization for $z > 1.84$ mm. The depolarization from V_r then diminishes to zero at about the rate of $\Phi_I(b,z)$ going to zero since, for large z, $V_m \doteq \Phi_I$ (Φ_E having decayed to zero at a faster rate). The area near the electrode where V_m' is negative represents the region where current is crossing the membrane into the cell. Away from the electrode (where V_m' is positive) the net current flow is out of the cell, on its return path to the reference electrode at infinity.

As in the case of an intracellular electrode, variations in the width of the electrode produce little effect at axial distances greater than 1 mm.[1] Near the electrode, the potential does change with electrode width as illustrated in Figure 3.14 where V_m is plotted near $z = 0$ for a 0.5 mm wide electrode, a 5μ wide electrode, and a delta function electrode. The delta function electrode produces a singularity at $z = 0$, as in this case $\Phi_E(a,0) \to \infty$ (giving $V_m \to -\infty$). As for the intracellular stimulus, decreasing the electrode width increases J^s (the current density supplied by the electrode) causing an increase in Φ_E at the electrode. This results in Φ_E diverging to infinity as $w \to 0$. Also as in the last section, the potential is relatively constant over the surface of the electrode but falls off very rapidly beyond the electrode. The intracellular potential (Φ_I) is not affected significantly by changing the electrode size, so that the variations in V_m seen in Figure 3.14 are mostly a result of changes in $\Phi_E(a,z)$.

---

[1] This is true for electrodes up to 1 mm wide and as narrow as a delta function electrode.

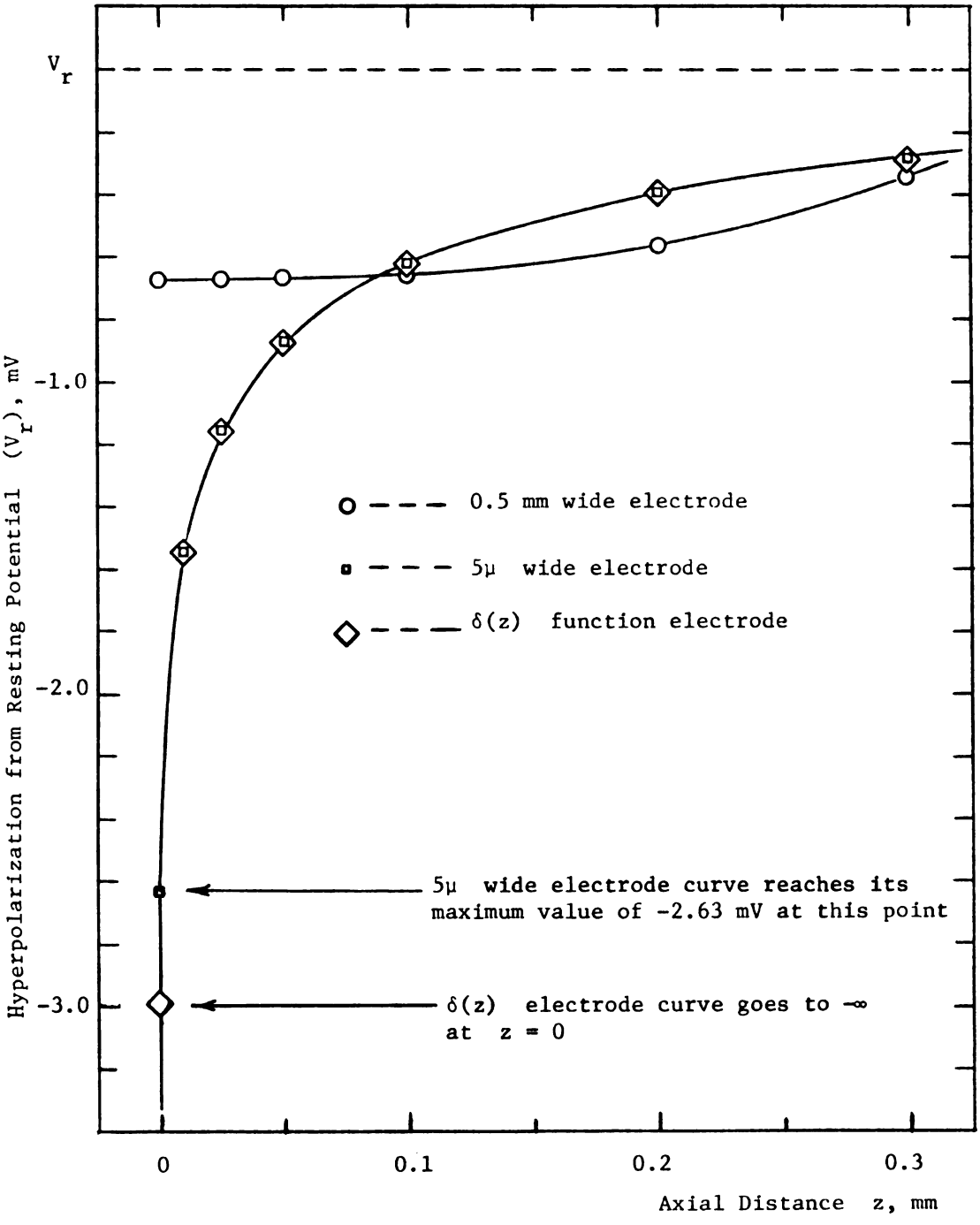

FIGURE 3.14

Transmembrane Potential as a Function of z
for Various Electrode Widths, Exterior Stimulus

Cable theory and the core-conductor model do not predict the transmembrane potential variation indicated by this model. Plonsey [60] solves the cable equation for extracellular ring electrodes, but the result is a response essentially the same as for an intracellular electrode. This result arises from restricting current flow in the extracellular media to the axial direction only. As indicated by Clark and Plonsey [8] this is a poor assumption and leads to significant deviations from the actual response. The Fourier transform model of this report supports this conclusion and indicates that for the case of an external stimulus and a large extracellular volume, the core-conductor approach is not applicable.

As noted above, varying the width of the electrode does not affect the transmembrane potential at axial distances greater than about 1 mm. Thus the point at which $\Phi_I(b,z) = \Phi_E(a,z)$ $(V_m' = 0)$ is seen to be invariant with electrode width. An investigation of what parameters do effect the location of this "zero point" (in transmembrane potential perturbation) was carried out. It was discovered that varying σ_E in the range of 10^{-3} to 1 mho/cm had no significant effect on the location of this point.[1] Also, no change was noted for variations in membrane thickness (for 25 to 200 Å) so long as the conductance (g_m) of the membrane per unit area was held constant.

As indicated in Figure 3.15(a), the zero point does depend upon the fiber radius. The curve in Figure 3.15(a) was obtained by

---

[1] It did increase both $\Phi_I(b,z)$ and $\Phi_E(a,z)$, but in the same proportion at $z = 1.84$ mm.

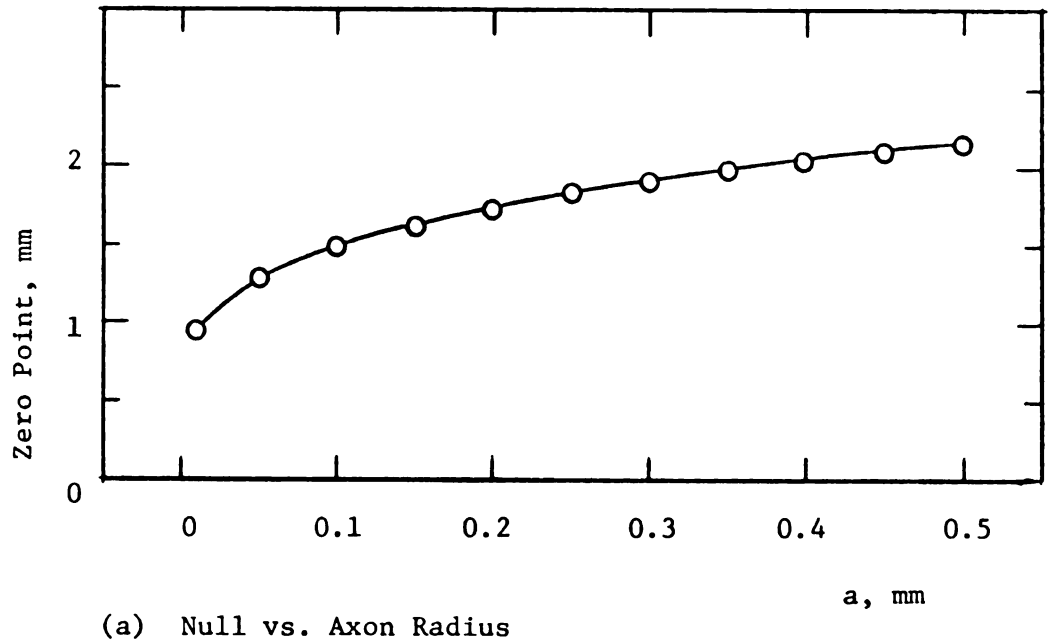

(a) Null vs. Axon Radius

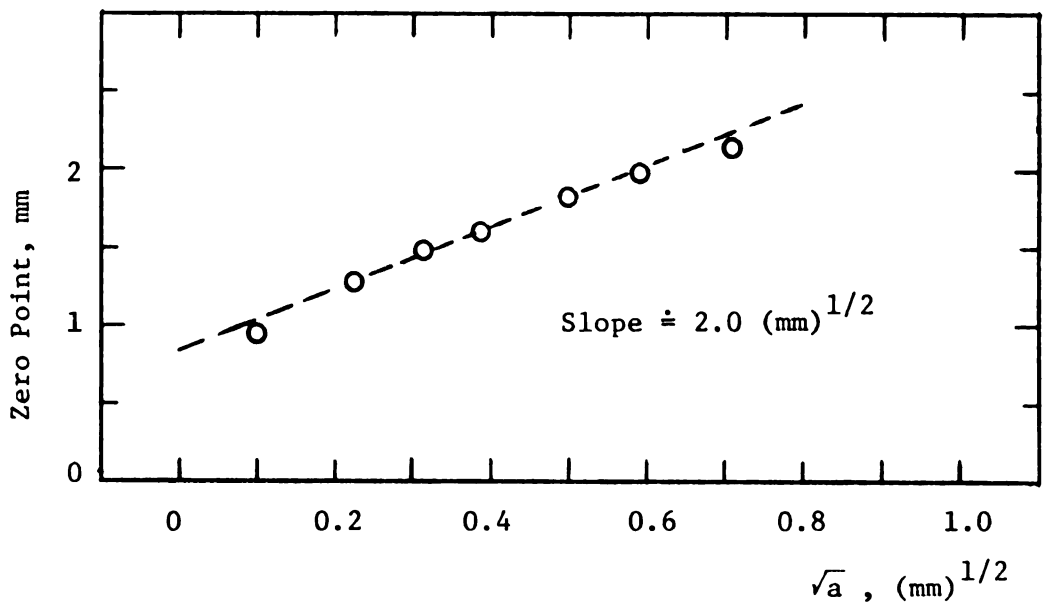

(b) Null vs. Square Root of Axon Radius

FIGURE 3.15

Variation of Transmembrane Potential Zero Point with Axon Radius

varying the radius while holding the length constant (λ) fixed. From the cable equation, λ varies directly with $\sqrt{a}$ (see equation (3.92)). λ increases for a larger internal volume per unit length as the net resistance to axial current flow in the intracellular space decreases. The length constant was held fixed by decreasing the membrane resistance per unit area (R_m) as fiber radius was increased. Plotting the variation of the zero point as a function of $\sqrt{a}$ (Figure 3.15(b)) yields an almost linear graph, with a slope of 2.0 $(mm)^{1/2}$. Thus it is seen that for radii in the range of 0.01 to 0.5 mm, the location of the point where $\Phi_I(b,z) = \Phi_E(a,z)$ is approximately a linear function of $\sqrt{a}$.

Changing R_m (membrane resistance per unit area) and holding all other parameters fixed gave another significant variation in the zero point. As illustrated in Figure 3.16, the effect is almost perfectly linear when plotted as a function of λ. As λ varies with the square root of R_m, this yields the location of the $V_m' = 0$ point as a linear function of $\sqrt{R_m}$ (or $1/\sqrt{\sigma_M}$ as $R_m = d/\sigma_M$ where d = membrane thickness). The slope of the line is 2.6 over the range of 1 to 10 mm for λ. Thus increasing either the fiber radius or the length constant (decreasing σ_M) moves the zero point in transmembrane potential perturbation farther away from the stimulus.

The radial variations in scalar potential are shown in Figures 3.17 - 3.19 for axial distances of 0, 1, 5, and 10 mm. Figure 3.17 indicates that $\Phi_I'(r,z)$ is constant with respect to r $(0 \leq r \leq b)$; the same result as for an intracellular stimulus. Thus the only electric field component expected in the intracellular

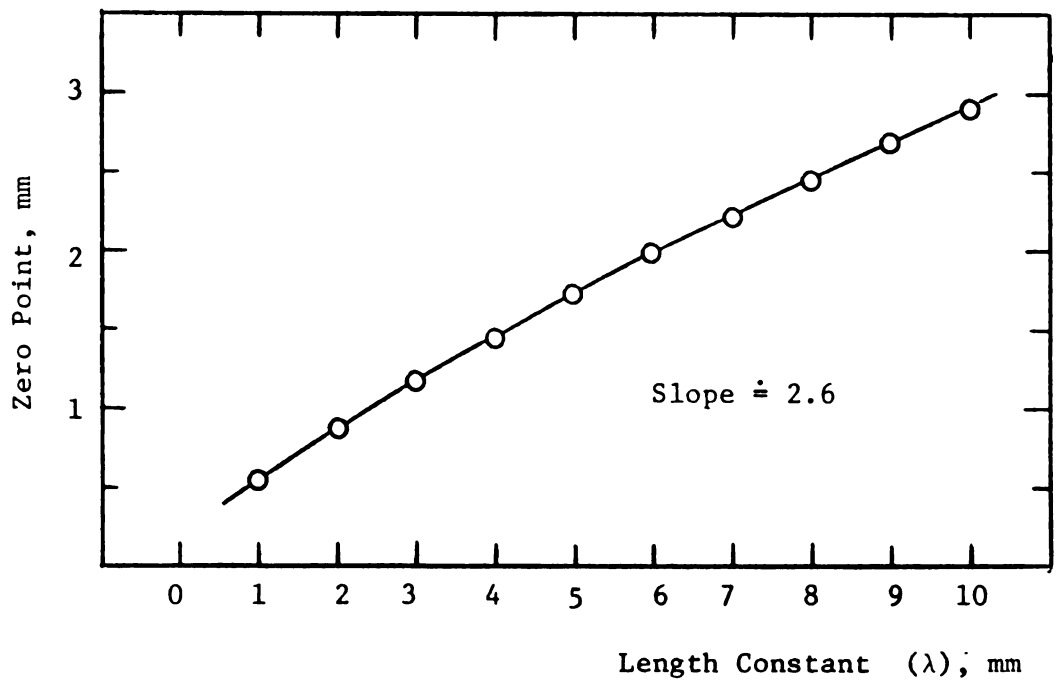

FIGURE 3.16

Variation of Transmembrane Potential Zero Point with Length Constant

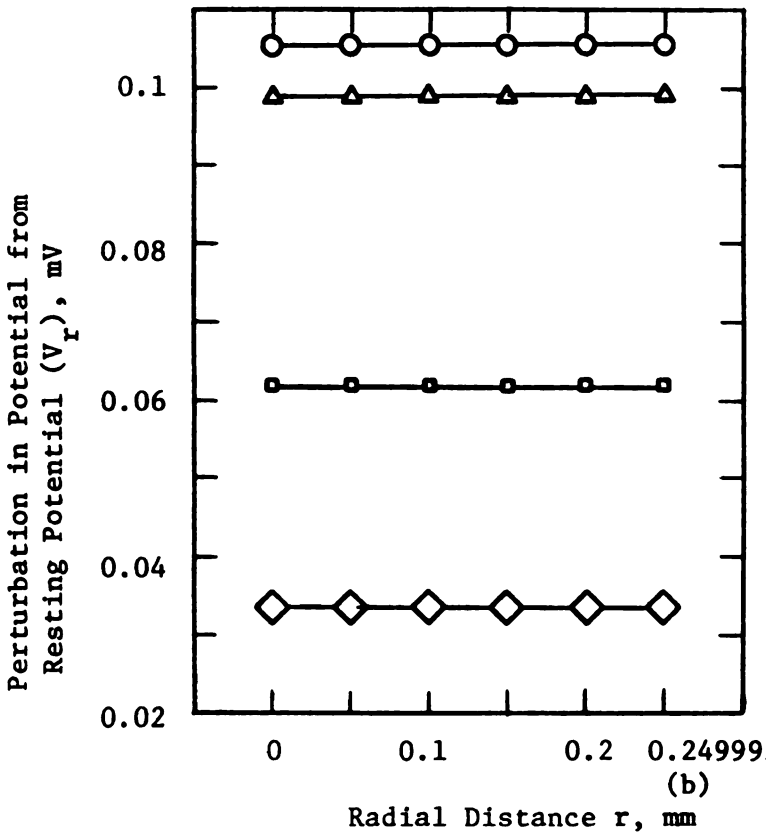

FIGURE 3.17

$\Phi_I'(r,z)$ as a Function of r for Several Values of z, 0.5 mm Wide External Electrode

KEY

○ - - - z = 0

△ - - - z = 1 mm

□ - - - z = 5 mm

◇ - - - z = 10 mm

(Both Graphs)

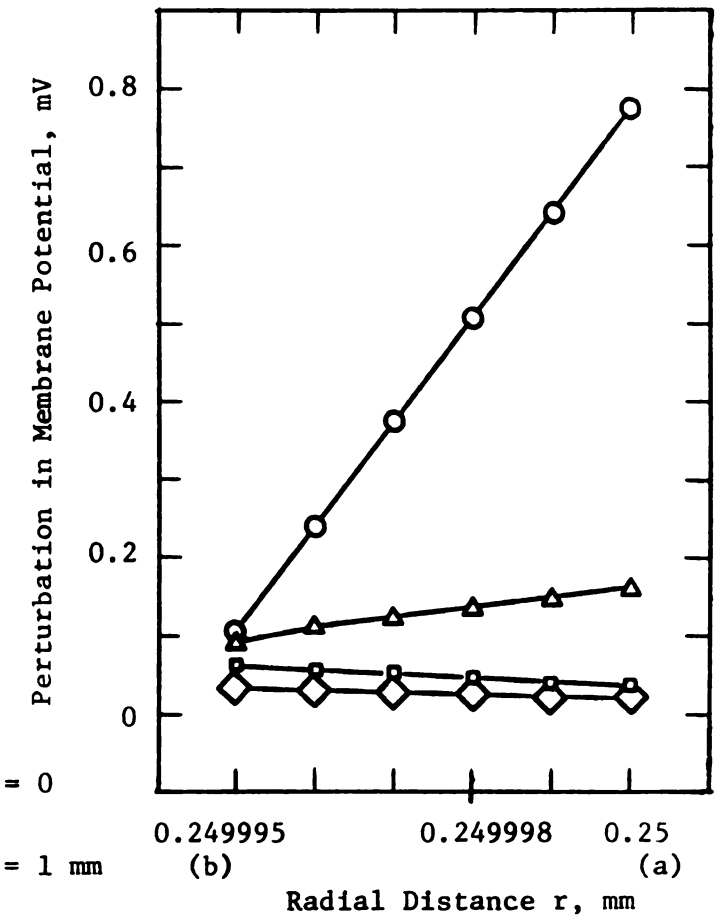

FIGURE 3.18

$\Phi_M'(r,z)$ as a Function of r for Several Values of z, 0.5 mm Wide External Electrode

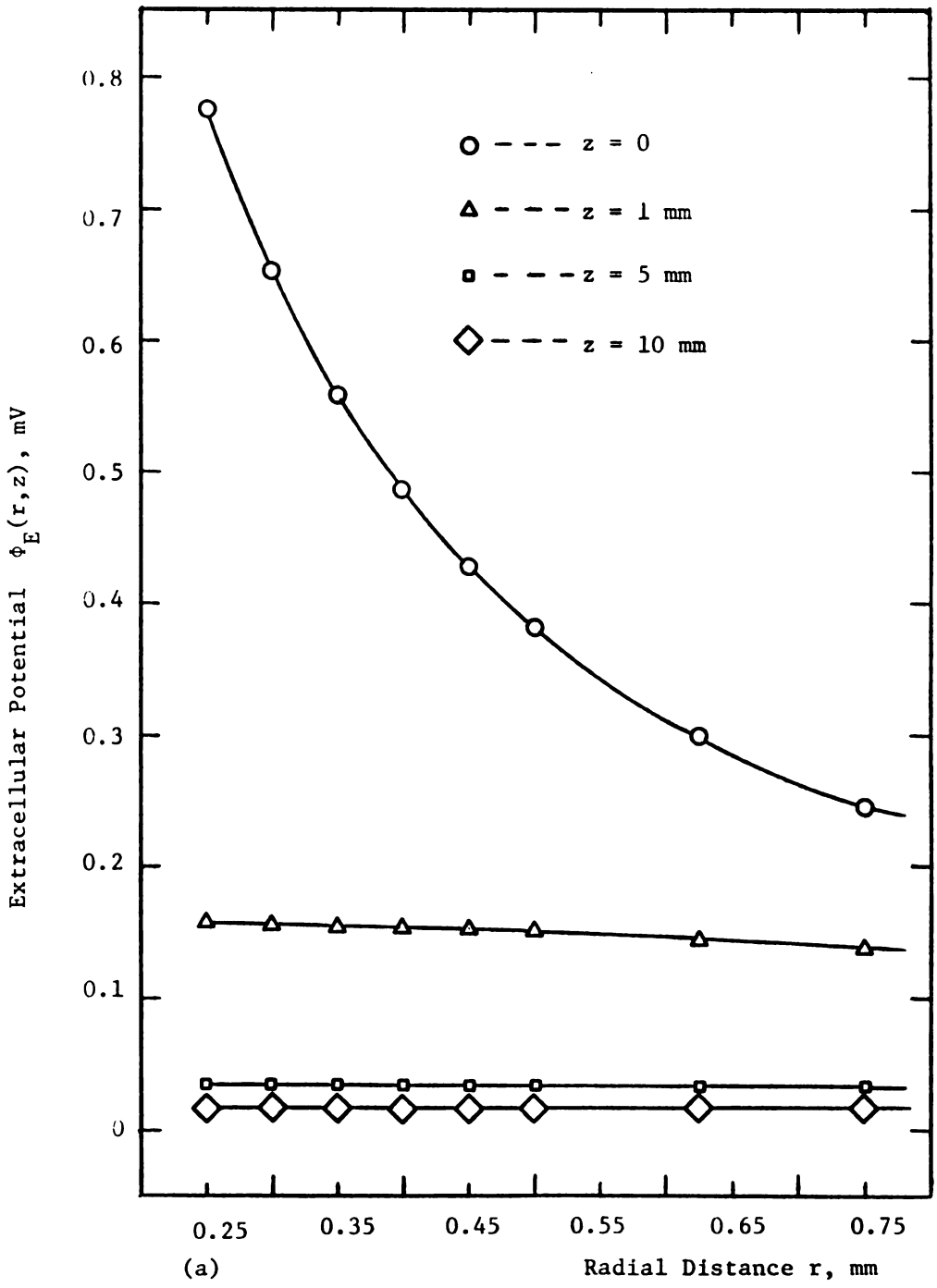

FIGURE 3.19

$\Phi_E(r,z)$ as a Function of r for Several Values of z, 0.5 mm Wide Electrode

region will be the $\hat{z}$ component. As illustrated in Figure 3.18, $\Phi'_M(r,z)$ is a linear function of r between the values of $\Phi'_I(b,z)$ and $\Phi_E(a,z)$ for any fixed z. Note that the slope of Φ'_M changes from positive at $z = 0$ and 1 mm to negative at $z = 5$ and 10 mm. This indicates an inward current in the first case and an outward (from the cell interior) current in the second case (as $\vec{E} = -\nabla\Phi$ and $\vec{J}_M = \sigma_M E$). The effect of the perturbation in transmembrane potential being a linear function of r was also seen in the intracellular electrode case.

The extracellular potential is a strong function of r near the electrode. As seen in Figure 3.19, there is a large radial gradient in Φ_E for $z = 0$, a very slight radial gradient for $z = 1$ mm, and essentially no radial gradient at $z = 5$ or 10 mm. This demonstrates that there is a large radial current density near the stimulus but a short axial distance away the only major component of current is in the z-direction[1]. The radial component of current observed near the electrode again indicates the unsuitability of the core-conductor model to be applied to the case of an extracellular stimulus.

The results of the Fourier transform field solution for the case of an external stimulating electrode may be summarized as follows.

i) Core-conductor theory does not apply as there is a large radial component of current near the stimulus.

---

[1] It is apparent that there is a large axial gradient in Φ_E by comparing the curves for various z points.

ii) The effect of supplying a positive current to the electrode is to hyperpolarize the membrane at the electrode and slightly depolarize the membrane a short axial distance away.

iii) The point that separates hyperpolarization from depolarization is constant for changes in electrode width, extracellular conductivity, and membrane thickness. The location is an increasing linear function of length constant or the square root of fiber radius.

iv) As in the case of an intracellular electrode, Φ_I is constant with respect to r, Φ_M is a linear function between Φ_I at $r = b$ and Φ_E at $r = a$, and Φ_E exhibits a radial gradient that is a smooth decreasing curve as $r \to \infty$.

3.3.4. Axial Electric Field, Surface Charge, and Capacitance

One of the purposes of considering a three-volume-conductor-region problem was to examine the assumption applied in Section 2.2.2 that axial currents in the membrane could be ignored if the membrane was very thin. The z-component of electric field (and current) in the membrane could be constructed from the graphs in the last two sections; however it is more direct and accurate to use expressions (3.66), (3.68) and (3.70) for E_{Iz}, E_{Mz}, and E_{Ez}. As $E_z = 0$ in the resting condition for all three regions, these equations yield the total z-component of electric field.

Figure 3.20 illustrates the z dependence of E_z at the center of the membrane and at the intracellular-membrane interface ($E_{Ez}(a,z)$ is on the order of 10^{-5} volts/cm, far too small to allow plotting on the scale of Figure 3.20) for the case of an intracellular stimulus. The maximum magnitude of E_z occurs at approximately $z = 0.5$ mm at the interior surface of the membrane, all other points in the membrane having a smaller field strength. This maximum is 0.07 volts/cm, and with a membrane conductivity of $\sigma_M = 7.143 \times 10^{-10}$ mhos/cm, yields a current density of $J_{Mz} = 5 \times 10^{-11}$ amps/cm^2. This certainly is a negligible current density, even as a maximum, when compared to the net radial current at the same point[1] of $\sigma_M E'_{Mr} = 5.7 \times 10^{-2}$ amps/cm^2. A check of the axial electric field in the membrane for an extracellular electrode gives the same result, as seen in Figure 3.21. The maximum E_{Mz}

---

[1] From Section 3.3.2, Figure 3.10 $E'_{Mr} = 8 \times 10^7$ volts/cm at $z = 0$, a constant with respect to r in the membrane.

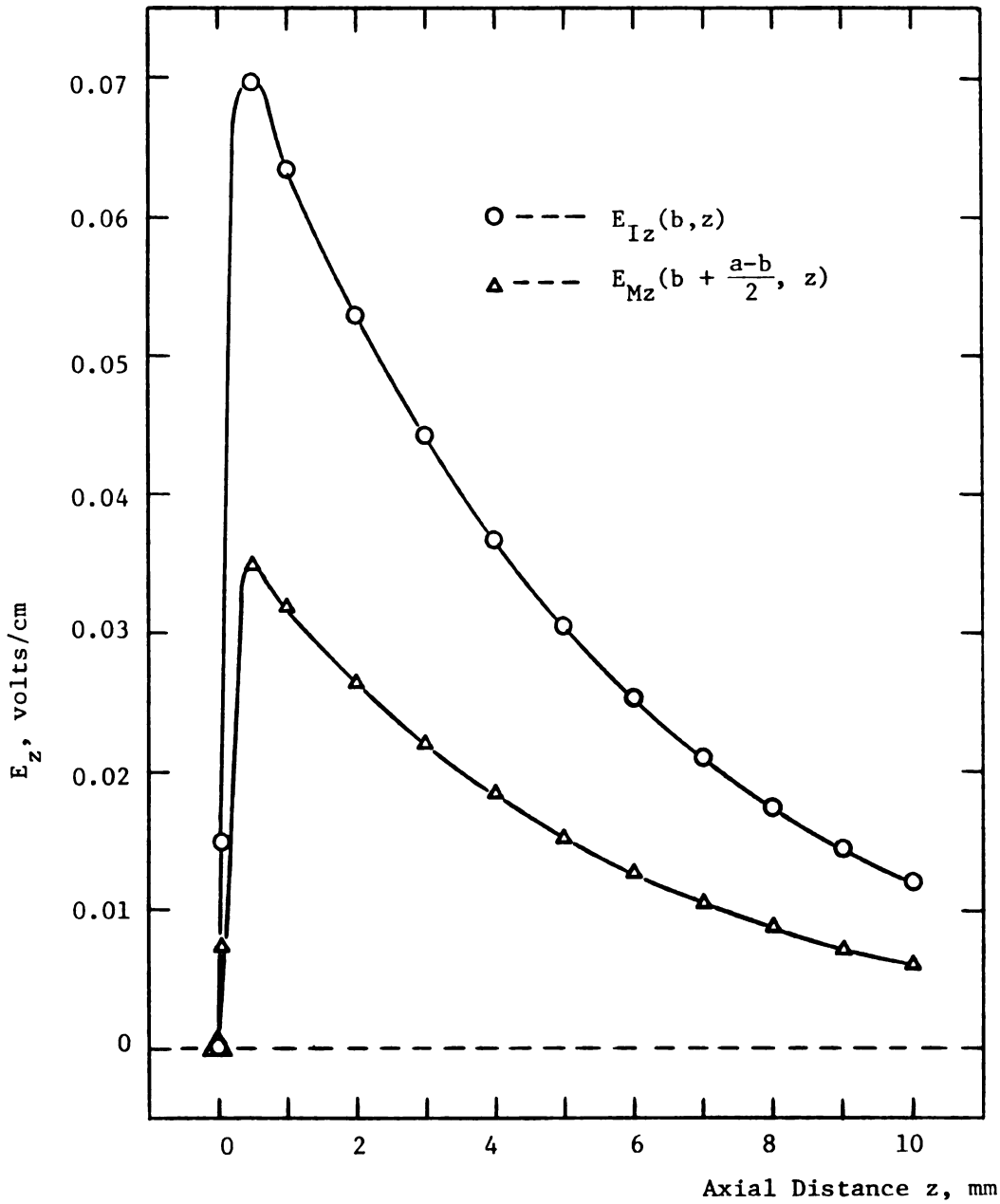

FIGURE 3.20

E_z as a Function of z for a
0.5 mm Wide Internal Electrode

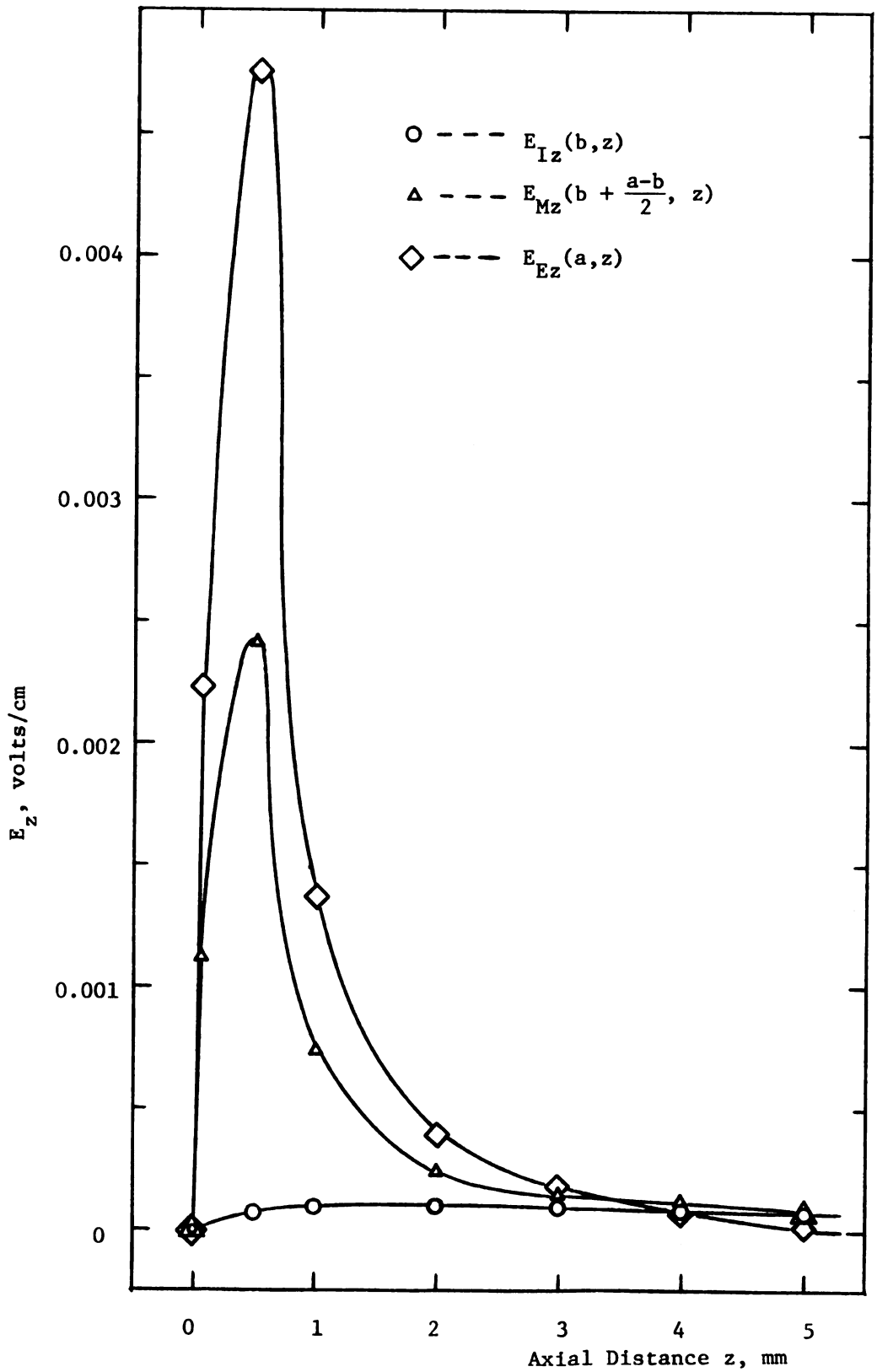

FIGURE 3.21

E_z as a Function of z for a 0.5 mm Wide External Electrode

is now less than 0.005 volts/cm, giving an even smaller J_{Mz} current density. Thus the assumption that membrane current may be taken to be totally radial is well founded even for a isotropic homogeneous membrane. If the membrane is anisotropic in the sense that current flow is confined to specific ionic channels (see Section 2.2.2) then this result also indicates that the solution presented in this report will give essentially the same answer as a channelized membrane (since J_{Mz} is negligible).

The solutions in this chapter also allow a check on the widely used assumptions that the surface charges on either side of the membrane are equal and opposite in sign, and that membrane capacitance is constant with respect to z and given by $C_m = \varepsilon_M/d$ (see Section 2.2.2). The surface charge density at the interior and exterior membrane interfaces was defined by boundary conditions (2.109) and (2.112) as

$$\varepsilon_M E_{Mr} - \varepsilon_I E_{Ir} = \eta_I \tag{3.93}$$

$$\varepsilon_E E_{Er} - \varepsilon_M E_{Mr} = \eta_E \quad . \tag{3.94}$$

By use of solutions (3.65), (3.67), and (3.69) the perturbation in η_I and η_E was calculated for the case of the extracellular electrode. The values $\varepsilon_I = \varepsilon_E = 80\varepsilon_o$ and $\varepsilon_M = 6\varepsilon_o$ were used for the permittivities of the three regions (values from Katz [40] or Plonsey [60]). Then by means of the definition $C_m = \eta_I'/V_m'$ (capacitance is the change in surface charge divided by the change in transmembrane potential) the results

as summarized in Table 3.1 were obtained.

Table 3.1

Surface Charge, Transmembrane Potential and Capacitance for an Extracellular Stimulus

z, mm	η_I', $\frac{\text{coulombs}}{\text{cm}^2}$	η_E', $\frac{\text{coulombs}}{\text{cm}}$	V_m, mV	C_m, $\mu f/cm^2$
0	-7.12×10^{-10}	7.12×10^{-10}	-0.670	1.063
0.05	-7.07×10^{-10}	7.07×10^{-10}	-0.665	1.063
0.5	-1.91×10^{-10}	1.91×10^{-10}	-0.180	1.061
1.0	-6.20×10^{-11}	6.20×10^{-11}	-0.0584	1.062
5.0	2.90×10^{-11}	-2.90×10^{-11}	0.0273	1.062
10.0	1.73×10^{-11}	-1.73×10^{-11}	0.0163	1.061

It is clear that $\eta_I' = -\eta_E'$ and that C_m is essentially constant. Furthermore, C_m as given by $C_m = \varepsilon_M/d$ is $1.062\ \mu f/cm^2$, agreeing very well with the direct calculation from $C_m = \eta_I'/V_m'$. The same results are obtained from the intracellular electrode case. Thus the assumptions made in arriving at the boundary conditions of Section 2.2.2 are confirmed to be well founded. With those boundary conditions, the problem may be solved in two regions (intracellular and extracellular) without the complication of finding a solution interior to the membrane. Before doing this, the next chapter considers time varying electrotonus for the three region problem as a generalization of the results of this chapter.

CHAPTER 4

TIME-DEPENDENT ELECTROTONUS

This chapter extends the three-region solutions of the last chapter to include time as a variable in the sources and fields. This will require a second transform to be applied to the time variable, but in this case the inverse transform is found analytically. Section 4.1 is a statement of the problem. Section 4.2 carries out the solution for the cases of a step, pulse, and delta function in the time variation of the stimulus. The last section presents the response of the standard test axon for these stimuli and an extension of the model to the case of a myelinated axon.

4.1. Statement of the Problem

The phenomena to be modeled in this chapter are identical to those in Chapter 3 with the exception of the inclusion of time variation. The model is thus for a nerve axon or dendrite as an infinitely long cylindrical structure subject to a subthreshold stimulus. The coordinate system will be cylindrical polar (r,ϕ,z), with rotational symmetry assumed so that no quantities are functions of ϕ. The three volume-conductor compartments are taken to be homogeneous, isotropic, and uniform; giving a constant σ and ε in each region. Macroscopic electroneutrality is assumed, the rotationally symmetric sources are at the membrane interfaces, and

solutions will be for perturbations from the resting condition[1].

The intracellular region is defined for radii in the range of $0 \leq r \leq b$, the membrane for $b < r < a$, and the extracellular space for $r \geq a$ (see Figure 3.1). Following the definitions in Chapter 3, the fields and their perturbations from the resting condition are given as

$$\vec{E}_I(r,z,t) = \vec{E}'_I(r,z,t) \tag{4.1}$$

$$\vec{E}_M(r,z,t) = \hat{r}E_{Mo}(r) + \vec{E}'_M(r,z,t) \tag{4.2}$$

$$\vec{E}_E(r,z,t) = \vec{E}'_E(r,z,t) \tag{4.3}$$

$$\Phi_I(r,z,t) = V_r + \Phi'_I(r,z,t) \tag{4.4}$$

$$\Phi_M(r,z,t) = \Phi_{Mo}(r) + \Phi'_M(r,z,t) \tag{4.5}$$

$$\Phi_E(r,z,t) = \Phi'_E(r,z,t) \tag{4.6}$$

where the primed quantities are the perturbations from the resting condition ("o" or unprimed) values. With the assumptions stated above, the equations satisfied by these fields are

$$\frac{1}{r}\frac{\partial}{\partial r}\left(r\frac{\partial \Phi'(r,z,t)}{\partial r}\right) + \frac{\partial^2 \Phi'(r,z,t)}{\partial z} = 0 \tag{4.7}$$

$$\vec{E}'(r,z,t) = -\nabla\Phi'(r,z,t) \tag{4.8}$$

---

[1] See Chapter 3 for the details and implications of these assumptions.

$$\vec{J}'(r,z,t) = \sigma\vec{E}'(r,z,t) \tag{4.9}$$

where ϕ', $\vec{E}'$, $\vec{J}'$ or σ are representative of any of the three space regions (I, M, or E).

The change in the problem due to the addition of the time variable is seen in the boundary conditions. The first boundary condition requiring continuity of potential (or tangential $\vec{E}$ field) is unchanged by the inclusion of time dependence and is given by[1]

$$\phi_E(a,z,t) = \phi'_M(a,z,t) \quad (\text{at } r = a) \tag{4.10}$$

and

$$\phi'_I(b,z,t) = \phi'_M(b,z,t) \quad (\text{at } r = b)\ . \tag{4.11}$$

However, in Chapter 3, the boundary condition on the continuity of normal current density contained a time derivative that was set to zero. Going back to Section 2.2.1 for the full boundary condition and defining source current densities J_I^s and J_E^s as in Chapter 3 gives

$$[\sigma_E + \epsilon_E \frac{\partial}{\partial t}]E_{Er}(a,z,t) - [\sigma_M + \epsilon_M \frac{\partial}{\partial t}]\ E'_{Mr}(a,z,t) = J_E^s(z,t) \tag{4.12}$$

$$[\sigma_M + \epsilon_M \frac{\partial}{\partial t}]E'_{Mr}(b,z,t) - [\sigma_I + \epsilon_I \frac{\partial}{\partial t}]E_{Ir}(b,z,t) = J_I^s(z,t) \tag{4.13}$$

---

[1] See Section 3.1.

with the sources now being functions of time.

Thus the only change from the problem that was solved in Chapter 3 is now all the field perturbations and source terms are functions of time. The single alteration in the defining equations appears in boundary conditions (4.12) and (4.13) where time derivatives of the radial components of electric field are now necessary. As a result, the more general time-varying problem is easily solved by an extension of the last chapter's solution and a second transform applied to the time variable.

4.2. Electrotonic Time-Dependent Solution in Fourier and Laplace Transform Domain

4.2.1. General Fourier and Laplace Transform Solution

The equation (4.7) for perturbations in potential in any of the three compartments is just Laplace's equation. Applying the Fourier transform on z as defined in equations (3.31) - (3.33) of Chapter 3 gives

$$\frac{\partial^2}{\partial r^2}\bar{\Phi}(r,k,t) + \frac{1}{r}\frac{\partial}{\partial r}\bar{\Phi}(r,k,t) - k^2\bar{\Phi}(r,k,t) = 0 \ . \qquad (4.14)$$

This second-order, ordinary differential equation was solved in the last chapter for each volume conductor region, yielding the solutions:

$$\bar{\Phi}_I'(r,k,t) = A(k,t)I_o(kr) \qquad (4.15)$$

$$\bar{\Phi}_M'(r,k,t) = B(k,t)I_o(kr) + C(k,t)K_o(kr) \qquad (4.16)$$

$$\bar{\Phi}_E(r,k,t) = D(k,t)K_o(kr) \ . \tag{4.17}$$

The only difference from steady-state conditions is that the integration constants A, B, C, and D are now functions of t as well as k (k is the Fourier transform domain variable).

Solutions (4.15) - (4.17) are not complete until coefficients A through D are determined via the boundary conditions. The Fourier transform of the required boundary conditions (4.10) - (4.13) leads to

$$\bar{\Phi}_E(a,k,t) = \bar{\Phi}'_M(a,k,t) \tag{4.18}$$

$$\bar{\Phi}'_I(b,k,t) = \bar{\Phi}'_M(b,k,t) \tag{4.19}$$

$$[\sigma_E + \varepsilon_E \frac{\partial}{\partial t}]\bar{E}_{Er}(a,k,t) - [\sigma_M + \varepsilon_M \frac{\partial}{\partial t}]\bar{E}'_{Mr}(a,k,t) = \bar{J}^s_E(k,t) \tag{4.20}$$

$$[\sigma_M + \varepsilon_M \frac{\partial}{\partial t}]\bar{E}'_{Mr}(b,k,t) - [\sigma_I + \varepsilon_I \frac{\partial}{\partial t}]\bar{E}_{Ir}(b,k,t) = \bar{J}^s_I(k,t) \ . \tag{4.21}$$

With the exception of the time derivative terms in expressions (4.20) and (4.21), the boundary conditions are the same as for the previous steady-state solutions.

If the boundary conditions were applied directly in their present form, the result would be three inhomogeneous partial differential equations with forcing functions $\bar{J}^s_I$ and $\bar{J}^s_E$. It is far simpler to use a second transform on the time variable and solve the resulting algebraic equations. A particularly well-

suited transform for this purpose is the Laplace transform, defined with the properties:

$$\mathcal{L}\{F(t)\} = f(s) = \int_0^\infty F(t)e^{-st}dt \tag{4.22}$$

$$\mathcal{L}\{\frac{\partial}{\partial t} F(t)\} = sf(s) - F(0) \tag{4.23}$$

$$\mathcal{L}\{F(t-b),\ (t > b)\} = e^{-bs}f(s) \quad (b > 0)\ . \tag{4.24}$$

The inverse transform is defined with

$$F(t) = \frac{1}{2\pi j} \lim_{\beta\to\infty} \int_{\gamma-j\beta}^{\gamma+j\beta} f(s)e^{ts}ds\ . \tag{4.25}$$

As the inversion requires an integration in the complex plane, it is easiest in practice to use the large number of tabulated Laplace transforms and their inverses. Two good sources for these are Churchill [7] and Erdélyi et al. [21].

With the restriction that the system is at rest at $t = 0$, the Laplace transform of expressions (4.15) - (4.21) yields[1]

$$\bar{\Phi}_I'(r,k,s) = A(k,s)I_o(kr) \tag{4.26}$$

$$\bar{\Phi}_M'(r,k,s) = B(k,s)I_o(kr) + C(k,s)K_o(kr) \tag{4.27}$$

---

[1] This assumption gives $\bar{E}_r(t = 0) = 0$ in applying property (4.23) for the time derivatives in expressions (4.20) and (4.21). It merely defines the stimulus starting point at $t = 0$ and implies $J_I^s = J_E^s \equiv 0$ for $t < 0$.

$$\bar{\Phi}_E(r,k,s) = D(k,s)K_o(kr) \tag{4.28}$$

$$\bar{\Phi}_E(a,k,s) = \bar{\Phi}'_M(a,k,s) \tag{4.29}$$

$$\bar{\Phi}'_I(b,k,s) = \bar{\Phi}'_M(b,k,s) \tag{4.30}$$

$$[\sigma_E + s\varepsilon_E]\bar{E}_{Er}(a,k,s) - [\sigma_M + s\varepsilon_M]\bar{E}'_{Mr}(a,k,s) = \bar{J}^s_E(k,s) \tag{4.31}$$

$$[\sigma_M + s\varepsilon_M]\bar{E}'_{Mr}(b,k,s) - [\sigma_I + s\varepsilon_I]\bar{E}_{Ir}(b,k,s) = \bar{J}^s_I(k,s) \tag{4.32}$$

where the application of the Laplace transform has been denoted by replacing t with s in the functional arguments. Defining generalized conductivites as

$$\eth_E = [\sigma_E + s\varepsilon_E] \tag{4.33}$$

$$\eth_M = [\sigma_M + s\varepsilon_M] \tag{4.34}$$

$$\eth_I = [\sigma_M + s\varepsilon_M] \tag{4.35}$$

leads to boundary conditions (4.31) and (4.32) having the form of

$$\eth_E\ \bar{E}_{Er}(a,k,s) - \eth_M\ \bar{E}'_{Mr}(a,k,s) = \bar{J}^s_E(k,s) \tag{4.36}$$

$$\eth_M\ \bar{E}'_{Mr}(b,k,s) - \eth_I\ \bar{E}_{Ir}(b,k,s) = \bar{J}^s_I(k,s)\ . \tag{4.37}$$

Comparing solutions (4.26) - (4.28) and boundary conditions (4.29), (4.30), (4.36) and (4.37) to the previous problem in Section 3.2.1 as defined in expressions (3.40) - (3.45) gives the immediate definition of A(k,s), B(k,s), C(k,s) and D(k,s) from equations (3.57) - (3.61) as

$$A(k,s) = \frac{-\sigma_M \bar{J}_E^s(k,s)}{k^2 b\, I_o(kb) I_1(kb) K_1(ka) F(k,s)} + \frac{\bar{J}_I^s(k,s)}{k\, I_1(kb) F(k,s)} \left[(\sigma_E - \sigma_M) - \frac{K_o(kb)}{I_o(kb)} \left(\sigma_E \frac{I_o(ka)}{K_o(ka)} + \sigma_M \frac{I_1(ka)}{K_1(ka)}\right)\right] \tag{4.38}$$

$$B(k,s) = \frac{-\bar{J}_E^s(k,s)}{k\, K_1(ka) F(k,s)} \left[\sigma_I \frac{K_o(kb)}{I_o(kb)} + \sigma_M \frac{K_1(kb)}{I_1(kb)}\right] + \frac{(\sigma_E - \sigma_M)\bar{J}_I^s(k,s)}{k\, I_1(kb) F(k,s)} \tag{4.39}$$

$$C(k,s) = \frac{(\sigma_I - \sigma_M)\bar{J}_E^s(k,s)}{k\, K_1(ka) F(k,s)} - \frac{\bar{J}_I^s(k,s)}{k\, I_1(kb) F(k,s)} \left[\sigma_E \frac{I_o(ka)}{K_o(ka)} + \sigma_M \frac{I_1(ka)}{K_1(ka)}\right] \tag{4.40}$$

$$D(k,s) = \frac{\bar{J}_E^s(k,s)}{k\, K_1(ka) F(k,s)} \left[(\sigma_I - \sigma_M) - \frac{I_o(ka)}{K_o(ka)} \left(\sigma_I \frac{K_o(kb)}{I_o(kb)} + \sigma_M \frac{K_1(kb)}{I_1(kb)}\right)\right] - \frac{\sigma_M \bar{J}_I^s(k,s)}{k^2 a I_1(kb) K_o(ka) K_1(ka) F(k,s)} \tag{4.41}$$

where $F(k,s)$ is defined with

$$F(k,s) = [(\sigma_I - \sigma_M)(\sigma_E - \sigma_M) - (\sigma_I \frac{K_o(kb)}{I_o(kb)} + \sigma_M \frac{K_1(kb)}{I_1(kb)})(\sigma_E \frac{I_o(ka)}{K_o(ka)}$$

$$+ \sigma_M \frac{I_1(ka)}{K_1(ka)})] \ . \qquad (4.42)$$

With the expressions for $A(k,s)$ through $D(k,s)$, the general solutions (4.26) - (4.28) for potential in Fourier and Laplace transform domain are complete.

4.2.2. Time-Varying Stimulus Functions

To proceed with inverting the solutions of the previous section back to the time and space domains requires specification of the source terms $\bar{J}_I^s(k,s)$ and $\bar{J}_E^s(k,s)$ in the Fourier and Laplace transform domains. The z-dependence of the source terms is assumed to be the same as discussed in Section 3.2.2. That is, the stimulus is supplied by a single metallic ring electrode, of finite width w, centered on $z = 0$, and driven by a total current I^s taken to be positive for current towards the electrode. The return path for the current is a second electrode at infinity and the current density over the surface area of the stimulating electrode is assumed constant. These assumptions are discussed in Section 3.2.2 and the electrodes are diagrammed in Figures 3.2 and 3.3.

For this type of stimulus, either source function ($\bar{J}_I^s(k,t)$ or $\bar{J}_E^s(k,t)$) will have a Fourier transform on z in the form of

$$\overline{J}^{s}(k,t) = \frac{2\ J^{s}(t)}{k} \sin(k\ w/2)\ , \qquad (4.43)$$

the transform being the same as for Section 3.2.2 except that the source current density magnitude $J^{s}(t)$ is now a function of time. The relationship of the current density magnitude to the input stimulating current $I^{s}(t)$ at any time t follows from Chapter 3 as

$$J_{I}^{s}(t) = \frac{I_{I}^{s}(t)}{w2\pi b} \quad \text{amps/m}^2 \qquad (4.44)$$

$$J_{E}^{s}(t) = \frac{I_{E}^{s}(t)}{w2\pi a} \quad \text{amps/m}^2\ , \qquad (4.45)$$

where the assumption of spatially constant current density gives its magnitude as the total current divided by the electrode surface area.

Three time functions for $I^{s}(t)$ are considered in this chapter. They are a step function, pulse function, and impulse (delta) function. These three time functions cover the most commonly used stimuli in experimental neurophysiology. Other time functions such as ramps, triangular pulses, etc., may be handled in exactly the same manner presented in the remainder of this chapter. Also, the solutions for multiple stimuli (trains of pulses, multi-level step functions) may be obtained by applying expression (4.24), the Laplace time-shifting theorem, just as multiple electrodes can be handled by space-shifting and linear superposition.

The Laplace transform of a unit step function starting at $t = 0$ is given by Churchill [7] as

$$\mathcal{L}\{U(t)\} = 1/s \ . \tag{4.46}$$

By the time-shifting theorem (4.24) and linear superposition, the transform of a pulse of unit magnitude and duration T_o is obtained as the sum of two step functions:

$$\mathcal{L}\{U(t) - U(t - T_o)\} = 1/s \ (1 - e^{-sT_o}) \ . \tag{4.47}$$

The transform of the Dirac delta function[1] is given by

$$\mathcal{L}\{\delta(t)\} = 1 \ . \tag{4.48}$$

Thus, with these transforms applied to expressions (4.44) and (4.45), the Fourier and Laplace transformed stimulus functions for either an internal or external electrode have the forms

$$\bar{J}^s(k,s) = \frac{2 \ J^s}{ks} \sin(k \ w/2) \tag{4.49}$$

for a step function time dependence,

$$\bar{J}^s(k,s) = \frac{2 \ J^s}{ks} [1 - e^{-sT_o}] \sin(k \ w/2) \tag{4.50}$$

---

[1] The impulse function is being considered for comparisons to other authors' solutions, just as a delta function width electrode was in the previous chapter.

for a pulse time function, and

$$\overline{J}^s(k,s) = \frac{2\,J^s}{k}\sin(k\,w/2) \tag{4.51}$$

for an impulse time dependence. The source current density magnitudes J_I^s or J_E^s are defined then as the peak (or weighting factor in the delta function case) of total current $I^s(t)$ divided by the surface area of the electrode. Following relationships (4.44) and (4.45), this gives

$$J_I^s = \frac{[I_I^s]_{max}}{w2\pi b} \tag{4.52}$$

$$J_E^s = \frac{[I_E^s]_{max}}{w2\pi a} \tag{4.53}$$

where either J_I^s or J_E^s is used in expressions (4.49) - (4.51) depending upon the type of electrode (and time function) desired.

4.2.3. Time Domain Solutions

In Section 4.2.1, the general solutions for pertubrations in potential in the intracellular, membrane or extracellular regions were given in expressions (4.26) - (4.28). These solutions are in the Fourier and Laplace transform domains (k and s replacing z and t respectively) and require two inverse transforms to express them as functions of z and t again. As in Chapter 3, the coefficients $A(k,s)$, $B(k,s)$, $C(k,s)$ and $D(k,s)$ are so hopelessly complicated as to rule out any analytical inversion of the Fourier transform. However, the Laplace transform can be inverted in a closed form so that numerical techniques need only be applied to invert the Fourier transform. The inversion back to the time domain is carried out for the stimulus functions of the previous section, but can also be accomplished for a wide variety of time functions by means of the extensive tables of Laplace transforms available (see Erdélyi, et al. [21]).

The k-space coefficients that are obtained from the Laplace transform inversion are complex and unwieldy. Were it not for the shorthand expression of $\delta = \sigma + s\varepsilon$ in the expressions (4.38) to (4.41) of integration constants $A(k,s)$ through $D(k,s)$, even these equations would be more cumbersome. To accomplish the Laplace inversion from s-space to the time domain, it becomes necessary to define a new series of coefficients and use these to express the solutions. This is done not only to reduce the complexity of the resulting expressions, but also because trial and error demonstrated these forms are the simplest to utilize in the computer routines for the Fourier transform inversion.

As the s-dependence in the solutions (4.26) - (4.28) occurs solely in the coefficients A(k,s) through D(k,s), it is only necessary to invert these coefficients back to the time domain. The time domain solutions are then obtained from expressions (4.15) - (4.17) with the Laplace-inverted coefficients A(k,t), B(k,t), C(k,t) and D(k,t). The k and s-space coefficients contain the source terms $\overline{J}_I^S(k,s)$ and $\overline{J}_E^S(k,s)$ which were given in Section 4.2.2 for the cases of a step, pulse, and impulse function stimulus time-dependence. It is convenient to express these stimulus terms in the form

$$\overline{J}^S(k,s) = \overline{J}^S(k) f(s) \tag{4.54}$$

where $\overline{J}^S(k,s)$ represents either $\overline{J}_I^S$ or $\overline{J}_E^S$, and $\overline{J}^S(k)$ is defined as the steady-state stimulus function[1] given by

$$\overline{J}^S(k) = \frac{2\ J^S}{k} \sin(k\ w/2)\ . \tag{4.55}$$

The function f(s) then represents the Laplace transform of the time-dependence of the stimulus and is given (by comparison with expressions (4.49) - (4.51)) as

$$f(s) = 1/s \tag{4.56}$$

for a step function stimulus,

---

[1] So labeled as it is the same as $\overline{J}^S(k)$ in Chapter 3 for steady-state conditions.

$$f(s) = 1/s\ (1 - e^{-sT_o}) \tag{4.57}$$

for a pulse of duration T_o, and

$$f(s) = 1 \tag{4.58}$$

for a Dirac delta function time-dependence.

The coefficients A(k,s) through D(k,s) (expressions (4.38) - (4.41)) can all be put in the form of

$$\psi(k,s) = \left[\frac{N_1(k) + sN_2(k)}{(s^2\alpha(k) + s\beta(k) + \gamma(k))}\right] f(s) \tag{4.59}$$

where ψ represents any coefficient A, B, C, or D and f(s) is the appropriate Laplace-transformed time dependence as given above. The time solution for the coefficients will be expressed in terms of the new coefficients N_1, N_2, α, β, and γ that are functions of k only. By comparison with expressions (4.38) - (4.41), these are found as follows. All four integration constants A, B, C, and D have the same denominator when α, β, and γ are defined as[1]

---

[1] Note that $s^2\alpha + s\beta + \gamma$ is being defined as equal to F(k,s), the common factor in the denominators of coefficients A(k,s) through D(k,s). Relation (4.62) redefines the common denominator factor F(k) (from the steady-state solution of Chapter 3) so as to avoid confusion between F(k,s) (of this chapter) and F(k) (of the last chapter). They are similar because F(k,s) was obtained from F(k) by replacing σ (in F(k)) with $\tilde{\sigma} = (\sigma + s\varepsilon)$.

$$\alpha(k) = [(\varepsilon_I - \varepsilon_M)(\varepsilon_E - \varepsilon_M) - (\varepsilon_I \frac{K_o(kb)}{I_o(kb)} + \varepsilon_M \frac{K_1(kb)}{I_1(kb)})(\varepsilon_E \frac{I_o(ka)}{K_o(ka)} + \varepsilon_M \frac{I_1(ka)}{K_1(ka)})] \tag{4.60}$$

$$\beta(k) = [(\varepsilon_I - \varepsilon_M)(\sigma_E - \sigma_M) + (\sigma_I - \sigma_M)(\varepsilon_E - \varepsilon_M) - (\varepsilon_I \frac{K_o(kb)}{I_o(kb)} + \varepsilon_M \frac{K_1(kb)}{I_1(kb)})(\sigma_E \frac{I_o(ka)}{K_o(ka)} + \sigma_M \frac{I_1(ka)}{K_1(ka)}) - (\sigma_I \frac{K_o(kb)}{I_o(kb)} + \sigma_M \frac{K_1(kb)}{I_1(kb)})(\varepsilon_E \frac{I_o(ka)}{K_o(ka)} + \varepsilon_M \frac{I_1(ka)}{K_1(ka)})] \tag{4.61}$$

$$\gamma(k) = F(k) \tag{4.62}$$

where $F(k)$ is the common factor in the denominators of the solutions in Chapter 3 and is defined in equation (3.58).

The numerator terms (with $s^2\alpha + s\beta + \gamma = F(k,s)$ as defined above) depend upon the particular coefficient A, B, C, or D. For $A(k,s)$, $N_1(k)$ and $N_2(k)$ are obtained by inspection from expression (4.38) as

$$N_{A1}(k) = A(k)\gamma(k) \tag{4.63}$$

$$N_{A2}(k) = \frac{-\varepsilon_M \overline{J}_E^s(k)}{k^2 b\, I_o(kb) I_1(kb) K_1(ka)} + \frac{\overline{J}_I^s(k)}{k\, I_1(kb)}[(\varepsilon_E - \varepsilon_M) - \frac{K_o(kb)}{I_o(kb)}(\varepsilon_E \frac{I_o(ka)}{K_o(ka)} + \varepsilon_M \frac{I_1(ka)}{K_1(ka)})] \tag{4.64}$$

where $A(k)$ and $\gamma(k)$ are defined in equations (3.60) and (4.62) and $\overline{J}_E^s(k)$ and $\overline{J}_I^s(k)$ are given by equation (4.55) with the appropriate choice of J^s as J_I^s or J_E^s (source current density magnitude)[1]. Note that N_{A1} may be obtained from N_{A2} (and vice-versa) by replacing ε_I, ε_E, and ε_M with σ_I, σ_E, and σ_M respectively. The subscript "A" is used to denote the defining solution coefficient $A(k,s)$.

In the same manner, the numerator coefficients for $B(k,s)$ are found to be

$$N_{B1}(k) = B(k)\gamma(k) \tag{4.65}$$

$$N_{B2}(k) = -\frac{\overline{J}_E^s(k)}{k\,K_1(ka)}\left(\varepsilon_I \frac{K_o(kb)}{I_o(kb)} + \varepsilon_M \frac{K_1(kb)}{I_1(kb)}\right) + \frac{\overline{J}_I^s(k)}{k\,I_1(kb)}\left(\varepsilon_E - \varepsilon_M\right) \tag{4.66}$$

where $B(k)$ is defined in expression (3.59). For $C(k,s)$, N_{C1} and N_{C2} are obtained as

$$N_{C1}(k) = C(k)\gamma(k) \tag{4.67}$$

$$N_{C2}(k) = \frac{\overline{J}_E^s(k)}{k\,K_1(ka)}\left(\varepsilon_I - \varepsilon_M\right) - \frac{\overline{J}_I^s(k)}{k\,I_1(kb)}\left[\varepsilon_E \frac{I_o(ka)}{K_o(ka)} + \varepsilon_M \frac{I_1(ka)}{K_1(ka)}\right] \tag{4.68}$$

where $C(k)$ was given in equation (3.57). Finally, for $D(k,s)$, the required terms are

---

[1] Either source is assumed to have the same time dependence so that $f(s)$ may be factored out as in equation (4.59).

$$N_{D1}(k) = D(k)\gamma(k) \tag{4.69}$$

$$N_{D2}(k) = \frac{\overline{J}_E^s(k)}{k\, K_1(ka)} \left[(\varepsilon_I - \varepsilon_M) - \frac{I_o(ka)}{K_o(ka)} \left(\varepsilon_I \frac{K_o(kb)}{I_o(kb)} + \varepsilon_M \frac{K_1(kb)}{I_1(kb)}\right)\right]$$

$$- \frac{\varepsilon_M \overline{J}_I^s(k)}{k^2 a\, I_1(kb) K_o(ka) K_1(ka)} \tag{4.70}$$

where $D(k)$ is defined in relation (3.61). Note that in each case, the N_1 coefficient is defined solely in terms of the steady-state coefficients for $A(k)$ through $D(k)$ defined in Chapter 3.

Before proceeding with the Laplace transform inversion, one more grouping of coefficients is made to simplify the solutions. The general denominator (that is the same for any coefficient A, B, C, or D) may be factored by means of the quadratic formula as

$$s^2\alpha(k) + s\beta(k) + \gamma(k) = \alpha(k)(s - P(k))(s - Q(k)) \tag{4.71}$$

where $P(k)$ and $Q(k)$ are defined as the quadratic roots of the polynomial $F(k,s)$ and are given by

$$P(k) = \frac{-\beta(k) + \sqrt{\beta^2(k) - 4\alpha(k)\gamma(k)}}{2\,\alpha(k)} \tag{4.72}$$

$$Q(k) = \frac{-\beta(k) - \sqrt{\beta^2(k) - 4\alpha(k)\gamma(k)}}{2\,\alpha(k)} \quad . \tag{4.73}$$

With this factoring, the general expression for any solution coefficient $\psi(k,s)$ becomes

$$\psi(k,s) = \left[\frac{N_1(k) + sN_2(k)}{\alpha(k)(s - P(k))(s - Q(k))}\right]f(s) \quad . \tag{4.74}$$

Now consider the case of a step function time dependence for the stimulus J_I^s and/or J_E^s. Any coefficient $A(k,s)$, $B(k,s)$, $C(k,s)$, or $D(k,s)$ has the form

$$\psi(k,s) = \left[\frac{N_1(k) + sN_2(k)}{\alpha(k)s(s - P(k))(s - Q(k))}\right] \tag{4.75}$$

where expression (4.56) has been used for $f(s)$. Applying a partial fraction expansion gives

$$\psi(k,s) = \frac{R_o(k)}{s} + \frac{R_1(k)}{s-P(k)} + \frac{R_2(k)}{s-Q(k)} \tag{4.76}$$

where the $R_i(k)$ are given by

$$R_o(k) = \frac{N_1(k)}{\gamma(k)} \tag{4.77}$$

$$R_1(k) = \frac{N_2(k)P(k) + N_1(k)}{\alpha(k)P(k)[P(k) - Q(k)]} \tag{4.78}$$

$$R_2(k) = \frac{N_2(k)Q(k) + N_1(k)}{\alpha(k)Q(k)[Q(k) - P(k)]} \quad . \tag{4.79}$$

With the Laplace transforms of

$$\mathcal{L}\{1\} = 1/s \tag{4.80}$$

and $$\mathcal{L}\{e^{at}\} = \frac{1}{s-a} , \tag{4.81}$$

the inverse Laplace transform of the general coefficient is immediately apparent as

$$\Psi(k,t) = R_o(k) + R_1(k)e^{P(k)t} + R_2(k)e^{Q(k)t}. \tag{4.82}$$

Thus by using the appropriate N_1 and N_2 coefficients in expressions (4.77) - (4.79), the solution coefficients $A(k,t)$, $B(k,t)$, $C(k,t)$ and $D(k,t)$ for a time step-function stimulus are given by equation (4.82).

A computer check of the factors $P(k)$ and $Q(k)$ in the exponentials of expression (4.82) showed that they were negative decreasing functions of k for all values of k. In the limit of $t \to \infty$, this forces the two exponential terms to vanish and leave only the steady state term of $R_o(k)$. By following back through all the definitions of the coefficients, $R_o(k)$ is found to be just the steady-state coefficient $A(k)$, $B(k)$, $C(k)$ or $D(k)$ as given in Chapter 3. Thus the solution to a step function in time has the expected limiting steady-state response as time approaches infinity and transients damp out. Another feature of the solution is that $\psi(k,0) = 0$, as expected from the assumption that the system is in the resting condition at $t = 0$. The time response of this system, after performing the numerical inversion of the Fourier transform, is discussed further in Section 4.3.1.

The Laplace transform inversion for the case of a pulse of duration T_o follows quickly from the case of a step function. The general coefficient now has the form

$$\psi(k,s) = \left[\frac{N_1 + sN_2}{\alpha s(s-P)(s-Q)}\right](1 - e^{-T_o s}) \tag{4.83}$$

where expression (4.57) has been used for $f(s)$ in equation (4.74). By use of the time-shifting theorem (4.24), the inverse is obtained from the same partial fraction expansion as used for the step function case as

$$\psi(k,t) = \begin{cases} R_o(k) + R_1(k)e^{P(k)t} + R_2(k)e^{Q(k)t} & (0 \leq t \leq T_o) \\ R_1(k)e^{P(k)t}(1 - e^{-P(k)T_o}) + R_2(k)e^{Q(k)t}(1-e^{-Q(k)T_o}) & (t \geq T_o) \end{cases} \tag{4.84}$$

where R_o, R_1, R_2, P, and Q are all the same as for the step function response. Note that this solution is the same as the linear superposition of two step function responses (one that starts at $t = 0$ and the second subtracted from the first after $t = T_o$). As such, it has the same properties as discussed for the step function response, with the exception that as t increases to infinity the steady-state solution is now zero (i.e., the resting condition). The pulse response is discussed further after inversion to the z-domain in Section 4.3.2.

The final time dependence to be considered is that of the impulse response. Using expression (4.58) for $f(s)$ in

equation (4.74) gives the general coefficient as

$$\psi(k,s) = \frac{N_1 + sN_2}{\alpha(s-P)(s-Q)} \quad . \tag{4.85}$$

This is expanded via partial fractions into

$$\psi(k,s) = \frac{\Delta_1}{s-P} + \frac{\Delta_2}{s-Q} \tag{4.86}$$

where Δ_1 and Δ_2 are given by

$$\Delta_1(k) = \frac{N_2(k)P(k) + N_1(k)}{\alpha(k)[P(k) - Q(k)]} \tag{4.87}$$

$$\Delta_2(k) = \frac{N_2(k)Q(k) + N_1(k)}{\alpha(k)[Q(k) - P(k)]} \quad . \tag{4.88}$$

From relation (4.81), the inverse to the time domain is found simply as

$$\psi(k,t) = \Delta_1(k)e^{P(k)t} + \Delta_2(k)e^{Q(k)t} \tag{4.89}$$

where P and Q are the same as in the previous cases and are defined (for all coefficients A, B, C, or D) in expressions (4.72) and (4.73). The features of the impulse response are discussed in Section 4.3.3.

By use of the appropriate constants N_1 and N_2 in the general time-domain coefficients given in expressions (4.82),

(4.84) and (4.89), the solution time-domain coefficients A(k,t), B(k,t), C(k,t) and D(k,t) are obtained for the cases of a step function, pulse function or impulse function stimulus time-dependence. With these coefficients and the inverse Fourier transform (3.32), the space and time domain solutions for perturbations of potential from the resting condition are found from equations (4.15) - (4.17) as

$$\Phi_I'(r,z,t) = \frac{1}{2\pi}\int_{-\infty}^{\infty} A(k,t)I_o(kr)e^{jkz}dk \tag{4.90}$$

$$\Phi_M'(r,z,t) = \frac{1}{2\pi}\int_{-\infty}^{\infty}[B(k,t)I_o(kr) + C(k,t)K_o(kr)]e^{jkz}dk \tag{4.91}$$

$$\Phi_E(r,z,t) = \frac{1}{2\pi}\int_{-\infty}^{\infty} D(k,t)K_o(kr)e^{jkz}dk\ . \tag{4.92}$$

The solutions for electric field and current density follow directly from equations (4.8) and (4.9), using the property (3.33) to arrive at

$$E_{Ir}(r,z,t) = -\frac{1}{2\pi}\int_{-\infty}^{\infty} kA(k,t)I_1(kr)e^{jkz}dk \tag{4.93}$$

$$E_{Iz}(r,z,t) = -\frac{1}{2\pi}\int_{-\infty}^{\infty} jkA(k,t)I_o(kr)e^{jkz}dk \tag{4.94}$$

$$E_{Mr}'(r,z,t) = -\frac{1}{2\pi}\int_{-\infty}^{\infty} k[B(k,t)I_1(kr) - C(k,t)K_1(k,r)]e^{jkz}dk \tag{4.95}$$

$$E_{Mz}(r,z,t) = -\frac{1}{2\pi}\int_{-\infty}^{\infty} jk[B(k,t)I_o(kr) + C(k,t)K_o(kr)]e^{jkz}dk \tag{4.96}$$

$$E_{Er}(r,z,t) = \frac{1}{2\pi} \int_{-\infty}^{\infty} kD(k,t)K_1(kr)e^{jkz}dk \qquad (4.97)$$

$$E_{Ez}(r,z,t) = -\frac{1}{2\pi} \int_{-\infty}^{\infty} jkD(k,t)K_o(kr)e^{jkz}dk \; . \qquad (4.98)$$

The current density at any point is obtained by the product of the appropriate conductivity with the electric field for that location.

The inverse Fourier transforms are obtained in the same manner as discussed in Chapter 3, with the same computer program[1]. The only differences are that the solution coefficients are now far more complicated and time-dependent. The rest of this chapter discusses features of this solution for the case of the standard test axon defined in Section 3.3.1. The permitivities ε_I, ε_M, and ε_E are also needed and are taken as $\varepsilon_I = \varepsilon_E = 80\varepsilon_o$, $\varepsilon_M = 6\varepsilon_o$ following Katz [40] and the definitions made in Section 3.3.4 for the surface charge development. A full list of the standard test axon parameters is given in Appendix D.

---

[1] See Appendix C.

4.3. Time-Dependent Electrotonic Response

The following subsections examine features of the time-dependent passive response of the standard axon. To simplify comparisons, a 0.5 mm wide electrode was used and the maximum current intensity I^s was fixed at 10^{-5} amps in sections 4.3.1 and 4.3.2. As in Chapter 3, results are given in terms of perturbations in potential from the resting condition. Though only potentials at the membrane are presented, potentials anywhere in the system and electric fields and current densities are easily obtained with the appropriate solutions from Section 4.2.3.

4.3.1. Response to a Step Function Stimulus

As in the steady-state case, the perturbation in transmembrane potential is fairly well predicted by cable theory when an intracellular stimulating electrode is used. The equivalent circuit used for time-dependent subthreshold phenomena in the core-conductor model is illustrated in Figure 4.1. In the diagram c_m and r_m are the membrane per-unit-length shunt capacitance and resistance, while r_1 and r_2 are the extracellular and intracellular axial resistances per unit length[1]. The time response to a step function stimulus (solution given in

---

[1] See Lorente de No [48] or Plonsey [60] for a discussion of this model. In terms of the conductivities and capacitances of this report, $r_2 = (\sigma_I \pi a^2)^{-1}$, $r_m = d/(\sigma_M 2\pi a)$, and $c_m = C_m 2\pi a$. As noted in Chapter 3, r_1 is poorly defined for fibers in a large extracellular volume.

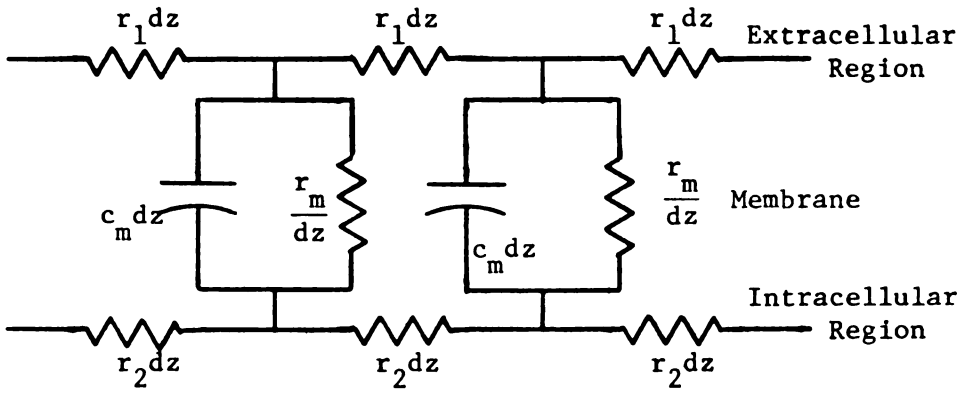

FIGURE 4.1

Cable Theory Equivalent Circuit

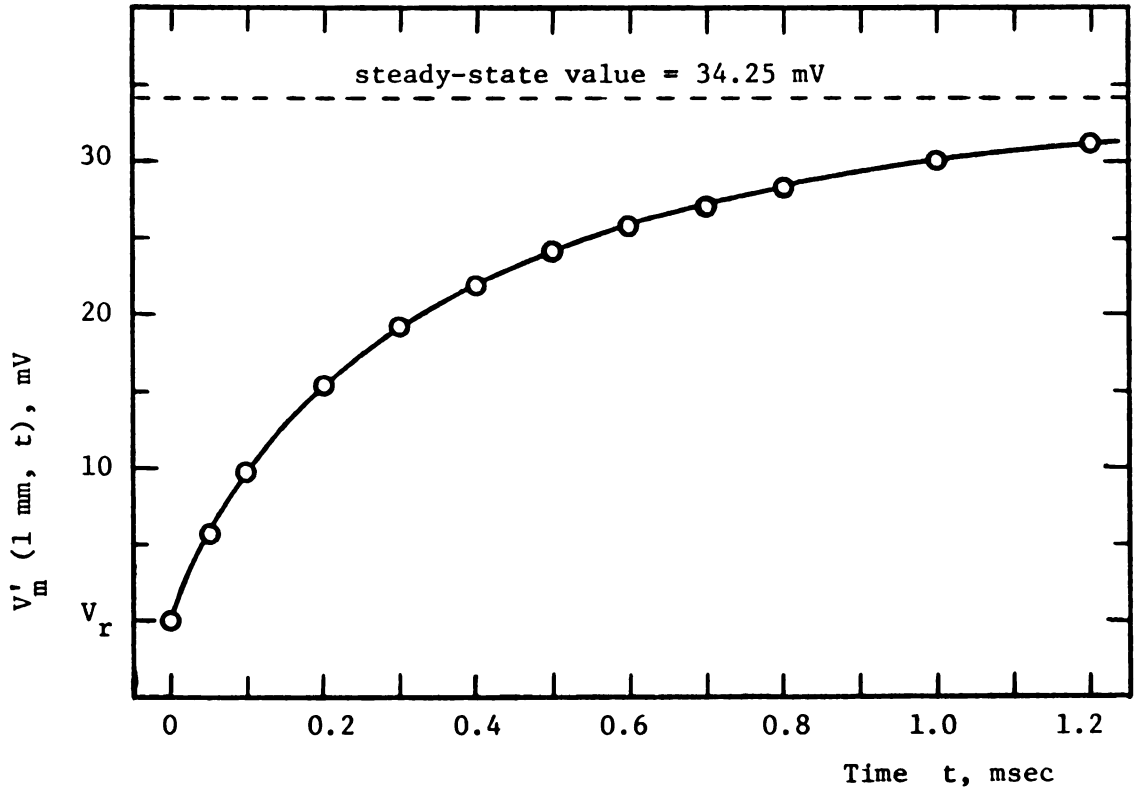

FIGURE 4.2

Transmembrane Potential Time Response at $z = 1$ mm for a Step Function Stimulus Applied Internally

Plonsey [60]) is expressed in terms of error functions, with the response at $z = 0$ given as an error function with a $\sqrt{t/r_m c_m}$ argument. A time constant τ is defined with

$$\tau = r_m c_m = \frac{d}{\sigma_M} C_m = \frac{\varepsilon_M}{\sigma_M} \tag{4.99}$$

so that at $z = 0$ and $t = \tau$, V_m is 84% of its steady-state value. The Fourier transform model of this report agrees very well with the cable equation response, with a time constant of $\tau = 0.743$ msec for the test axon[1].

The two models give different results near the electrode (as noted in Chapter 3) in the magnitude and z-dependence of V_m. However, the time response is essentially the same for the percent of the steady-state value reached after any time t. The response of both models away from the electrode is virtually identical and is illustrated for $z = 1$ mm in Figure 4.2. Near $t = 0$, the membrane capacitance (displacement current density in the membrane) provides a "short circuited" path for current flow from the cell interior into the extracellular region. As this capacitance becomes charged, the only path for current flow is the resistive one represented by r_m in the core conductor model or σ_M in the present field model. At steady-state, all current density through the membrane is resistive; giving $V_m(z, t \to \infty)$ as found in Chapter 3.

The field model of this report also allows accurate determination of the electric scalar potential at either side of the membrane.

---

[1] See the $z = 0$ curve in Figure 4.4.

Figure 4.3 is a plot of $\Phi_E(a, 1\ mm, t)$ versus time. It indicates an effect not predicted by the core-conductor model in the overshoot seen near $t = 0$. Φ_E quickly rises from zero to more than 200% of its steady-state value, then decays to the steady-state response over a period of about 1 msec. This effect is due to the initial surge of charge through the membrane carried by the large displacement (capacitive) currents near $t = 0$. The decay to the steady-state value occurs as the surface charge densities on either membrane interface reach their steady-state values and this current path "closes" as discussed above. Note that as in Chapter 3, the magnitude of Φ_E is far smaller than V_m' at all time t (except very close to $t = 0$). Thus Figure 4.2 is also a graph of $\Phi_I'(b, 1\ mm, t)$ as (to the resolution inherent in the scale) $V_m'(z,t) \doteq \Phi_I'(b,z,t)$.

Figure 4.4 is a time plot of V_m' for the axial distances of $z = 0$, 5, and 10 mm. At the larger axial distances, it is apparent that there is a time lag before the effect of the internal stimulus is seen. This is due to the initial low impedance current path at $t = 0$ of the membrane capacitance allowing the current to leave the intracellular space near the electrode. Figure 4.5 is a plot of V_m' as a function of z for various time points. The delay mentioned above for the stimulus effect to spread down the axon is even more clearly seen. A velocity for this passive spread of potential cannot be determined as there is no distinct feature (as in a traveling spike) to take time versus distance measurements from. As seen in Figure 4.5, the transmembrane potential is very close to its steady-state distribution at

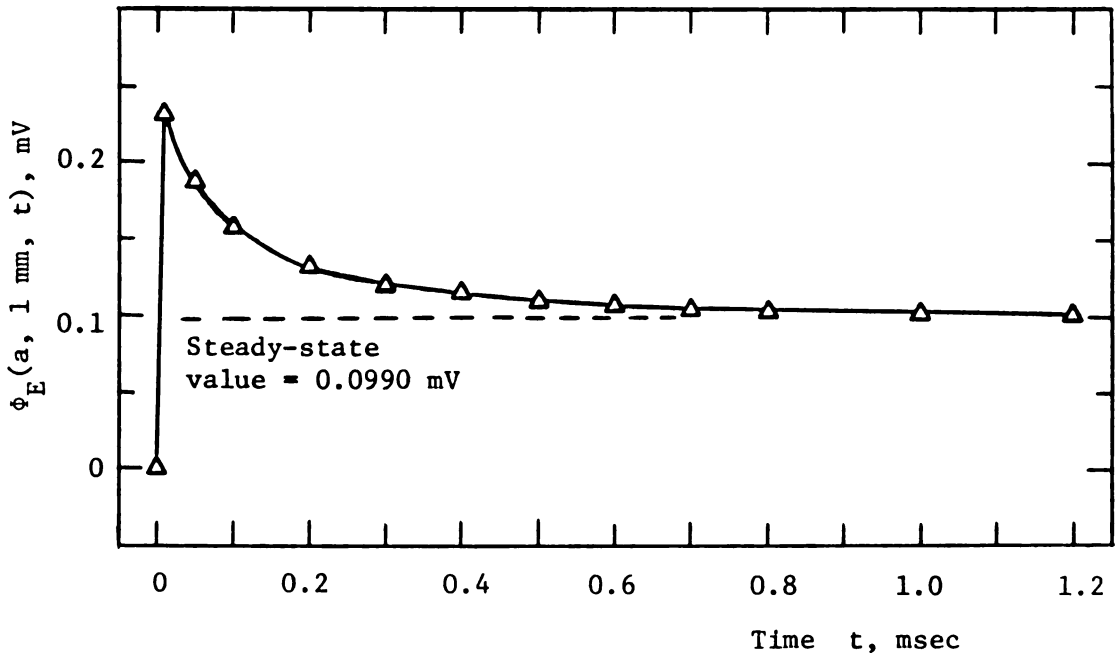

(a) Plot on the same time scale of Figure 4.2

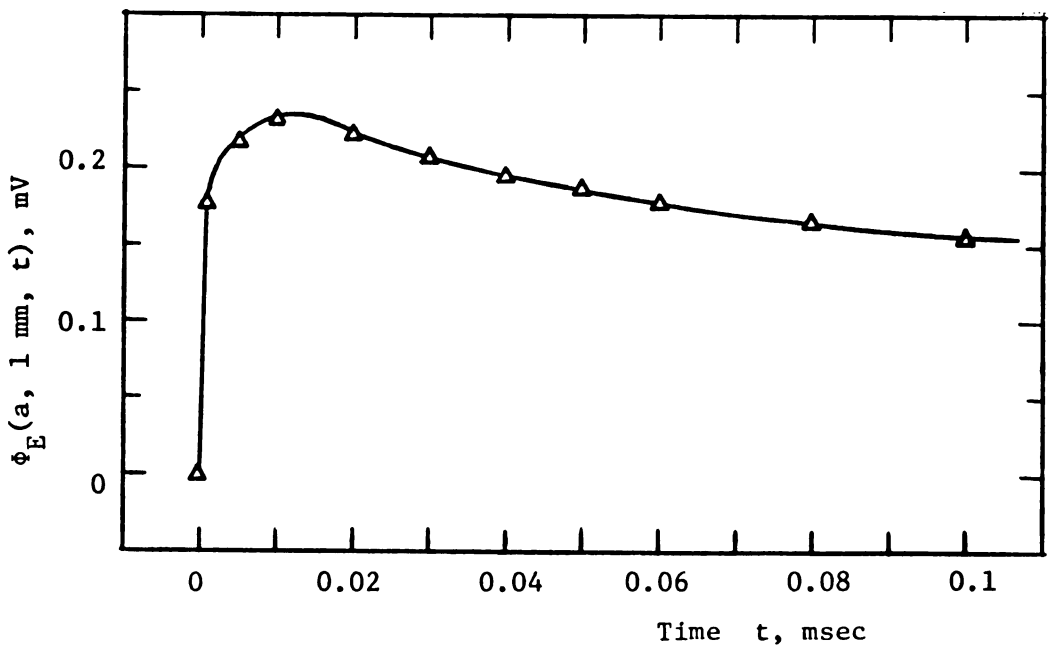

(b) Detail near t = 0

FIGURE 4.3

Φ_E(a, 1 mm, t) Time Response at z = 1 mm for a Step Function Stimulus Applied Internally

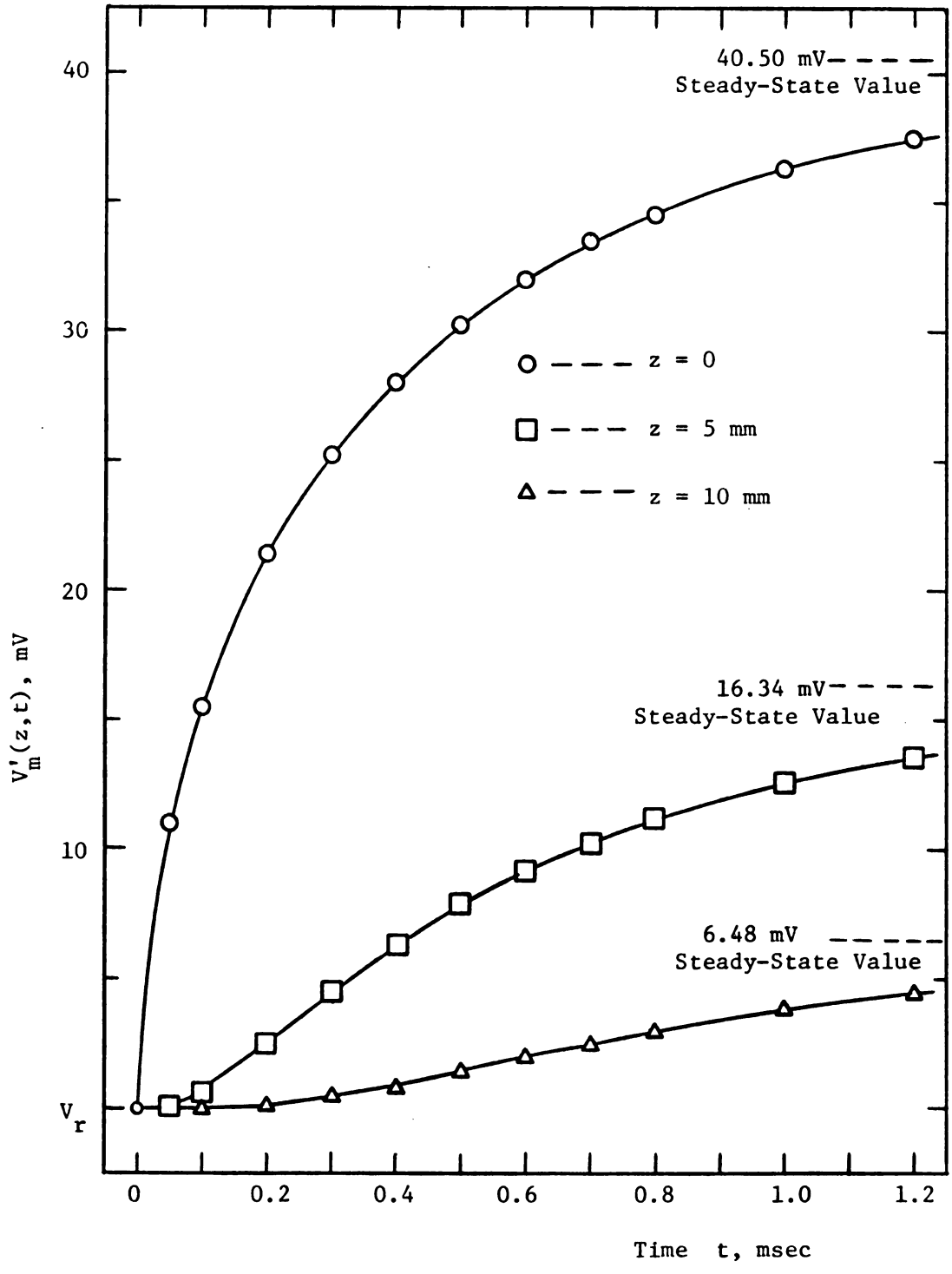

FIGURE 4.4

Transmembrane Potential Time Response at z = 0, 5, and 10 mm for a Step Function Stimulus Applied Internally

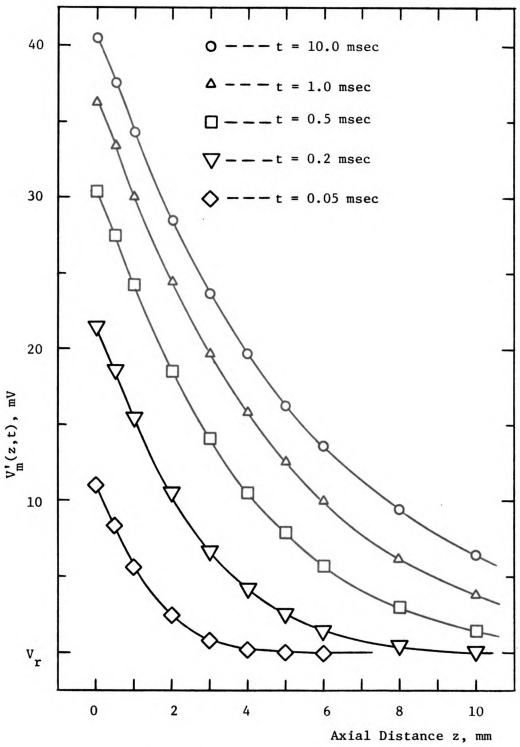

FIGURE 4.5

Transmembrane Potential as a Function of z for t = 0.05, 0.2, 0.5, 1.0, and 10.0 msec, Step Function Stimulus Internally Applied

t = 1 msec and it reaches steady-state by 10 msec.

All of the discussion above applies only to an intracellular stimulating electrode. If the stimulus is supplied via an extracellular electrode, the response is totally different. Figure 4.6 illustrates this with a graph of V_m', Φ_I' and Φ_E at z = 0.5 mm. The steady-state values of each potential are reached much more quickly than in the internal electrode case. In Chapter 3, it was demonstrated that the steady-state z-dependence for this stimulating electrode was not predicted by cable theory. Likewise the time response is also not given by cable theory, for the same reason that considering only axial current flow in the extracellular region is a poor assumption.

As seen in Figure 4.6, and in greater detail in Figure 4.7, Φ_I' and Φ_E both overshoot their steady-state values near $t = 0$, resulting in a brief period where $V_m'(0.5\text{ mm}, t)$ is positive. $\Phi_E(a, 0.5\text{ mm}, t)$ has a small overshoot very close to $t = 0$, followed by a slight drop below the steady-state value, and reaches steady-state by $t \doteq 0.02$ msec. The time response of $\Phi_I'(b, 0.5\text{ mm}, t)$ shows a far greater overshoot (more than 300% of the steady-state value) and a much slower decay to the steady state. Unlike the steady-state case of Chatper 3 where $\Phi_E(a,z)$ for the <u>intracellular</u> stimulus case was essentially equal to $\Phi_I'(b,z)$ from the <u>extracellular</u> stimulus case, $\Phi_E(a,z,t)$ for a time-dependent internal stimulus does not equal $\Phi_I'(b,z,t)$ from a time-dependent external stimulus[1].

---

[1] Compare Figures 4.3, 4.6, and 4.7. In the steady-state (as $t \to \infty$) they again become equal.

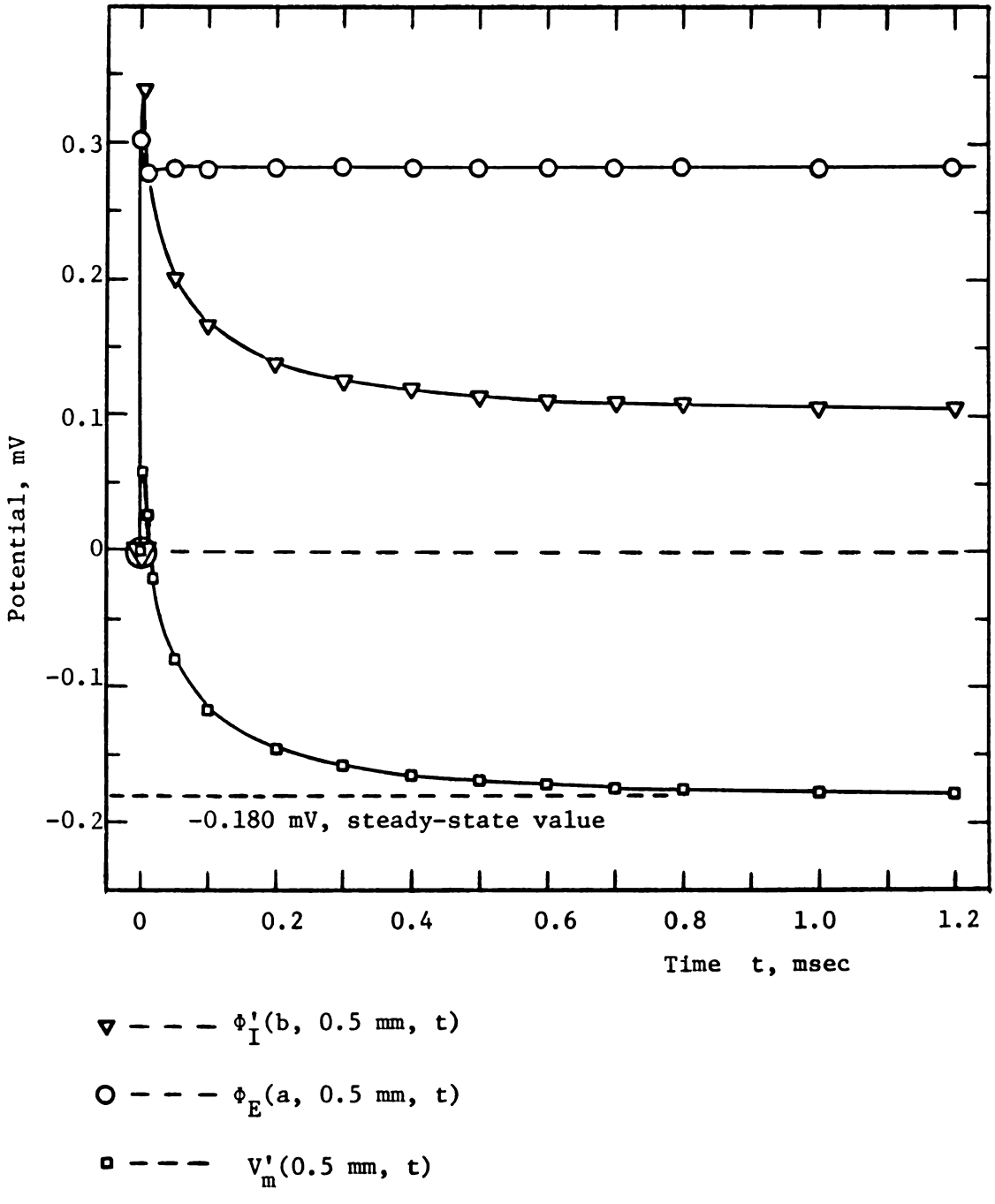

FIGURE 4.6

Time Response at z = 0.5 mm to an Externally Applied Step Function Stimulus

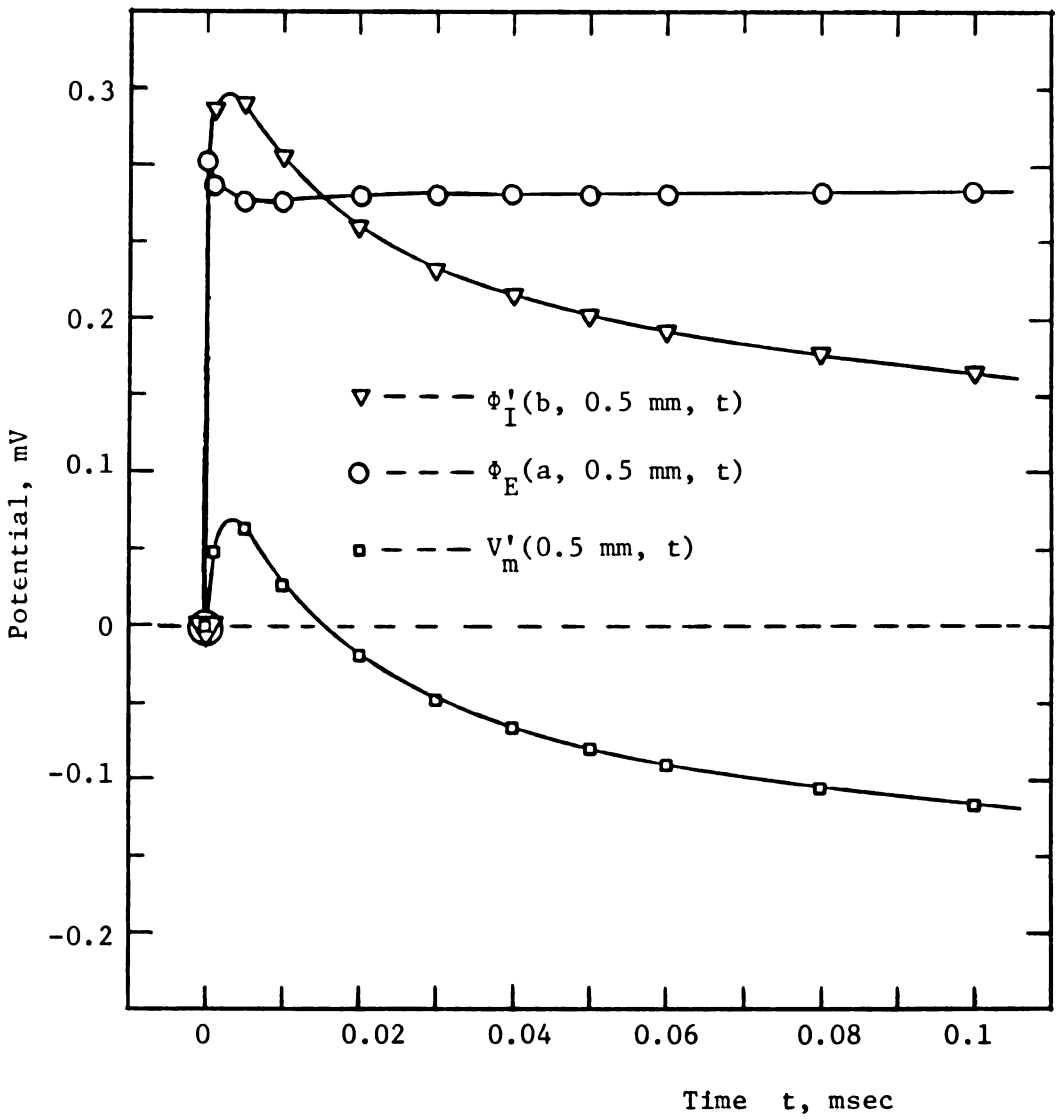

FIGURE 4.7

Detail of Time Response at z = 0.5 mm for an Externally Applied Step Function Stimulus

Also note that the time response of V_m' is mostly due to the slower decay of Φ_I', as Φ_E reaches steady-state almost immediately.

The overshoot of Φ_I and its subsequent slow return to the steady-state value is an effect of the membrane capacitance. As in the intracellular electrode case, near $t = 0$ the capacitance provides a low-impedance shunt path for a surge of charge through the membrane. This excess charge is retained within the cell until it can leak back out via the now highly resistive membrane. The time required for this return to the steady-state is shorter than in the intracellular stimulus case. This is because, after the initial surge, the electrode no longer supplies the excess charge and there is the additional axial path of the intracellular medium for the excess charge to disperse along before leaving the cell interior via the membrane[1].

These effects are further illustrated in Figure 4.8. At $z = 0$, there is a very brief overshoot of V_m' positive, followed by a rapid decay to the steady-state value. At $z = 1$ mm, the overshoot is delayed and dispersed in time, with a slower drop to the (negative) steady-state value. At $z = 5$ mm, almost no overshoot is seen, with V_m' rising smoothly to its steady-state. Figure 4.9, a plot of V_m' versus z for $t = 0.05$, 0.2, and 1.0 msec, shows the same response in a slightly different manner. Again the overshoot is seen to nearly vanish at larger values of z. Note

---

[1] The potential overshoots (along with other stray capacitive effects in the stimulating and recording circuits) are seen in neural experiments as a stimulus artifact. See the results of Hodgkin, Huxley, and Katz [38]. Note that this effect is also present in Φ_E for the intracellular stimulus case.

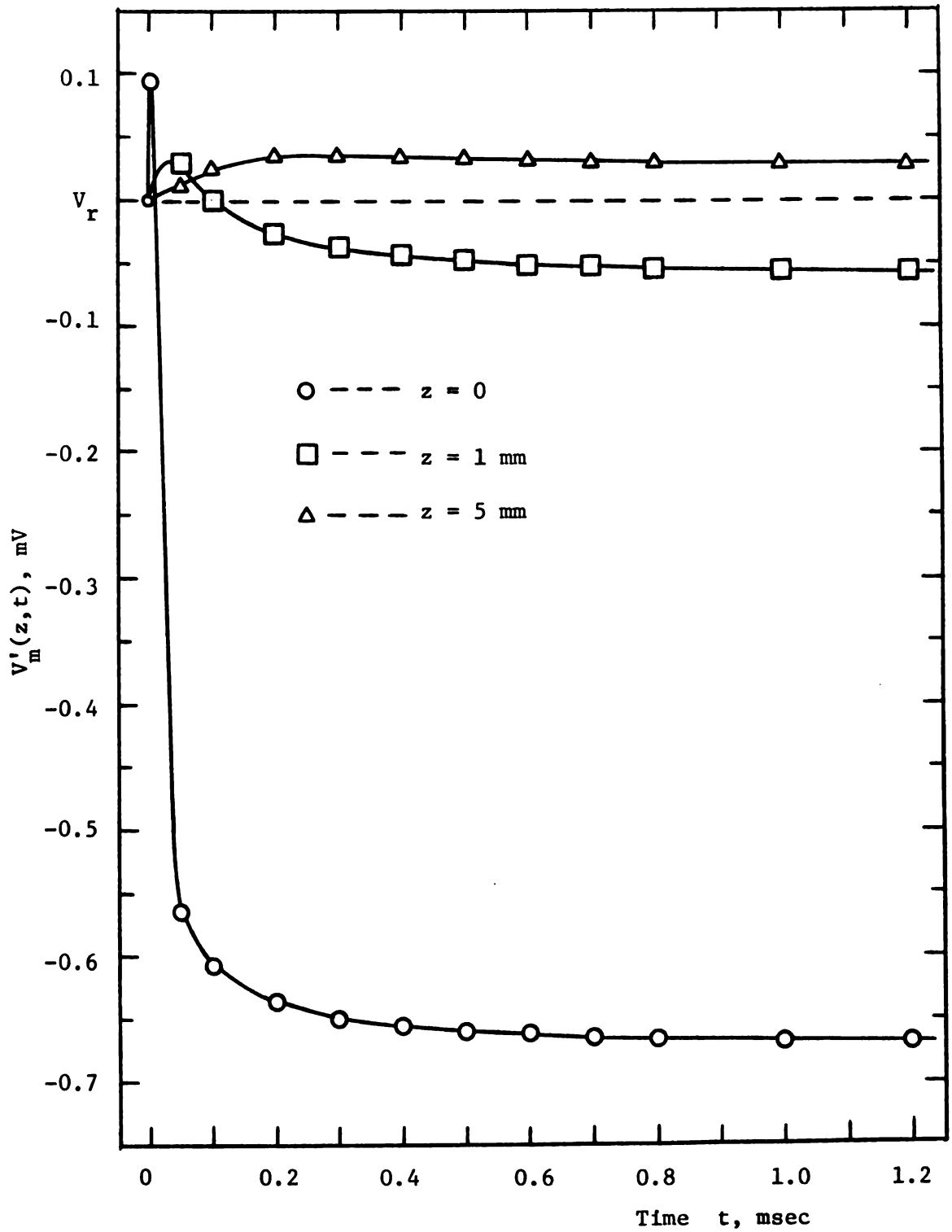

FIGURE 4.8

Transmembrane Potential Time Response at z = 0, 1, and 5 mm for a Step Function Stimulus Applied Externally

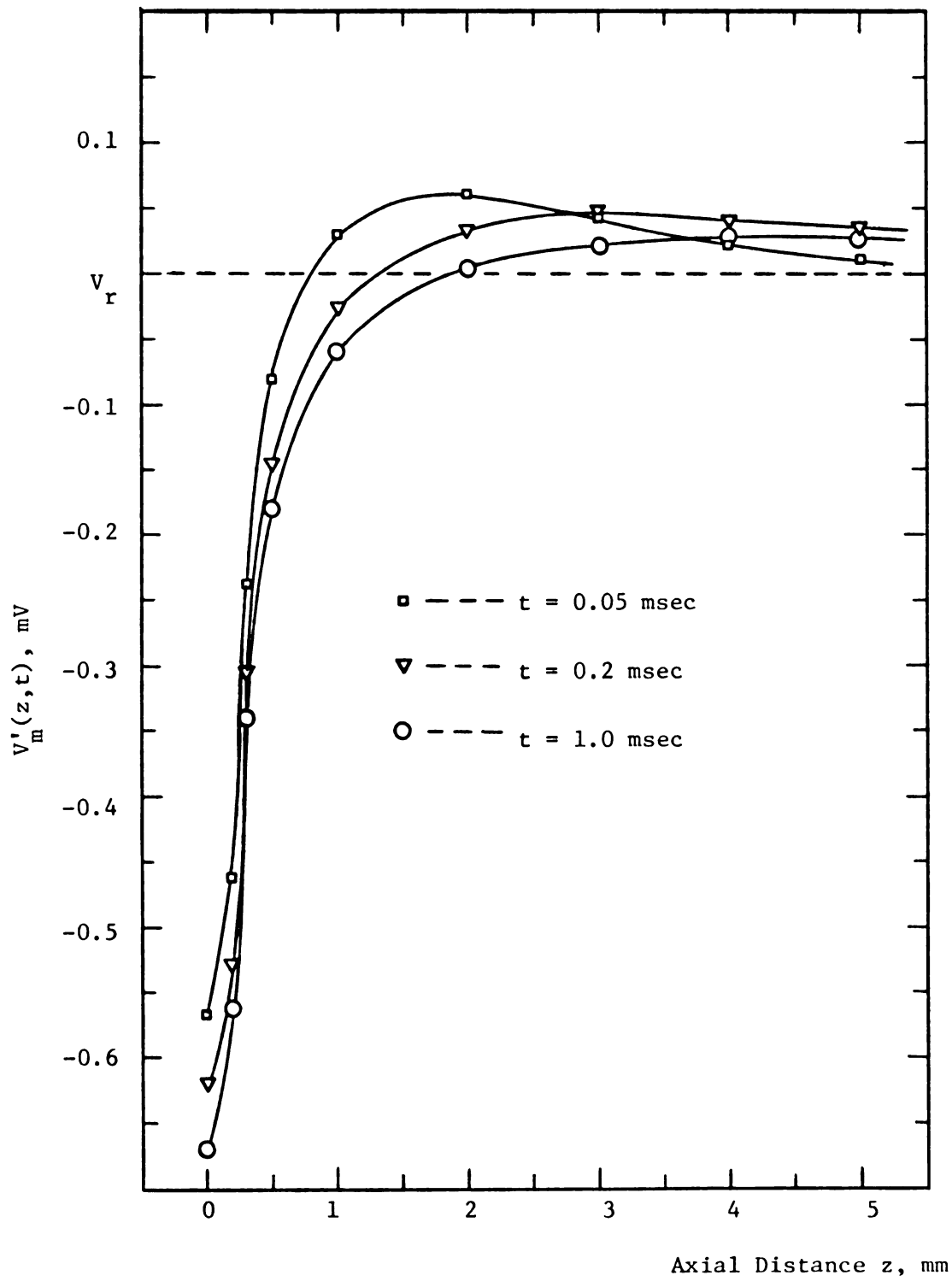

FIGURE 4.9

Transmembrane Potential as a Function of z for t = 0.05, 0.2, and 1.0 msec, Step Function Stimulus Externally Applied

that the point where $V_m' = 0$ moves to the right with increasing time. Steady-state is also observed to be attained much more quickly than for an intracellular stimulus, this being the case at $t = 1.0$ msec (as compared with about 10 msec for an internal stimulus).

The results for a step function stimulus may be summarized as follows.

i) The time response of V_m' is well predicted by cable theory for the case of an intracellular electrode, but not for an external stimulus.

ii) The low impedance path due to capacitive effects near $t = 0$ gives rise to an overshoot in the Φ_E response for the internal stimulus case, and an overshoot for Φ_I', Φ_E, and V_m' in the extracellular electrode case.

iii) As $t \to \infty$, the response becomes that of the steady-state model of Chapter 3.

4.3.2. Response to a Pulse Function Stimulus

The transmembrane potential time response to a rectangular stimulating current pulse of 0.5 msec duration is illustrated in Figure 4.10. Only times greater than 0.3 msec are plotted as (by equation (4.84)) the response for $0 \leq t \leq 0.5$ msec is the same as for a step function stimulus. Thus Figures 4.1 and 4.4 of the previous section supply the portion of the response between $t = 0$ and $t = 0.3$ msec. This solution may be obtained by the linear superposition of two step responses, one at $t = 0$ and the second (subtracted from the first) starting at $t = 0.5$ msec. As before, the Fourier transform field model gives essentially the same time response as the core-conductor model.

As observed in both Figures 4.10 and 4.11, the effect of switching off the stimulus is seen immediately at the electrode ($z = 0$), but the response is delayed and diffused at greater axial distances. This is especially clear in Figure 4.11 (a plot of V_m' vs. z for various $t \geq 0.5$ msec) in that V_m' continues to increase after $t = 0.5$ msec for axial distances greater than a few millimeters. These effects are due to the discharging of the membrane capacitance (relaxation of polarization effects within the membrane and loss of excess surface charge density). Even though the transmembrane potential near the electrode at $t > 0.5$ msec has started to decay to V_r, the potential still has a decreasing axial gradient that causes an axial current flow to the right, resulting in a continued increase in V_m' at points away from the electrode. Thus the sharp edge seen in the $z = 0$ and 1 mm

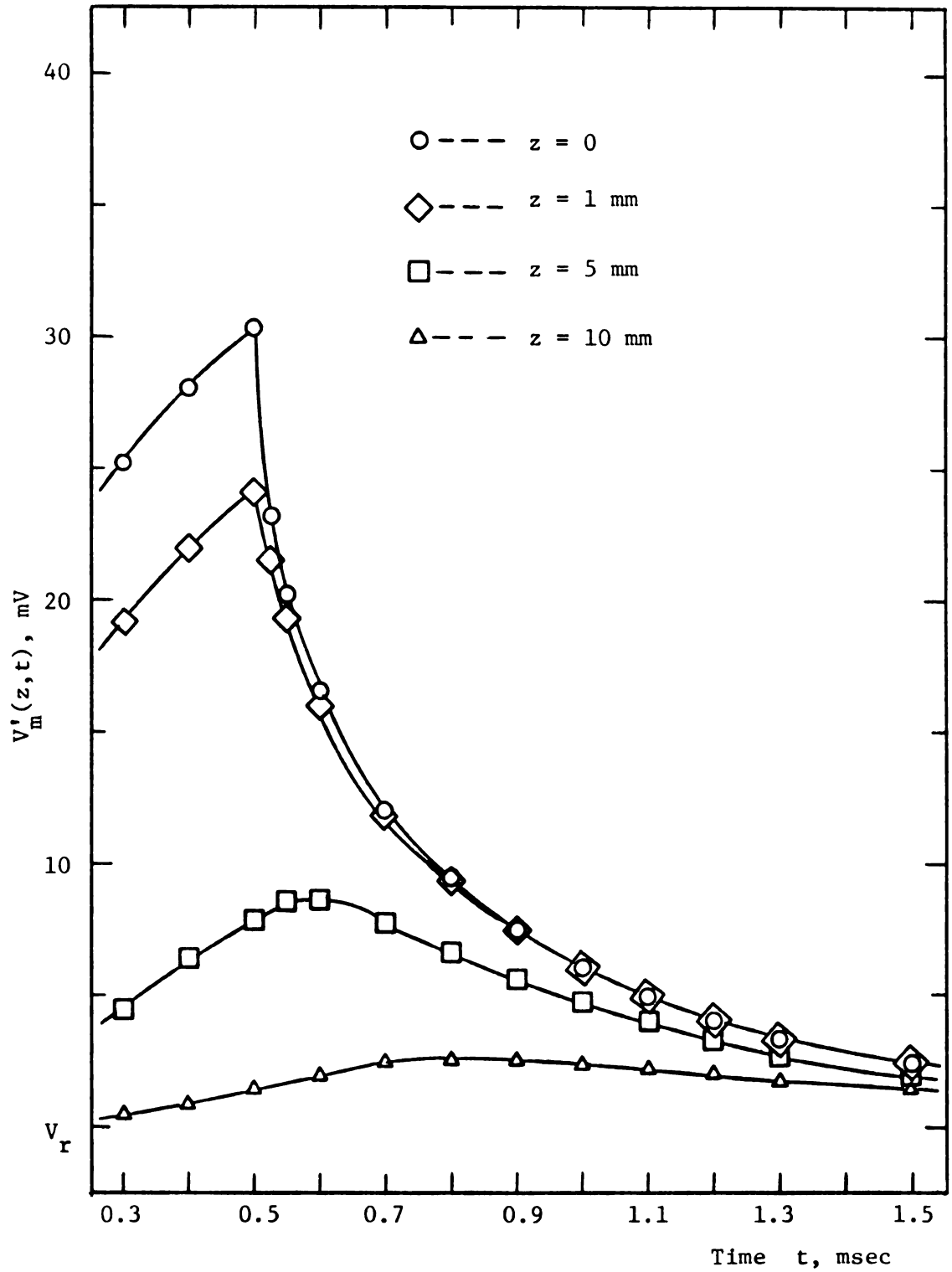

FIGURE 4.10

Transmembrane Potential Time Response at z = 0, 1, 5, and 10 mm for a 0.5 msec Duration Pulse Stimulus Applied Internally

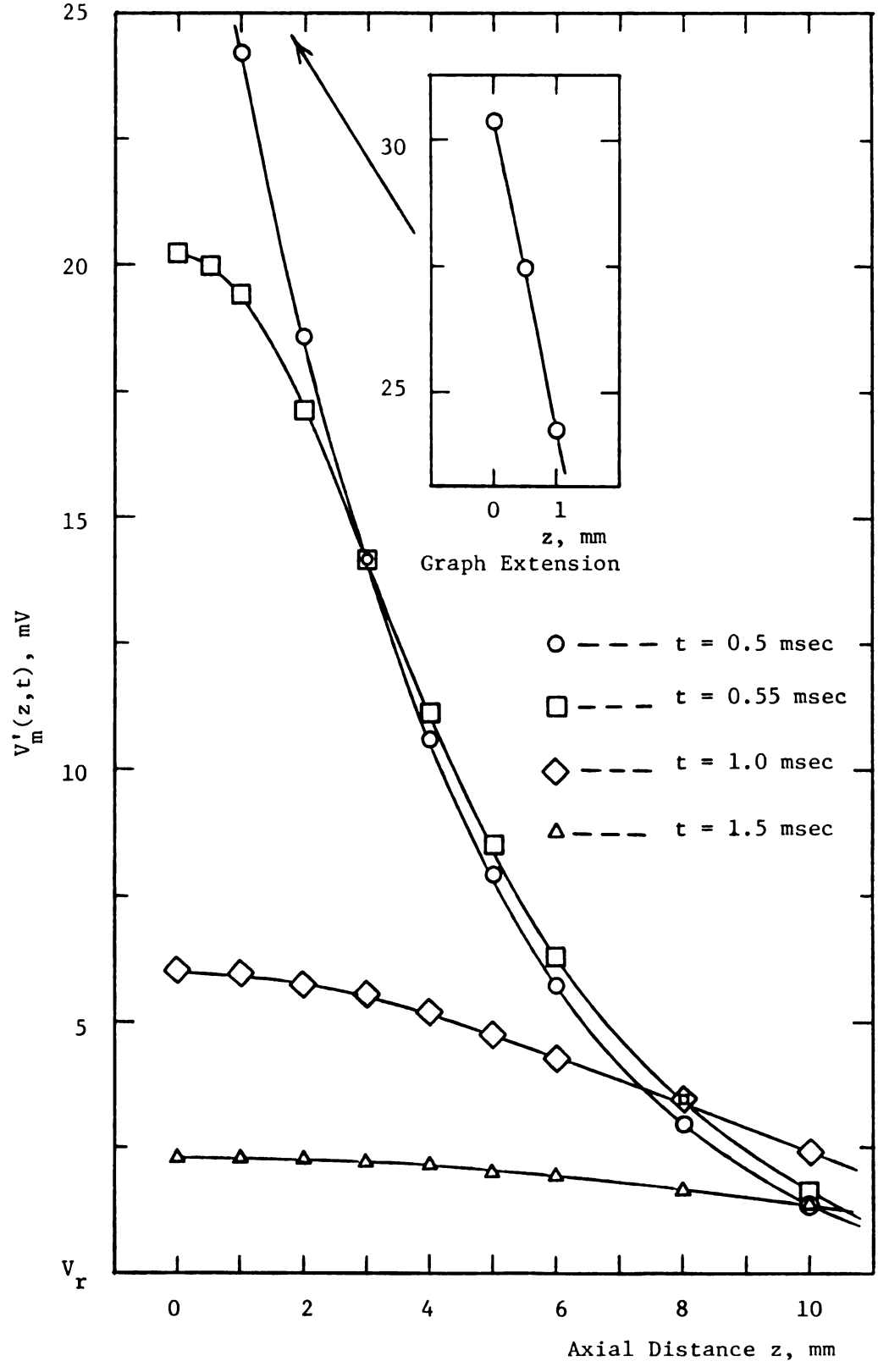

FIGURE 4.11

Transmembrane Potential as a Function of z for t = 0.5, 0.55, 1.0, and 1.5 msec, 0.5 msec Pulse Stimulus Internally Applied

curves of Figure 4.10 is diffused into the smooth hump seen in the $z = 5$ and 10 mm curves.

As in the previous step function case, the extracellular potential at the membrane ($\Phi_E(a,z,t)$) reaches its steady-state value almost immediately and is far smaller in magnitude than $\Phi_I'(b,z,t)$. Thus Figures 4.10 and 4.11 also give (at the resolution of their scale) the time and axial dependence of $\Phi_I'(b,z,t)$. $\Phi_E(a,z,t)$ shows a brief and small undershoot (i.e., becomes negative) near $t = 0.5$ msec, then returns to the steady-state value of zero (as the stimulus is absent at $t \to \infty$). The response of $\Phi_E(a,z,t)$ may be obtained as indicated above by the linear superposition of the results of the previous section (Figure 4.3).

The time response associated with terminating the stimulating current to an <u>extracellular</u> electrode is shown in Figure 4.12, with Figures 4.6 to 4.8 of Section 4.3.1 supplying the curves for $0 \leq t \leq 0.4$ msec. As in the case of an external step function stimulus, the response to a change in stimulating current is very fast (as compared to an intracellular stimulus) and shows a stimulus artifact in the form of a brief spike at the termination of the pulse stimulus. Linear superposition again gives the solution from the results of Section 4.3.1.

Figure 4.13 provides a more detailed picture of the stimulus artifact near $t = 0.5$ msec. The artifact is apparent only near the electrode, diffusing and vanishing for increasing z. At $z = 5$ mm, its only trace is a very leisurely excursion of V_m slightly below the resting potential. These effects are again due to the discharge of the membrane capacitance, and the discussion

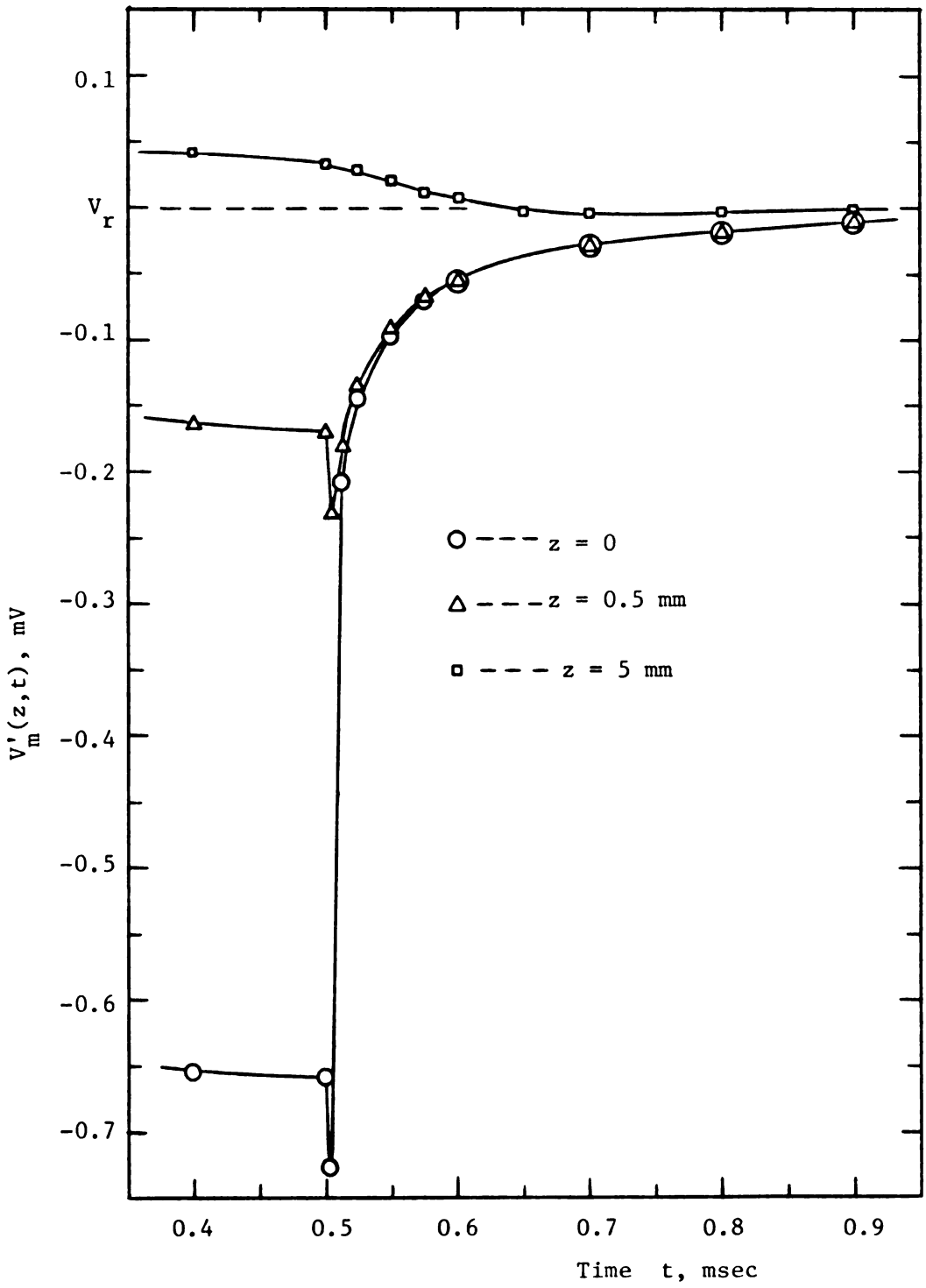

FIGURE 4.12

Transmembrane Potential Time Response at z = 0, 0.5, and 5 mm for a 0.5 msec Duration Pulse Stimulus Applied Externally

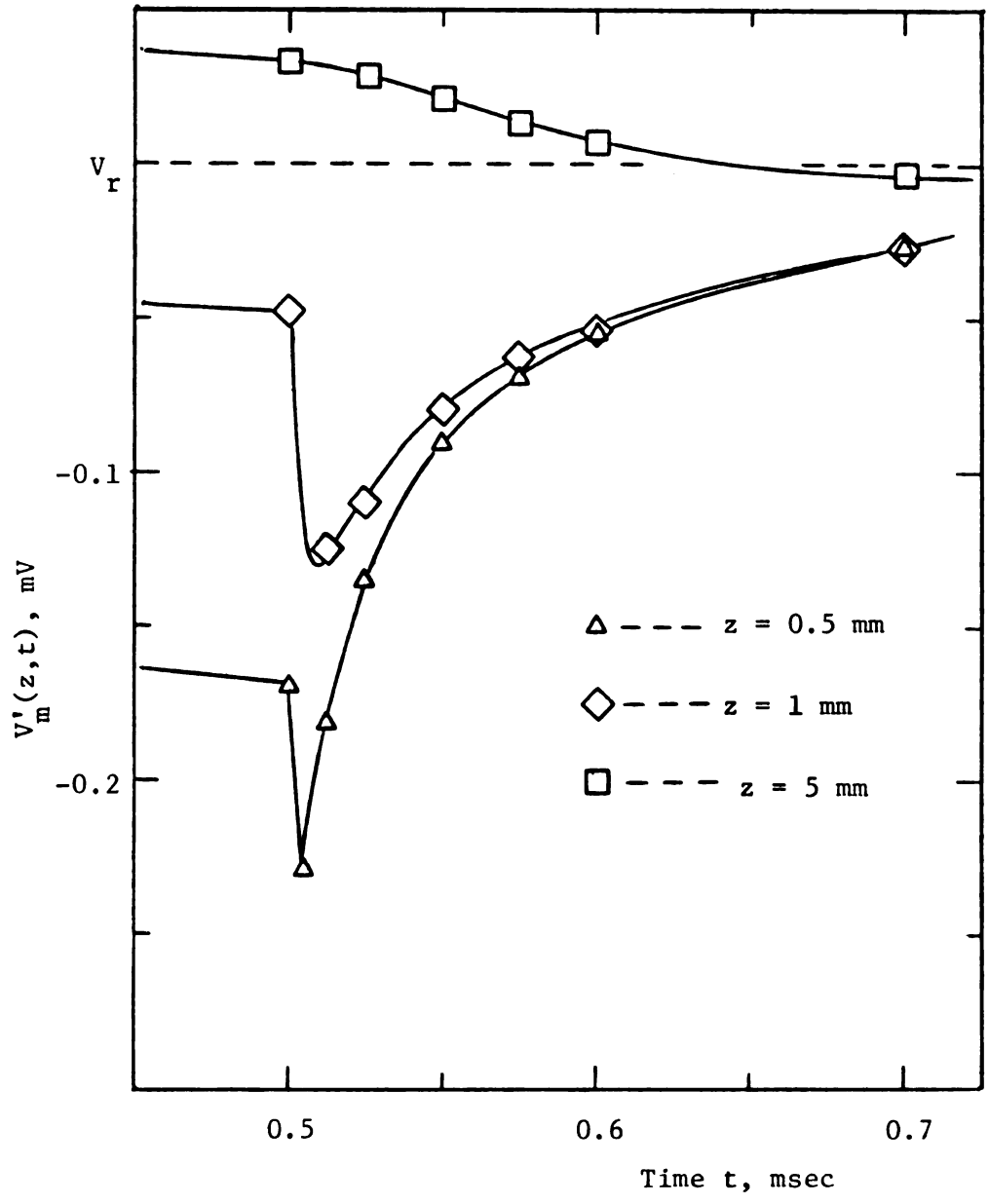

FIGURE 4.13

Transmembrane Potential Time Response to External Pulse Stimulus, Detail Near t = 0.5 msec for z = 0.5, 1, and 5 mm

in the previous section on the overshoot transients for the step-function extracellular stimulus applies to this case.

As in the intracellular stimulus case, the axial locations away from the electrode do not respond immediately to the end of the stimulating current. This is seen in Figure 4.14 (a plot of V_m' vs. z at $t = 0.5$, 0.5125, and 0.55 msec) as well as a much faster return of V_m to the steady-state condition of $V_m = V_r$ than for an internally applied pulse (compare with Figure 4.11). In terms of scalar potential at the membrane interfaces, the response is mostly due to $\Phi_I'(b,z,t)$; as $\Phi_E(a,z,t)$ returns to zero almost immediately after $t = 0.5$ msec (with a brief undershoot at $t = 0.5$ msec, see Figure 4.7 of the step function response). Also, as discussed in the previous section, the effect of an extracellular stimulus (a pulse time function in this case) is not predicted by the core-conductor model.

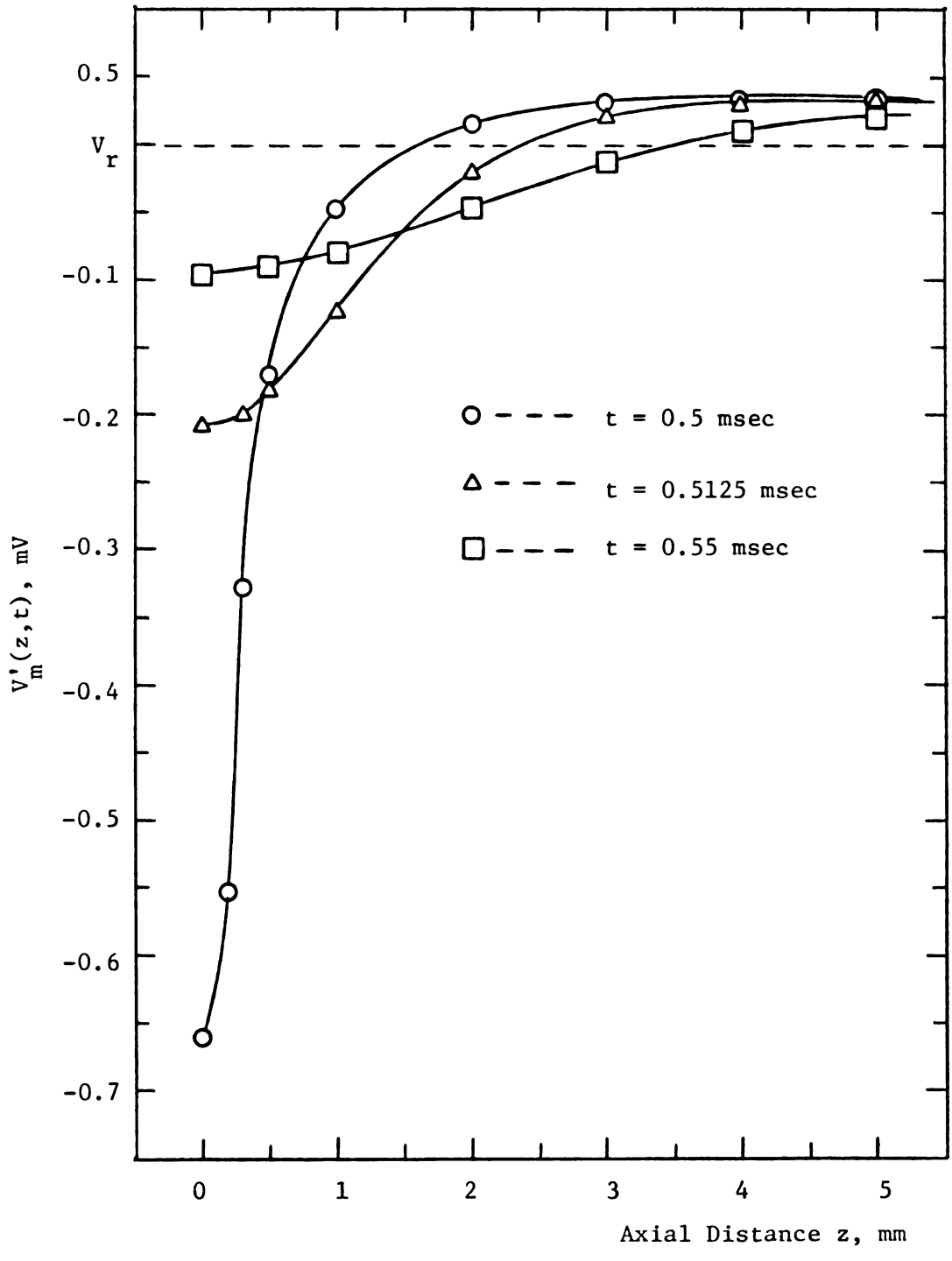

FIGURE 4.14

Transmembrane Potential as a Function of z for t = 0.5, 0.5125, and 0.55 msec, Externally Applied 0.5 msec Pulse Stimulus

4.3.3. Response to an Impulse Function Stimulus

The previous section dealt with a pulse stimulus that consisted of a step in the current to the electrode at $t = 0$ that ended a finite time later at T_o. The total charge supplied by the stimulating circuit is then just $T_o I^s$ where I^s is the magnitude of the total current to the electrode. As T_o becomes smaller, the charge delivered becomes less, with the limiting case of $T_o \to 0$ being no stimulus at all, and no evoked response. However, it is possible to mathematically define an impulse stimulus that delivers a finite charge in an infinitely brief time by means of a Dirac delta function, $\delta(t)$. This was done in equation (4.51) and the solution was found in Section 4.2.3 , relations (4.87) - (4.89). Previous authors have used delta functions both for electrode space extent (see Chapter 3) and stimulus time response[1]. It is included in this report primarily for comparison purposes.

For the results presented in this section, the current density magnitude J^s (in equation (4.51)) was adjusted by multiplying by 0.0005. This was done to make the total charge supplied by the impulse the same as that delivered by a 0.5 msec pulse stimulus (the delta function has unit magnitude when current is integrated to obtain charge). Thus the results in this section may be compared with those of the previous section to study the limiting case of shortening the pulse duration and increasing pulse magnitude so as to deliver the same total charge[2].

---

[1] For example, Stevens [74] models a synapase with a $\delta(z)\delta(t)$ type of source in the core-conductor model.

[2] The total charge is 10^{-5} amps $\times$ 0.5 msec $= 5 \times 10^{-9}$ coulombs for the numerical results presented.

Figures 4.15 and 4.16 present the time and axial dependence of transmembrane potential for the case of the impulse current supplied via a 0.5 mm width intracellular electrode. Perhaps the most outstanding feature of the response is the singularity at $t = 0$ and $z = 0$ where V_m diverges to $+\infty$. This is a result of the requirement of an infinite potential at the electrode (Φ_I at $r = b$, $|z| < 0.25$ mm in this case) to deliver a finite charge in an infinitely brief interval (i.e., via an infinitely large current at that point and time). After the injection of this charge, a very rapid relaxation in time and space occurs. As seen in Figure 4.16, the response is far more localized about the electrode than for the finite pulse, and Figure 4.15 indicates the transient period ends much more quickly (than for a pulse). This is because it takes little time or space for the charge delivered by the electrode to dissipate into the intracellular volume conductor. Even in the small intracellular volume, the total charge is so minute as to decay to an insignificant density very quickly as the resultant currents diffuse it throughout the system.

From Figure 4.15, a velocity for the axial spread of potential can be discerned. At $z = 0$, the peak of the curve of V_m' is essentially at $t = 0$ (the time of the impulse). The $z = 0.5$ mm curve shows the peak as diffused and occurring at $t \doteq 0.005$ msec. At $z = 1.0$ mm, the maximum is even more diffuse, but can be discerned as occurring at $t \doteq 0.01$ msec. This gives a velocity for the passive spread of potential as $v = 0.5$ mm/0.005 msec = 1.0 mm/0.01 msec = 100 m/sec. This velocity is only a measure of

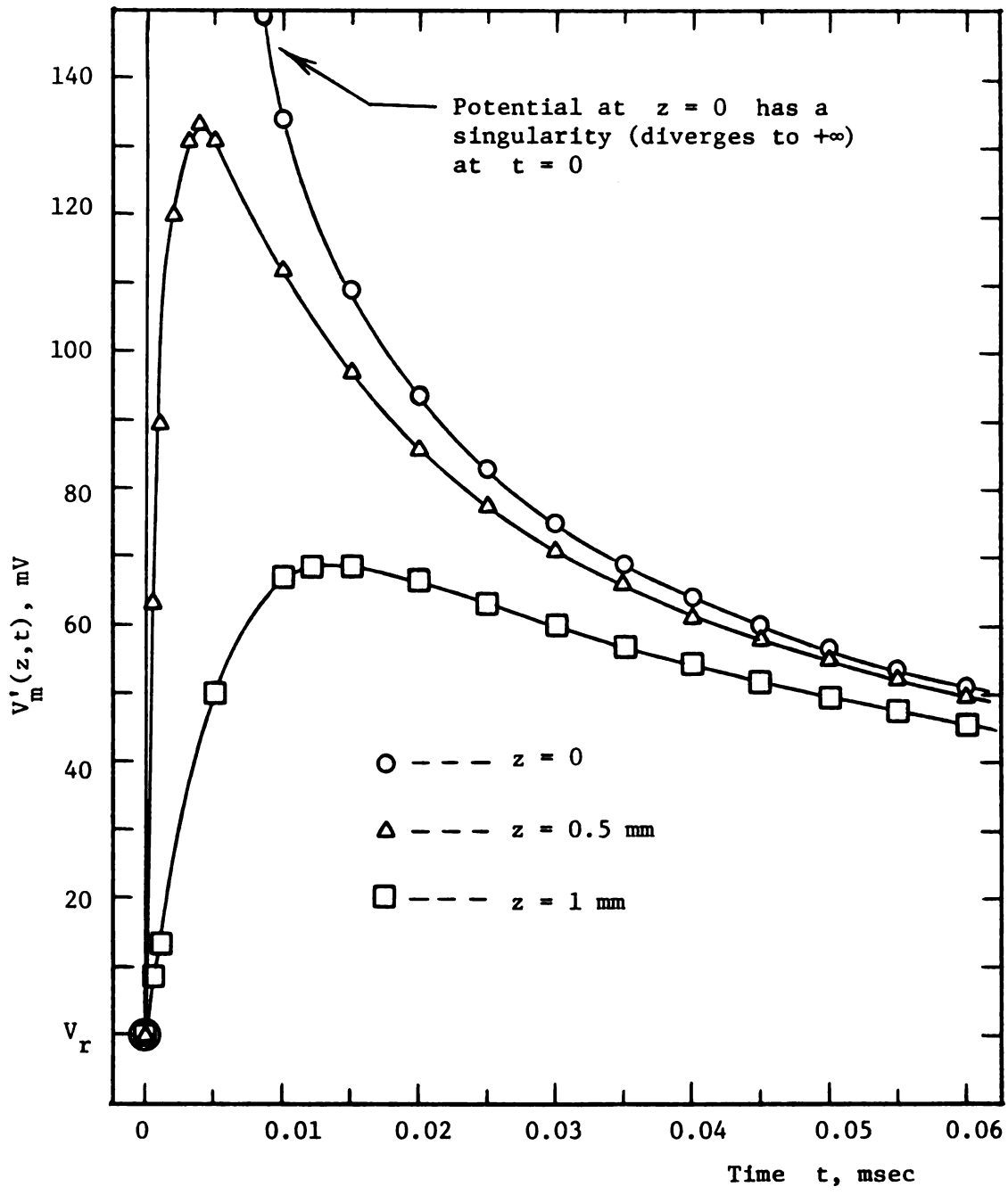

FIGURE 4.15

Transmembrane Potential Time Response at z = 0, 0.5, and 1 mm for an Internal Impulse Stimulus

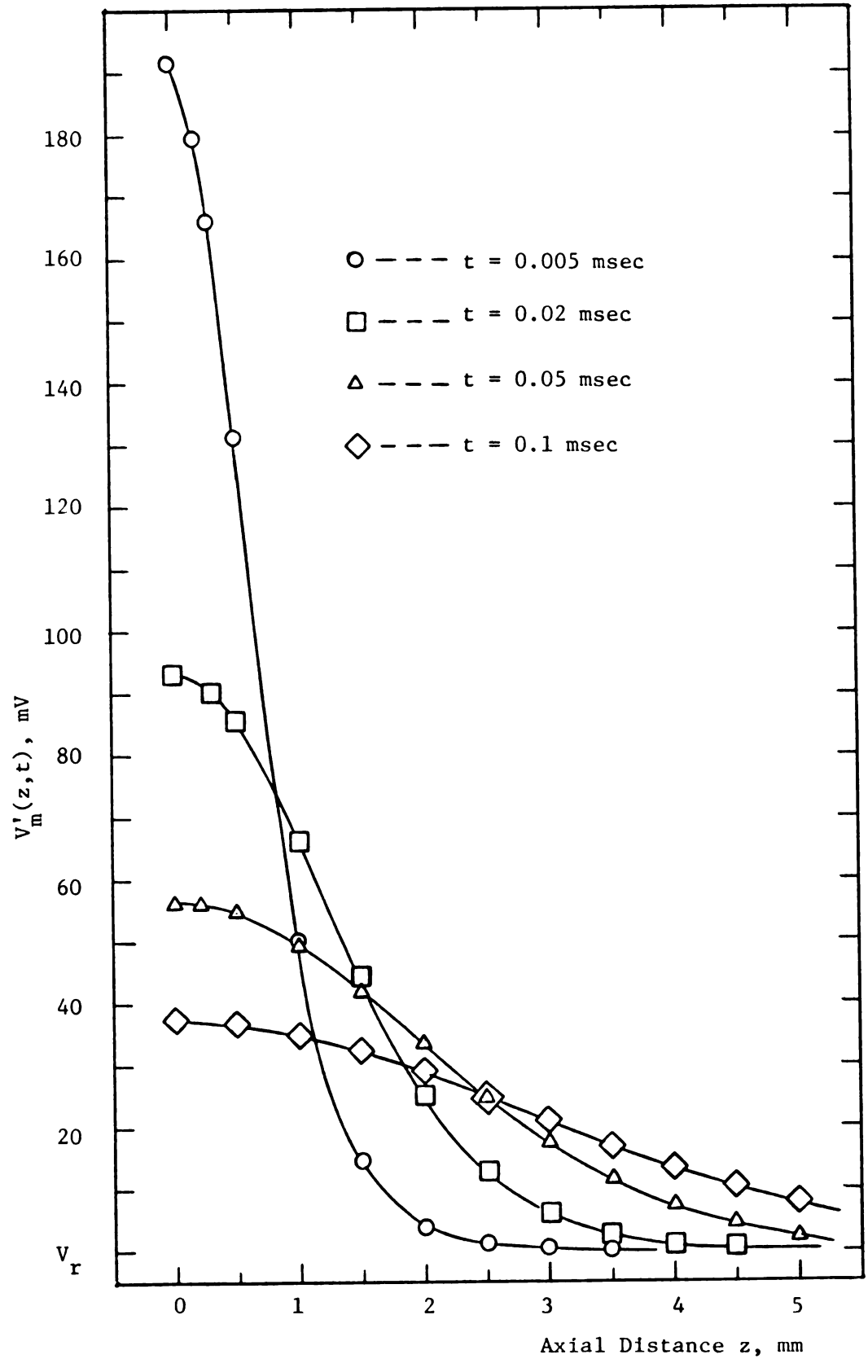

FIGURE 4.16

Transmembrane Potential as a Function of z for t = 0.005, 0.02, 0.05, and 0.1 msec, Internal Impulse Stimulus

the rapidity of the spread of the passive response, and does not represent an action potential propagation velocity[1].

The results are essentially the same for the extracellular electrode case, as illustrated in Figures 4.17 and 4.18. The major differences lie in the fact that V_m' now diverges to $-\infty$ at $t = z = 0$ and that the decay times and distances of the response are even smaller. V_m' goes to $-\infty$ because, with the electrode at the external membrane interface, the singularity caused by the impulse is in $\Phi_E \to +\infty$ at the location of the electrode and $V_m' = \Phi_I' - \Phi_E$ gives $V_m' \to -\infty$. The more rapid time and spatial decay are the result of the large extracellular volume for the charge to immediately diffuse into, no longer being confined within a highly resistive membrane as in the intracellular stimulus case. Also note in Figure 4.18 the wild swings in V_m' from positive to negative at times near $t = 0$ that quickly die out as seen in the $t = .005$ msec curve. This is a result of the alternate charging and subsequent discharging of the membrane capacitance by the charge supplied by the impulse.

The net conclusion from this section is that except for a brief infinite spike at $t = z = 0$, an impulse stimulus does not produce an effect that has the space or time extent of a finite duration pulse, especially when the decay times or distances are defined as a percentage drop from a value of $|V_m'|$ very near

---

[1] Other effects are included in determining action potential velocity (such as latency, the time between a supra-threshold stimulus and the peak of the resultant action potential).

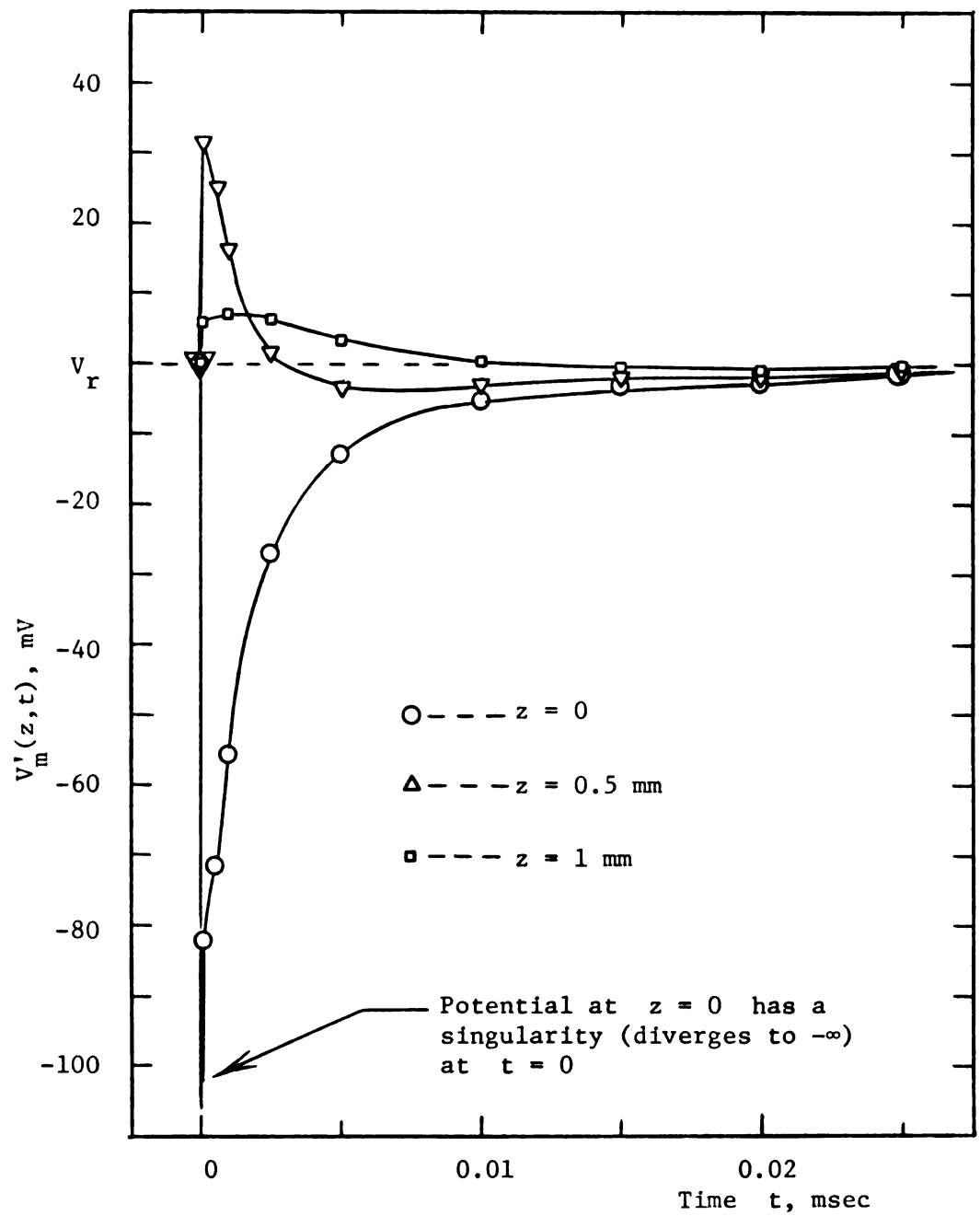

FIGURE 4.17

Transmembrane Potential Time Response at z = 0, 0.5, and 1 mm for an External Impulse Stimulus

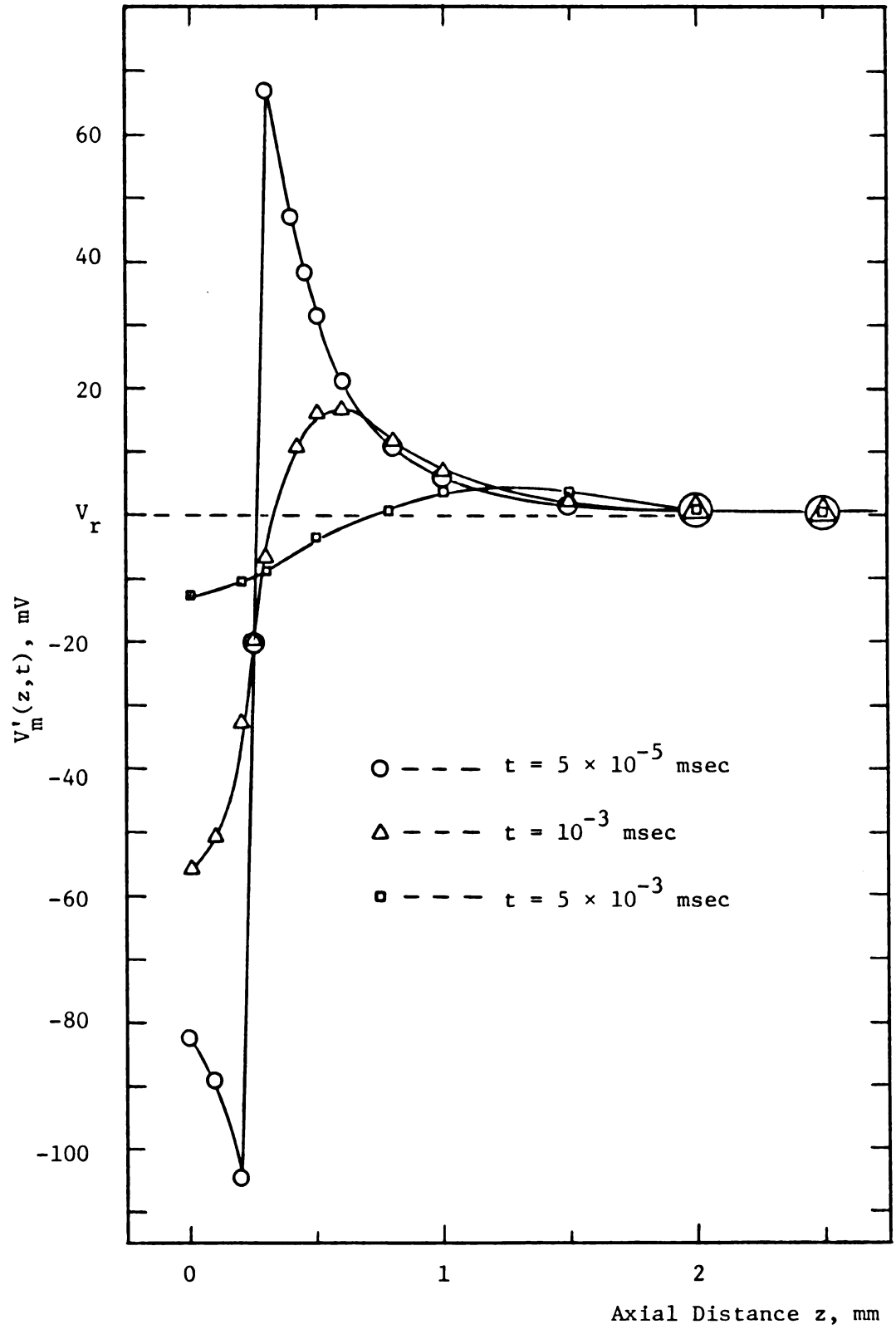

FIGURE 4.18

Transmembrane Potential as a Function of z for t = 50, 1000, and 5000 μsec, External Impulse Stimulus

$t = z = 0$. The response does not display the R-C time constant of the core-conductor model, even for the intracellular electrode case. With the singularity in V_m' and the brevity of response, the impulse response does not appear to model very well any observed neural phenomena. Its characteristics make it a poor approximation of such phenomena as action potential spikes or synapses (as some authors have done, see Stevens [74]), especially in a field-type model such as presently being considered.

4.3.4. Simulation of a Myelinated Axon

The three-volume-conductor-region solution of this chapter can be used to obtain an interesting model of a myelinated axon. As discussed in Section 2.1.2, many axons have a periodically interrupted insulating sheath formed by Schwann cells wrapping several layers of their membrane about the axon. The action of this myelin sheath is to allow only a passive (electrotonic) spread of potential between nodes (interruptions in the sheath) and generation of the action potential only at the nodes. Nerve impulse propagation velocity is increased by not allowing action potential generation at every point and by decreasing the electrotonic axial decay for the regions covered by the myelin. These effects are discussed in Ochs [54] and Plonsey [60].

To simulate response characteristics that occur during the active event of saltatory conduction with this electrotonic (passive) model requires a few approximations and a realization of the limited number of features that the model will give. The simplifications of the simulation are illustrated in Figure 4.19 in a three-part

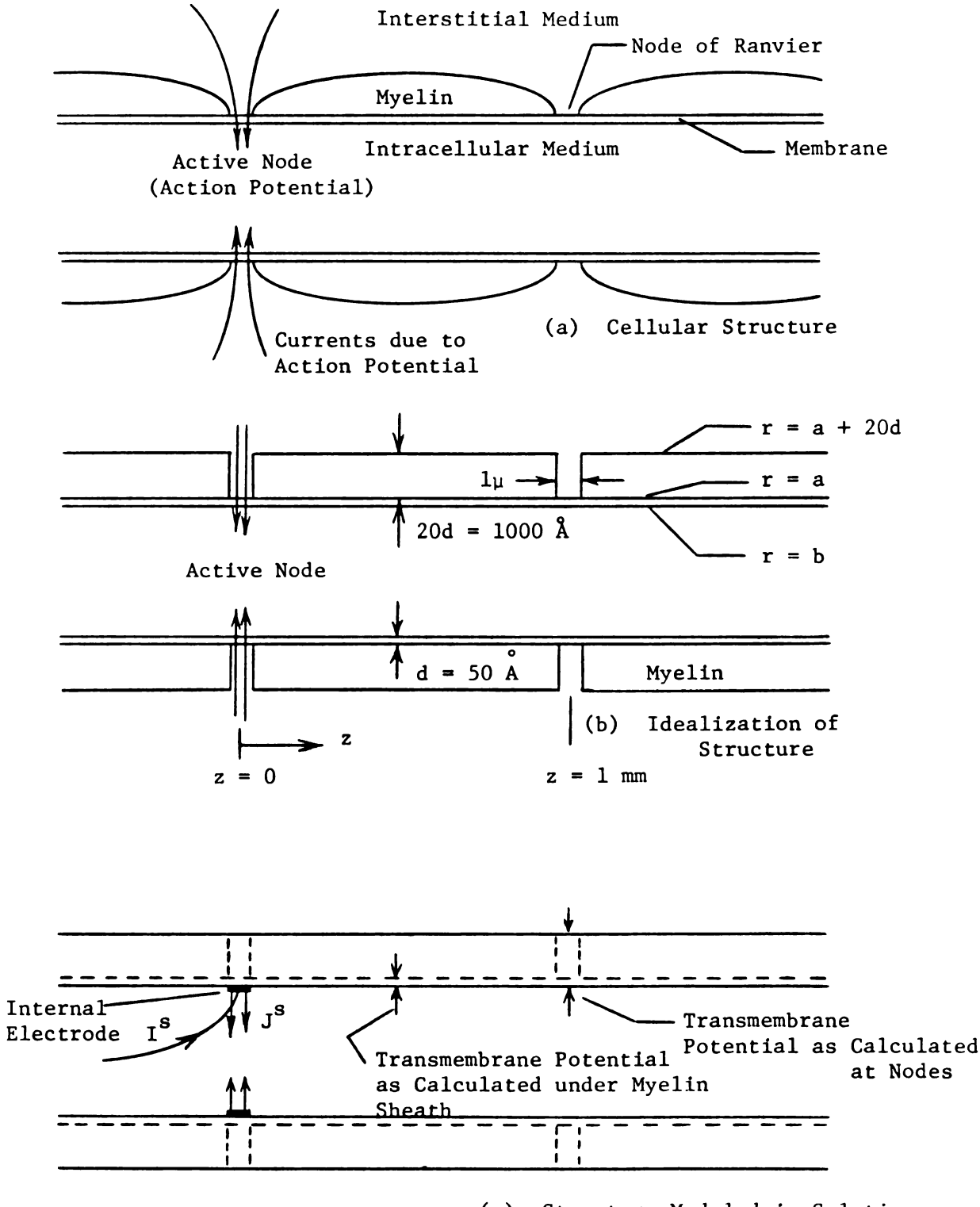

FIGURE 4.19

Geometry for Myelinated Axon Model

fashion. Figure 4.19(a) diagrams the actual cellular structure that consists of four regions: intracellular, interstitial (extracellular), membrane, and the myelin sheath. One node (at the left) is assumed "active" in the sense that an action potential has been excited there. What will be examined is the passive spread of potential from this active node to the adjacent node at the right.

Figure 4.19(b) shows the idealized structure to be modeled. The myelin sheath is assumed to be uniform in thickness between nodes, with the origin ($z = 0$) at the center of the active node and the adjacent node centered at $z = 1$ mm. The nodes are taken as 1μ wide and the myelin sheath as 1000 Å thick (as might be the case for a Schwann cell wrapping its 50 Å membrane 10 times about the axon, with two layers per wrap)[1]. The axon is otherwise the same as the standard test axon, with its outer membrane interface at $r = a = 0.25$ mm and inner radius as $b = a - d$ where $d = 50$ Å = membrane thickness.

As the field model of this chapter is for three regions rather than four, the closest cellular structure that can be described by this model is diagrammed in Figure 4.19(c). The myelin sheath and axonal membrane have been combined into a single homogeneous region defined between $r = b$ and $r = b + 21d$. As the myelin sheath is considered to be constructed of tightly laminated layers of unit membrane, with properties similar to the axonal membrane in the passive state (see Ochs [54]), this assumption is

---

[1] See Ochs [54], these values are representative of the dimensions of the actual structures. Note that Figure 4.19 is not drawn to scale.

not unreasonable. The outer boundary of the axon membrane is indicated at $r = b + 50\ \mathring{A} = 0.25$ mm with a dashed line. In terms of the Fourier transform solutions of Section 4.2.3, the inner radius b is defined as the same as for the test axon, the outer axon radius is at $b + 50\ \mathring{A}$ (as for the test axon) with its potential now defined by means of Φ'_M evaluated at $r = b + 50\ \mathring{A}$, and the outer radius a in the solutions is now taken as $b + 1050\ \mathring{A}$ $(b + 21d)$. The potential in the extracellular region (Φ_E) is thus defined for $r \geq b + 1050\ \mathring{A}$.

The nodes are modeled as follows. The active node at $z = 0$ is simulated by a 1μ wide intracellular electrode supplying a current density J^s at that location. This approximates the depolarization that results during an action potential from the influx of positive sodium ions. The stimulus current I^s is taken as a 0.5 msec duration pulse, similar to the duration of an action potential. As it was demonstrated in Chapter 3 (and seen also in the results of this chapter) for an intracellular stimulus, $\Phi_E << \Phi'_I$ and Φ_E is not a very strong function of r for distances within $1000\ \mathring{A}$ of the cell membrane (see Figure 3.11 of Chapter 3). Thus the perturbed transmembrane potential at the nodes may be approximated by $\Phi'_I(b,z,t) - \Phi_E(b + 21d, z, t)$ as indicated in Figure 4.19(c). This assumes that V'_m at the nodes is given essentially by Φ'_I, with the extracellular medium being isopotential between $r = b + 50\ \mathring{A}$ and $r = b + 1050\ \mathring{A}$. A further assumption is that the relatively low impedance paths for current presented by the nodes are insignificant because of their size and infrequent spacing. The

model will only examine potential between $z = 0$ (the active node) and $z = 1$ mm (the first adjacent node) so that the effects of other nodes at greater axial distances will be minimal. Between nodes, the perturbation in transmembrane potential will be given by $V'_m \doteq \Phi'_I(b,z,t) - \Phi'_M(b + d, z, t)$, the perturbed potential across the membrane of the axon alone ($\Phi'_M(b + d, z, t)$ being taken as the electric scalar potential perturbation at the outer <u>axonal</u> membrane surface).[1]

With the above assumptions and definitions, the solution was carried out using the equations of Section 4.2.3. The axon parameters (exclusive of the radius definitions above) were the same as for the test axon (Appendix D) with the stimulating current I^s at the 10^{-5} amps standard value. With the same membrane conductivity of $\sigma_M = 7.143 \times 10^{-10}$ mhos/cm as for the unmyelinated axon, this gave a net membrane resistance per-unit-area 21 times larger than for the unmyelinated case[2]. As it is realized that a 0.5 msec pulse of current is not the same as the time course of currents through the membrane during an action potential, it is not expected that the simulation will give the same potential magnitudes and time courses as due to a nerve impulse. The model does give information on time constants, axial decay, and potential magnitudes at the nodes as compared with those between the nodes.

---

[1] The resting potential V_r is assumed to exist only across the axon membrane with $\Phi_{Mo}(r)$ given by Section 2.3 for $b < r < b + d$.

[2] Essentially 21 identical membranes in a laminar structure form the axon membrane-myelin sheath complex.

The response obtained is illustrated in Figures 4.20 and 4.21. In Figure 4.20, it is observed that the peak depolarization at the active node is about 145 mV,[1] and has decayed only slightly at the adjacent node at $z = 1$ mm. Though the depolarization is about 50% larger than for an action potential at $z = 0$, the maximum depolarization at $z = 0.5$ mm where the myelin sheath covers the axon is only on the order of 7 mV. The decay in potential perturbation from the magnitude at the active node to the second node at $z = 1$ mm is far less than seen in the unmyelinated axon[2]. Another response characteristic is that the rise time is the same as for a non-myelinated axon; as can be observed by comparing Figures 4.4 and 4.20.

Figure 4.21 graphs the variation V_m' as a function of z at $t = 0.01$, 0.05, and 0.1 msec. Note that the transmembrane potential at either node ($z = 0$, 1 mm) is far greater than for the region covered by the myelin sheath. The dashed lines indicate the edges of the myelin and the change in V_m' that occurs at those points. This also denotes that the transition in V_m' from its value at a node to its value under the sheath is ill-defined and thus the portion of the curve for those points cannot be specified[3]. Figure

---

[1] A result of the chosen stimulus intensity. By the linearity of the model, all potentials could be multiplied by 2/3, giving about a 100 mV depolarization (similar to the action potential magnitude) that would result from 2/3 the stimulus intensity.

[2] Compare Figures 4.10 and 4.20. In this case the decay is 6.8% as compared to 23% for the unmyelinated axon.

[3] It is expected that in a real cell there would be a smooth transition in transmembrane potential between nodal and trans-nodal magnitudes.

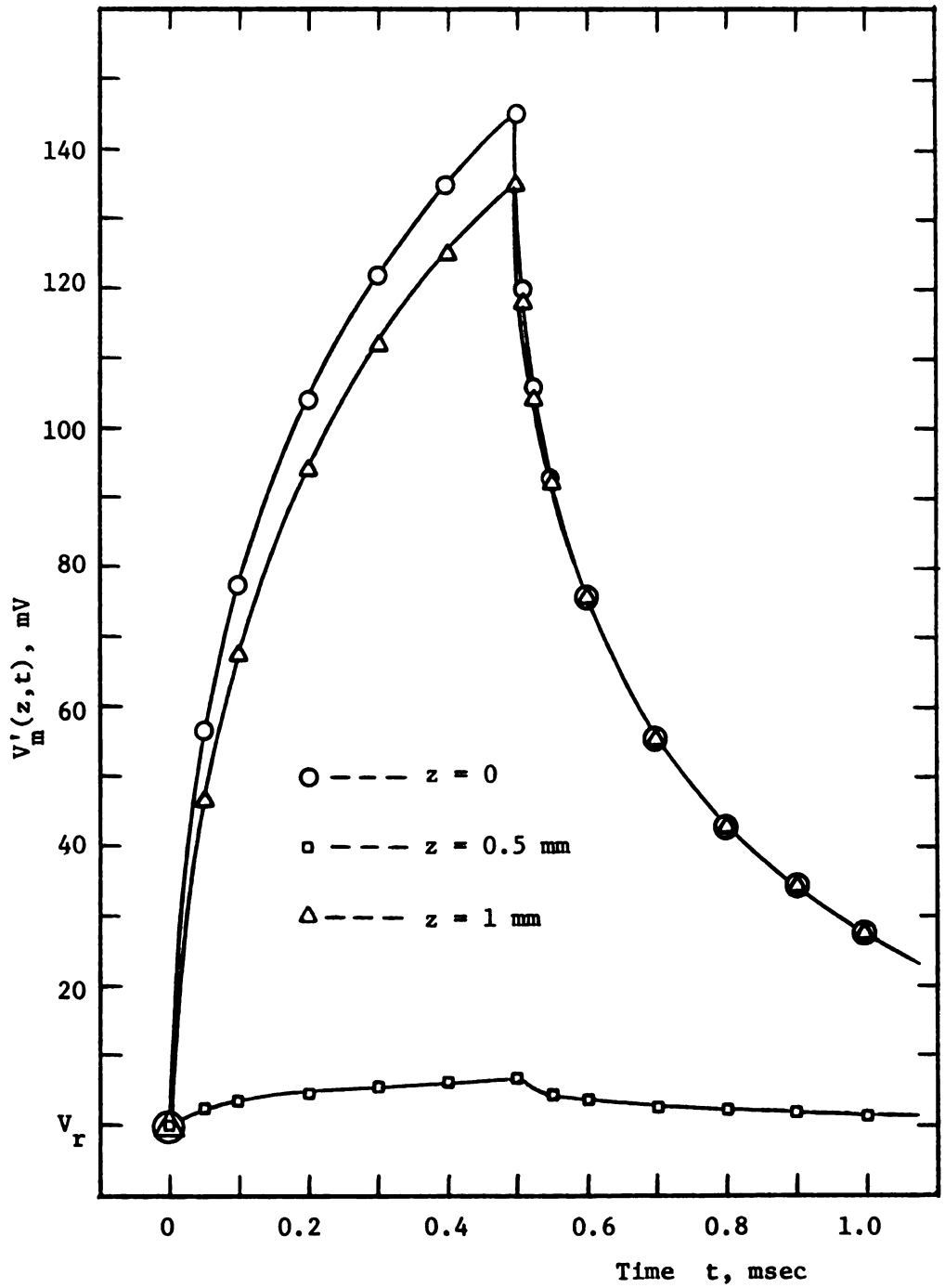

FIGURE 4.20

Transmembrane Potential Time Response at z = 0, 0.5, and 1 mm, Myelinated Axon Model

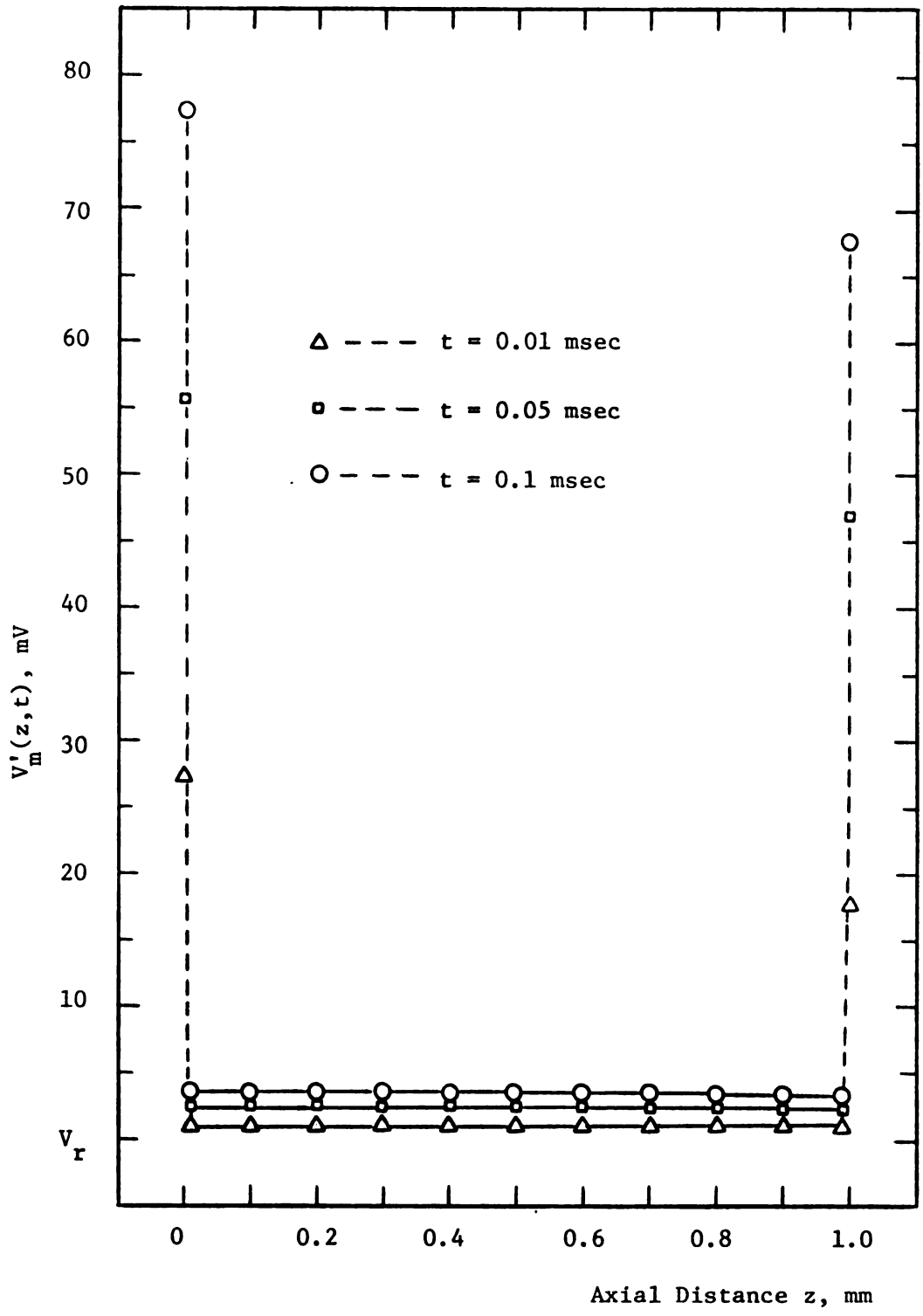

FIGURE 4.21

Transmembrane Potential as a Function of z at t = 0.01, 0.05, and 0.1 msec, Myelinated Axon Model

4.21 clearly demonstrates that while the depolarization between nodes has reached only 3.3 to 3.5 mV, the node at $z = 1$ mm has been depolarized some 67 mV (at $t = 0.1$ msec), a value well above the threshold required to excite an action potential (less than a 40 mV depolarization, see Plonsey [60]). The interesting feature of this model is that it indicates that the reason action potential excitation is prevented between nodes is not necessarily the blocking of ionic currents by the myelin, but gives the slightly different view that the neuronal membrane never reaches threshold. Thus even if the myelin sheath allowed a small leakage of extracellular fluid between it and the axon, the action potential would still be prevented by there being an insufficient depolarization of the axon membrane (between nodes) to reach threshold.

The response of the model may be explained by considering the physical characteristics of the system. The increased length constant (smaller decay from $z = 0$ to $z = 1$ mm in V_m' with the sheath) arises from the increase in net resistance to current flow through the membrane. The membrane-myelin complex is equivalent to a single thick membrane of the same conductivity as of the non-myelinated axon membrane. This feature has been incorporated into a core-conductor model by increasing r_m (see FitzHugh [25], Plonsey [60]). There is no change in the membrane time constant, as from Section 4.3.1 (equation 4.99) $\tau = \varepsilon_M/\sigma_M$. Since neither σ_M or ε_M has changed, τ is unchanged[1].

---

[1] The membrane capacitance, C_m, is inversely proportional to membrane thickness while R_m is directly proportional. Thus the increase in effective membrane thickness cancels in $\tau = R_m C_m = r_m c_m$.

The decreased transmembrane depolarization of the axonal membrane under the myelin sheath may be seen as essentially a simple voltage-divider network effect. As observed in Section 3.3.2, the perturbation in potential within the membrane is very close to a linear function between Φ_I' and Φ_E at either side of the membrane. With the total thickness of the membrane-myelin complex 21 times that of the excitable axonal membrane, the effect is that only 1/21 of the potential difference across the entire complex appears across the axon membrane (i.e., the membrane and myelin are similar to resistances in series for radial current flow). The fact that V_m' under the sheath is approximately 1/21 of $\Phi_I'(b,z,t) - \Phi_E(b + 21d, z, t)$ was verified from the numerical solutions, and may be observed to be the case by extrapolating values from the curves in Figures 4.20 and 4.21. The conclusion arises that the action potential is blocked between nodes in a myelinated axon because the excitable membrane of the axon never reaches threshold. The depolarization is shared in a voltage-divider fashion with the non-excitable membrane layers of the myelin sheath. Thus even if ions from the interstitial fluid manage to penetrate between the myelin layers in a sufficient quantity that theoretically could produce an action potential, the excitable membrane is prevented from reaching the threshold for this event. This is similar but slightly different from the prevailing notion that the myelin acts as an insulator, physically preventing ionic currents through its high resistance.

CHAPTER 5

REDUCTION OF THE SYSTEM TO A TWO-COMPARTMENT MODEL

The problem is greatly simplified if the fields and currents interior to the membrane are not required in the solution. For this situation, the boundary conditions developed in Section 2.2.2 are combined with the volume-conductor equations for the intracellular and extracellular regions to obtain the solutions for only those two regions. The advantage of this approach is that the resultant simplification not only yields expressions that require less computer time for Fourier inversion, but also allows the model to be extended to include time and space-dependent ion-selective conductance changes in the membrane. This enables the modeling of active as well as passive neural phenomena.

The first section of this chapter states the defining equations for the two-compartment model. Section 5.2 carries out the solution in a general form for both the electrotonus (passive response) and variable membrane conductance cases. The last section examines the response characteristics for a few examples of variable conductance in modeling synaptic events.

5.1. Description of the Two-Compartment System

Once again the structure to be modeled is a membrane cylinder, its geometry represented in cylindrical coordinates as shown in

Figure 5.1. The cylinder's axis and the z-axis are coincidental, the cell is taken to be infinite and uniform in the $\pm \hat{z}$ directions, and the system rotationally symmetric. As before, the intracellular space is defined by $0 \leq r \leq b$ and the extracellular region by $r \geq a$. The membrane exists between $r = b$ and $r = a$, but fields within this region are <u>not</u> part of the model[1]. Only the fields of the intracellular and extracellular volume conductors are to be solved for, with the boundary conditions of Section 2.2.2 used to relate these fields across the membrane.

As in the previous chapters, the volume conductor regions of the intracellular and extracellular spaces are assumed to be linear, homogeneous, isotropic, and electroneutral media; with any externally applied sources only at the membrane interfaces. Following Chapters 3 and 4, the fields and currents will thus satisfy the relations:

$$\Phi_I(r,z,t) = V_r + \Phi_I'(r,z,t) \tag{5.1}$$

$$\nabla^2 \begin{Bmatrix} \Phi_I'(r,z,t) \\ \\ \Phi_E(r,z,t) \end{Bmatrix} = 0 \qquad \text{(Laplace's equation)} \tag{5.2}$$

$$\vec{J}_I(r,z,t) = \sigma_I \vec{E}_I(r,z,t) \tag{5.3}$$

$$\vec{J}_E(r,z,t) = \sigma_E \vec{E}_E(r,z,t) \tag{5.4}$$

---

[1] If desired, the membrane may be considered infinitely thin by setting $a = b$ in all equations in this chapter.

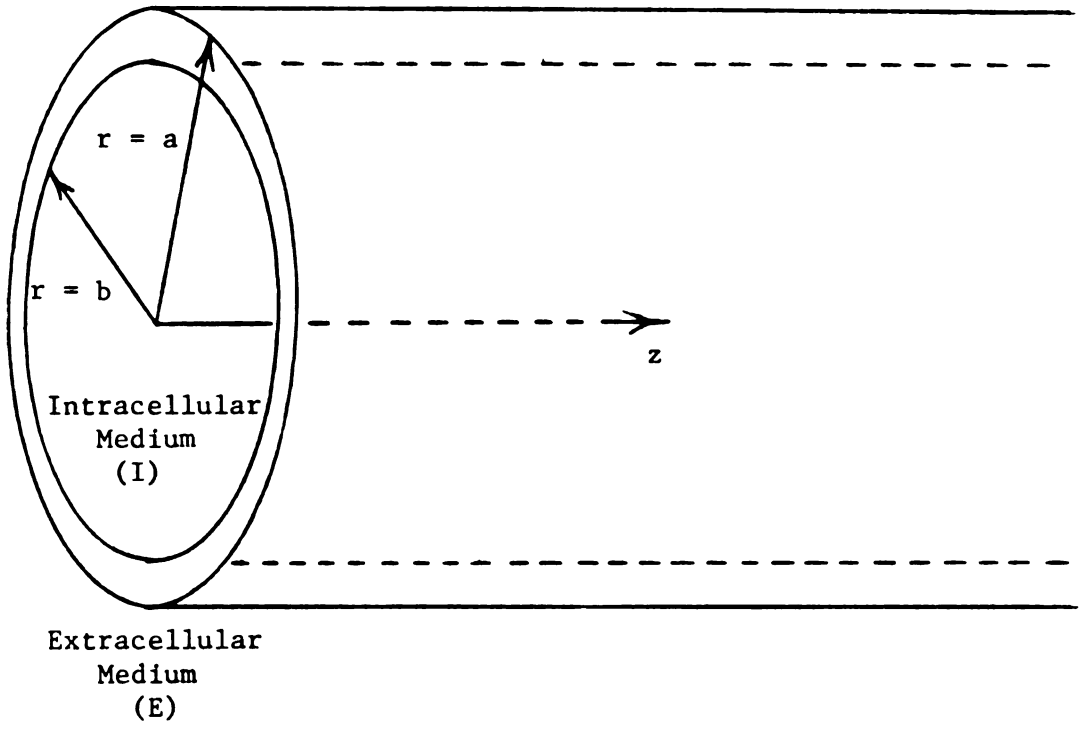

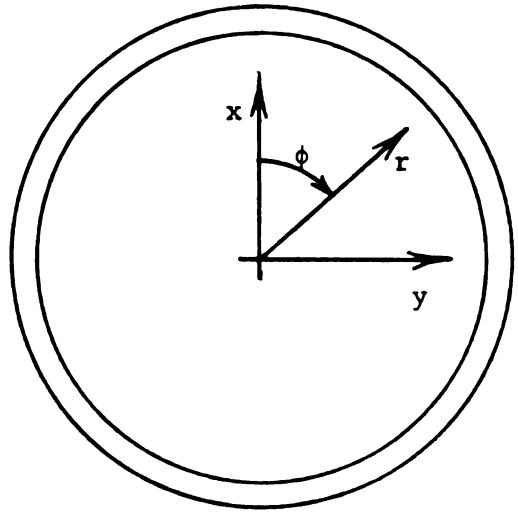

FIGURE 5.1

Geometry for Two-Region Cylindrical Model

$$\begin{Bmatrix} \vec{E}_I(r,z,t) \\ \vec{E}_E(r,z,t) \end{Bmatrix} = -\nabla \begin{Bmatrix} \Phi'_I(r,z,t) \\ \Phi_E(r,z,t) \end{Bmatrix} \tag{5.5}$$

where V_r is the resting transmembrane potential and Φ'_I the perturbation from $\Phi_I = V_r$ in the resting state[1].

The boundary conditions were developed in Section 2.2.2, with Chapter 3 demonstrating that the assumptions necessary for their derivation were valid. For the geometry of this system, they are obtained from equations (2.164) and (2.165) as

$$\sum_i g_i(z,t)[V_m(z,t) - V_i^e] + C_m \frac{\partial}{\partial t} V_m(z,t) - \sigma_I E_{Ir}(b,z,t) = 0 \tag{5.6}$$

$$\sigma_E E_{Er}(a,z,t) - \sum_i g_i(z,t)[V_m(z,t) - V_i^e] - C_m \frac{\partial}{\partial t} V_m(z,t) = 0 \tag{5.7}$$

$$\text{where } g_i(z,t) = \left[\int_a^b \frac{dr}{\sigma_{Mi}(r,z,t)}\right]^{-1} \quad \begin{matrix}\text{(membrane conductance of the} \\ \text{ith ion species, mhos/m}^2\text{)}\end{matrix} \tag{5.8}$$

$$C_m = \varepsilon_M/d \quad \text{(membrane capacitance, farads/m}^2\text{)} \tag{5.9}$$

$$V_i^e = -\frac{RT}{z_i F} \ell n \frac{[C_{Ii}]_b}{[C_{Ei}]_a} \quad \begin{matrix}\text{(Nernst potential of the ith ion} \\ \text{species, volts).}\end{matrix} \tag{5.10}$$

Following Section 3.2.2, any externally applied stimulus will be considered as originating from metallic ring electrodes at either

---

[1] See Section 3.1 for a discussion of the assumptions made above. Also note that both Φ_I and Φ'_I satisfy Laplace's equation (5.1) as V_r is space (and time) independent.

membrane interface. Thus, recognizing that $\sum_i g_i[V_m - V_i^e]$ was derived from J_{Mr} (the radial membrane current density), the sources $J_I^s(z,t)$ and $J_E^s(z,t)$ are added to relations (5.6) and (5.7) in the same manner as in Sections 3.1 and 4.1. The boundary conditions are then

$$\sum_i g_i(z,t)[V_m'(z,t) + V_r - V_i^e] + C_m \frac{\partial}{\partial t} V_m'(z,t) - \sigma_I E_{Ir}(b,z,t) = J_I^s(z,t) \qquad (5.11)$$

$$\sigma_E E_{Er}(a,z,t) - \sum_i g_i(z,t)[V_m'(z,t) + V_r - V_i^e] - C_m \frac{\partial}{\partial t} V_m'(z,t) = J_E^s(z,t) \qquad (5.12)$$

with J_I^s and J_E^s being defined as externally supplied discontinuties in the radial current densities at the appropriate membrane interface (see Section 3.2.2). Note that the expansion of

$$V_m(z,t) = V_m'(z,t) + V_r \qquad (5.13)$$

where $V_m'(z,t) = \Phi_I'(b,z,t) - \Phi_E(a,z,t)$ (5.14)

(the perturbation from the resting potential, V_r) has been used in expressions (5.11) and (5.12)[1]. This will prove convenient in developing the solutions.

---

[1] It also gives $C_m \frac{\partial V_m}{\partial t} = C_m \frac{\partial V_m'}{\partial t}$ in expressions (5.11) and (5.12).

The system is completely described in equations (5.1) - (5.5) and boundary conditions (5.11) and (5.12). The advantage of reducing the problem to two regions is that it allows a far more general simulation of neural phenomena than the three-compartment model of Chapters 3 and 4. This model, in not specifying the fields within the membrane, works for any membrane description (fixed charge, r-dependent conductivity or mobility, etc.). It also avoids the difficulty of having to define macroscopic parameters in a membrane that is so narrow as to make these definitions theoretically unsound. As indicated in the boundary conditions, the membrane conductance need not be assumed constant. This enables the appropriate solutions to describe active as well as passive neural events.

5.2. Fourier Transform Solutions for the Two-Compartment Model

This section is concerned with the development of the two-region model in the form of a set of general Fourier-space solutions and a series of solution coefficients for a wide variety of neural phenomena. The first subsection gives the general solution in terms of two time-dependent coefficients (A(k,t) and D(k,t)). Subsection 5.2.2 develops these solution coefficients for the passive neural response to either an intracellular or extracellular stimulating electrode. This material is essentially a parallel of Chapters 3 and 4; the result being a simplified two-region model for the electrotonus problem solved in those chapters. The next subsection (5.2.3) handles the case of a spatially non-uniform membrane conductance, leaving the solution coefficients in terms of

the Fourier transform of the perturbation from the resting condition conductance. Finally, Subsection 5.2.4 presents the solution coefficients for the general case of a space and time-dependent membrane conductance. Thus the field-model solutions are extended to cover both the passive response due to an impressed (electrode supplied) stimulus and the active response resulting from ion-selective membrane conductance changes.

5.2.1. The General Solution; Resting Condition Results

As in the previous two chapters, the Fourier transform on z is applied to Laplace's equation (5.2) in cylindrical coordinates to obtain

$$\frac{\partial^2}{\partial r^2}\,\bar{\Phi}(r,k,t) + \frac{1}{r}\frac{\partial}{\partial r}\,\bar{\Phi}(r,k,t) - k^2\,\bar{\Phi}(r,k,t) = 0 \qquad (5.15)$$

where k is the Fourier-domain variable and $\bar{\Phi}$ represents the transform of either Φ_I' or Φ_E. The general solution to equation (5.15) is specified in Chapter 3, relation (3.37)[1]. Applying the physical constraint of potential being finite at $r = 0$ and $r \to \infty$ plus the Bessel function properties (3.38) and (3.39) on $I_o(kr)$ and $K_o(kr)$ at those locations leads to the k-space potential functions as

$$\bar{\Phi}_I'(r,k,t) = A(k,t)I_o(kr) \qquad 0 \leq r \leq b \qquad (5.16)$$

---

[1] With the integration constants now being functions of t as well as k (as in Chapter 4).

$$\bar{\Phi}_E(r,k,t) = D(k,t)K_o(kr) \qquad r \geq a \ . \tag{5.17}$$

The coefficients A and D depend upon the stimulus (if any) and the boundary conditions. They will be found for a variety of cases in the following subsections.

Once A and D have been obtained, the z-space solution is again given by the inverse Fourier integrals as[1]

$$\Phi_I(r,z,t) = V_r + \frac{1}{2\pi}\int_{-\infty}^{\infty} A(k,t)I_o(kr)e^{jkz}dk \tag{5.18}$$

$$\Phi_E(r,z,t) = \frac{1}{2\pi}\int_{-\infty}^{\infty} D(k,t)K_o(kr)e^{jkz}dk \ . \tag{5.19}$$

These inversion integrals are evaluated numerically on a digital computer (as discussed in Section 3.3.1 and Appendix C) to obtain the final results. If the solutions for $\vec{E}_I$, $\vec{E}_E$, $\vec{J}_I$, or $\vec{J}_E$ are desired, they are immediately obtained from equations (4.93), (4.94), (4.97), and (4.98) in Chapter 4, with the $A(k,t)$ and $D(k,t)$ coefficients as specified in this chapter.

Before proceeding with applying the boundary conditions, it is convenient to solve for the resting transmembrane potential in terms of the parameters of this model. As discussed in Section 2.3, in the resting state $\vec{J}_I(b,z,t) = \vec{J}_E(a,z,t) = 0$, no stimulus is present, the system is time independent, and the membrane parameters are constants with respect to z and t. Thus boundary

---

[1] Note that the resting potential V_r has been included in equation (5.18) so that the total potential Φ_I is recovered.

conditions (5.11) and (5.12) reduce to the single relation

$$\sigma_I E_{Ir} = \sigma_E E_{Er} = \sum_i g_{io}[V_r - V_i^e] = 0 \tag{5.20}$$

where g_{io} is defined as the resting state (invariant) membrane conductance of the ith ion species, and V_m' is taken as zero (by definition) in the resting condition. The resting transmembrane potential is then found simply as

$$V_r = \frac{\sum_i g_{io} V_i^e}{g_r} \tag{5.21}$$

where

$$g_r = \sum_i g_{io} \tag{5.22}$$

is the total resting-state membrane conductance, defined as the sum of the individual conductances due to each ion species carrying charge through the membrane.

It is noted that result (5.21) could have been obtained from a Fourier transform solution for Φ_I and Φ_E in the form of solutions (5.16) and (5.17). The transform of the boundary conditions would yield a $2\pi\delta(k)V_i^e$ term for the Nernst potentials, and this would allow (by the integral property of the delta function) the inversion integrals (5.18) and (5.19) to be evaluated analytically. Carrying this out, one obtains $\Phi_I(r,z,t)$ as equal to expression (5.21) (i.e., $\Phi_I = V_r$ as expected) and $\Phi_E \equiv 0$. However, the approach above is far simpler and, by applying (via linear superposition) the transform to only the perturbed potentials,

avoids complex terms in the Fourier solution that reduce to the trivial form above for the resting state portion of the solution.

5.2.2. Two-Compartment Electrotonus

This section evaluates the solution coefficients $A(k,t)$ and $D(k,t)$ for the case of subthreshold stimuli supplied by electrodes. The result is a simplified version of the model developed in Chapters 3 and 4. Because of this, the notation used will follow the conventions and definitions of those chapters wherever possible. The development includes time dependent stimulus functions, so that the Laplace transform on the time variable (with analytical inversion back to the time domain) is applied as in Chapter 4.

For subthreshold stimuli only a passive response is evoked, with the conductance of each ion species remaining at its resting value g_{io}. This gives boundary condition (5.11) the form

$$\sum_i g_{io}[V'_m(z,t) + V_r - V_i^e] + C_m \frac{\partial}{\partial t} V'_m(z,t) - \sigma_I E_{Ir}(b,z,t) = J_I^s(z,t). \tag{5.23}$$

The resting potential and Nernst potential terms cancel each other, as by result (5.21) $\sum_i g_{io} V_r = \sum_i g_{io} V_i^e$. Then applying definition (5.22) for g_r, the Fourier transform on z, and the Laplace transform on time (with the assumption of the system at rest for $t \leq 0$) gives

$$(g_r + sC_m)\bar{V}'_m(k,s) - \sigma_I \bar{E}_{Ir}(b,k,s) = \bar{J}_I^s(k,s) \ . \tag{5.24}$$

Following the same procedure with boundary condition (5.12) leads to

$$\sigma_E \bar{E}_{Er}(a,k,s) - (g_r + sC_m)\bar{V}_m'(k,s) = \bar{J}_E^s(k,s) \ . \tag{5.25}$$

The general solutions (5.16) and (5.17) are Laplace transformed and substituted into boundary conditions (5.24) and (5.25) using definition (5.14), relation (5.5) and the Bessel function properties $I_1(x) = \frac{\partial}{\partial x} I_o(x)$, $-K_1(x) = \frac{\partial}{\partial x} K_o(x)$ to obtain

$$(g_r + sC_m)[A(k,s)I_o(kb) - D(k,s)K_o(kb)] + \sigma_I k\, A(k,s)I_1(kb) = \bar{J}_I^s(k,s) \tag{5.26}$$

$$\sigma_E k\, D(k,s)K_1(ka) - (g_r + sC_m)[A(k,s)I_o(kb) - D(k,s)K_o(kb)] = \bar{J}_E^s(k,s) \ . \tag{5.27}$$

These two equations are solved simultaneously to yield the Laplace and Fourier transform solution coefficients as

$$A(k,s) = \frac{(g_r + sC_m)K_o(ka)\bar{J}_E^s(k,s)}{F(k,s)} + \frac{[(g_r + sC_m)K_o(ka) + \sigma_E k\, K_1(ka)]\bar{J}_I^s(k,s)}{F(k,s)} \tag{5.28}$$

$$D(k,s) = \frac{[(g_r + sC_m)I_o(kb) + \sigma_I k\, I_1(kb)]\bar{J}_E^s(k,s)}{F(k,s)} + \frac{(g_r + sC_m)I_o(kb)\bar{J}_I^s(k,s)}{F(k,s)} \tag{5.29}$$

where the denominator $F(k,s)$ is defined by

$$F(k,s) = k\{(g_r + sC_m)[\sigma_E I_o(kb)K_1(ka) + \sigma_I K_o(ka)I_1(kb)]$$

$$+ \sigma_I\sigma_E k\, I_1(kb)K_1(ka)\} \quad . \tag{5.30}$$

With the assumption applied in Chapters 3 and 4 that the source current densities are uniform over the electrode's surface, either stimulus term $\overline{J}_I^s$ or $\overline{J}_E^s$ can be expressed in the form[1]

$$\overline{J}^s(k,s) = \overline{J}^s(k)f(s) \tag{5.31}$$

where $$\overline{J}^s(k) = \frac{2J^s}{k}\sin(k\, w/2) \ , \tag{5.32}$$

w is the electrode width, J^s represents either J_I^s or J_E^s, and $f(s)$ is the Laplace transform of the stimulus time function[2] $F(t)$. Using expression (5.31) in equations (5.28) and (5.29) allows solution coefficients $A(k,s)$ and $D(k,s)$ to be re-written as

$$\psi(k,s) = \frac{N_1(k) + sN_2(k)}{\alpha(k)[s + P(k)]}\, f(s) \tag{5.33}$$

where ψ represents either coefficient with the appropriate definition of N_1, N_2, α, and P.

---

[1] See Chapter 4, Sections 4.2.2 and 4.2.3 for the development of this time-dependent source term and the definitions (4.44) and (4.45) of J_I^s and J_E^s in terms of the total stimulus current.

[2] The total current to either electrode is defined with $I^sF(t)$.

The common denominator $F(k,s)$ for coefficients A and D immediately defines $\alpha(k)$ and $P(k)$ (by comparison with equation (5.30)) as being

$$\alpha(k) = kC_m[\sigma_E I_o(kb)K_1(ka) + \sigma_I K_o(ka)I_1(kb)] \tag{5.34}$$

$$P(k) = g_r/C_m + \frac{\sigma_I\sigma_E k^2 I_1(kb)K_1(ka)}{\alpha(k)} \quad . \tag{5.35}$$

The numerator terms $N_1(k)$ and $N_2(k)$ depend upon the particular coefficient being expressed. They are found by inspection from equations (5.28) and (5.29) as

$$N_{A1}(k) = g_r K_o(ka)\bar{J}_E^s(k) + [g_r K_o(ka) + \sigma_E k\, K_1(ka)]\bar{J}_I^s(k) \tag{5.36}$$

$$N_{A2}(k) = C_m K_o(ka)[\bar{J}_E^s(k) + \bar{J}_I^s(k)] \tag{5.37}$$

for coefficient $A(k,s)$, and

$$N_{D1}(k) = [g_r I_o(kb) + \sigma_I k\, I_1(kb)]\bar{J}_E^s(k) + g_r I_o(kb)\bar{J}_I^s(k) \tag{5.38}$$

$$N_{D2}(k) = C_m I_o(kb)[\bar{J}_E^s(k) + \bar{J}_I^s(k)] \tag{5.39}$$

for coefficient $D(k,s)$. Note that the source terms $\bar{J}_I^s(k)$ and $\bar{J}_E^s(k)$ are those defined in expressions (5.31) and (5.32).

Now the inverse Laplace transform of the solution coefficients may be found for specific stimulus time functions as in Chapter 4.

Using the Laplace transform of a unit step function, $f(s) = 1/s$ (equation (4.46)) leads to the general coefficient (5.33) having the form

$$\psi(k,s) = \frac{N_1(k) + sN_2(k)}{\alpha(k)s[s + P(k)]} , \tag{5.40}$$

which can be expanded with partial fractions into

$$\psi(k,s) = \frac{R_o(k)}{s} + \frac{R_1(k)}{s + P(k)} \tag{5.41}$$

where

$$R_o(k) = \frac{N_1(k)}{\alpha(k)P(k)} \tag{5.42}$$

$$R_1(k) = \frac{P(k)N_2(k) - N_1(k)}{\alpha(k)P(k)} . \tag{5.43}$$

With inverse transforms (4.80) and (4.81), the time-domain general coefficient becomes

$$\psi(k,t) = R_o(k) + R_1(k)e^{-P(k)t} . \tag{5.44}$$

Thus, by use of the appropriate N_1 and N_2 in expressions (5.42) and (5.43) and definitions (5.34) and (5.35) for α and P, the time domain coefficients $A(k,t)$ and $D(k,t)$ are defined by equation (5.44).

From its definition, it is apparent that $P(k)$ must be positive for all k. Thus as $t \to \infty$, the exponential term $e^{-P(k)t}$

in expression (5.44) decays to zero, leaving the steady-state coefficients for a constant, maintained stimulus as

$$A(k) = \frac{N_{A1}(k)}{\alpha(k)P(k)} \tag{5.45}$$

$$D(k) = \frac{N_{D1}(k)}{\alpha(k)P(k)} \; . \tag{5.46}$$

The use of the above $A(k)$ and $D(k)$ in place of $A(k,t)$ and $D(k,t)$ in general solutions (5.18) and (5.19) gives the response of the two-compartment model for steady-state electrotonus (the case handled in Chapter 3 for a three-region system). Note that the steady-state response is obtained from the step function response just as it was for the three-compartment model in Chapter 4 by taking $t \to \infty$.

As discussed in Chapter 4, the response to a stimulating current pulse of duration T_o may be obtained by time shifting and linear superposition from the step function response. This yields

$$\psi(k,t) = \begin{cases} R_o(k) + R_1(k)e^{-P(k)t} & 0 \leq t \leq T_o \\ R_1(k)e^{-P(k)t}[1 - e^{P(k)T_o}] & t \geq T_o \end{cases} \tag{5.47}$$

where R_o, R_1, and P are the same as in the step function stimulus case (expressions (5.35), (5.41), and (5.42)).

The impulse stimulus response cannot be found for the general two-compartment model, as the singularity involved yields

a solution in Laplace transform space that has no simple inverse. It is possible to invert the solution for $\bar{V}_m'(k,s)$ back to the time domain, as the offending terms cancel in subtracting $\bar{\Phi}_E(a,k,s)$ from $\bar{\Phi}_I'(b,k,s)$. The impulse response was noted in Chapter 4 as just being the limiting case of letting $T_o \to 0$ in the pulse response while forcing the same amount of charge to be delivered by the electrode to the system. As such, and considering the physical objection to requiring a finite charge to be injected into the system in an infinitely brief interval, it does not seem worthwhile to pursue this case further with the two-compartment model.

A series of comparisons were made of the solutions for $\Phi_I'(r,z,t)$, $\Phi_E(r,z,t)$ and $V_m'(z,t)$ as predicted by the two and three-region models. It was found that the two-compartment model gave the same response (to three significant figures) as the three-region models of Chapters 3 and 4. These checks were made using the same numerical inversion techniques as discussed in Chapter 3 and Appendix C for the parameters of the standard test axon and stimulus intensity (Appendix D). Since the response was the same, the reader is referred to the discussion in Chapters 3 and 4 for the details and conclusions that apply to either model, even though those results were all specifically obtained from the three-region system. As the present two-compartment model is mathematically simpler and requires less computer time for the numerical inversions, it is the logical model to use if one desires a solution for only the intracellular, extracellular, or transmembrane potentials. For fields within the membrane or for the myelinated axon simulation

of Chapter 4, it would be necessary to use the full (and more complex) three-region model of the previous chapters.

All previous results in this report have been found for the case of either an intracellular or extracellular stimulus. Before proceeding to the case of variable membrane conductance, it is worthwhile to briefly examine a special-case electrotonic solution that is later demonstrated to have a similar form to a variable g_i solution. This is the situation where an intracellular electrode supplies exactly the same current that an extracellular electrode removes. In this case, with both electrodes centered at $z = 0$ and of width w, $J_I^s(z,t) = -J_E^s(z,t)$. The boundary conditions (5.24) and (5.25) reduce to the single expression:

$$\sigma_I \bar{E}_{Ir}(b,k,s) = \sigma_E \bar{E}_{Er}(a,k,s) = (g_r + sC_m)\bar{V}_m'(k,s) - \bar{J}^s(k,s). \quad (5.48)$$

Setting $\bar{J}_I^s = -\bar{J}_E^s = \bar{J}_s$ in the solution coefficients (5.28) and (5.29) immediately obtains

$$A(k,s) = \frac{\sigma_E k\, K_1(ka)}{F(k,s)}\, \bar{J}^s(k,s) \quad (5.49)$$

$$D(k,s) = -\frac{\sigma_I k\, I_1(kb)}{F(k,s)}\, \bar{J}^s(k,s) \quad (5.50)$$

where $F(k,s)$ was specified in relation (5.30).

The response for this special case is found via linear superposition by subtracting the response of an extracellular electrode from that for an intracellular electrode where both

electrodes are supplied with the same total current. By the results of Chapters 3 and 4, the transmembrane potential response for the intracellular stimulus was consistently far greater in magnitude than the response to an extracellular stimulus of identical strength. Thus the response for this system is essentially identical to the transmembrane potential response of the intracellular electrode case presented in the previous two chapters; the extracellular electrode having little net effect[1].

5.2.3. Spatially-Dependent Membrane Conductance

This subsection considers the case of g_i as a function of the axial variable z, partly as a prelude to Section 5.2.4 where the situation of a time and space dependent membrane conductance is handled. The solution gives the response for a membrane with a region where the conductance of one or more ion species is either higher or lower than the resting state conductance[2]. The source term for perturbations in potential arises from the difference in $V_m(z)$ and the Nernst potentials, a distinctly different situation than an electrode-supplied stimulus. Applications of this response include the determination of an upper (or lower)

---

[1] Hellerstein [30] solved a similar two-compartment problem (current source and sink on opposing sides of the membrane) for the passive response to delta function width electrodes supplying a time-step in current. His solutions used a cosine transform (on z) inverted analytically after assuming an infinitely thin R-C membrane, $\sigma_I = \sigma_E$, and making several approximations in the transform-domain solutions by discarding certain terms as negligible.

[2] See Klee and Plonsey [43] for an integral equation approach to a similar problem involving a spherical cell with a low resistance window in the membrane immersed in a static electric field.

bound for a given combination of changes in the conductance of one or more ion species, the potentials that would result from a maintained conductance change (as in continued application of transmitter substance at a synapse), and perhaps another model for a myelinated axon (see Chapter 6).

An expansion for the axially-dependent conductance of the ith ion species is defined with

$$g_i(z) = g_{io} + g_i'(z) \tag{5.51}$$

where g_i' is the perturbation from the resting condition conductance g_{io} (a constant). It will be assumed that there are no electrodes or other outside sources in the system, so that boundary conditions (5.11) and (5.12) become

$$\sum_i g_i'(z)[V_m'(z) + V_r - V_i^e] + \sum_i g_{io}[V_m'(z) + V_r - V_i^e] - \sigma_I E_{Ir}(b,z) = 0 \tag{5.52}$$

$$\sigma_E E_{Er}(a,z) - \sum_i g_i'(z)[V_m'(z) + V_r - V_i^e] - \sum_i g_{io}[V_m'(z) + V_r - V_i^e] = 0 \tag{5.53}$$

where the steady-state assumption gives all quantities as time-independent. As in the previous section, $\sum_i g_{io}V_r = \sum_i g_{io}V_i^e$ (from equations (5.21), (5.22)) simplifying the boundary conditions to

$$g_r V_m'(z) - \sigma_I E_{Ir}(b,z) = \sum_i g_i'(z)[V_i^e - V_r - V_m'(z)] \tag{5.54}$$

$$\sigma_I E_{Ir}(b,z) = \sigma_E E_{Er}(a,z) \tag{5.55}$$

where $g_r = \sum_i g_{io}$ and boundary conditions (5.52) and (5.53) were added to obtain alternate boundary condition (5.55).

The boundary conditions (5.54) and (5.55) state that the normal component of current density is continuous across the membrane and that the forcing (or source) term for the system is the sum of the membrane conductance change of each ion species multiplying the difference in that ion's Nernst potential and V_m. As this system is time invariant, only the Fourier transform on z is needed, with the general solution as given in expressions (5.16) and (5.17)[1]. Taking the Fourier transform of the boundary conditions, and substituting for $\overline{V}'_m$, $\overline{E}_{Ir}$, and $\overline{E}_{Er}$ as in the previous section, gives

$$g_r[A(k)I_o(kb) - D(k)K_o(ka)] + \sigma_I k\, A(k)I_1(kb) = S(k) \quad (5.56)$$

$$-\sigma_I A(k)I_1(kb) = \sigma_E D(k)K_1(ka) \quad (5.57)$$

where

$$S(k) = \mathcal{F}_k\{\sum_i g'_i(z)[V_i^e - V_r - V'_m(z)]\} \quad (5.58)$$

is the Fourier transform of the indicated source term. The solution coefficients are obtained from (5.56) and (5.57) as

$$A(k) = \frac{\sigma_E k\, K_1(ka)}{H(k)}\ S(k) \quad (5.59)$$

---

[1] The coefficients $A(k,t)$ and $D(k,t)$ reduce to $A(k)$ and $D(k)$ (functions of k only) since this solution is not time-dependent.

$$D(k) = - \frac{\sigma_I k\, I_1(kb)}{H(k)}\, S(k) \tag{5.60}$$

where the denominator term $H(k)$ is defined by

$$H(k) = g_r[\sigma_E I_o(kb)K_1(ka) + \sigma_I K_o(ka)I_1(kb)] + \sigma_I \sigma_E k\, I_1(kb)K_1(ka). \tag{5.61}$$

Note that $H(k) = \alpha(k)P(k)$, in terms of the coefficients α and P of the electrotonus solution of the previous section.

The transform of the source term ($S(k)$) has yet to be determined. Unfortunately it cannot be found in the general case. This is because it contains the product of two z functions ($g_i'(z)V_m'(z)$), one of which is an unknown[1]. The transform of a product is found with a convolution integral on the product of the transforms. With $V_m'(z)$ being part of the solution that is being sought, this leads to a form with no general solution. There is an approximation that bypasses this difficulty and is valid in many situations. Consider the definition of $S(k)$ in terms of the transform integral:

$$S(k) = \sum_i \int_{-\infty}^{\infty} g_i'(z)[V_i^e - V_r - V_m'(z)]e^{-jkz}dz\ . \tag{5.62}$$

If it is assumed that the perturbation in the conductance of the ith ion species is non-zero only for $|z| < w/2$, then with a mean-

---

[1] It is assumed that $g_i'(z)$ is a known function. $V_m'(z)$ is an unknown as it is defined in terms of the solutions for Φ_I' and Φ_E.

value theorem (see Olmsted [58]) applied to $V_m(z)$ expression (5.62) becomes

$$S(k) = \sum_i [V_i^e - V_m^*] \int_{-w/2}^{w/2} g_i'(z) e^{-jkz} dz \qquad (5.63)$$

where $V_m^* \in [V_m(-w/2), V_m(w/2)]$ and $V_m(z) = V_m'(z) + V_r$ has been used. Noting that the integral in equation (5.63) is just the Fourier transform of $g_i'(z)$ leads to[1]

$$S(k) = \sum_i [V_i^e - V_m^*] \bar{g}_i'(k) \ . \qquad (5.64)$$

A characteristic of the response for electrode-supplied stimuli noted in Chapters 3 and 4 was that $V_m'(z)$ is essentially constant over $[-w/2, w/2]$, the width of the electrode[2]. It will be assumed that the conductance perturbation width is narrow enough to give the same effect; i.e. $V_m(z) =$ constant for $|z| \leq w/2$. This gives $V_m^* = V_m(0)$ in equation (5.64), where $V_m(0)$ is the transmembrane potential at $z = 0$. The validity of this approximation is reinforced by noting that with the definition (5.62) of the source term, solution coefficients $A(k)$ and $D(k)$ for the

---

[1] In the Fourier transform (5.63), $g_i'(z)$ need not be symmetric about $z = 0$. If not, w is chosen so that $w/2$ is the larger distance from the origin where g_i' becomes zero.

[2] This was demonstrated for $w \leq 2a$, where $2a$ is the fiber diameter.

z-dependent membrane conductance have the same form as the electrotonus coefficients (5.49) and (5.50) of the $J_I^s = -J_E^s$ case of Section 5.2.2 in the steady-state. This implies the response in the present situation should be somewhat similar to the steady-state electrotonus response of an intracellular electrode (discussed in Chapter 3). Even if this approximation is not valid[1], the solution may be obtained by setting $V_m^* = V_m(0)$ and using the result to start an iterative procedure with equation (5.62).

With the above approximation, the source term becomes

$$S(k) = \sum_i [V_i^e - V_m(0)]\bar{g}_i'(k) \quad . \tag{5.65}$$

It is still necessary to find $V_m(0)$, at present an unknown. With coefficients $A(k)$ and $D(k)$ (expressions (5.59) and (5.60)), source term $S(k)$ as given in equation (5.65), and the general solutions (5.18) and (5.19) for Φ_I and Φ_E, $V_m(0)$ is expressed by definition as

$$V_m(0) = V_r + \frac{1}{2\pi} \sum_i [V_i^e - V_m(0)] \int_{-\infty}^{\infty} \frac{\bar{g}_i'(k)}{H(k)} [\sigma_E k\, I_o(kb) K_1(ka) + \sigma_I k\, K_o(ka) I_1(kb)]dk \quad . \tag{5.66}$$

Equation (5.66) may be solved for $V_m(0)$, giving

---

[1] This would be indicated if the $V_m(z)$ obtained with $V_m^* = V_m(0)$ was not constant over $|z| \leq w/2$.

$$V_m(0) = \frac{V_r + \frac{1}{2\pi}\int_{-\infty}^{\infty} \frac{\Sigma V_i^e \bar{g}_i'(k)}{H(k)} [\sigma_E k I_o(kb) K_1(ka) + \sigma_I k K_o(ka) I_1(kb)]dk}{1 + \frac{1}{2\pi}\int_{-\infty}^{\infty} \frac{\Sigma \bar{g}_i'(k)}{H(k)} [\sigma_E k I_o(kb) K_1(ka) + \sigma_I k K_o(ka) I_1(kb)]dk} \quad . \tag{5.67}$$

As all quantities on the right-hand-side of expression (5.67) are known, $V_m(0)$ is easily calculated by means of the numerical Fourier inversion computer program being used to evaluate the integrals.

The solution for a z-dependent membrane conductance (that varies from resting-state conductance only in the narrow region $|z| \leq w/2$) is now complete. With the transform of the conductance perturbation $\bar{g}_i'(k)$, first the transmembrane potential at $z = 0$ is evaluated numerically from expression (5.67). Then with this $V_m(0)$ value and equation (5.65) for the source term $S(k)$, the solution coefficients $A(k)$ and $D(k)$ are fully specified and may be used in the general solutions (Section 5.2.1) for the fields at any point in the system. The case of maintained increase of sodium conductance in the membrane of a dendritic-size fiber is discussed in Section 5.3.1 as one application of this model.

5.2.4. Time and Spatially-Dependent Membrane Conductance

This subsection develops the solution coefficients $A(k,t)$ and $D(k,t)$ for the situation where the neuronal membrane conductance has both a time and space dependence. As in the previous subsection, it is assumed that $g_i(z,t)$ is a known function. The conductance of each ion species is expanded into the form

$$g_i(z,t) = g_{io} + g_i'(z,t) \tag{5.68}$$

where g_{io} is the constant resting condition membrane conductance of that ion species and g_i' is the perturbation from the resting-state value. This expansion for g_i is substituted into boundary conditions (5.11) and (5.12) to obtain

$$\sigma_I E_{Ir}(b,z,t) = \sigma_E E_{Er}(a,z,t) \tag{5.69}$$

$$g_r V_m'(z,t) + C_m \frac{\partial}{\partial t} V_m'(z,t) - \sigma_I E_{Ir}(b,z,t) = \sum_i g_i'(z,t)[V_i^e - V_r - V_m'(z,t)] \tag{5.70}$$

where it has been assumed that there are no electrode-supplied sources present and the procedure used to arrive at expressions (5.54) and (5.55) has been followed (Section 5.2.3).

The Fourier transform on axial variable z and the Laplace transform on time (see Chapters 3 and 4) are applied to boundary conditions (5.69) and (5.70) to yield

$$\sigma_I \bar{E}_{Ir}(b,k,t) = \sigma_E \bar{E}_{Er}(a,k,t) \tag{5.71}$$

$$(g_r + sC_m)\bar{V}'_m(k,s) - \sigma_I \bar{E}_{Ir}(k,s) = S(k,s) \qquad (5.72)$$

where the assumption has been made that the system is at rest at $t = 0$, k is the Fourier domain variable, s is the Laplace domain variable, and the source function is given by

$$S(k,s) = \mathcal{L}\{\mathfrak{F}_k\{\Sigma_i\, g'_i(z,t)[V^e_i - V_r - V'_m(z,t)]\}\} \quad . \qquad (5.73)$$

A comparison of boundary conditions (5.71) and (5.72) with the boundary conditions (expression (5.48)) of Section 5.2.2 for the case of $J^s_I = -J^s_E$ demonstrates that the mathematical form is identical if $\bar{J}^s(k,s)$ (in Section 5.2.2) is replaced with $S(k,s)$. This immediately gives the solution coefficients from equations (5.49) and (5.50) as

$$A(k,s) = \frac{\sigma_E k\, K_1(ka)}{F(k,s)}\; S(k,s) \qquad (5.74)$$

$$D(k,s) = \frac{-\sigma_I k\, I_I(kb)}{F(k,s)}\; S(k,s) \qquad (5.75)$$

where $F(k,s)$ is defined by relation (5.30).

After some manipulation of source term $S(k,s)$ and solution coefficients (5.74) and (5.75), it is possible to express $A(k,t)$ and $D(k,t)$ (the time-domain solution coefficients) in terms of the Fourier transform of the perturbation in membrane conductance. To start, it is assumed (as in the previous section) that all the perturbations $g'_i(z,t)$ are non-zero within a narrow

region defined by $|z| \leq w/2$. The criterion for the width of this region is that $V'_m(z,t)$ may be approximated by $V'_m(z,t) = V'_m(0,t)$ = spatially constant for $|z| \leq w/2$. With this approximation, the Fourier transform in expression (5.73) avoids a convolution integral (from $g'_i(z,t)V'_m(z,t)$) that cannot be handled, and gives the result

$$S(k,s) = \mathcal{L}\{\sum_i \bar{g}'_i(k,t)[V^e_i - V_r - V'_m(0,t)]\} \tag{5.76}$$

where $\bar{g}'_i(k,t)$ is the Fourier transform on z of $g'_i(z,t)$.

The Laplace transform is carried out on the terms involving the product of time function $\bar{g}'_i$ and the constants V^e_i and V_r to obtain

$$S(k,s) = \sum_i \bar{g}'_i(k,s)[V^e_i - V_r] - \mathcal{L}\{\sum_i \bar{g}'_i(k,t)V'_m(0,t)\} \tag{5.77}$$

where $\bar{g}'_i(k,s)$ is the Laplace and Fourier transformed perturbation in membrane conductance of the ith ion species. The $\bar{g}'_i(k,t)V'_m(0,t)$ terms in relation (5.77) cannot be transformed as $V'_m(0,t)$ is at present an unknown. Altering the present expressions so as to obtain an explicit equation for $V'_m(0,t)$ from the implicit form above is the next manipulation and leads to the final solution.

The source term (5.77) is inserted into the k and s-space transmembrane potential perturbation defined by $\bar{V}'_m(k,s) = \bar{\Phi}'_I(b,k,s) - \bar{\Phi}_E(a,k,s)$ giving

$$\bar{V}_m'(k,s) = A(k,s)I_o(kb) - D(k,s)K_o(ka)$$

$$= \frac{\sigma_E k\, I_o(kb)K_1(ka) + \sigma_I k\, K_o(ka)I_1(kb)}{F(k,s)}\left[\sum_i \bar{g}_i'(k,s)[V_i^e - V_r]\right.$$

$$\left. - \mathcal{L}\{\sum_i \bar{g}_i'(k,t)V_m'(0,t)\}\right] . \qquad (5.78)$$

Using the expansion introduced in equation (5.33) of $F(k,s) = \alpha(k)[s + P(k)]$, with α and P defined in relations (5.34) and (5.35), leads to

$$\bar{V}_m'(k,s) = \frac{\sum_i \bar{g}_i'(k,s)[V_i^e - V_r] - \mathcal{L}\{\sum_i \bar{g}_i'(k,t)V_m'(0,t)\}}{C_m[s + P(k)]} \qquad (5.79)$$

where it is noted that the numerator in expression (5.78) is just $\alpha(k)/C_m$, canceling the $\alpha(k)$ factor in $F(k,s)$.

Now the convolution property for Laplace transforms is applied. This property is given by Churchill [7] as

$$\mathcal{L}^{-1}\{f(s)h(s)\} = \int_o^t F(\tau)H(t - \tau)d\tau \qquad (5.80)$$

where $f(s)$ and $h(s)$ are the Laplace transforms of any functions $F(t)$ and $H(t)$. With the Laplace transform (4.81) of an exponential ($\mathcal{L}\{e^{at}\} = \frac{1}{s-a}$), the convolution property (5.80) applied to expression (5.79) gives

$$\bar{V}'_m(k,t) = \frac{1}{C_m} \int_o^t \sum_i \bar{g}'_i(k,\tau)[V_i^e - V_r]e^{-P(k)[t-\tau]}d\tau$$

$$- \frac{1}{C_m} \int_o^t \sum_i \bar{g}'_i(k,\tau)V'_m(0,\tau)e^{-P(k)[t-\tau]}d\tau \qquad (5.81)$$

where now all quantities have been inverted back to the time domain.

The second integral containing $V'_m(0,\tau)$ in equation (5.81) is numerically approximated by means of the trapezoidal rule (see Henrici [31]). This numerical integration is defined by

$$\int_o^t H(\tau)d\tau \doteq \frac{\Delta\tau}{2} [H(0) + H(t) + 2 \sum_{n=1}^{N-1} H(n\Delta\tau)] \qquad (5.82)$$

where $N = t/\Delta\tau$ and $\Delta\tau$ is the integration step size. As illustrated in Figure 5.2, this approximates the integral of a smooth function with respect to continuous variable τ by the sum of the areas of N trapezoids. These trapezoids are defined by the function at the $N + 1$ points $n\Delta\tau$; $n = 0,1,2,\ldots,N$. In the limit of $\Delta\tau \to 0$ $(N \to \infty)$, the trapezoidal integration converges to the exact value. Applying this numerical algorithm to the second integral in expression (5.81) yields

$$\int_o^t \sum_i \bar{g}'_i(k,\tau)V'_m(0,\tau)e^{-P(k)[t-\tau]}d\tau = \frac{\Delta\tau}{2} [\sum_i \bar{g}'_i(k,t)V'_m(0,t)$$

$$+ 2 \sum_{n=1}^{N-1} (\sum_i \bar{g}'_i(k,n\Delta\tau)V'_m(0, n\Delta\tau)e^{-P(k)[t-n\Delta\tau]})] \qquad (5.83)$$

where the assumption of $V'_m(z,0) = 0$ (the system is at rest for $t \leq 0$) gives $\bar{g}'_i(k,0)V'_m(0,0) = 0$.

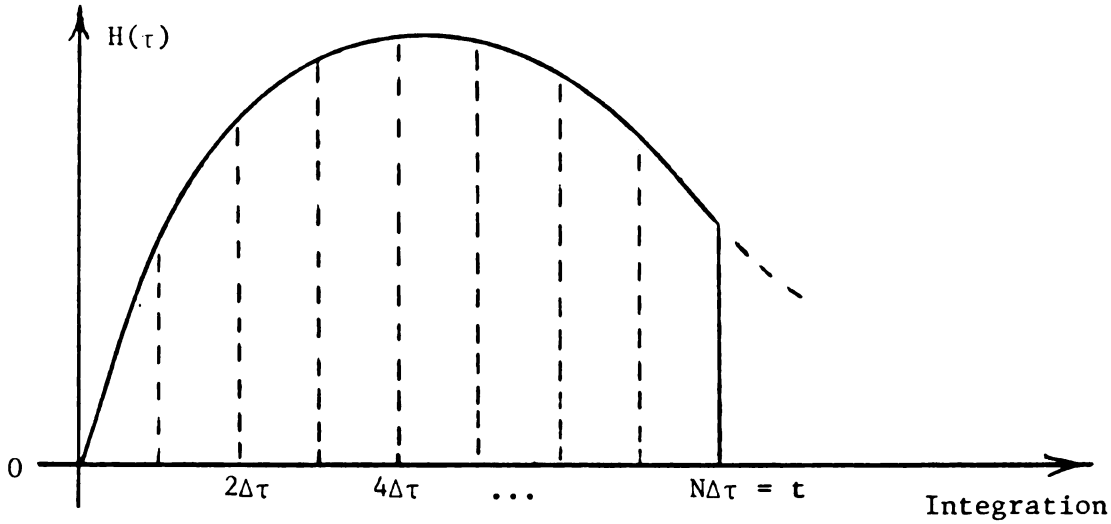

(a) Continuous function $H(\tau)$, integrated for its area between $\tau = 0$ and $\tau = t$

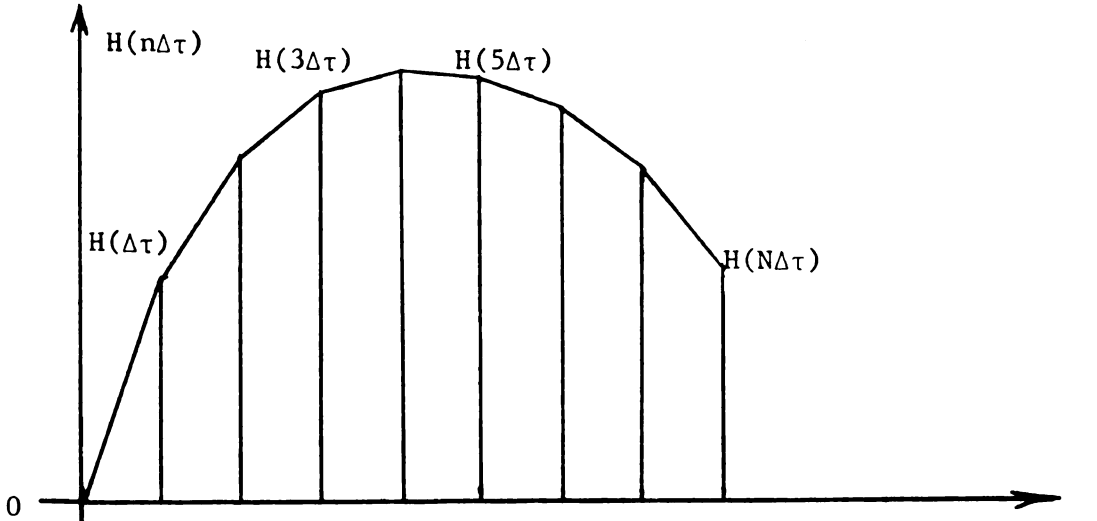

(b) Numerical integration of $H(\tau)$ as a sum of N trapezoids using the function $H(\tau)$ at $\tau = n\Delta\tau$

FIGURE 5.2

Trapezoidal Rule Integration Approximation

The trapezoidal rule integration is substituted into expression (5.81) and the inverse Fourier transform (definition (3.32)) is applied to obtain $V'_m(0,t)$ as follows:

$$V'_m(0,t) = \frac{1}{2\pi}\int_{-\infty}^{\infty} \bar{V}'_m(k,t)dk$$

$$= \frac{1}{2\pi C_m}\int_{-\infty}^{\infty}\int_{o}^{t}\sum_i \bar{g}'_i(k,\tau)[V_i^e - V_r]e^{-P(k)[t-\tau]}d\tau\, dk$$

$$- \frac{\Delta\tau}{4\pi C_m}\int_{-\infty}^{\infty}[\sum_i \bar{g}'_i(k,t)V'_m(0,t)$$

$$+ 2\sum_{n=1}^{N-1}(\sum_i \bar{g}'_i(k,n\Delta\tau)V'_m(0,n\Delta\tau)e^{-P(k)[t-n\Delta\tau]})]dk$$

$$V'_m(0,t) = \frac{1}{2\pi C_m}\frac{\int_{-\infty}^{\infty}\int_{o}^{t}\sum_i \bar{g}'_i(k,\tau)[V_i^e - V_r]e^{-P(k)[t-\tau]}d\tau\, dk}{1 + \frac{\Delta\tau}{2C_m}\sum_i g'_i(0,t)}$$

$$- \frac{\Delta\tau}{2\pi C_m}\frac{\int_{-\infty}^{\infty}\sum_{n=1}^{N-1}[\sum_i \bar{g}'_i(k,n\Delta\tau)V'_m(0,n\Delta\tau)e^{-P(k)[t-n\Delta\tau]}]dk}{1 + \frac{\Delta\tau}{2C_m}\sum_i g'_i(0,t)} \qquad (5.84)$$

where the Fourier inverse of $g'_i(0,t) = \frac{1}{2\pi}\int_{-\infty}^{\infty}\bar{g}'_i(k,t)dk$ has been used in the denominator terms. Though equation (5.84) looks very complex, it may be evaluated on the digital computer with the same program used for all Fourier inversions in this report.

After obtaining $V'_m(0,t)$ from expression (5.84), the transmembrane potential is given by the Fourier inverse of equation (5.81) as

$$V_m(z,t) = V_r + \frac{1}{2\pi C_m} \int_{-\infty}^{\infty} \int_o^t \sum_i \bar{g}_i'(k,\tau)[V_i^e - V_r]e^{-P(k)[t-\tau]}d\tau\, e^{jkz}dk$$

$$- \frac{\Delta\tau}{4\pi C_m} \int_{-\infty}^{\infty} [\sum_i \bar{g}_i'(k,t)V_m'(0,t)$$

$$+ 2 \sum_{n=1}^{N-1} \sum_i \bar{g}_i'(k,n\Delta\tau)V_m'(0,n\Delta\tau)e^{-P(k)[t-n\Delta\tau]}e^{jkz}dk \qquad (5.85)$$

where $V_m = V_r + V_m'$ and the trapezoidal rule approximation for the second integral in expression (5.81) have been applied. If the desired result is the transmembrane potential, then the solution is complete. First $V_m'(0,t)$ is evaluated by means of expression (5.84) for the times $t = \Delta\tau, 2\Delta\tau, 3\Delta\tau,\ldots,N\Delta\tau$; where $t = N\Delta\tau$ is the maximum time point of interest. By performing the calculations sequentially for increasing times t, the successive values of V_m' from $t = 0$ to $t = N\Delta\tau$ are obtained; with the previous $(n - 1)$ values used to calculate the nth value of V_m'[1]. In practice, $\Delta\tau$ must be chosen small enough to make the trapezoidal approximation accurate, requiring a large number of sequential $V_m'(0,n\Delta\tau)$ values to be calculated. The transmembrane potential for $z \neq 0$ is then obtained from expression (5.85), the calculation being performed only at the time points of interest by use of the previously obtained values of $V_m'(0,n\Delta\tau)$.

In most cases, the integral $\int_o^t \sum_i \bar{g}_i'(k,\tau)[V_i^e - V_r]e^{-P(k)[t-\tau]}d\tau$ found in both expressions (5.84) and (5.85) can be evaluated

---

[1] $V_m'(0,0) = 0$ is used as the starting point.

analytically. This is the reason it was left in that form. For the cases where it cannot be evaluated, it may be included in the trapezoidal numerical integration that was applied to the V'_m terms. It is noted that the term containing $V'_m(0,n\Delta\tau)$ in both equations (5.84) and (5.85) is an insignificant second-order correction term in the special case where $V'_m(0,t) << V^e_i - V_r$ for all ion species "i" that have a significant conductance change. For this situation, the solutions are greatly simplified as the trapezoidal rule integration terms may be discarded. Section 5.3.2 presents an example of this situation in a simulation of the excitatory postsynaptic potential and discusses this approximation. In cases where $V'_m(0,t)$ is large with respect to $V^e_i - V_r$, the full expressions must be applied. An example of this is discussed in Section 5.3.3 in a simulation of an inhibitory postsynaptic potential. As the transmembrane potential experiences a change larger than the magnitude of V_r in an action potential, the complete expressions would always be required in a calculation of nerve impulse events.

If the desired result is the scalar potential, electric field, or current density, then the solution coefficients $A(k,t)$ and $D(k,t)$ are needed for the general solutions presented in Section 5.2.1. The solution coefficients (5.74) and (5.75) in s-space contain the common factor $S(k,s)/F(k,s)$; the only s-dependent portion of either coefficient. Following the development in equations (5.78) - (5.83), $F(k,s)$ is expanded into $\alpha(k)[s - P(k)]$, the convolution property is applied, and the trapezoidal integration is used as follows:

$$\frac{S(k,s)}{F(k,s)} = \frac{\sum_i \bar{g}_i'(k,s)[V_i^e - V_r] - \mathcal{L}\{\sum_i \bar{g}_i'(k,t)V_m'(0,t)\}}{\alpha(k)[s + P(k)]} \tag{5.86}$$

$$\frac{S(k,t)}{F(k,t)} = \mathcal{L}^{-1}\{\frac{S(k,s)}{F(k,s)}\}$$

$$= \frac{1}{\alpha(k)} \int_o^t \sum_i \bar{g}_i'(k,\tau)[V_i^e - V_r]e^{-P(k)[t-\tau]}d\tau$$

$$- \frac{\Delta\tau}{2\alpha(k)} [\sum_i \bar{g}_i'(k,t)V_m'(0,t)$$

$$+ 2 \sum_{n=1}^{N-1} \sum_i \bar{g}_i'(k,n\Delta\tau)V_m'(0,n\Delta\tau)e^{-P(k)[t-n\Delta\tau]}] . \tag{5.87}$$

This gives $A(k,t)$ and $D(k,t)$ immediately as

$$A(k,t) = \sigma_E k K_1(ka) \frac{S(k,t)}{F(k,t)} \tag{5.88}$$

$$D(k,t) = - \sigma_I k I_1(kb) \frac{S(k,t)}{F(k,t)} \tag{5.89}$$

with $S(k,t)/F(k,t)$ as defined in relation (5.87). As discussed above, $V_m'(0,t)$ is obtained at the sequential time points $\Delta\tau, 2\Delta\tau, 3\Delta\tau,\ldots,N\Delta\tau$ from expression (5.84) and the convolution integral containing $[V_i^e - V_r]$ is either evaluated analytically (see Section 5.3.2) or approximated with a trapezoidal rule. The

coefficients are then evaluated at the desired time points and used in the Fourier inversion integrals (as discussed in Section 5.2.1) to obtain the z-space end result.

5.3. Response for Spatial and Time-Dependent Membrane Conductance

5.3.1. Characteristics of the Response Due to a Spatially-Variant Membrane Conductance

It has been repeatedly demonstrated that naturally occurring neural electrical phenomena are the result of changes in the individual membrane conductivities of the various ion species within the system[1]. The resting neuron has a transmembrane potential generally very close to the Nernst potential of the choloride (Cl^-) ions, with depolarizations a result of an increase in sodium (Na^+) conductance and hyperpolarizations a result of potassium (K^+) conductance increases (see Katz [40], Plonsey [60]). This section considers the effect of a maintained (steady-state) increase in Na^+ conductance over a small region of the membrane. The resultant depolarization may be considered as due to a "window" in the membrane that selectively allows an influx of sodium ions. This conductance "window" for sodium might be the result of a continued application of transmitter substance to a postsynaptic membrane. As such, this model will give the maximum magnitude and spatial extent of the depolarization across the postsynaptic membrane for a repeated series of excitatory postsynaptic potentials (EPSP's).

---

[1] See Cole and Curtis [13], Hille [32], Hodgkin and Huxley [34], and Smith, Wuerker, and Frank [73] for examples of specific (and classical) experiments.

Consider the case where the perturbation in sodium conductance is constant and non-zero for a region of width w centered on $z = 0$. This is stated mathematically by

$$g'_{Na^+}(z) = \begin{cases} g'_{Na^+} & |z| \leq w/2 \\ 0 & \text{elsewhere} \end{cases} \tag{5.90}$$

where g'_{Na^+} is the (positive) magnitude of the increase in membrane sodium conductance. From Section 3.2.2, $\bar{g}'_{Na^+}(k)$ (the Fourier transform of $g'_{Na^+}(z)$) is obtained immediately as

$$\bar{g}'_{Na^+}(k) = g'_{Na^+} \frac{2 \sin(k\, w/2)}{k} \quad . \tag{5.91}$$

With relation (5.91) (and the assumption of only the sodium conductance changing from its resting condition value), the solutions (5.64) and (5.67) for the source term $S(k)$ and $V_m(0)$ from Section 5.2.3 are

$$S(k) = [V_{Na^+} - V_m(0)]\bar{g}'_{Na^+}(k) \tag{5.92}$$

$$V_m(0) = \frac{V_r + \frac{V_{Na^+}}{2\pi} \int_{-\infty}^{\infty} \frac{\bar{g}'_{Na^+}(k)}{H(k)} [\sigma_E k I_o(kb) K_1(ka) + \sigma_I k K_o(ka) I_1(kb)]dk}{1 + \frac{1}{2\pi} \int_{-\infty}^{\infty} \frac{\bar{g}'_{Na^+}(k)}{H(k)} [\sigma_E k I_o(kb) K_1(ka) + \sigma_I k K_o(ka) I_1(kb)]dk} \tag{5.93}$$

where V_{Na^+} is the sodium Nernst potential and $H(k)$ was defined in relation (5.61). Numerical integration of the Fourier integrals in expression (5.93) obtains $V_m(0)$; which may then be used to specify the source term (5.92). Note that $V_m(0)$ is a constant and that the difference between its magnitude and the sodium Nernst potential (V_{Na^+}) determines the magnitude of $S(k)$. With the source term $S(k)$, the solution coefficients (5.59) and (5.60) of Section 5.2.3 may be used to find the fields anywhere in the intracellular or extracellular spaces and the transmembrane potential for $z \neq 0$.

The parameters for the example in this section are representative of a dendritic membrane cylinder[1]. They are:

$a = 2.5\mu$ radius (5μ diameter)

$d = 50\ \text{Å}$ membrane thickness

$\sigma_I = 0.01667$ mhos/cm intracellular conductivity

$\sigma_E = 0.04546$ mhos/cm extracellular conductivity

$g_r = 2.0 \times 10^{-4}$ mhos/cm^2 resting-state membrane conductance

$V_r = -60$ mV resting transmembrane potential

$V_{Na^+} = 55$ mV sodium Nernst potential

$w = 1\mu$ width of conductance perturbation "window".

The transmembrane potential response for this system is illustrated in Figure 5.3 for conductance changes of $g'_{Na^+} = 0.01$

---

[1] The values are from Katz [40] and Plonsey [60]. The magnitudes of g'_{Na^+} used are indicated by Eccles [18] to lie within the range of experimentally observed values.

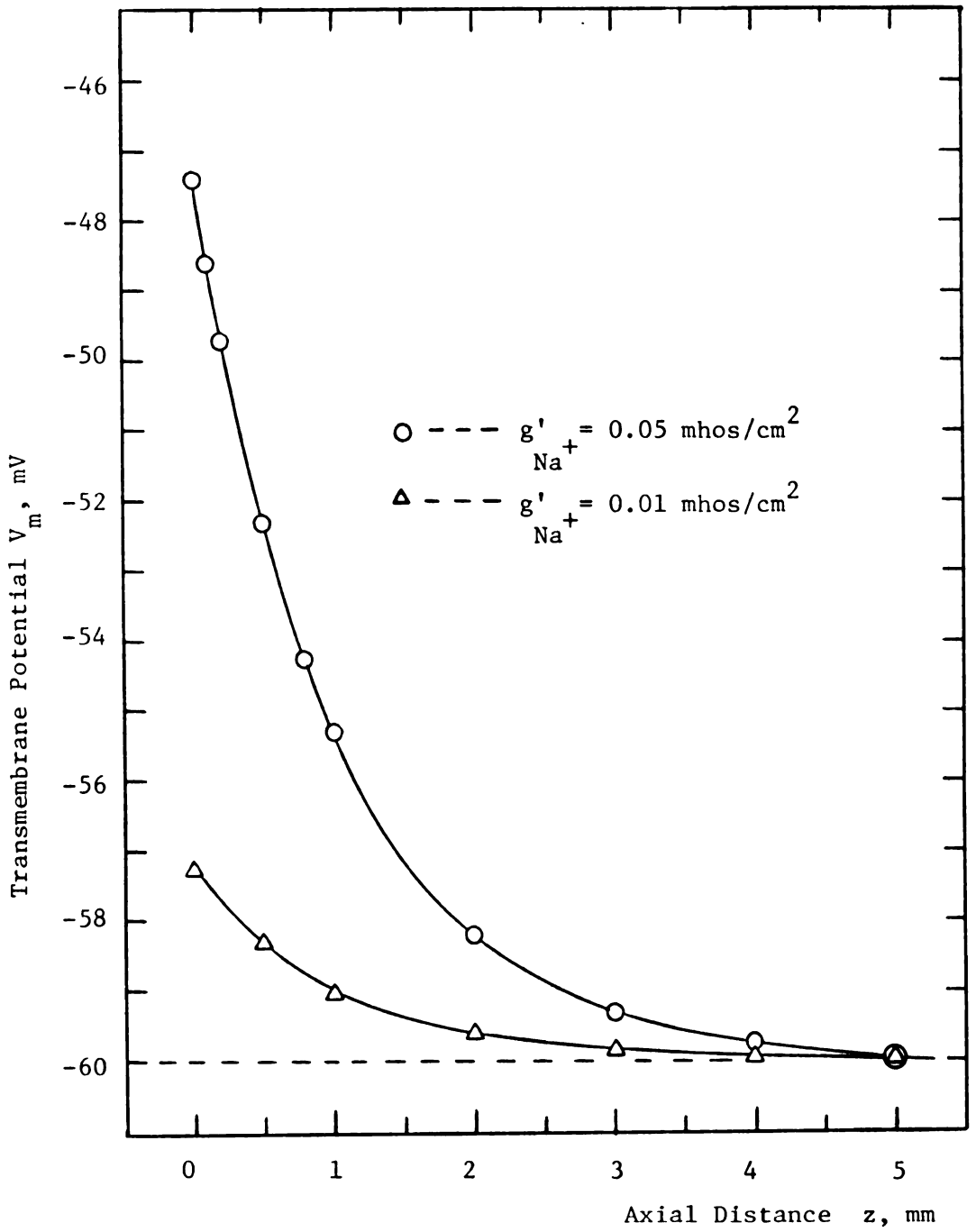

FIGURE 5.3

Transmembrane Potential Response for a Maintained Increase in Sodium Conductance

and 0.05 mhos/cm^2. The curves are exponential (for $z > 10\mu$)[1] with a length constant of about 1 mm. Since the length constant of this fiber given by cable theory (for passive response) is $\lambda = 1.02$ mm (see Section 3.3.2), the axial decay is essentially the same as that expected for a transmembrane potential perturbation in the case of steady-state electrotonus. Although $\bar{g}'_{Na^+}(k)$ has the same form as $\bar{J}^s(k)$ (the source term in Chapter 3 for electrode current density), the response to a change in the perturbation magnitude g'_{Na^+} is not linear as it was for changes in stimulating current magnitudes. This may be observed by considering that $g'_{Na^+} = 0.01$ mhos/cm^2 produced a depolarization at $z = 0$ of 2.76 mV ($V_m(0) = -57.24$ mV) while $g'_{Na^+} = 0.05$ mhos/cm^2 gave a depolarization of 12.58 mV ($V_m(0) = -47.42$ mV). The response to a five-fold increase in g'_{Na^+} is not five times the depolarization ($5 \times 2.76 = 13.80$ mV), which contrasts with the solutions in Chapters 3 and 4 that are always directly proportional to stimulating current intensity (I^s).

The reason for this difference becomes apparent when the source of the depolarization in each case is considered. With an electrode-impressed source current density, the depolarization is a result of a source current (I^s) that can have any magnitude since an external generator (battery) drives the stimulating circuit. Doubling I^s means the charge/unit time that is injected into the system at the electrode is doubled; resulting in a response twice as large. For the present case, the current that flows into the

---

[1] For $|z| \leq 0.5\mu$, $V_m(z)$ is virtually constant, satisfying the assumption applied in Section 5.2.3.

cell interior is driven by a "battery" that consists of the difference between V_{Na^+} and $V_m(0)$ (see equation (5.92) for $S(k)$). As the conductance perturbation is increased, the charge carried into the cell interior depolarizes the membrane so that $V_m(0)$ approaches V_{Na^+}, reducing the magnitude of the source term $S(k)$. In effect, a negative feedback occurs where a depolarization has the result of reducing the effect of further increases in conductance. The limiting case is $V_m(0) = V_{Na^+}$, where $S(k) = 0$; a situation that corresponds to $g'_{Na^+} \to \infty$. This non-linear response to changes in g'_{Na^+} may be noted by considering that V_m is confined to the range V_r to V_{Na^+} for variations in g'_{Na^+} between zero and infinity. As such, the depolarization for $g'_{Na^+} = 0.05$ mhos/cm^2 in Figure 5.3 is not five times that for $g'_{Na^+} = 0.01$ mhos/cm^2 because the resultant further depolarization from increasing g'_{Na^+} has reduced the magnitude of the driving term $S(k)$.

The magnitude of the response is also dependent upon the area of the conductance window. The relationship is nonlinear in a manner similar to that discussed for changes in g'_{Na^+}. Increasing w leads to a greater depolarization for fixed g'_{Na^+}, but the response is limited by the point where $S(k) = 0$ $(V_m(0) = V_{Na^+})$. Thus, for this case of a spatially dependent sodium conductance, the amount of depolarization seen at any point depends upon three factors that determine the overall magnitude of the source term $S(k)$. These are the amount of conductance change (g'_{Na^+}), the difference between the sodium Nernst potential and the transmembrane potential at $z = 0$ $(V_{Na^+} - V_m(0))$, and the area affected by the conductance change.

It would be a simple matter to apply the solutions of Section 5.2.3 to changes in the conductance of several ion species. The major response characteristics would be the same as noted here since the effect would be to add one or more additional $[V_i^e - V_m(0)]\bar{g}_i'(k)$ terms to $S(k)$. Each of these terms would be similar and vary only in magnitude. The major difference would be a shift in the amount of depolarization necessary to give $S(k) = 0$, this potential being solved for from expression (5.65) as

$$V_m(0) = \frac{\Sigma_i \bar{g}_i'(k) V_i^e}{\Sigma_i \bar{g}_i'(k)} \quad . \tag{5.94}$$

For a single ion species, this reduces to $V_m(0) = V_i^e$ as in the example above.

5.3.2. Use of the Two-Compartment Model to Simulate Excitatory Postsynaptic Potentials

A synapse is the junction at which information (incident action potentials) is passed from the presynaptic axon to the postsynaptic cell (often a second neuron). The presynaptic cell releases a chemical transmitter substance that diffuses across the synaptic cleft where it alters the permeability of the postsynaptic membrane to one or more ion species. This causes a depolarization or hyperpolarization of the postsynaptic membrane, referred to as a postsynaptic potential (PSP). If the potential change is towards threshold (positive, a depolarization) the event is called an excitatory postsynaptic potential (EPSP). If the effect is a

hyperpolarization (negative, away from threshold), the PSP is labeled an inhibitory postsynaptic potential (IPSP)[1]. The solutions of Section 5.2.4 are used in this section to simulate an EPSP, where the nature of the driving term $S(k,t)$ will allow a simplification in the calculations.

An EPSP is the result of an increase in the membrane's sodium conductance (permeability), since (of the three major ion species Na^+, K^+, and Cl^-) only sodium has a Nernst potential that is above threshold. Assuming that only the sodium conductance changes[2], that the area of the synapse is small, and that the conductance change is a constant over the affected region leads to

$$\bar{g}'_{Na^+}(k,t) = g'_{Na^+}(t) \frac{2 \sin(k\, w/2)}{k} \tag{5.95}$$

where $g'_{Na^+}(t)$ is the time-dependence and magnitude of the conductance perturbation and w is the width of the region where $g'_{Na^+}(z,t) \neq 0$ (see Section 5.3.1)[3].

---

[1] See Katz [40] or Plonsey [60] for a basic discussion of synaptic structure and events. Eccles [18] offers a more complete treatment.

[2] There is evidence (Eccles [18], Smith, Wuerker, and Frank [73]) that indicates that an increase in K^+ conductance also occurs. The effect is smaller than the Na^+ conductance increase and is neglected in this model. If it was included, the only result would be that the magnitude of $S(k,t)$ would be slightly smaller.

[3] The nature of the solutions requires the affected area to be rotationally symmetric, so that the synaptic area is $2\pi aw$.

The time-dependence is obtained from Rall [64] as

$$g'_{\underset{Na}{+}}(t) = g'_{\underset{Na}{+}} \frac{t}{T_p} e^{(1-t/T_p)} \tag{5.96}$$

where $g'_{\underset{Na}{+}}$ is the peak magnitude of the conductance perturbation. This $g'_{\underset{Na}{+}}(t)$ function represents the time course of the chemical transmitter that causes the change in conductance. The function is essentially linear for $0 \leq t \leq T_p$, representing the arrival (via diffusion) of the transmitter substance at the postsynaptic membrane. After T_p (the time of maximum or peak conductance change) there is an exponential decay that simulates the enzymatic degradation of the transmitter. The duration of the conductance perturbation is altered by changing T_p, the time of the conductance peak[1].

The solutions of Section 5.2.4 (relations (5.84), (5.85), and (5.87)) all contain a convolution integral which can be analytically carried out even with the complicated time function assumed for $g'_{\underset{Na}{+}}(t)$. With expressions (5.95) and (5.96), the convolution becomes

---

[1] This function assumes that the arrival of transmitter at the postsynaptic membrane begins at $t = 0$. The time of transmitter release is at some $t < 0$.

$$\int_0^t \sum_i \bar{g}'_i(k,\tau)[V_i^e - V_r]e^{-P(k)[t-\tau]}d\tau$$

$$= \int_0^t g'_{\overset{+}{Na}} \frac{2\sin(k\,w/2)}{k}\,[V_{\overset{+}{Na}} - V_r]\frac{\tau}{T_p}\,e^{(1-\tau/T_p-P(k)[t-\tau])}\,d\tau$$

$$= \bar{g}'_{\overset{+}{Na}}(k)\,\frac{[V_{\overset{+}{Na}} - V_r]}{T_p}\,e^1 \int_0^t \tau\, e^{(\tau/T_p-P(k)[t-\tau])}\,d\tau \qquad (5.97)$$

where $\bar{g}'_{\overset{+}{Na}}(k) = g'_{\overset{+}{Na}} \frac{2\sin(k\,w/2)}{k}$ as defined for the steady-state case in relation (5.91), Section 5.3.1. Applying integration by parts to equation (5.97) leads to the desired analytical expression:

$$\bar{g}'_{\overset{+}{Na}}(k)\,\frac{[V_{\overset{+}{Na}} - V_r]e^1}{T_p} \int_0^t \tau\, e^{(\tau/T_p-P(k)[t-\tau])}\,d\tau$$

$$= \bar{g}'_{\overset{+}{Na}}(k)\,\frac{[V_{\overset{+}{Na}} - V_r]e^1}{T_p}\left\{\frac{e^{-t/T_p}[(P(k) - 1/T_p)t - 1] + e^{-P(k)t}}{(P(k) - 1/T_p)^2}\right\}. \qquad (5.98)$$

The response for the example in this section is calculated with the parameters (a, d, σ_I, σ_E, etc) listed in the previous section for a dendritic-size fiber.[1] These solutions also require the membrane capacitance/unit area; taken as $C_m = 1.062\ \mu f/cm^2$ (this value is obtained from $C_m = \varepsilon_M/d$ with $\varepsilon_M = 6\varepsilon_o$ and $d = 50\ \mathring{A}$). The peak magnitude of the sodium conductance perturbation $g'_{\overset{+}{Na}}$ is chosen as $0.05\ mhos/cm^2$ occurring at $T_p = 0.2$ msec, and the width of the synaptic area w taken as 1μ. This allows

---

[1] Test parameters are also summarized in Appendix D.

comparison of the time-dependent response with the steady-state response presented in Section 5.3.1.

As discussed in Section 5.2.4, the calculation of the numerical response first requires the transmembrane potential perturbation at $z = 0$. Solution (5.84) defines $V_m'(0,t)$ as the difference of two Fourier inversion integrals. The first integral contains the source term and convolution integral defined analytically in expression (5.98) for this present example. The second integral contains a sum on n of the product $\bar{g}_1'(k,n\Delta\tau)V_m'(0, n\Delta\tau)$, this sum arising from the trapezoidal integration rule being applied to a convolution containing $V_m'(0,t)$. In general, $V_m'(0,t)$ would be evaluated for the sequential time series $t = n\Delta\tau$, $n = 1,2,3,...$; where $\Delta\tau$ must be chosen sufficiently small for the trapezoidal rule to converge to the correct response. This second term (of equation (5.84) for $V_m'(0,t)$) is a correction term in the sense that it modifies the response of the transmembrane potential at time t by a factor dependent upon the past history of the transmembrane potential perturbation.

Figure 5.4 illustrates the effect of the second integral term in solution (5.84) as a correction term. As $\Delta\tau$ is decreased, the response converges to the correct result. The only problem is that this requires a $\Delta\tau$ that is so small as to require a very large number of time steps to be calculated. However, in this particular case the correction term can be discarded. As seen in Figure 5.4, the curves for decreasing $\Delta\tau$ are bounded by the response

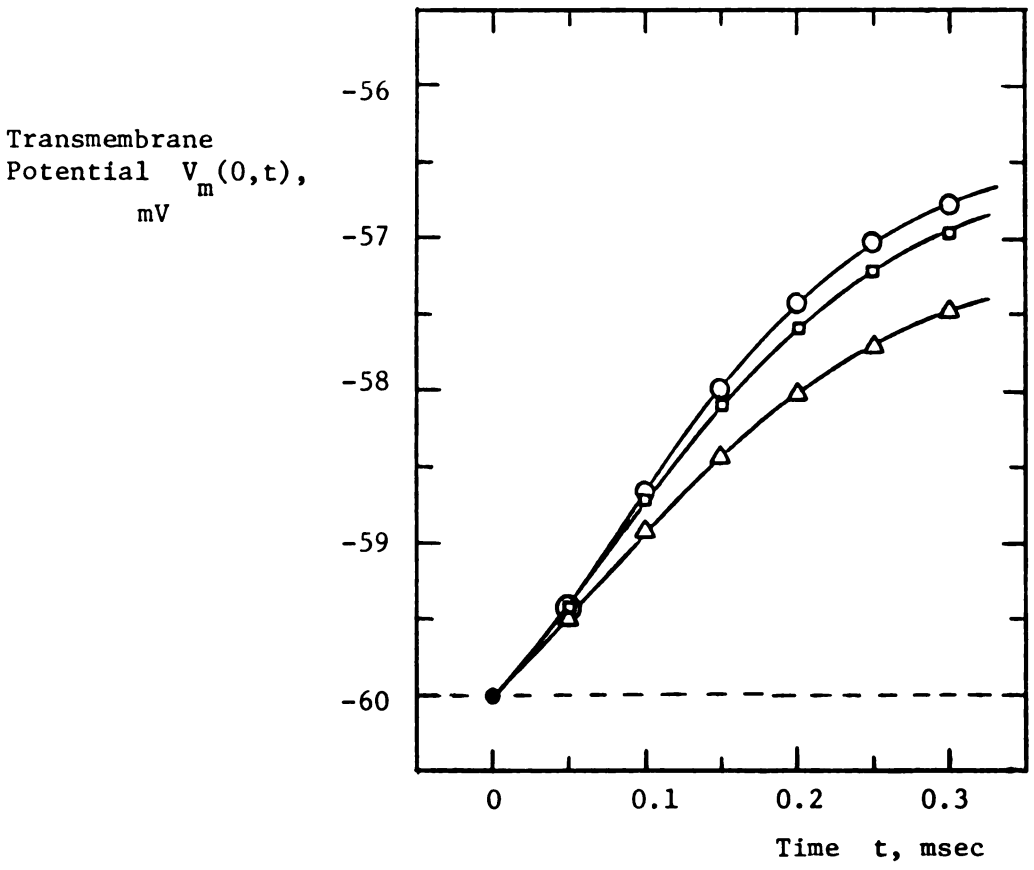

FIGURE 5.4

Convergence of Solution for Decreasing Values of $\Delta\tau$

curve calculated without the second term of solution (5.84) (the "correction term"). By decreasing $\Delta\tau$[1], it was discovered that the full solution converged to a curve that was within 0.1 mV of the curve for the solution without the correction term. Thus it appears that the solution without the correction term yields a response that is acceptably accurate[2] without the enormous amount of calculation required to include this term.

The above approximation (dropping the correction term) may be verified by considering the origin of the two terms in solution (5.84). They arose from the Laplace transform of the source term $S(k,s)$ defined in (5.76). The first term of expression (5.84) (the convolution carried out in relation (5.98)) is invariant for changes in the transmembrane potential, as this term represents the influx of sodium ions driven by $V_{Na^+} - V_r$. The second (correction) term came from the transmembrane potential perturbation term in $S(k,s)$. This term reflects the nature of the natural bioelectric source due to sodium to decrease its magnitude as the membrane depolarizes. Considering the driving potential in $S(k,s)$ as $V_{Na^+} - V_r - V'_m(0,t) = V_{Na^+} - V_m(0,t)$ (for this case of only g'_{Na^+} non-zero) demonstrates that the correction term represents the change in the source term magnitude due to changes in $V_m(0,t)$ from the resting potential. Since the sodium Nernst potential (in this example) is 55 mV and resting potential is

---

[1] This required taking $\Delta\tau$ as small as 0.005 msec.

[2] The peak of the response is a depolarization of about 3.5 mV. Better than 0.1 mV accuracy thus gives less than 3% error.

-60 mV, the driving potential for the source term is $55 - (-60) - V'_m(0,t) = 115 - V'_m(0,t)$ mV. As the magnitude of a single EPSP is normally in the range of 1 to 10 mV[1], $V'_m(0,t)$ modifies $S(k,t)$ by less than 10% even at the peak of the EPSP. For the present example, the peak of the EPSP was found to be a depolarization of 3.5 mV, so that the correction term modifies the solution at most 3%. Since 3% of 3.5 mV is on the order of 0.1 mV, the result noted by direct numerical calculation is verified.

The net conclusion that can be reached from the above discussion is that when the difference between V_i^e and V_r for all ion species involved in the source term $S(k,s)$ is far greater than the expected perturbation in transmembrane potential at $z = 0$ the correction term represented by the second Fourier integral in solution (5.84) may be discarded as negligible. If the conductance changes result in a transmembrane potential where $V'_m(0,t)$ becomes significant with respect to $V_i^e - V_r$, this term must be included. An example of the latter situation is presented in the next section.

For the present EPSP simulation, the correction term is discarded to give the solution for transmembrane potential as

$$V_m(z,t) = V_r + \frac{[V_{Na^+} - V_r]e^1}{2\pi C_m T_p} \int_{-\infty}^{\infty} \bar{g}'_{Na^+}(k) e^{jkz} \left\{ \frac{e^{-t/T_p}[(P(k) - 1/T_p)t - 1] + e^{-P(k)t}}{(P(k) - 1/T_p)^2} \right\} dk . \qquad (5.99)$$

---

[1] See Eccles [18], Plonsey [60].

This expression is obtained by dropping the second term[1] in equation (5.81) for $\bar{V}'_m(k,t)$, applying the Fourier inverse transform, and adding V_r. The same result is obtained from following the development of solution (5.85) when the correction term is discarded in expression (5.84) for $V'_m(0,t)$ and $\Delta\tau \to 0$ is taken to eliminate the $\frac{\Delta\tau}{2C_m} \sum_i g'_i(0,t)$ term in the denominator of the remaining term[2]. Solution (5.99) is the expression used to obtain the EPSP transmembrane potential response in this section.

Figure 5.5 presents the transmembrane potential time response at $z = 0$. Also illustrated is the time course of the sodium conductance perturbation that is the source of this response. The depolarization of the cell membrane is due to an influx of Na^+ ions during the conductance change. Because of the time required to charge the membrane capacitance C_m, the potential change lags behind this current influx giving the V_m peak some 0.2 msec after the time of maximum conductance change ($T_p = 0.2$ msec). Although the conductance perturbation is essentially zero by $t = 1.5$ msec, the return of V_m to the resting potential (-60 mV) is far slower. This reflects the time required for the membrane capacitance to discharge through the low conductivity that the membrane presents to ionic current flow. The R-C time constant for this fiber as given by the core-conductor model for passive events is 5 msec, which agrees fairly well with the decay rate of this response.

---

[1] The trapezoidal integration was applied to the integral in this term, giving the correction term in solution (5.84).

[2] This expresses the fact that the trapezoidal-rule integration yields the exact result for $\Delta\tau \to 0$.

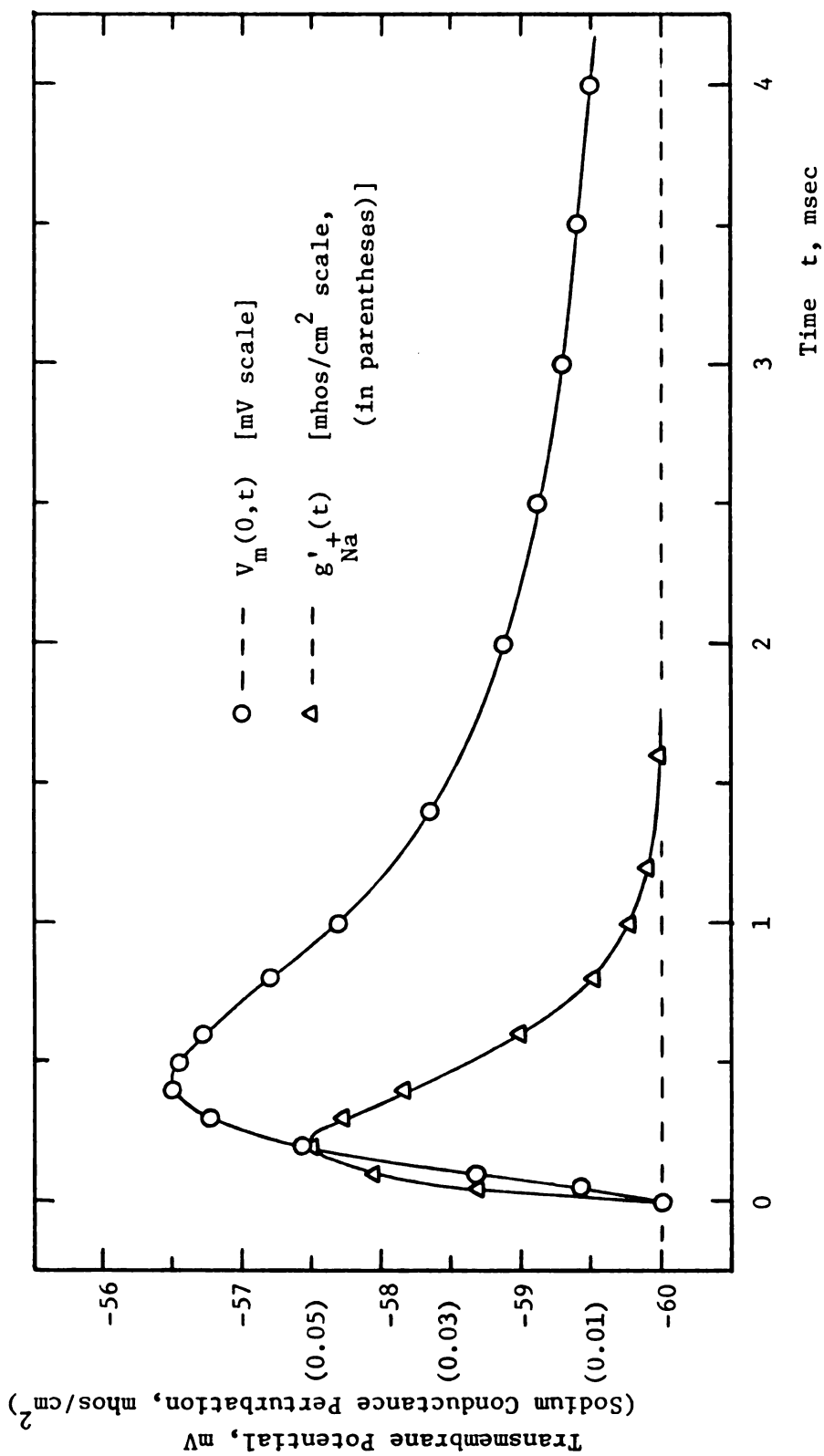

FIGURE 5.5

Conductance Change and Time Response of Transmembrane Potential at z = 0 for EPSP Simulation

The time course of $V_m(0,t)$ is quite different in this case than for the passive response to a pulse, reflecting the considerably different time-dependence of the source. Overall the response magnitude and shape agrees well with experimentally observed EPSP's (see Eccles [18], Katz [40], or Smith, Wuerker, and Frank [73]).

The spread of this response axially down the fiber is illustrated in Figure 5.6. The primary characteristic to be noted is the increasing delay in the start of the response. Also, the axial decay and dispersion of the charge that decreases the response magnitude and broadens the peak are clearly observed. Comparing Figures (5.5) and (5.6) with the steady-state response to a maintained sodium conductance change of the same magnitude (0.05 mhos/cm^2) as presented in Figure 5.3 shows that the axial decay is similar near the time of the $V_m(0,t)$ peak, but the time case never reaches the magnitude of the steady-state situation. This simply reflects the fact that the conductance perturbation (and thus the Na^+ ion influx) occurs in a time period far shorter than the time necessary to charge the membrane capacitance.

Figure 5.7 presents an alternate view of the response. When plotted vs. axial distance z, the time-delay in the spread of the depolarization down the fiber is clearly discerned. Note that while V_m has begun to return to the resting potential near the point of synapse (z = 0), the membrane near z = 1 mm is still experiencing an increasing depolarization. Since any given neuron receives synaptic input from many locations, the time delays and axial decay noted in this response become important

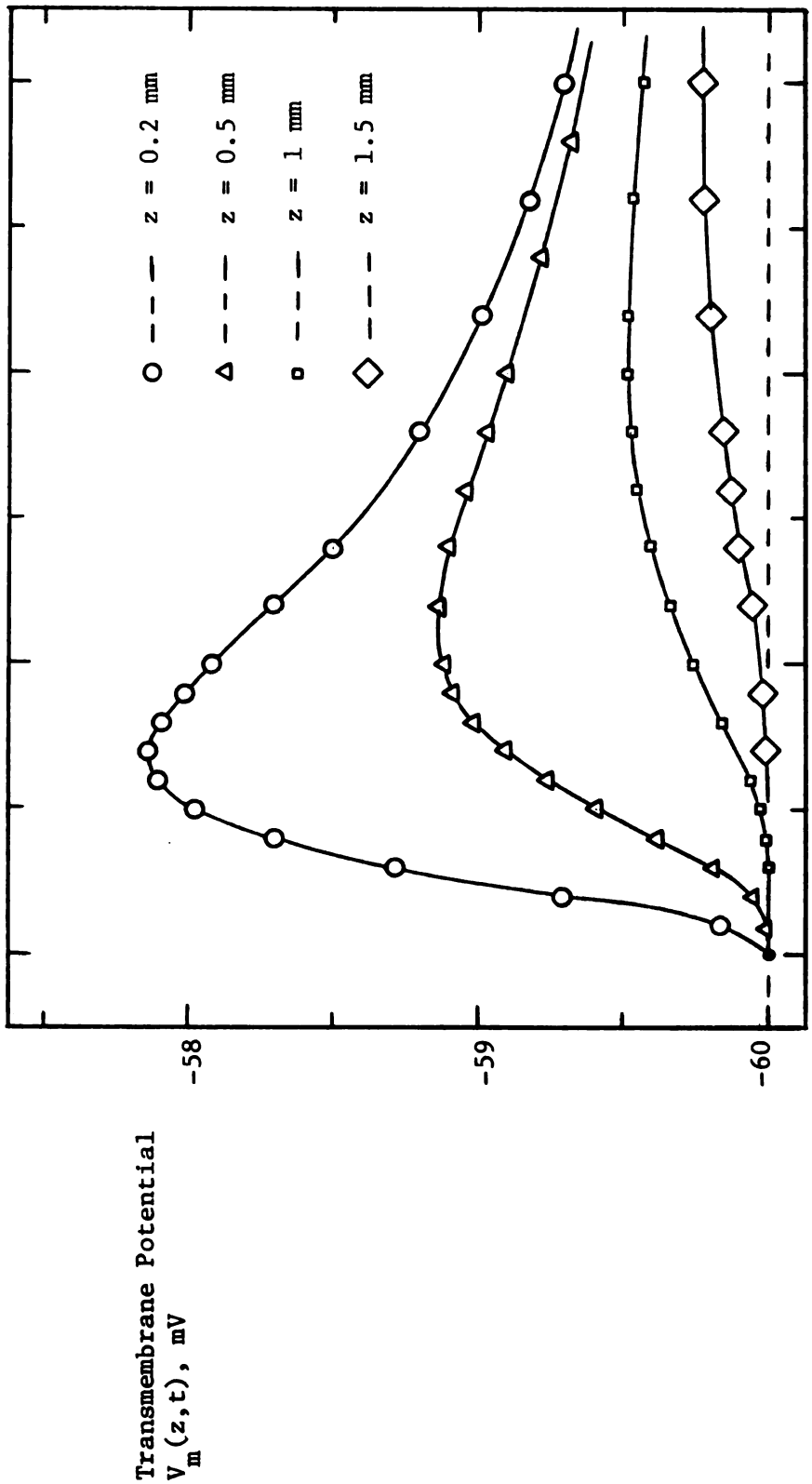

FIGURE 5.6

Transmembrane Potential Time Response at Various Axial Distances, EPSP Simulation

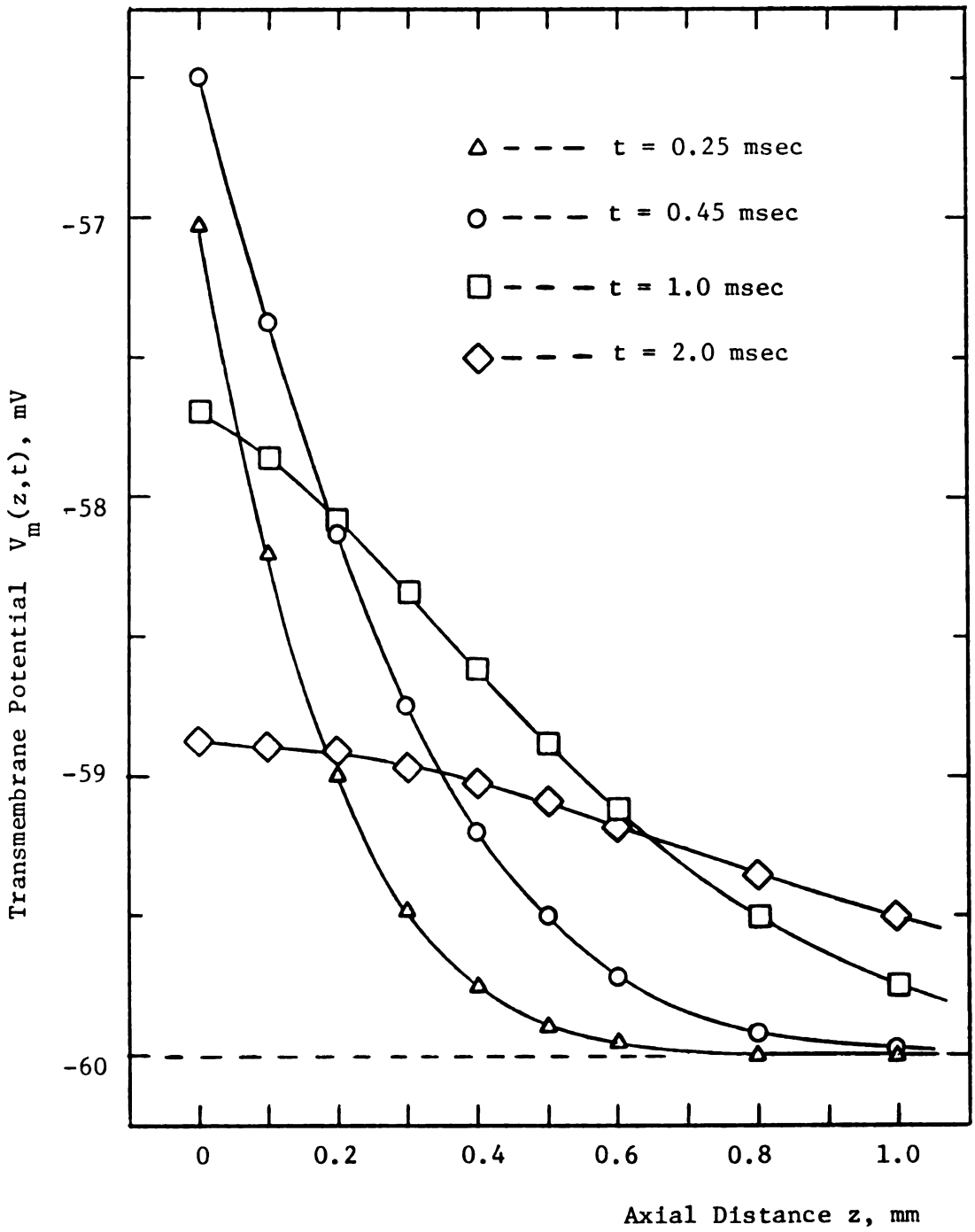

FIGURE 5.7

Transmembrane Potential Axial Response at Various Time Points, EPSP Simulation

in determining the net transmembrane potential response that would occur at the point of action potential generation (the axon hillock) from the time and spatial summation of many synapses.[1]

An effect that is not seen in the EPSP response presented here is the non-linearity to changes in g'_{Na^+} noted in Section 5.3.1. This is due to dropping the correction term from perturbations in transmembrane potential in the source term $S(k,s)$. As discussed previously, for a single EPSP this term is unimportant. For multiple synapses occurring in a time span where their responses would add, a point would be reached where the correction term would be necessary to predict the response accurately. Since for many bioelectric phenomena[2] V'_m is large enough with respect to $V^e_i - V_r$ to require the full solution of Section 5.2.4 to be used, the next section presents an example of this calculation in the simulation of an inhibitory postsynaptic potential.

5.3.3. Simulation of Inhibitory Postsynaptic Potentials; A Case Requiring the V'_m Correction Term

If the action at a synapse of the transmitter substance is to increase the postsynaptic membrane's conductivity to potassium ions, the transmembrane potential moves toward the Nernst potential for K^+. Since the potassium Nernst potential is normally more negative than the resting potential, the result is a hyperpolarization

---

[1] See Rall [63], [64].

[2] For example, multiple synapses where V_m approaches threshold, the action potential, and any conductance changes for ion species where $V^e_i - V_r$ is small.

of the cell membrane. This event is referred to as an inhibitory postsynaptic potential, since the response moves the transmembrane potential away from threshold. This section uses the solutions of Section 5.2.4 to model an IPSP.

The parameters used for the numerical example presented here are identical to those for the EPSP simulation in the previous section. The single exception is that now it is assumed that only the membrane conductance to potassium ions increases from its resting value. The additional parameters of g'_{K^+} and V_{K^+} are thus needed. V_{K^+} (the potassium Nernst potential) is taken as -95 mV (representative value from Katz [40]). This yields the difference $V_{K^+} - V_r$ as $-95 - (-60) = -35$ mV, a factor about three times smaller than the similar factor in the EPSP simulation's source term of $V_{Na^+} - V_r = 115$ mV. To keep the magnitude of the response about the same, $g'_{K^+} = 0.2$ mhos/cm^2 was chosen (four times larger than g'_{Na^+} for the EPSP response)[1].

With the parameters as listed above, it is apparent that the so-called "correction term" in solutions (5.84) and (5.85) for transmembrane potential is now far more important than it was for the EPSP case. Paralleling the argument of the previous section; with $V_{K^+} - V_r = -35$ mV, a change in transmembrane potential of $V'_m \doteq 4$ mV will now alter the $[V_{K^+} - V_m]$ factor in the source term $S(k,s)$ (relation (5.76)) by about 12%. Since 12% of 4 mV is on the order of 0.5 mV, this could result in as much as a 12%

---

[1] This value is still in the physiological range, see Eccles [18].

error in the response if the correction term containing V'_m is discarded (as compared to a 3% error in the EPSP case). To eliminate this error, the full solutions are used to obtain the response presented in this section. This also serves to illustrate the application of the technique to neural events where the correction term is even more essential.

The same assumptions and time-course for the conductance perturbation that were used in the previous section are applied to this case. Thus expression (5.98) for the convolution integral may be used by replacing g'_{Na^+} and V_{Na^+} with g'_{K^+} and V_{K^+} respectively. With these definitions substituted into solution (5.84), the transmembrane potential perturbation at $z = 0$ is obtained for the IPSP model as

$$V'_m(0,t) = \frac{[V_{K^+} - V_r]e^1}{2\pi C_m T_p} \int_{-\infty}^{\infty} \bar{g}'_{K^+}(k)\{\frac{e^{-t/T_p}[(P(k) - 1/T_p)t - 1] + e^{-P(k)t}}{(P(k) - 1/T_p)^2}\} dk$$

$$- \frac{\Delta\tau}{2\pi C_m} \frac{\int_{-\infty}^{\infty} \sum_{n=1}^{N-1} \bar{g}'_{K^+}(k, n\Delta\tau)V'_m(0,n\Delta\tau)e^{-P(k)[t-n\Delta\tau]}dk}{1 + \frac{\Delta\tau}{2C_m} g'_{K^+}(0,t)}, \qquad (5.100)$$

where $\bar{g}'_{K^+}(k) = g'_{K^+} \frac{2 \sin(k\, w/2)}{k}$ (following the definition of $\bar{g}'_{Na^+}(k)$ in Section 5.3.2). The factors $\bar{g}'_{K^+}(k,n\Delta\tau)$ and $g'_{K^+}(0,t)$ are defined by $\bar{g}'_{K^+}(k)f(n\Delta\tau)$ and $g'_{K^+}f(t)$ with $f(t) = t/T_p e^{(1-t/T_p)}$ being the conductance perturbation time-dependence. Note that the $\frac{\Delta\tau}{2C_m} g'_{K^+}(0,t)$ term has been dropped from the denominator of the first term in obtaining solution (5.100) from expression (5.84).

It was discovered (by numerical calculation) the solution converged for a much larger value of $\Delta\tau$ without that denominator term. As noted in the last section, when $\Delta\tau \to 0$ (and the trapezoidal rule integration becomes exact) that particular term vanishes in the denominator of the first term in solution (5.84). Thus as $\Delta\tau$ is taken very small, it may be discarded for convenience in the first term of the solution. This is not the case for the denominator of the second term in the solution, as there is also a $\Delta\tau$ factor in the numerator[1].

The time of the conductance perturbation peak was chosen as $T_p = 0.2$ msec, the same as for the EPSP simulation. By the graph of $g'_{Na^+}(t)$ in Figure 5.5, it is apparent that the conductance perturbation is effectively zero after 1.5 msec (as $g'_{K^+}(t)$ has the same time course). Setting $g'_{K^+}(t) = 0$ for $t > 1.5$ msec, the trapezoidal rule integration in the second term of solution (5.100) has at most $1.5/\Delta\tau$ terms in its summation, since any n larger than $1.5/\Delta\tau$ yields a time greater than 1.5 msec in $\bar{g}'_{K^+}(k,n\Delta\tau)$. This sets an upper bound on the number of sequential time steps $t = n\Delta\tau$ that must be calculated to obtain the response.

The IPSP response was obtained as follows. First $V'_m(0, n\Delta\tau)$ was calculated from expression (5.100), yielding some 600 values for $\Delta\tau = 0.025$ msec ($1.5/0.025 = 600$). For any time

---

[1] By making this alteration in the solution, convergence was obtained with $\Delta\tau = 0.025$ msec. With the $\Delta\tau/2C_m\, g'_{K^+}(0,t)$ term present in the first term's denominator, $\Delta\tau = 0.005$ msec was required.

greater than 1.5 msec, $V_m'(0,t)$ was found from the same expression by using all 600 previously calculated values in the second term. At axial points $z \neq 0$, the transmembrane potential was obtained by means of solution (5.85), that for this example becomes

$$V_m(z,t) = V_r + \frac{[V_{K^+} - V_r]e^1}{2\pi C_m T_p} \int_{-\infty}^{\infty} \bar{g}'_{K^+}(k) \left\{\frac{e^{-t/T_p}[(P(k)-1/T_p)t-1]+e^{-P(k)t}}{(P(k) - 1/T_p)^2}\right\} e^{jkz} dk$$

$$- \frac{\Delta\tau}{4\pi C_m} \int_{-\infty}^{\infty} [\bar{g}'_{K^+}(k,t)V_m'(0,t)$$

$$+ 2 \sum_{n=1}^{N-1} \bar{g}'_{K^+}(k,n\Delta\tau)V_m'(0,n\Delta\tau)e^{-P(k)(t-n\Delta\tau)}]e^{jkz} dk \ . \qquad (5.101)$$

The calculation of the 600 consecutive time points for $V_m'(0,t)$ was expensive in terms of computer time, but once these values were obtained the rest of the response was inexpensive and simple to obtain.

The response at $z = 0$ is illustrated in Figure 5.8. The transmembrane potential as obtained from the full solution is plotted with a solid line. For comparison purposes, the response that is obtained without the correction term (the second term in relation (5.100)) is also included as a dashed line. Note that at the point of maximum hyperpolarization, the two curves differ by an amount in the range of the expected 0.5 mV (12%). The apparent effect of the correction term is to decrease the magnitude of the response (since the source term decreases as V_m

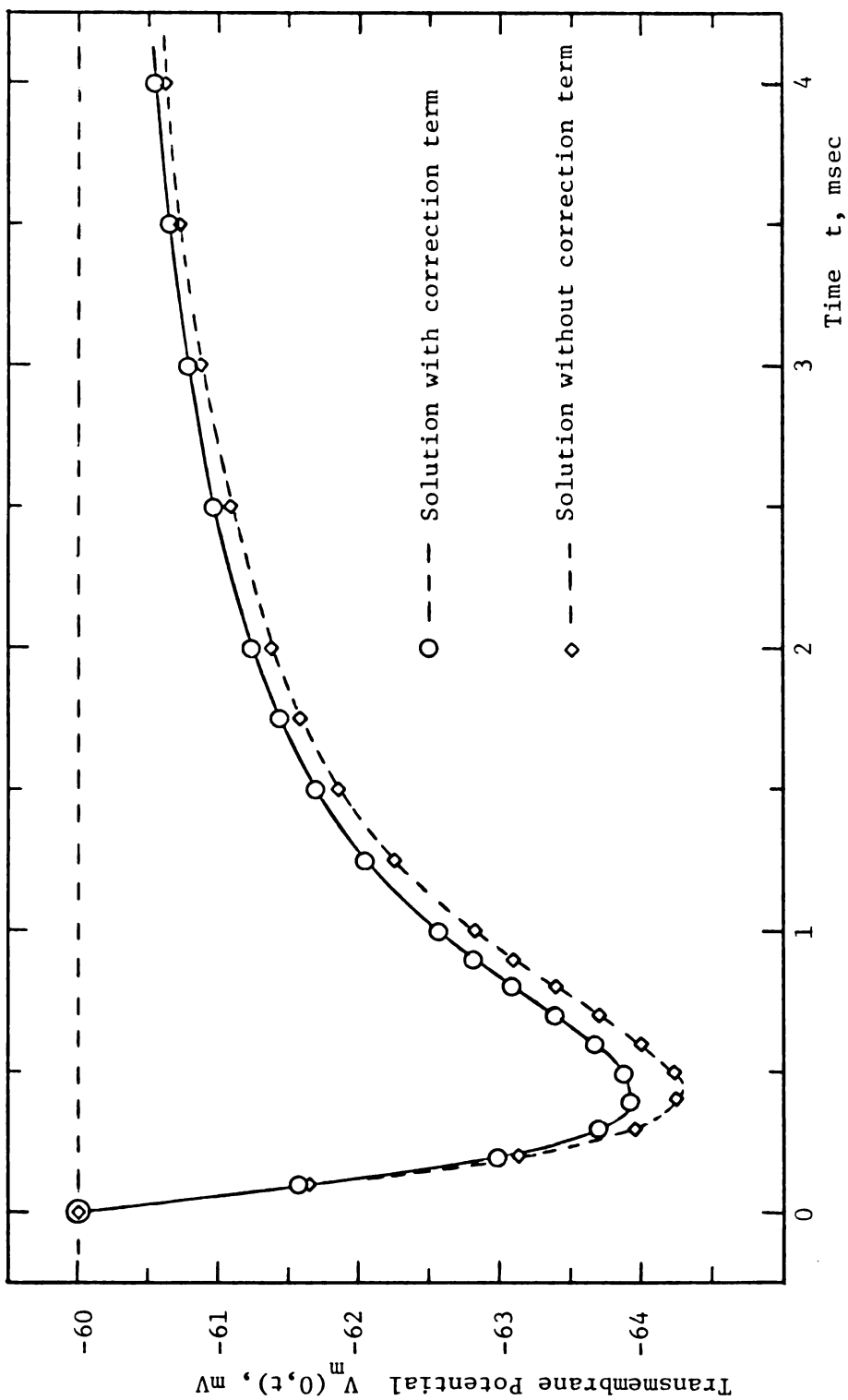

FIGURE 5.8

Transmembrane Potential Time Response at z = 0, IPSP Simulation

approaches V_{K^+}) and there is a slight shift in the time of maximum hyperpolarization.

The time response at other axial distances is indicated in Figure 5.9. Overall, the response is essentially similar to the EPSP case except the perturbation in transmembrane potential is inverted (as expected since the "driving potential" $V_{K^+} - V_r$ is now negative as opposed to positive for $V_{Na^+} - V_r$ in the EPSP simulation). The physical basis for the hyperpolarization that is evident in the IPSP response is an efflux of K^+ ions from the intracellular space at the synapse during the conductance perturbation. The duration and axial extent of the response are about the same as for the EPSP case, and the discussion in the previous section on the role of capacitive effects applies here. Figure 5.10 is a plot of the axial response at various time points and also similar (though inverted) to the graph in Figure 5.7 of the EPSP axial response. The IPSP response obtained by this simulation resembles experimentally observed IPSP's as given in Eccles [18], Katz [40], or Plonsey [60]. The greatest difference between this simulation and the EPSP response of the previous section is that, with the inclusion of the correction term, the IPSP response is non-linear to changes in g'_{K^+} and for $g'_{K^+} \to \infty$ has a maximum hyperpolarization of $V_m(0,t) = V_{K^+}$.

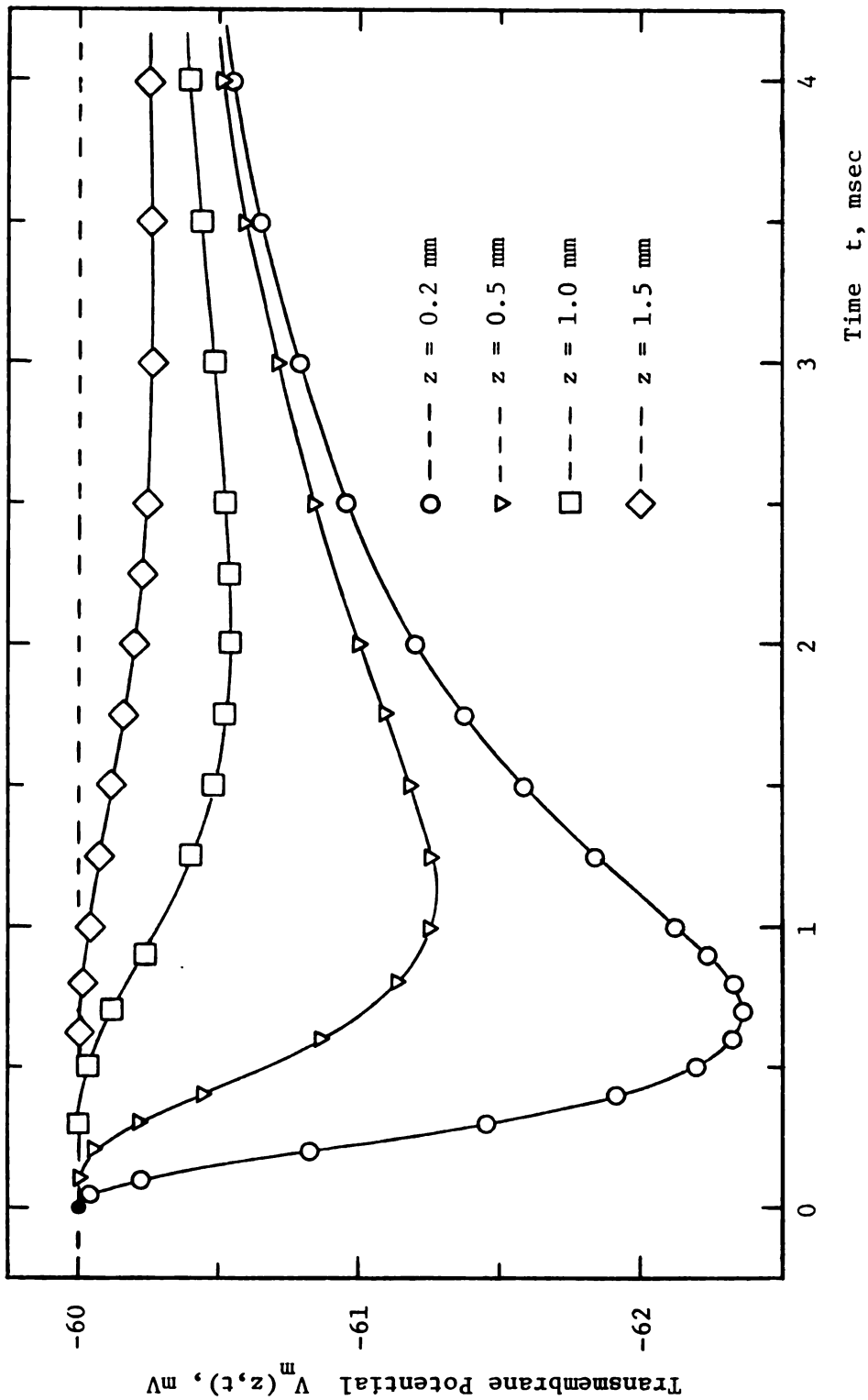

FIGURE 5.9

Transmembrane Potential Time Response at Various Axial Distances, IPSP Simulation

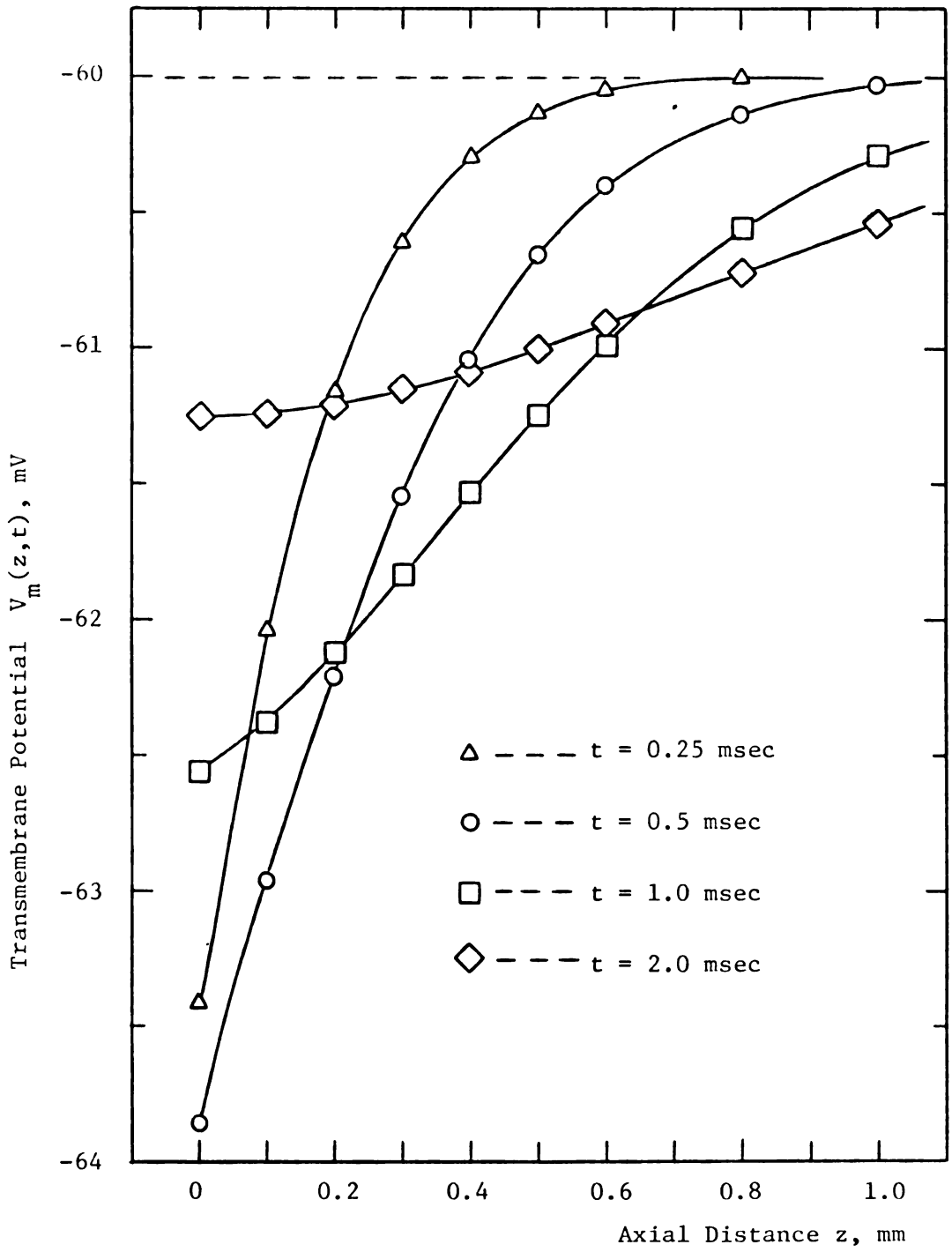

FIGURE 5.10

Transmembrane Potential Axial Response at Various Time Points, IPSP Simulation

CHAPTER 6

SUMMARY, CONCLUSIONS, AND RECOMMENDATIONS FOR FURTHER STUDY

6.1. Summary and Conclusions

The observations and conclusions of this research report are best summarized by considering the material in each of the major chapters (2 through 5) in order. Chapter 2 was primarily concerned with the development of a general set of volume-conductor equations and boundary conditions that apply to any bioelectric field problem. In Section 2.1.2, the possibility of an ion-acoustic wave being excited in a nerve axon during the action potential was considered and rejected. The fact that collisional damping forces overwhelm relaxation effects was demonstrated in this ion-acoustic phenomena exploration. In the last section of Chapter 2, a "constant field" derivation was carried out in cylindrical coordinates. The conclusions reached were that the Goldman equation for the resting transmembrane potential has the identical form in either cylindrical or rectangular coordinates and that the fields and individual ionic current densities in the membrane reduce to the rectangular coordinate system results when the membrane thickness is insignificant with respect to the fiber radius.

Chapter 3 solved for and examined the steady-state passive response of a cylindrical cell in three volume-conductor compartments

for an impressed stimulus delivered by a metallic ring electrode. The Fourier transform solution allowed these electrodes to be modeled as finite-sized structures, eliminating a singularity found in previous solutions. For the case of an intracellular stimulus, it was shown that the transmembrane potential response away from the electrode was well predicted by the cable equation from core-conductor theory. Near the electrode, the response of the two models differed, with the field solution being correctly dependent upon the width of the electrode. Also demonstrated was the fact that the cable equation incorrectly predicts the axial decay of the extracellular potential at the membrane. According to the core-conductor model, $\Phi_E(a,z)$ decays exponentially with the same length constant λ that describes transmembrane potential perturbation decay. The model in this report indicated that $\Phi_E(a,z)$ had a significantly slower decay rate than $V_m'(z)$, leading to the conclusion that the length constant can only be correctly determined by means of intracellular recording electrodes and not by extracellular measurements as indicated by core-conductor theory (see Plonsey [60]).

For the case of an extracellular stimulus, the response was found to be totally at odds with the cable equation prediction. The response to a current injected into the system at the external membrane surface was a hyperpolarization near the electrode and a slight depolarization a short axial distance away. This response was far smaller in magnitude than for an intracellular stimulus of the same strength. The point where $V_m' = 0$ was found to be a linear function of $\sqrt{a}$ and λ (a = fiber radius, λ = cable theory length constant). An examination of the radial variation in

potential demonstrated the flaw in core-conductor theory to be the assumption of only axially directed currents in the extracellular medium, supporting the conclusion of Clark and Plonsey [8].

The final section in Chapter 3 showed that the axial current density within the membrane was insignificant compared to radial currents. A solution and direct numerical calculation of membrane capacitance and surface charge density on the membrane interfaces demonstrated that the relations $C_m = \varepsilon_M/d$ and $\eta_I = -\eta_E$ were valid. This supported the assumptions necessary in Section 2.2.2 in the development of transmembrane boundary conditions that allow the field problem to be reduced to two volume-conductor regions (the intracellular and extracellular).

In Chapter 4, the three-region solutions of Chapter 3 were extended to cover the passive response to impressed time-dependent stimulating currents. The same conclusions (of the intracellular stimulus giving a transmembrane potential response similar to that predicted by the cable equation and an extracellular stimulus yielding a response not at all predicted by core-conductor theory) were again demonstrated for the time-dependent response. This model also had the observed (but not predicted in cable-equation solutions) phenomena known as the stimulus artifact as part of its response. An impulse stimulus (delta function in time) was shown to produce a singularity at $t = 0$, and demonstrated that although delta functions simplify many solutions (as carried out by previous authors), they give rise to responses that do not simulate observable neural phenomena very accurately. The final section in Chapter 4

examined a simulation of the myelinated axon using the three-region field model of this report. The result suggests that the myelin sheath blocks action potential generation by a voltage-divider effect that prevents the excitable neural membrane from reaching threshold. This explanation of the effect of the myelin sheath is somewhat different than the view that the myelin prevents ions in the extracellular medium from reaching the axonal membrane.

Chapter 5 presented a reduced, two-compartment model for the fields and current in the intracellular and extracellular regions. For the case of the passive response to subthreshold impressed stimuli, this reduced model gave the same results as the interior and exterior portions of the solutions in Chapters 3 and 4. The inherently simpler form of the two-compartment model makes it the logical form to utilize if only the intracellular and/or extracellular fields and currents are desired. Chapter 5 also extended the solution to cover ion-selective perturbations in membrane conductance, allowing the modeling of active neural phenomena. The solution required the conductance change to be confined to a narrow region such that the transmembrane potential was essentially constant across that region. The source current in this latter case was the movement of ions of one or more specific species through the membrane, driven by the difference between their Nernst potential and the transmembrane potential. This gave a non-linear response to changes in the magnitude of the conductance perturbation, with the response (for the case of the involvement of a single ion species) being limited by $V_m = V_i^e$ where the driving

force goes to zero. The same non-linearity also applied to changing the amount of area involved in a given conductance perturbation.

Section 5.3.2 presented a simulation of an EPSP and demonstrated that when $V_i^e - V_r$ is large with respect to the perturbation in transmembrane potential[1], the correction term in the source term $S(k,t)$ that is responsible for non-linearity of the response can be discarded. This greatly simplifies the numerical calculations. The last section in Chapter 5 was a IPSP simulation, where the full solution (with the correction term) was required to obtain the response accurately. These PSP simulations showed that the field model of this report can be used to find the two-dimensional response (in terms of potentials, fields, and currents) of active as well as passive neural events. The criterion for inclusion of the correction term also gives a measure of the importance of the nonlinear portion of the response due to a specified conductance change.

Looking at the report as a whole, it is apparent that the Fourier transform provides a powerful technique for obtaining solutions for bioelectric field problems. By use of the digital computer, complex Fourier domain solutions are easily invertable, eliminating the need for many simplifying assumptions to obtain an analytical result. The solutions presented in this dissertation have a multitude of response characteristics not found in previous

---

[1] This is checked by calculating the response <u>without</u> the correction term as the effect of the correction term is to reduce the magnitude of the response as V_m varies from V_r.

models. These effects include the accurate response to an extracellular stimulating electrode, stimulus artifacts, and the dependence of response upon the physical size of electrodes or conductance perturbation regions. Singularities due to unrealistic infinitely narrow or brief stimuli have been eliminated. The solutions can yield the potential, electric field, or current density at any point in the system; not just the transmembrane potential. Finally, one expects the response of the class of models in this report would be more accurate than the cable equation solutions since the present solutions are mathematical descriptions of a system very similar to real neural structures.

6.2. Recommendations for Future Research

Perhaps one of the greatest strengths of the neural model presented in this report is that the possibilities for further study are nearly limitless. A few recommendations are offered by the present author as suggestions for future work; mostly they concern extensions of the model of Chapter 5.

The steady-state axially-dependent membrane conductance solution of Section 5.2.3 could be altered for a very accurate simulation of a myelinated axon. By the Fourier space-shifting theorem, a series of conductance windows of 1μ width and 1 mm apart could be included in a "thick" membrane representing the myelin sheath. The response to a stimulus at one node could then be evaluated for the entire fiber.

Another possibility would be to use the solutions in Sections 5.2.3 and 5.2.4 to conduct an examination into the effects

of varying such parameters as synaptic area, resting state conductance, internal or external conductivity, etc. upon the transmembrane potential response of an ion-selective conductance perturbation (as occurs in a synapse or action potential).

A final suggestion would be to explore the possibility of using such membrane conductance functions as derived by Hodgkin and Huxley [37] to simulate action potentials with this model. Since these conductances are intrinsic functions of V_m, it would require further development of the numerical techniques used in the handling of the convolution integrals containing $\bar{g}_i'(k,t)$. A possibility here would be to apply an adaptive integration routine in place of the trapezoidal-rule integration, perhaps using a Simpson's-rule algorithm. This would reduce the amount of numerical calculation required to obtain convergence of the solutions. A preliminary investigation along these lines was started by the present author that looked very promising, but lack of time forced its termination. If a general and efficient technique for finding the solution for any conductance perturbation function could be developed, then the model in this report could be used to evaluate various theoretical membrane descriptions for comparison of their response to experimental evidence.

APPENDICES

APPENDIX A

LIST OF SYMBOLS AND NOTATION

This appendix defines and describes the major symbols and notations used throughout the report. Symbols used only where defined are omitted. For example, the solution coefficients (i.e. A(k,s), P(k), $\alpha(k)$, etc.) are local to each chapter and are not included in this list. On rare occasions, duplicate notation has been used, but only where totally unavoidable and in separate sections of the text where their meaning is unambiguous (the primary usage is given here). Subscript and superscript conventions are listed separately at the end, but they are also used in the main list when necessary to differentiate between symbols or where that symbol only appears with the indicated subscript or superscript.

$\vec{A}$	vector potential (webers/m)
a	outer radius of membrane cylinder (m)
$\vec{B}$	magnetic induction (webers/m^2)
b	inner radius of membrane cylinder (m)
C_i	concentration of the ith ion species (moles/m^3)
C_m	membrane capacitance/unit area (farads/m^2)
d	membrane thickness, d = a - b (m)
$\vec{E}$	electric field strength (volts/m)

E_r, E_z	electric field component, subscript specifies associated direction (volts/m)
e	absolute value of electronic charge (1.6×10^{-19} coulombs) (Also used as symbol for exponential function, differentiated from above by exponent.)
F	Faraday's constant (9.65×10^{4} coulombs/mole)
g	conductivity (defined only for membrane, mhos/m^2)
I^s	total source current to electrode (amps)
$\vec{J}$	current density (amps/m^2)
J_r, J_z	current density component, subscript identifies associated direction (amps/m^2)
J^s	source current density (amps/m^2)
j	$\sqrt{-1}$
k	Boltzmann's constant, used in Chapter 2 (1.38×10^{-23} joules/°K)
k	Fourier transform domain variable, used in Chapters 3, 4, and 5 (1/m)
L	Avogadro's number (6.02×10^{23} particles/mole)
m_i	effective mass of the ith ion species (kg)
$\hat{n}$	unit vector normal to boundary surface
n_i	number density of the ith ion species (ions/m^3)
P_i	permeability coefficient of the ith ion species (m/sec)
q_i	effective charge of the ith ion species (coulombs)
R	gas constant (8.31 joules/mole - °K)
R_i, R_o, R_m	cable equation distributed resistances, defined in Appendix D
$\vec{r}$	position vector, any coordinate system
$\hat{r}$	unit vector in radial direction, cylindrical coordinates
r	radial variable, cylindrical coordinates (m)
s	Laplace transform domain variable (1/sec)
T	temperature (°K)

T_o pulse function duration (sec)

T_p time of conductance perturbation peak (sec)

t time variable (sec)

u_i electric mobility of the ith ion species (m^2/volt-sec)

V_i^e Nernst potential of the ith ion species (volts)
Note: when i is specified, e superscript is dropped (eg. V_{Na^+})

V_m transmembrane potential, $V_m = \Phi_I(r = b) - \Phi_E(r = a)$ (volts)

V_r resting transmembrane potential (volts)

$\vec{v}_i$ average velocity of the ith ion species (m/sec)

v_{it} ion thermal velocity (m/sec)

w width of electrode or conductance change region (m)

$\hat{z}$ unit vector in axial direction, cylindrical coordinates

z axial variable, cylindrical coordinates (m)

z_i valence of ith ion species (signed)

β_i partition coefficient (unitless)

ε permittivity of the medium (farads/m)

ε_o permittivity of free space (8.854×10^{-12} farads/m)

η surface charge density (coulombs/m^2)

λ length constant, axial distance for e^{-1} decay (m)

μ magnetic permeability of the medium (henrys/m)

μ_o magnetic permeability of free space ($4\pi \times 10^{-7}$ henrys/m)

ν_i effective collision frequency of the ith ion species (1/sec)

ρ volume charge density (coulombs/m)

σ conductivity of the medium (mhos/m)

τ	time constant, e^{-1} decay or decrease of 84% in core-conductor model (sec)
$\hat{\tau}$	unit vector tangential to boundary surface
Φ	electric scalar potential (volts)
ϕ	angular variable, cylindrical coordinates (radians)
ω_{ip}	ion resonance frequency of the ith ion species (1/sec)

Subscripts

E	quantity defined for extracellular region
I	quantity defined for intracellular region
i	signifies ith ion species
M	quantity defined interior to membrane
m	used to denote quantities defined across the membrane (eg. V_m, transmembrane potential; C_m, membrane capacitance/unit area)
o	denotes resting-state value of quantity
r	radial component of a vector in cylindrical coordinates (exception: also used to denote resting potential (V_r) and resting state value of total membrane conductance (g_r))
s	source quantity (eg. ρ_s, impressed charge density)
z	axial component of a vector in cylindrical coordinates

Superscripts

e	denotes impressed field quantity (eg. V_i^e, Nernst potential)
s	used to signify currents and current densities supplied by an electrode
'	denotes perturbation from resting-state value (eg. $V_m' = V_m - V_r$)
*	denotes quantities defined from application of a mean value theorem

$\hat{}$ denotes unit vector

$\rightarrow$ denotes vector

$\bar{}$ signifies functions that are Fourier or Laplace transformed physical quantities (eg. $\bar{\Phi}(k,s)$, $\bar{V}'_m(k)$)
Note: transform specified by functional argument (k and/or s).

APPENDIX B

MATHEMATICAL DETAILS, CONVERGENCE, AND ERROR ESTIMATION

B.1. Axial Symmetry

It is apparent on physical grounds that if the source functions in the system are symmetric about $z = 0$, then the scalar potentials share the same symmetry. The Fourier-domain solutions will then also be symmetric about $k = 0$, as can be demonstrated by considering the transform definition (3.31). Taking $k = -k$ obtains exactly the same function $\bar{F}(k)$ when $F(x) = F(-x)$ (use the substitution $\tilde{x} = -x$ in the transform integral). Thus axially symmetric sources yield potential functions in k-space that are even functions of k.

With $\bar{\Phi}(r,k,t)$ being an even function of k, the inversion integral reduces to just

$$\Phi(r,z,t) = \frac{1}{\pi} \int_0^\infty \bar{\Phi}(r,k,t)\cos(kz)dk \qquad (B.1)$$

as noted in Section 3.3.1. If $\bar{\Phi}$ is not an even function of k, then it can be expressed as the sum of an even and an odd function; where the even function is real and the odd function is pure imaginary. The inversion integral may then be written as the difference of two integrals:

$$\Phi(r,z,t) = \frac{1}{\pi}\int_0^\infty \mathrm{Re}\{\bar{\Phi}(r,k,t)\}\cos(kz)\,dk$$

$$- \frac{1}{\pi}\int_0^\infty \mathrm{Im}\{\bar{\Phi}(r,k,t)\}\sin(kz)\,dk \ . \qquad (B.2)$$

This form is obtained from the application of Euler's formula for e^{jkz} and noting that since Φ must be real, then $\mathrm{Im}\{\bar{\Phi}\}$ must be an odd function of k. Thus for the case of a non-axially symmetric stimulus, the Fourier inverse may still be obtained without the use of complex numbers in the computer routines. The same discussion applies to the electric field and current density, with the exception that E_z and J_z for symmetric stimuli are pure imaginary and odd functions of k. Then (for E_z and J_z) the kernel in integral (B.1) is $j\sin(kz)$ (relation (B.2) is correct in any case). These general properties may also be observed to hold for each Fourier-domain solution given in this report by direct consideration of the symmetry properties of the functions they contain.

B.2. Considerations Near $k = 0$

The Fourier-domain solutions of this report commonly contain the modified Bessel functions $I_o(x)$ and $I_1(x)$ which diverge to $+\infty$ as $x \to 0$. This causes numerical problems in the computer routines when trying to evaluate the inversion integral near $k = 0$. To avoid these difficulties, the lower integration limit is taken as a small number δ rather than 0 in relation (B.1). Choosing δ small enough results in negligible error from discarding the contribution between 0 and δ, as can be shown by considering the asymptotic forms of the solutions as $k \to 0$.

From Abramowitz and Stegun [1], the asymptotic forms of the modified Bessel functions involved are[1]

$$\left.\begin{aligned} I_o(x) &\sim 1 \\ I_1(x) &\sim x/2 \\ K_o(x) &\sim -\ell n(x) \\ K_1(x) &\sim 1/x \end{aligned}\right\} \quad \text{as} \quad x \to 0 \; . \tag{B.3}$$

Substituting these into the steady-state solutions for Fourier-domain potential from Chapter 3 and taking the limit as $k \to 0$ leads to

$$\bar{\Phi}_I(r,k \to 0) \sim \frac{-\ell n(ka)}{2\pi\sigma_E} (I_E^s + I_I^s) + \frac{\ell n(a/b)}{2\pi\sigma_M} I_I^s \tag{B.4}$$

$$\bar{\Phi}_M(r,k \to 0) \sim \frac{-\ell n(ka)}{2\pi\sigma_E} (I_E^s + I_I^s) + \frac{\ell n(a/r)}{2\pi\sigma_M} I_I^s \tag{B.5}$$

$$\bar{\Phi}_E(r,k \to 0) \sim \frac{-\ell n(kr)}{2\pi\sigma_E} (I_E^s + I_I^s) \tag{B.6}$$

where $\lim_{x\to 0} x\ell n(cx) = 0$, $\lim_{x\to 0} \frac{\sin x}{x} = 1$, and the definitions (in Section 3.2.2) for $\bar{J}_I^s(k)$ and $\bar{J}_E^s(k)$ have been applied[2]. The behavior of $\bar{\Phi}_M$ is bracketed by $\bar{\Phi}_I$ and $\bar{\Phi}_E$, since in the membrane $b < r < a$. Also, the worst case for $\bar{\Phi}_E$ is $r = a$ since $\ell n(kr)$ diverges fastest as $k \to 0$ for that value of r of

---

[1] The symbol "~" represents "asymptotically equal to".

[2] The asymptotic forms are identical for either finite-width or delta function electrodes since in taking $\lim_{k\to 0}$, $\bar{J}_E^s(k) \sim I_E^s/2\pi a$ and $\bar{J}_I^s(k) \sim I_I^s/2\pi b$ for both classes of electrodes.

the allowed extracellular range of $r \geq a$. Thus with $r = a$ in relation (B.6), it is apparent that the desired error bound may be obtained from asymptotic form (B.4) alone.

The error bound is obtained by integrating the product of $\bar{\Phi}_I(r,k \to 0)$ and $\frac{\cos kz}{\pi}$ between the limits $k = 0$ and $k = \delta$. For $k \to 0$, $\cos kz \sim 1$, giving an upper bound on error as

$$\text{error} \leq \frac{1}{\pi} \int_o^\delta \left[\frac{-\ell n(ka)}{2\pi\sigma_E} (I_E^s + I_I^s) + \frac{\ell n(a/b)}{2\pi\sigma_M} I_I^s\right] dk$$

$$= \frac{1}{2\pi^2} \left[\frac{I_E^s + I_I^s}{\sigma_E} (\delta - \delta\, \ell n\delta) + \frac{I_I^s}{\sigma_M} \delta \ell n(a/b)\right] . \qquad (B.7)$$

For the parameters of the "test axon" (Appendix D), the standard stimulus intensity of $I^s = 10^{-5}$ amps, and $\delta = 10^{-9}$ (the value used for all numerical calculations in this report), the error from using δ as the lower integration limit in the Fourier inversion integral is obtained from relation (B.7) as

$$\text{error} \leq 1.4 \times 10^{-8} \text{ mV} .$$

Since 10^{-5} amps stimulus intensity gave a response in the mV range, an error of 10^{-8} mV is clearly negligible. This was also verified by trying values of δ in the range of 10^{-7} to 10^{-11} in the computer routines. The largest alteration produced was in the 9th significant figure of the numerical result.

The above conclusion that negligible error is introduced by discarding the contribution to the inversion integral between

0 and δ also holds for the time case in Chapter 4. The exponential terms are well behaved as $k \to 0$ and, in the solution for a step function stimulus, the non-exponential term is just the steady-state response discussed above. The same is true of the two-compartment solutions of Chapter 5, with the steady-state response giving exactly the same asymptotic forms as above. In calculating electric field or current density, the error introduced from using δ as the lower integration limit is even smaller since taking $\lim_{k\to 0}$ of their Fourier-domain solutions produces zero.

B.3. Consideration of Convergence; Errors from Truncation

To examine the question of the inversion integral's convergence to a finite value at its upper (infinite) limit, and the error introduced by truncating the infinite integration, requires consideration of the integrand's behavior as $k \to \infty$. The asymptotic forms of the Bessel functions for large argument are given by Abramowitz and Stegun [1] as

$$\left.\begin{aligned} I_o(x) \sim I_1(x) &\sim \frac{e^x}{\sqrt{2\pi x}} \\ K_o(x) \sim K_1(x) &\sim \sqrt{\frac{\pi}{2x}}\, e^{-x} \end{aligned}\right\} \quad \text{as} \quad x \to \infty \,. \tag{B.8}$$

Substituting these into the steady-state solutions of Chapter 3 and taking the limit as $k \to \infty$ obtains

$$\bar{\Phi}_I(r,k\to\infty) \sim \frac{2\sigma_M \bar{J}_E^s(k)}{k\sqrt{r/a}\,(\sigma_I+\sigma_M)(\sigma_E+\sigma_M)e^{kd}e^{k(b-r)}}$$

$$+\frac{\bar{J}_I^s(k)(\sigma_E+\sigma_M)}{k\sqrt{r/b}\,e^{k(b-r)}[(\sigma_I+\sigma_M)(\sigma_E+\sigma_M)-e^{-2kd}(\sigma_I-\sigma_M)(\sigma_E-\sigma_M)]}$$

$$0 \le r \le b \qquad \text{(B.9)}$$

$$\bar{\Phi}_E(r,k\to\infty) \sim \frac{\bar{J}_E^s(k)}{k\sqrt{r/a}\,(\sigma_E+\sigma_M)e^{k(r-a)}}$$

$$+\frac{2\sigma_M \bar{J}_I^s(k)}{k\sqrt{r/b}\,(\sigma_I+\sigma_M)(\sigma_E+\sigma_M)e^{kd}e^{k(r-a)}} \quad r \ge a \qquad \text{(B.10)}$$

where $\bar{\Phi}_M(r,k\to\infty)$ has its behavior bracketed by $\bar{\Phi}_I$ and $\bar{\Phi}_E$ given above. The "worst case" as defined by the slowest decay to zero is for $r = b$ in relation (B.9) and for $r = a$ in relation (B.10), giving

$$\bar{\Phi}_I(b,k\to\infty) \sim \frac{\bar{J}_I^s(k)}{k(\sigma_I+\sigma_M)} \qquad \text{(B.11)}$$

$$\bar{\Phi}_E(a,k\to\infty) \sim \frac{\bar{J}_E^s(k)}{k(\sigma_E+\sigma_M)} \qquad \text{(B.12)}$$

where only those terms having the most gradual decay have been retained.

First the case of a delta function electrode is considered. From Section 3.2.2, $\bar{J}_I^s(k)$ and $\bar{J}_E^s(k)$ are the constants J_I^s and

J_E^s for an infinitely narrow electrode. This gives the asymptotic k-dependence of the integrand in the inversion integral (B.1) for either an intracellular or extracellular stimulus as

$$\bar{\Phi}(k \to \infty) \sim G \frac{\cos(kz)}{k} \tag{B.13}$$

where G = constant. If $z \neq 0$ (ie., the location specified is not at the electrode) the inversion integral is clearly convergent, since

$$I = \lim_{u\to\infty} \int_c^u \frac{\cos(\alpha t)}{t}\, dt \qquad (c > 0) \tag{B.14}$$

has a finite limit[1]. If $z = 0$, this form reduces to

$$I = \lim_{u\to\infty} \int_c^u \frac{dt}{t}$$

$$= \lim_{u\to\infty} [\ell n u/c] \to \infty \tag{B.15}$$

which indicates that the delta function electrode response has a singularity at $z = 0$ in its scalar potential. Examination of asymptotic forms (B.11) and (B.12) reveals this singularity is at the location of the electrode for either an intracellular or extracellular stimulating electrode. In both cases the potential at

---

[1] Integral I (B.14) is just $-\alpha C_i(\alpha c)$ where $C_i(\cdot)$ is the cosine integral function (Abramowitz and Stegun [1]) which has a finite value for $\alpha c > 0$.

the electrode diverges to $+\infty$ and is finite elsewhere, confirming the results noted in Chapter 3 for a delta function stimulus.

For a finite-width electrode, the inversion integral yields a finite result for the potential at any point. Using the definitions of $\bar{J}_I^s(k)$ and $\bar{J}_E^s(k)$ from Section 3.2.2 for an electrode of width w in the asymptotic forms (B.11) and (B.12) leads to

$$\bar{\Phi}_I(b,k \to \infty) \sim \frac{I_I^s \sin(k\, w/2)}{k^2 w \pi b(\sigma_I + \sigma_M)} \tag{B.16}$$

$$\bar{\Phi}_E(a,k \to \infty) \sim \frac{I_E^s \sin(k\, w/2)}{k^2 w \pi a(\sigma_E + \sigma_M)} \tag{B.17}$$

where I^s is the total current to the electrode. Since $|\sin(k\, w/2)| \leq 1$, the integrand of the inversion integral (B.1) is bounded by

$$\bar{\Phi}(k \to \infty) \sim G \frac{\cos(kz)}{k^2} \tag{B.18}$$

where G = constant. Thus the inversion integral is clearly convergent, since

$$I = \lim_{u \to \infty} \int_c^u \frac{\cos(\alpha t)}{t^2}\, dt \qquad (c > 0) \tag{B.19}$$

has a finite limit for any value of α (see Olmsted [58])[1]. Thus

---

[1] At $z = 0$ the form is now $\lim_{u \to \infty} \int_c^u \frac{dt}{t^2}$ which is finite, unlike the similar integral (B.15) for the delta function electrode.

it is apparent that the inversion integral will converge to a finite result at any point (r,z) in the system.

These results also hold for the time-dependent case of Chapter 4 and the two-compartment solutions of Chapter 5 since the exponential functions contained in those Fourier-domain solutions have arguments that are negative decreasing functions of k. As $k \to \infty$, the exponentials decay to zero faster than any k^{-n} (Arfken [2]). A similar result holds for the solutions for $\vec{E}$ or $\vec{J}$. The conclusion is that with the single exception of the fields or currents at the location of an infinitely narrow electrode, all Fourier-domain solutions in this report yield a finite result when inverted back to the z-domain.

The asymptotic forms for $k \to \infty$ given above can be used to obtain an estimate of the error that results from truncating the infinite upper limit of the inversion integral. Assuming that the truncation point is high enough so that relations (B.16) and (B.17) for Fourier-domain potential as $k \to \infty$ are accurate, then the error for truncating the integration at $k = k_u$ is[1]

$$\text{error} \leq \frac{1}{\pi} \int_{k_u}^{\infty} \bar{\Phi}(k)\cos(kz)\,dk \qquad \text{(B.20)}$$

where $\bar{\Phi}(k)$ represents either $\bar{\Phi}_I(b,k \to \infty)$ or $\bar{\Phi}_E(a,k \to \infty)$. The integrand in (B.20) has the form $G\,\frac{\cos(kz)\sin(k\,w/2)}{k^2}$ where

---

[1] The discarded terms tend to decrease the magnitude of $\bar{\Phi}_I$ or $\bar{\Phi}_E$ from the value given by the asymptotic forms (B.16) or (B.17).

$$G = \begin{cases} \dfrac{I_I^s}{w\pi^2 b(\sigma_I + \sigma_M)} & \text{for } \bar{\Phi}_I \\ \dfrac{I_E^s}{w\pi^2 a(\sigma_E + \sigma_M)} & \text{for } \bar{\Phi}_E \ . \end{cases} \tag{B.21}$$

This integral may then be evaluated as follows:

$$I = G \int_{k_u}^{\infty} \frac{\cos(kz)\sin(k\, w/2)}{k^2}\, dk$$

$$= \frac{G}{2} \int_{k_u}^{\infty} \frac{\sin(k(w/2 + z)) + \sin(k(w/2 - z))}{k^2}\, dk$$

$$= \frac{G}{2} \left\{ (w/2 + z)^2 \left[\frac{\sin(k_u(w/2 + z))}{k_u(w/2 + z)} + \int_{k_u}^{\infty} \frac{\cos(k(w/2 + z))}{k(w/2 + z)}\, dk \right] \right.$$

$$\left. + (w/2 - z)^2 \left[\frac{\sin k_u(w/2 - z)}{k_u(w/2 - z)} + \int_{k_u}^{\infty} \frac{\cos(k(w/2 - z))}{k(w/2 - z)}\, dk \right] \right\}$$

$$= \frac{G}{2} \left\{ \frac{(w/2 + z)}{k_u} \sin(k_u(w/2 + z)) - (w/2 + z)^2 C_i(k_u(w/2 + z)) \right.$$

$$\left. + \frac{(w/2 - z)}{k_u} \sin(k_u(w/2 - z)) - (w/2 - z)^2 C_i(k_u(w/2 - z)) \right\} \tag{B.22}$$

where $C_i(x)$ is the cosine integral function defined by

$$C_i(x) = -\int_x^{\infty} \frac{\cos(t)}{t}\, dt \ . \tag{B.23}$$

The desired error bound is given by expression (B.22) with the appropriate choice of G from relation (B.21). This

expression is easily evaluated by means of tabulated values of $C_i(x)$ (Abramowitz and Stegun [1]) or may be numerically evaluated as part of the inversion routine on the computer. As the truncation error due to terminating the numerical integration at k_u is shown in expression (B.22) to depend upon the value of z and the width of the electrode, it is not possible to specify a fixed error bound for a given k_u. However, with the termination criterion used in the integration program (see Section 3.3.1 or Appendix C), the truncation point k_u was found to be sufficiently large to result in an error of less than 0.05% for a series of specific evaluations using expression (B.22). This was further verified by forcing the integration to continue to a value of k_u 10 to 100 times larger, with the effect being a change in at most the 5th significant figure of the integration result[1].

Similar techniques may be used to obtain error bounds for $\vec{E}$ or $\vec{J}$, with the same result being that the truncation error is insignificant when the termination criterion specified in Section 3.3.1 or Appendix C is used. These results also apply to the time-dependent response since the exponentials involved decay to zero faster than the asymptotic forms used to obtain the error bounds of expression (B.22).

B.4. Errors from Integration Interval Segmentation

If the integration involved in the Fourier inversion were performed in a single segment as

---

[1] The expression (B.22) is an error bound, so that the actual truncation error is often far less.

$$\Phi(r,z,t) = \frac{1}{\pi}\int_{\delta}^{k_u} \bar{\Phi}(r,k,t)\cos(kz)dk \ , \qquad (B.24)$$

then the net error would be due to three sources: truncation of the upper infinite limit to k_u, starting the integration at δ rather than 0, and the accuracy of the integration routine that evaluates the integral between δ and k_u. The previous sub-sections indicated that the error arising from the first two sources was insignificant if δ was small and k_u large, and error bounds were given for estimating these errors. The third source of error depends upon the numerical integrator, and typically can also be made as small as desired by specification of an error tolerance in the integration program (see Appendix C). However, the integration between δ and k_u is normally broken into segments defined by the period of the cosine function in expression (B.24), so that there is an additional consideration in the error estimation.

The expression actually used for performing the inverse Fourier transforms on the computer is given in relation (3.87). The integration interval is broken into $N + 1$ subintervals, with N determined in the integration routine by terminating when the $N + 1$ segment's contribution is insignificant with respect to the previous N segments. If the error of each segment is bounded by the same value, then the overall error is bounded by $(N + 1)$ times that of the single segment (see Henrici [31]). For example, if the numerical routine returns a value that is accurate to 1%, then $N + 1$ segments added together give a result that is at least accurate to $(N + 1)$% (this being the case if the errors were additive and didn't tend to cancel each other). However, since the k-domain

functions in this report have their maximum value at or near $k = 0$ and then decay at $\frac{1}{k^2}$ as $k \to \infty$ (for a finite-width electrode), the usual situation is that the largest contribution to the total integration result is given by the first one or two subintervals. The other segments added together return a contribution that is typically far smaller. Thus the actual accuracy on a percent basis is determined by the first few segments.

The net result of the discussion above is that the error tolerance of the integration routine on the first segments determines the overall accuracy of the numerical integration; with the error from truncation, discarding the area from 0 to δ, and the latter segments being insignificant. In the calculations performed for this report, the error tolerance was normally set at 1%. The adaptive integration routine normally was far more accurate than this would indicate, as decreasing the tolerance to 0.001% only gave an alteration in the 4th or 5th significant figure of the result in periodic tests performed on nearly all the solution inversions. Thus the responses presented in this report can be taken to be accurate to at least 1%.

APPENDIX C

PROGRAMMING CONSIDERATIONS

The responses presented in this report were obtained by numerical inversion of the Fourier-domain solutions using a program written in FORTRAN Extended language, carried out on a CDC 6500 computer system. Mathematical details such as integrand form, segmentation of the integration range, truncation, error determination, etc. are given in Section 3.3.1 and Appendix B. This appendix outlines the programming involved and lists the two key subprograms that form the necessary numerical integrator.

The overall program is divided into nine sections, consisting of a main program and eight subprograms. These eight subprograms include a routine to initialize axon parameters, a subroutine that does the segmented integration and determines the truncation point, the actual Simpson's rule adaptive integrator, the function to be integrated, and the four modified Bessel functions ($I_o(x)$, $I_1(x)$, $K_o(x)$ and $K_1(x)$) necessary to evaluate the Fourier-domain solutions. In practice, all but the main program and the integrand (solution) function are stored in a permanent file; eliminating the need to compile those portions of the program every time it is used. Each of the program's sections are discussed in the following paragraphs.

The main program provides the structural framework of the overall program and is modified as necessary for the particular response being calculated. First it calls the parameter initialization routine. Then the desired response points (r,z,t) are input and stored in three arrays. The body of the main program steps through these arrays to calculate the response at each (r,z,t) by calling the appropriate subroutines. The order of these calculations varies with the type of plot wanted. For example, for $V_m(z,t)$ vs. t; z is held fixed while the t values are varied. After each calculation, the result is output before continuing. The most often desired response was the transmembrane potential. This was obtained by first calculating $\Phi_I'(b,z,t)$ and $\Phi_E(a,z,t)$ separately and then applying $V_m' = \Phi_I' - \Phi_E$. In this manner, the intracellular and extracellular potentials at the membrane are obtained as well as the transmembrane potential. After finishing the Fourier inversions at each (r,z,t), the program terminates.

Subroutine READIN is the parameter initialization routine. Called by the main program, READIN inputs the necessary neuron parameters and the desired error tolerances for truncation and the numerical integrator. Such physical constants as π or ε_o are also initialized in this subprogram (eg. $\pi = 4 \tan^{-1}(1)$ is used to obtain π). Labeled common blocks are used to pass this information to the rest of the program.

INTEG, given in Table C.1, is the subroutine that performs the segmented integration and determines the truncation point. Values in its parameter list (and common block) are as follows:

DELTA	δ, the inversion integral's starting point (see Appendix B or Section 3.3.1)
PERIOD	the period of the cosine kernel, cos kz, taken to be $2\pi/z$ or, if $z = 0$, $4\pi/w$ (w = electrode width)
MAXK	maximum value of k_u allowed (a default parameter that terminates integration if convergence is not obtained)
ACTEST	truncation criterion, percentage of total area (typically 0.001 (0.1%) was used)
FUN	name of function to be integrated
AIN	total area obtained from integration
K	value of k reached at the end of any segment
ACHK	actual percentage of total area returned by last segment before termination
TEST	error tolerance for numerical integrator SIMP.

TABLE C.1

Subroutine INTEG

```
      SUBROUTINE INTEG (DELTA,PERIOD,MAXK,ACTEST,FUN,AIN,K,ACHK)
      COMMON /BLK1/  TEST
      X1 = DELTA
      XEND = 0.1
      AREA = SIMP (X1, XEND, TEST, FUN)
      AIN = AREA
      X1 = XEND
      XEND = PERIOD
      K = XEND
      AREA = SIMP (X1, XEND, TEST, FUN)
      AIN = AIN + AREA
   10 X1 = XEND
      XEND = XEND +PERIOD
      ATEST = AIN
      AREA = SIMP (X1, XEND, TEST, FUN)
      AIN = AIN + AREA
      IF (AIN) 11,15,11
   11 ACHK = ABS((ATEST-AIN)/AIN)
      IF (ACHK .LT.ACTEST) GO TO 15
      K = XEND
      IF (K .GT. MAXK) GO TO 15
      GO TO 10
   15 RETURN
      END
```

INTEG first calculates the inversion integral's contribution from δ to 0.1 and from 0.1 to PERIOD. Normally these are the major contributions to the total integration since the Fourier-domain solutions have both the greatest magnitude and slope near $k = 0$. The integration then continues in segments of width PERIOD until either the latest segment increases the total area by less than the percentage specified by ACTEST, or MAXK is reached. INTEG is called by the main program, with FUN in the calling statement being the name of the k-domain solution function to be integrated.

SIMP is the adaptive Simpson's-rule numerical integrator, called by INTEG. It is written in the form of a FORTRAN function and is listed in Table C.2. This function is from Davis and Rabinowitz [16], and the form given here has been modified for the CDC 6500 computer and has had some minor programming errors removed[1]. SIMP calculates the area under the curve of function FUN(X) between the limits A1 and B to an error tolerance of EP. Typically, EP = 0.01 (1%) was used, with SIMP usually terminating with far less error (a characteristic of the program, discussed in Davis and Rabinowitz [16] along with the theory involved). The routine is adaptive in the sense that it uses a non-fixed integration step size, taking more points in regions where FUN(X) has a large second derivative than where FUN(X) or its slope is relatively constant.

The Fourier-domain solution is specified in the function FUN(X). Whatever name is used for this function is declared in an

---

[1] These involved problems that occurred when the integrand returned zero as its value in the first few integration steps.

TABLE C.2

Function SIMP, Adaptive Simpson's Rule Integrator

```
      FUNCTION SIMP (A1,B,EP,FUN)
C   NON-RECURSIVE ADAPTIVE INTEGRATION
      DIMENSION DX(30),EPSP(30),X2(30),X3(30),F2(30),F3(30),F4(30),
     1 FMP(30),FBP(30),EST2(30),EST3(30),PVAL(30,3),NRTR(30)
      COMMON PVAL, SUM, LVL, L1
C   PARAMETER SETUP FOR INITIAL CALL
      A = A1
      EPS = EP
      LVL = 0
      ABSAR = 0.
      EST = 0.
      DA = B -A
      FA = FUN(A)
      FM = 4.*FUN((A+B)*.5)
      FB = FUN(B)
C   1 = RECUR
    1 LVL = LVL+1
      DX(LVL) = DA/3.
      SX = DX(LVL)/6.
      F1 = 4.*FUN(.5*DX(LVL)+A)
      X2(LVL) = A+DX(LVL)
      F2(LVL) = FUN(X2(LVL))
      X3(LVL) = X2(LVL)+DX(LVL)
      F3(LVL) = FUN(X3(LVL))
      EPSP(LVL) = EPS
      F4(LVL) = 4.*FUN(DX(LVL)*.5 +X3(LVL))
      FMP(LVL) = FM
      EST1 = SX*(FA +F1 +F2(LVL))
      FBP(LVL) = FB
      EST2(LVL) = SX*(F2(LVL) +F3(LVL) +FM)
      EST3(LVL) = SX*(F3(LVL) +F4(LVL) +FB)
      SUM = EST1 +EST2(LVL) +EST3(LVL)
      ABSAR = ABSAR -ABS(EST) +ABS(EST1) +ABS(EST2(LVL)) +ABS(EST3(LVL))
      IF(ABS(EST -SUM) -EPSP(LVL)*ABSAR) 2,2,3
    3 IF(LVL -30) 4,2,2
C   2 = UP
    2 LVL = LVL -1
      IF (LVL) 8,8,6
    6 L = NRTR(LVL)
      PVAL(LVL,L) = SUM
      GO TO (11,12,13)L
C   11 = R1, 12 = R2, 13 = R3
    8 LVL = 1
    4 NRTR(LVL) = 1
      EST = EST1
      FM = F1
      FB = F2(LVL)
    7 EPS = EPSP(LVL)/1.7
      DA = DX(LVL)
      GO TO 1
   11 NRTR(LVL) = 2
      FA = F2(LVL)
      FM = FMP(LVL)
      FB = F3(LVL)
      EST = EST2(LVL)
      A = X2(LVL)
      GO TO 7
   12 NRTR(LVL) = 3
      FA = F3(LVL)
      FM = F4(LVL)
      FB = FBP(LVL)
      EST = EST3(LVL)
      A = X3(LVL)
      GO TO 7
   13 SUM = PVAL(LVL,1) +PVAL(LVL,2) +PVAL(LVL,3)
      IF(LVL-1) 5,5,2
    5 SIMP = SUM
      RETURN
      END
```

EXTERNAL statement in the main program. The single argument X in the parameter list represents the transform variable k of the solution functions, with all other necessary data (stimulus intensity, fiber parameters, etc.) being supplied to FUN(X) via labeled common blocks. Since most of the Fourier-domain solutions contain several identical factors, it is convenient to use one function FUN(X) to calculate any of several solutions (eg., Φ_I, Φ_M, and Φ_E); using a computed GO TO statement to branch to the desired function calculation after performing the calculations common to all solutions. The index for this computed GO TO statement is set in the main program and passed to FUN(X) in a common block.

The last four subprograms calculate the modified Bessel functions $I_o(x)$, $I_1(x)$, $K_o(x)$, and $K_1(x)$. Although these functions are available at most computer facilities, the programs are generally not written for optimum performance in this particular application. These Bessel functions are calculated literally thousands of times for a single numerical Fourier inversion, making it necessary that they be as efficient as possible in terms of computer time. The FORTRAN functions used for the calculation of responses presented in this report were written using the polynomial approximations given in Abramowitz and Stegun [1], Section 9.8. These polynomials evaluate the Bessel functions with an error of less than 10^{-7}, and it was found by direct comparison with the computer lab's programs that they were far more efficient time-wise than the available routines. $I_o(x)$ and $I_1(x)$ are evaluated first for any value x, since the polynomials for $K_o(x)$ and $K_1(x)$ use those values in their calculation. Each of the four functions has two polynomial approximations;

one for x near zero and one for large x. It is a simple matter to use an IF statement to branch to the appropriate polynomial. The simplest way to program these four Bessel functions is to write an individual FORTRAN function subprogram for each.

APPENDIX D

NEURAL PARAMETERS USED IN OBTAINING NUMERICAL RESULTS

The responses presented in Chapters 3, 4, and 5 for steady-state and time-dependent electrotonus were obtained from the following set of "test axon" parameters.

$a = 0.25$ mm	axon radius
$d = 50$ Å	membrane thickness
$\sigma_I = 0.03333$ mhos/cm	intracellular conductivity
$\sigma_E = 0.04546$ mhos/cm	extracellular conductivity
$\sigma_M = 7.143 \times 10^{-10}$ mhos/cm	membrane conductivity
$\varepsilon_I = \varepsilon_E = 80\varepsilon_o$ $= 7.08 \times 10^{-12}$ farads/cm	intracellular and extracellular permittivity
$\varepsilon_M = 6\varepsilon_o = 5.31 \times 10^{-12}$ farads/cm	membrane permittivity
$w = 0.5$ mm	electrode width
I_I^s, $I_E^s = 10^{-5}$ amps	total current to either electrode
J_I^s, $J_E^s = 1.273 \times 10^{-3}$ amps/cm^2	current density at either electrode

The last three values define the standardized electrode size and stimulus intensity. Any deviations from the above values for purposes of showing the effects of varying a parameter are noted and defined in the text. These axon parameters are from Katz [40], where they are listed in the forms more appropriate to core-conductor theory as:

$R_i = \frac{1}{\sigma_I} = 30$ ohm-cm resistivity of cell interior

$R_o = \frac{1}{\sigma_E} = 22$ ohm-cm resistivity of extracellular fluid

$R_m = \frac{d}{\sigma_M} = 700$ ohm-cm^2 membrane resistance.

The membrane capacitance is defined with

$$C_m = \varepsilon_M/d = 1.062 \ \mu f/cm^2 \ .$$

These parameters give the cable equation length constant and time constant (see Sections 3.3.2 and 4.3.1) as

$$\lambda = 5.4 \text{ mm}$$

$$\tau = 0.743 \text{ msec} \ .$$

Since the solutions were carried out for electrotonic perturbations from the resting state, it was not necessary to specify the Nernst potentials, individual ion conductivities, or resting transmembrane potential.

For the responses presented in the latter part of Chapter 5 in the simulations of postsynaptic potentials, the parameter set was changed to represent a dendritic-size fiber. These were obtained from Eccles [18] and Katz [40] and are listed as follows:

$a = 2.5 \ \mu$ dendrite radius

$d = 50 \ \text{Å}$ membrane thickness

$\sigma_I = 0.01667$ mhos/cm intracellular conductivity

$\sigma_E = 0.04546$ mhos/cm extracellular conductivity

$g_r = 2.0 \times 10^{-4}$ mhos/cm^2	resting-state membrane conductance
$C_m = 1.062$ μf/cm^2	membrane capacitance
$V_r = -60$ mV	resting transmembrane potential
$V_{Na^+} = 55$ mV	sodium Nernst potential
$V_{K^+} = -95$ mV	potassium Nernst potential
$w = 1\mu$	width of conductance perturbation "window".

C_m was obtained from ε_M/d with $\varepsilon_M = 6\varepsilon_o$. Also, g_r is the sum of all individual resting-state ion conductances[1]. The conductance perturbation magnitudes are given in the appropriate sections where they were used (Sections 5.3.1, 5.3.2, and 5.3.3). The Nernst potentials and resting potential had to be specified in this case as they are involved in the source term that arises from ion-selective conductance perturbations. For core-conductor theory, the appropriate forms for the above conductances and conductivities are

$R_i = 60$ ohm-cm	resistivity of cell interior
$R_o = 22$ ohm-cm	resistivity of extracellular fluid
$R_m = 1/g_m = 5{,}000$ ohm-cm^2	membrane resistance.

These give electrotonic time and length constants (see Sections 3.3.2 and 4.3.1) of

$$\lambda = 2.5 \text{ mm}$$

$$\tau = 5.31 \text{ msec.}$$

---

[1] In the resting-state the membrane conductance is primarily due to the conductances of potassium and chloride ions.

BIBLIOGRAPHY

BIBLIOGRAPHY

1. Abramowitz, M. and I.A. Stegun (editors), Handbook of Mathematical Functions. New York: Dover, 1965.

2. Arfken, G., Mathematical Methods for Physicists, 2nd ed. New York: Academic Press, 1970.

3. Arndt, R.A., J.D. Bond, and L.D. Roper, "An exact constant-field solution for a simple membrane," Biophys. J., vol. 10, pp. 1149-1153, December 1970.

4. Arndt, R.A., J.D. Bond, and L.D. Roper, "Numerical solution of steady-state electrodiffusion equations for a simple membrane," Biophys. J., vol. 11, pp. 265-294, March 1971.

5. Berg, P.W. and J.L. McGregor, Elementary Partial Differential Equations. San Francisco: Holden-Day, 1966.

6. Carslaw, H.S. and J.C. Jaeger, Conduction of Heat in Solids, 2nd ed. London: Oxford Press, 1959.

7. Churchill, R.V., Operational Mathematics, 3rd ed. New York: McGraw-Hill, 1972.

8. Clark, J.W. and R. Plonsey, "A mathematical evaluation of the core conductor model," Biophys. J., vol. 6, pp. 95-112, January 1966.

9. Clark, J.W. and R. Plonsey, "The extracellular potential field of the single active nerve fiber in a volume conductor," Biophys. J., vol. 8, pp. 842-864, July 1968.

10. Clark, J.W. and R. Plonsey, "A mathematical study of nerve fiber interaction," Biophys. J., vol. 10, pp. 937-957, October 1970.

11. Cole, K.S., "The advance of electrical models for cells and axons," Biophys. J., vol. 2, pp. 101-119, part 2, March 1962.

12. Cole, K.S., Membranes, Ions, and Impulses, Berkeley, Calif.: Univ. of California Press, 1968.

13. Cole, K.S. and H.J. Curtis, "Electrical impedance of the squid giant axon during activity," J. Gen. Physiol., vol. 22, pp. 649-670, May 1939.

14. Cooley, J.W. and H. Cohen, "The numerical solution of the time-dependent Nernst-Planck equations," Biophys. J., vol. 5, pp. 145-162, March 1965.

15. Cooley, J.W. and F.A. Dodge, Jr., "Digital computer solutions for excitation and propagation of the nerve impulse," Biophys. J., vol. 6, pp. 583-599, September 1966.

16. Davis, P.J. and P. Rabinowitz, Numerical Integration. Waltham, Mass.: Blaisdell, 1967.

17. Eccles, J.C., The Physiology of Nerve Cells. Baltimore: Johns Hopkins Press, 1957.

18. Eccles, J.C., The Physiology of Synapses. Berlin: Springer-Verlag, 1964.

19. Eccles, J.C., The Understanding of the Brain. New York: McGraw-Hill, 1973.

20. Eisenberg, R.S. and E.A. Johnson, "Three-dimensional electric field problems in physiology," in Progress in Biophysics and Molecular Biology, vol. 20, edited by J.A. Butler and D. Noble, New York: Pergamon Press, 1970.

21. Erdélyi, A., W. Magnus, F. Oberhettinger, and F.G. Tricomi, Tables of Integral Transforms, vol. 1. New York: McGraw-Hill, 1954.

22. Evans, J. and N. Shenk, "Solutions to axon equations," Biophys. J., vol. 10, pp. 1090-1101, November 1970.

23. Finkelstein, A. and A. Mauro, "Equivalent circuits as related to ionic systems," Biophys. J., vol. 3, pp. 215-237, May 1963.

24. FitzHugh, R., "Impulses and physiological states in theoretical models of nerve membrane," Biophys. J., vol. 1, pp. 445-466, July 1961.

25. FitzHugh, R., "Computation of impulse initiation and saltatory conduction in a myelinated nerve fiber," Biophys. J., vol. 2, pp. 11-21, January 1962.

26. FitzHugh, R., "Mathematical models of excitation and propagation in nerve," in Biological Engineering, edited by H.P. Schwan, New York: McGraw-Hill, 1969.

27. Ganong, W.F., Review of Medical Physiology, 5th ed. Los Altos, Calif.: Lange Medical Publications, 1971.

28. Goldman, L. and J.S. Albus, "Computation of impulse conduction in myelinated fibers; theoretical basis of the velocity-diameter relation," Biophys. J., vol. 8, pp. 596-607, May 1968.

29. Goldstein, S.S. and W. Rall, "Changes of action potential shape and velocity for changing core conductor geometry," Biophys. J., vol. 14, pp. 731-758, October 1974.

30. Hellerstein, D., "Passive membrane potentials, a generalization of the theory of electrotonus," Biophys. J., vol. 8, pp. 358-379, March 1968.

31. Henrici, P., Elements of Numerical Analysis. New York: John Wiley and Sons, 1964.

32. Hille, B., "Ionic channels in membranes," in Progress in Biophysics and Molecular Biology, vol. 21, edited by J.A.V. Butler and D. Noble, New York: Pergamon Press, 1970.

33. Hodgkin, A.L., The Conduction of the Nervous Impulse. Liverpool: Liverpool University Press, 1964.

34. Hodgkin, A.L. and A.F. Huxley, "Currents carried by sodium and potassium ions through the membrane of the giant axon of Loligo," J. Physiol., vol. 116, pp. 449-472, April 1952.

35. Hodgkin, A.L. and A.F. Huxley, "The components of membrane conductance in the giant axon of Loligo," J. Physiol., vol. 116, pp. 473-496, April 1952.

36. Hodgkin, A.L. and A.F. Huxley, "The dual effect of membrane potential on sodium conductance in the giant axon of Loligo," J. Physiol., vol. 116, pp. 497-506, April 1952.

37. Hodgkin, A.L. and A.F. Huxley, "A quantitative description of membrane current and its application to conduction and excitation in nerve," J. Physiol., vol. 117, pp. 500-544, August 1952.

38. Hodgkin, A.L., A.F. Huxley, and B. Katz, "Measurement of current-voltage relations in the membrane of the giant axon of Loligo," J. Physiol., vol. 116, pp. 424-448, April 1952.

39. Hoyt, R., "Independence of the sodium and potassium conductance channel. A kinetic argument," Biophys. J., vol. 11, pp. 110-122, January 1971.

40. Katz, B., Nerve, Muscle, and Synapse. New York: McGraw-Hill, 1966.

41. King, R.W.P., Fundamental Electromagnetic Theory, 2nd ed. New York: Dover, 1963.

42. Klee, M., "Intracellular biopotentials during static extracellular stimulation," Biophys. J., vol. 13, pp. 822-831, August 1973.

43. Klee, M. and R. Plonsey, "Finite difference solution for biopotentials of axially symmetric cells," Biophys. J., vol. 12, pp. 1661-1675, December 1972.

44. Klee, M. and R. Plonsey, "Integral equation solution for biopotentials of single cells," Biophys. J., vol. 12, pp. 1676-1686, December 1972.

45. Kortum, G., Treatise on Electrochemistry, 2nd ed. Amsterdam: Elsevier Publishing Co., 1965.

46. Lehninger, A.L., Biochemistry. New York: Worth, 1970.

47. Lillie, R.S., "The passive iron wire model of protoplasmic and nervous transmission and its physiological analogies," Biol. Rev., vol. 11, pp. 181-209, April 1936.

48. Lorente de No, R., "A study of nerve physiology," Stud. Rockefeller Inst. Med. Research, vol. 131 and 132, 1947.

49. Morse, P.M, and H. Feshbach, Methods of Theoretical Physics. New York: McGraw-Hill, 1953.

50. Mountcastle, V.B. (editor), Medical Physiology, 13th ed. Saint Louis: C.V. Mosby, 1974.

51. Mullins, L.J., "An analysis of conductance changes in squid axon," J. Gen. Physiol., vol. 42, pp. 1013-1035, May 1959.

52. Nagumo, J., S. Arimoto, and S. Yoshizawa, "An active pulse transmission line simulating nerve axon," Proc. IRE, vol. 50, pp. 2061-2070, October 1962.

53. Norman, R.S., "Cable theory for finite length dendritic cylinders with initial and boundary conditions," Biophys. J., vol. 12, pp. 25-45, January 1972.

54. Ochs, S., Elements of Neurophysiology. New York: John Wiley and Sons, 1965.

55. Offner, F.F., "Kinetics of excitable membranes, voltage amplification in a diffusion regime," J. Gen. Physiol., vol. 56, pp. 272-296, August 1970.

56. Offner, F.F., "Nernst-Planck-Poisson diffusion equation: numerical solution of the boundary value problem," J. Theor. Biol., vol. 31, pp. 215-227, May 1971.

57. Offner, F.F., "The excitable membrane, a physiochemical model," Biophys. J., vol. 12, pp. 1583-1629, December 1972.

58. Olmsted, J.M.H., Advanced Calculus. New York: Appleton-Century-Crofts, 1961.

59. Papoulis, A., The Fourier Integral and Its Applications. New York: McGraw-Hill, 1962.

60. Plonsey, R., Bioelectric Phenomena. New York: McGraw-Hill, 1969.

61. Plonsey, R. and D. Heppner, "Considerations of quasi-stationarity in electrophysiological systems," Bull. Math. Biophys., vol. 29, pp. 657-664, December 1967.

62. Rall, W., "Electrophysiology of a dendritic neuron model," Biophys. J., vol. 2, pp. 145-167, part 2, March 1962.

63. Rall, W., "Theoretical significance of dendritic trees for neuronal input-output relations," in Neural Theory and Modeling, edited by R.F. Reiss, Stanford: Stanford Univ. Press, 1964.

64. Rall, W., "Distinguishing theoretical synaptic potentials computed for different soma-dendritic distributions of synaptic input," J. Neurophysiol., vol. 30, pp. 1138-1168, September 1967.

65. Rall, W., "Distributions of potential in cylindrical coordinates and time constants for a membrane cylinder," Biophys. J., vol. 9, pp. 1509-1541, December 1969.

66. Rall, W., R.E. Burke, T.G. Smith, P.G. Nelson, and K. Frank, "Dendritic location of synapses and possible mechanisms for the monosynaptic EPSP in motoneurons," J. Neurophysiol., vol. 30, pp. 1169-1193, September 1967.

67. Ramo, S., J.R. Whinnery, and T. VanDuzer, Fields and Waves in Communication Electronics. New York: John Wiley and Sons, 1965.

68. Rinzel, J. and J.B. Keller, "Traveling wave solutions of a nerve conduction equation," Biophys. J., vol. 13, pp. 1313-1337, December 1973.

69. Roberts, G.E. and H. Kaufman, Tables of Laplace Transforms. Philadelphia: Saunders, 1966.

70. Ruch, T.C. and H.D. Patton, Physiology and Biophysics. Philadelphia: Saunders, 1965.

71. Sagan, H., Boundary and Eigenvalue Problems in Mathematical Physics. New York: John Wiley and Sons, 1961.

72. Schmidt, G., Physics of High Temperature Plasmas, An Introduction. New York: Academic Press, 1966.

73. Smith, T.G., R.B. Wuerker, and K. Frank, "Membrane impedance changes during synaptic transmission in cat spinal motoneurons," J. Neurophysiol., vol. 30, pp. 1072-1096, September 1967.

74. Stevens, C.F., Neurophysiology: A Primer. New York: John Wiley and Sons, 1966.

75. Tanenbaum, B.S., Plasma Physics. New York: McGraw-Hill, 1967.

76. Taylor, R.E., "Cable theory," in Physical Techniques in Biological Research, vol. VIB, edited by W.L. Nastuk, New York: Academic Press, 1963.